

## ABSTRACT

ADOTEYE, KASKA. Biological Applications of Uncertainty Quantification, Including Multiscale *Daphnia magna* Population Modeling. (Under the direction of H.T. Banks.)

Mathematical modeling, inverse problems, and uncertainty quantification have become increasingly important parts of biological and ecotoxicological studies. Mathematics is used to create models to try and explain and predict biological phenomenon, inverse problems are used to find values for the parameters in these models, and uncertainty quantification is then used to understand the certainty we have in our parameter estimates and the relation of our estimators to each other.

In this dissertation we seek to use mathematical modeling and uncertainty quantification to attain novel insights concerning biological phenomenon. We begin by exploring a few uncertainty quantification techniques themselves to glean their efficacy. That is, we explore correlation of parametric estimators through the use of correlation coefficients, frequentist techniques (asymptotic and exact confidence regions), and Bayesian uncertainty analysis through the use of the DRAM algorithm. We find that only the DRAM algorithm and exact confidence regions are able to give the full nonlinear scope of estimator correlation, if it exists, and that the computation time for the creation of the exact confidence regions is far less than that for the DRAM algorithm. We also find that the use of asymptotic confidence regions and correlation coefficients can provide a quick technique to see if any correlation exists, but not necessarily the nature of that correlation.

We then turn to a commonly studied organism, *Daphnia magna*. While there is a plethora of work concerning individual daphnid dynamics, whether perturbed by toxicants or undisturbed, there is much less work done on the population level dynamics. There are several important mechanisms that affect populations of daphnids. Not only are there random effects on the individual level (e.g., the number of offspring produced per brood by adult female daphnids is highly variable) but there are also effects that occur at the population level (e.g., daphnids that are in crowded conditions produce less offspring). The modeling efforts of the past have in some cases overlooked important effects, or have not given the same level of experimental, mathematical, and statistical scrutiny that we have. Here we design and run experiments to tease out the individual and population-level effects that drive daphnid population dynamics. We quantify individual daphnid mortality using linear spline approximations, verify that individual daphnid fecundity is best modeled on the population level using averages (as the underlying process is random), and fully quantify individual daphnid growth. In addition, we verify previously discovered density-dependent effects, including a delayed reduction in fecundity and a reduction in mortality. In addition, we discover there is a delay in the density-dependent effect on mortality, and see the tremendous effect that daphnid life history has on these outcomes, which is an effect that, to our knowledge, has not been seen before. We then create a multi-scale, discrete daphnid population model using some of our findings, calibrated

with our experimental data and verified using uncertainty quantification. We also lay out a more comprehensive model that incorporates everything that we know about daphnids.



© Copyright 2015 by Kaska Adoteye

All Rights Reserved

Biological Applications of Uncertainty Quantification, Including Multiscale *Daphnia magna*  
Population Modeling

by  
Kaska Adoteye

A dissertation submitted to the Graduate Faculty of  
North Carolina State University  
in partial fulfillment of the  
requirements for the Degree of  
Doctor of Philosophy

Applied Mathematics

Raleigh, North Carolina

2015

APPROVED BY:

---

Hien Tran

---

Gerald LeBlanc

---

Alun Lloyd

---

H.T. Banks  
Chair of Advisory Committee

## **DEDICATION**

To anyone who ever pursued a dream, even if that dream was a moving target. To my family and friends, who stood by me as I followed mine.

## **BIOGRAPHY**

Kaska Adoteye was born in Northern Virginia on August 21, 1989 where he spent his childhood among his two older brothers. He graduated magna cum laude from the University of Pittsburgh in 2011 with a B.S. in Mathematics and Fiction Writing. He received is Masters in Applied Mathematics from North Carolina State University in 2013.

## ACKNOWLEDGEMENTS

This dissertation has been the combination of projects that a lot of people contributed to. First and foremost I must thank my advisor, Dr. H.T. Banks, for making all of this possible, and for giving me repeated chances to prove my worth on such a complex set of tasks. Thank you for your patience, your guidance, your advice, your expertise, your resources, and your friendship.

Thanks must go to Dr. Gerald A. LeBlanc, Dr. H.T. Banks, and the CRSC, for the funds to create and run the wet lab that produced the experiments shown throughout this dissertation. The opportunity to create and run a lab is an experience that few graduate students get, and I feel honored that I was given that rare opportunity.

To Elizabeth Medlock, Stephanie Eytcheson, and the other researchers in Dr. LeBlanc's lab, thank you for taking the time to show me how to run a lab and take care of daphnids.

To Kevin Flores, thank you for being there every single step of the way. I can't think of a single part of this dissertation that you were not a part of. Thank you for your help with everything: setting up the lab, modeling, analyzing data, and being a good friend. Thank you for your knowledge and guidance, and for being there with me going through this process.

To Dr. Jonathan Rubin, thank you for helping me pick graduate schools, and to introducing me to research. I can't think of better preparation when entering NC State. To Dr. Nehash Medhin, thank you for working with me for two and a half years, and for introducing me to research at a higher level.

All of the people that helped with the mathematical and biological aspects of this project: Dr. H. T. Banks, Dr. Kevin Flores, Dr. Shuhua Hu, Dr. Gerald A. LeBlanc, Elizabeth Medlock, Stephanie Eytcheson, Chelsea Ross, Karissa Cross, Michael Stemkovski, Sarah Stokely, Emmaline Smith, Timothy Nguyen, Amanda Laubmeier, Kristen Tillman, and anyone I might have missed.

Now, of course, these years would not have been possible without the support and love of my friends and family. I could go on and on for days thanking people, but here I'll name but a few. George Lankford and Christina Battista, you've been with me every step of this entire process, from recruitment weekend at State up until the end. We've shared laughs, tears, excitement, anger, frustration, hopes, and dreams, and I wouldn't trade any of it for a second. And thank you to my brothers and parents, all three of them, for your continued encouragement and endless love.

While the journey has been wild and challenging, I know that I'm a better person, researcher, scientist, and mathematician because of it, and I was able to get through it with the support of all of you. Thank you.

## TABLE OF CONTENTS

<b>LIST OF TABLES</b> . . . . .	<b>viii</b>
<b>LIST OF FIGURES</b> . . . . .	<b>xi</b>
<b>Chapter 1 Introduction</b> . . . . .	<b>1</b>
<b>Chapter 2 Methods to Determine Correlation of Parameter Estimates from Inverse Problems Given Different Model Parametrizations</b> . . . . .	<b>5</b>
2.1 Introduction . . . . .	5
2.2 Methodology . . . . .	7
2.2.1 Statistical Analysis and Inverse Problem Methods . . . . .	7
2.2.2 Confidence "Ellipsoids" or Regions . . . . .	9
2.2.3 DRAM (Bayesian Analysis) . . . . .	12
2.2.4 Complex-Step Method of Sensitivity Calculations . . . . .	13
2.3 Mathematical Models . . . . .	14
2.3.1 Logistic . . . . .	14
2.3.2 Richards . . . . .	15
2.3.3 Spring Equation . . . . .	16
2.3.4 Adding Noise . . . . .	17
2.4 Results . . . . .	18
2.4.1 Covariance Results . . . . .	18
2.4.2 Ellipsoidal and DRAM Results . . . . .	21
2.5 Discussion and Concluding Remarks . . . . .	30
<b>Chapter 3 A Discrete Multi-Scale Population Model for <i>Daphnia magna</i></b> . . . . .	<b>32</b>
3.1 Introduction . . . . .	32
3.2 Methods . . . . .	34
3.2.1 Population models . . . . .	34
3.2.2 Laboratory studies . . . . .	37
3.2.3 Estimation of density-independent rates . . . . .	41
3.2.4 Parameter Estimation . . . . .	42
3.2.5 Testing Constant Error Assumption . . . . .	44
3.2.6 Model Comparisons . . . . .	45
3.2.7 Parameter Uncertainty Quantification . . . . .	46
3.3 Results . . . . .	48
3.3.1 Model Selection . . . . .	48
3.3.2 Verification of Constant Error Assumption . . . . .	48
3.3.3 Uncertainty Analysis . . . . .	52
3.3.4 Parameter Sensitivities . . . . .	57
3.3.5 Parameter Correlation . . . . .	60
3.4 Conclusions and Discussion . . . . .	63
<b>Chapter 4 Estimation of Age-Varying Mortality Rates for <i>Daphnia magna</i></b> . . . . .	<b>66</b>

4.1	Introduction	66
4.2	Data and Methods	67
4.2.1	Density-independent <i>Daphnia magna</i> survival data	67
4.2.2	Mathematical models	68
4.2.3	Inverse problem methodology	68
4.2.4	Model comparisons	70
4.3	Results	70
4.4	Discussion	73
<b>Chapter 5</b>	<b>Determining Delay on Density-Dependent Effect on Fecundity from Experimental Data of <i>Daphnia magna</i>, and Ramifications for Future Modeling</b>	<b>75</b>
5.1	Introduction	75
5.2	Continuous Model	76
5.3	Data and Methods	78
5.3.1	Experimental Design and Data	78
5.3.2	Statistical Analysis	79
5.4	Statistical Analysis Results	84
5.5	Discussion and Concluding Remarks	84
5.5.1	Fecundity Delay	84
5.5.2	Mortality Delay and Effect of Developmental Environment	89
5.5.3	Future Work	90
<b>Chapter 6</b>	<b>Discussion and Concluding Remarks</b>	<b>92</b>
	<b>BIBLIOGRAPHY</b>	<b>94</b>
	<b>APPENDICES</b>	<b>106</b>
Appendix A	Other Daphnid Work	107
A.1	Considering Probabilistic Fecundity	107
A.1.1	Background and Data	107
A.1.2	Introducing Probability	110
A.1.3	Population Model Incorporating Probabilistic Fecundity/Testing Within a Population Model	111
A.2	Supplemental Experiments	115
A.2.1	Feeding Experiment	115
A.2.2	Replicates 3 and 4 of Population Experiment	119
A.2.3	Pyriproxyfen and Ethanol Population and Individual Experiments	122
A.2.4	Pesticide Resistance	131
Appendix B	Implementation Details for Chapter 3	136
B.1	Computing Non-linear Mixed Effects Model	136
B.1.1	Initial NLME Growth Model Computation	137
B.1.2	Simbiology NLME Growth Model Computation	138
B.2	Sensitivity Equations for Discrete Model D	139
Appendix C	Optimal Design of Non-Equilibrium Experiments for Genetic Network Interrogation	144

C.1	Introduction . . . . .	144
C.2	Data and Methods . . . . .	145
C.2.1	Mathematical models, statistical models, and parameter uncertainty quantification . . . . .	145
C.2.2	Optimal design measures . . . . .	146
C.2.3	Non-equilibrium experimental design algorithm . . . . .	147
C.3	Results . . . . .	147
C.3.1	A gene network model for RNA3 recruitment in Brome Mosaic Virus . . .	147
C.4	Discussion . . . . .	151



## LIST OF TABLES

Table 2.1	These show the forward solves $f(t_j, \theta_0)$ of the models using the parameters specified in Section 2.3, along with data $y_j$ collected at evenly spaced time points $t_j$ , and perturbed by noise $\mathcal{E}_j$ from a normal distribution with standard deviation $nl$ . The forward solve is plotted as a solid line, while the data (with noise added) are plotted as open circles. Each column corresponds to a different model, while each row corresponds to a different noise level. . . . .	18
Table 2.2	These are the covariance matrices for each parametrization for each model, and for each noise level. The first parameter corresponds to the first diagonal, and the second parameter to the second. So, for example, the logistic $(r, K)$ covariance matrix has the variance in the $r$ estimate as the top left entry, and the variance in the $K$ estimate in the bottom right entry. . . . .	19
Table 2.3	Here we show the parameter estimates $\hat{\theta}_k$ and standard errors $SE(\hat{\theta}_k)$ for each parameterization for each model at each noise level considered in this chapter. Each row corresponds to a different parameter. For example, the second to last row corresponds to the parameter $c$ in the $(c, \omega)$ parametrization for the spring equation, with the first two columns corresponding to the noise level $nl = 0.01$ , the next two columns corresponding to the noise level $nl = 0.05$ , and the last two columns corresponding to the noise level $nl = 0.2$ . . . . .	20
Table 2.4	Here we show the correlation coefficients $\rho_{ij}$ for each parametrization of each model at each noise level considered in this chapter. Each column corresponds to a different noise level, while each row corresponds to a different model parametrization. . . . .	21
Table 2.5	These show the results for the logistic curve with the $(r, K)$ parametrization. The left column of plots are the asymptotic ellipsoids, the middle column of plots are the exact ellipsoids, and the right column of plots are the DRAM Monte Carlo plots. The top row of plots correspond to noise level $nl = 0.01$ , the middle row to noise level $nl = 0.05$ , and the bottom row to noise level $nl = 0.2$ . . . . .	23
Table 2.6	These show the results for the logistic curve with the $(A, B)$ parametrization. The left column of plots are the asymptotic ellipsoids, the middle column of plots are the exact ellipsoids, and the right column of plots are the DRAM Monte Carlo plots. The top row of plots correspond to noise level $nl = 0.01$ , the middle row to noise level $nl = 0.05$ , and the bottom row to noise level $nl = 0.2$ . . . . .	24
Table 2.7	These show the results for the logistic curve with the $(C, D)$ parametrization. The left column of plots are the asymptotic ellipsoids, the middle column of plots are the exact ellipsoids, and the right column of plots are the DRAM Monte Carlo plots. The top row of plots correspond to noise level $nl = 0.01$ , the middle row to noise level $nl = 0.05$ , and the bottom row to noise level $nl = 0.2$ . . . . .	25
Table 2.8	These show the results for the Richards curve with the $(\kappa, \delta)$ parametrization. The left column of plots are the asymptotic ellipsoids, the middle column of plots are the exact ellipsoids, and the right column of plots are the DRAM Monte Carlo plots. The top row of plots correspond to noise level $nl = 0.01$ , the middle row to noise level $nl = 0.05$ , and the bottom row to noise level $nl = 0.2$ . . . . .	26

Table 2.9	These show the results for the Richards curve with the $(A, B)$ parametrization. The left column of plots are the asymptotic ellipsoids, the middle column of plots are the exact ellipsoids, and the right column of plots are the DRAM Monte Carlo plots. The top row of plots correspond to noise level $nl = 0.01$ , the middle row to noise level $nl = 0.05$ , and the bottom row to noise level $nl = 0.2$ .	27
Table 2.10	These show the results for the spring equation with the $(C, K)$ parametrization. The left column of plots are the asymptotic ellipsoids, the middle column of plots are the exact ellipsoids, and the right column of plots are the DRAM Monte Carlo plots. The top row of plots correspond to noise level $nl = 0.01$ , the middle row to noise level $nl = 0.05$ , and the bottom row to noise level $nl = 0.2$ .	28
Table 2.11	These show the results for the spring equation with the $(C, \omega)$ parametrization. The left column of plots are the asymptotic ellipsoids, the middle column of plots are the exact ellipsoids, and the right column of plots are the DRAM Monte Carlo plots. The top row of plots correspond to noise level $nl = 0.01$ , the middle row to noise level $nl = 0.05$ , and the bottom row to noise level $nl = 0.2$ .	29
Table 2.12	This table contains the actual time it took to compute each figure shown in Tables 2.5 - 2.11. Each of these computations were done in serial, and each time is reported in seconds.	30
Table 3.1	Descriptions of models, parameters, and variables with unknown parameters $\theta = (\mu, q)$ in Models A and B and $\theta = (\mu, q, c)$ in Models C and D to be estimated.	36
Table 3.2	Mean parameter estimates and variances along with individual daphnid parameter estimates for the logistic equation using a nonlinear mixed effects model (see Figure 3.2).	43
Table 3.3	Results from uncertainty quantification with asymptotic theory and bootstrapping for model D.	54
Table 3.4	Our estimates for the observation standard errors are shown here. For example, $\hat{\sigma}_{A,0}$ is what our uncertainty quantification returned as our best estimate for the standard deviation of the error seen in observing adult daphnids during data collection.	56
Table 3.5	The percentage (% accuracy) and fraction of observed data points that were contained in the 68 % confidence bands of our model solution. Results are shown for the number of juveniles, number of adults, and total population size for each replicate	57
Table 4.1	The $AIC_C$ values for the Leslie model and PDE model using age-varying mortality with different interval lengths for the step function (for the Leslie model) and linear splines (for the PDE model)	72
Table 5.1	This is the mortality data seen for each Group of the experiment. The data shown here are the total number of deaths seen in that Group (Column 'A'), and the total number of deaths per daphnid each day (Column 'B') in that Group.	80

Table 5.2	This table contains the number of daphnids per beaker (labeled density) and the number of beakers for each experimental Group for Phases 1 and 2 of the the experiment. . . . .	81
Table A.1	Fecundity parameters for our daphnids from our individual experiments. $\gamma_i$ is the proportion of living daphnids that create zero offspring in brood $i$ . The other daphnids produce a number of offspring pulled from the distribution $N(\mu_i, \sigma_i^2)$ for brood $i$ . . . . .	112
Table A.2	The food concentrations for each group of the experiment. The algae solution used to feed the beakers contains the number of cells specified, and the fish food solution contains the specified mg of fish food. . . . .	116
Table B.1	This table shows which model had the largest Akaike weight for each daphnid given each type of measurement. So, for example, when trying to model the major axis length for the Control daphnids, the Gompertz curve had the largest Akaike weight for one of the 24 daphnids used, the logistic curve had the largest weight for 23 daphnids, and the linear model had the largest weight for none of the 24 daphnids, and all of this is expressed in the first row of this table. . . .	138
Table B.2	These are the $AIC_C$ values computed by Simbiology for the logistic model $f_1$ , the linear model $f_2$ , the Gompertz growth model $f_3$ , and the exponential model $f_4$ using the major axis length data for each daphnid. Here we see that the logistic model provides the best fit to the data since it has the lowest $AIC_C$ score. . . . .	139
Table C.1	BMV model results for naive time points and naive inputs (A), optimized time points and naive inputs for D-, E-, and SE-optimal design (B-D through B-SE), or naive time points and optimized inputs for D-, E-, and SE- optimal design (C-D through C-SE). NSE = normalized standard error. . . . .	149
Table C.2	BMV model results for optimized time points and inputs using D-optimal design criteria (D), E-optimal design criteria (E), or SE-optimal design criteria (SE). . . . .	151

## LIST OF FIGURES

Figure 3.1	Calibration of the maximum size for classification of juveniles. We determined the maximum juvenile daphnid size by simulating the logistic growth curve with mean parameter values from the nonlinear mixed effects model (Figure 3.2, Table 3.2). The pore size of the mesh we used to separate juveniles from adults was 1.62 mm, and this value is plotted as a horizontal line. The vertical line gives the average daphnid age at which their major axis length is equal to the mesh pore size. Based on this calculation, we inferred that the maximum age at which daphnids can fit through the mesh was 4 days old. Thus, we chose to classify juveniles in our models as $\leq 4$ days old. . . . .	38
Figure 3.2	Results for nonlinear regression performed on individual-level growth data using a logistic equation within a nonlinear mixed effects model (NLMEM). Growth data are represented by star symbols (to view growth data on a single graph, see Control Beaker plot in Figure A.8). Best model fits are drawn as lines for each individual. We collected data for thirty daphnids, but these plots show results for twenty four daphnids for which an adequate number of data was collected to fit a NLMEM (the other six daphnids died very early in the experiment). Nonlinear regression was performed using Simbiology in Matlab. We tested several models for growth, including logistic, Gompertz, constant, and linear equations. Based on $AIC_C$ values, it was determined that the logistic model provided the most accurate fit to the data. See Table 3.2 for estimated parameters and variances, including fixed effects and random effects, and Appendix B.1 for details on how the computation was completed. . . . .	39
Figure 3.3	The number of neonates produced per female daphnid per day. Data were collected from thirty female daphnids whose birth was known to within two hours of accuracy. Daily data are represented by star symbols and connecting lines are drawn to show general trends. This data was used as the age-dependent function $\alpha(i)$ (see Table 3.1). . . . .	41
Figure 3.4	These are the plots of the observation error estimates $\hat{\epsilon}_{J,j}$ and $\hat{\epsilon}_{A,j}$ for juveniles and adults, respectively, plotted against time $t_j$ for $\gamma = 0.5$ . The plots for Replicate 1 are on the left, and for Replicate 2 are on the right. . . . .	49
Figure 3.5	These are the plots of the observation error estimates $\hat{\epsilon}_{J,j}$ and $\hat{\epsilon}_{A,j}$ for juveniles and adults, respectively, plotted against time $t_j$ for $\gamma = 1.0$ . The plots for Replicate 1 are on the left, and for Replicate 2 are on the right. . . . .	50
Figure 3.6	These are the plots of the observation error estimates $\hat{\epsilon}_{J,j}$ and $\hat{\epsilon}_{A,j}$ for juveniles and adults, respectively, plotted against time $t_j$ for $\gamma = 1.5$ . The plots for Replicate 1 are on the left, and for Replicate 2 are on the right. . . . .	51
Figure 3.7	These are the plots of the observation error estimates $\hat{\epsilon}_{J,j}$ and $\hat{\epsilon}_{A,j}$ for juveniles and adults, respectively, plotted against time $t_j$ . The plots for $\gamma = 0$ are on the top, and the corresponding plots for $\gamma = 0.2$ are on the bottom. . . . .	52

Figure 3.8	These are the plots of the residual $r_j^J$ plotted against the model solution for juveniles $f_j(t_j, \theta)$ on top and $r_j^A$ plotted against the model solution for adults $f_A(t_j, \theta)$ on the bottom. The plots for Replicate 1 are on the left, and for Replicate 2 are on the right. . . . .	53
Figure 3.9	The parameter distributions obtained from bootstrapping for each estimated parameter ( $\mu, q, c$ ) and each replicate for model D. . . . .	55
Figure 3.10	Results from fitting our discrete daphnid population model to adult and juvenile longitudinal data. Black lines: model simulation results using parameter estimates. Black circles: our data. Gray region: 68 % confidence band, with the error coming from our statistical model, which assumes constant error. . . . .	58
Figure 3.11	Results from fitting our discrete daphnid population model to adult and juvenile longitudinal data. Black lines: model simulation results using parameter estimates. Black circles: our data. Gray region: 95 % confidence band, with the error coming from our statistical model, which assumes constant error. . . . .	59
Figure 3.12	The relative time-dependent sensitivities for juveniles, adults, and the total population with respect to each of the estimated parameters ( $\mu, q, c$ ) for model D. Sensitivities were calculated for the number of juveniles $f_j(t, \hat{\theta})$ (top row), the number of adults $f_A(t, \hat{\theta})$ (middle row), and the total population size $f_N(t, \hat{\theta})$ (bottom row). The left column corresponds to $\mu$ , the middle column to $q$ , and the right column to $c$ . Solid lines: Replicate 1. Dashed lines: Replicate 2. . . . .	61
Figure 3.13	Longitudinal data for the total population size for two population replicates. The vertical dashed line is at 19 days, and shows the division between the early phase and late phase dynamics. . . . .	62
Figure 3.14	The average of the relative sensitivities during the early and late phases for juvenile, $J(t)$ , adult, $A(t)$ , and total population, $N(t)$ , counts with respect to the survival parameter, $\mu$ , the effect of density on fecundity, $q$ , and the effect of density on survival, $c$ . Sensitivities are divided between the early phase of the population experiments (before the peak size is reached on day 19) and the late phase (after day 19). . . . .	62
Figure 3.15	These are the asymptotic confidence ellipsoids for the parameters in model D. In each figure, the solid black line corresponds to the 90% confidence ellipsoid, the dash-dot red line corresponds to the 95% confidence ellipsoid, and the solid blue line corresponds to the 99% confidence ellipsoid. The top row of figures correspond to Replicate 1, while the bottom row correspond to Replicate 2. . . . .	63
Figure 4.1	This is the pseudo measurement error based on second-order differencing of the data shown in Figure 4.2 using Equation (3.4). . . . .	69
Figure 4.2	Left: The proportion of surviving daphnids from three groups: no exposure (No treatment), exposure to ethanol (Carrier), or exposure to pyriproxyfen and ethanol (Pyriproxyfen + Carrier). Right: The proportion of surviving daphnids from the no exposure group (No treatment) and the combined set of daphnids from all three groups (Combined). . . . .	71

Figure 4.3	Results from fitting different functional forms for the mortality rate in the PDE and Leslie models. . . . .	72
Figure 4.4	Left: Daphnid survival data. Right: The estimated age-varying mortality function $\tilde{\mu}(t)$ for the Sinko-Streifer model using linear splines. Both plots are shown with dashed vertical lines representing the division between three possible subpopulations. . . . .	73
Figure 5.1	For each experimental group these show the average fecundity per daphnid per day. The vertical dashed line in each graph depicts the time when Phase 2 began for that beaker. So, for example, for Group 2 Phase 2 began on day 18, and so that is the vertical dashed line in that plot, and all data to the left of that vertical dashed line is Phase 1. Notice that each graph is plot on a different scale. . . . .	81
Figure 5.2	Here we have the fecundity data for each beaker in Group 1, as well as the fit using our model from Equation (5.1). The fecundity data is depicted by red stars, and gives the actual number of offspring recorded for each beaker. The model fit, using the optimal parameter values for that beaker, is depicted by a solid black line. We see that the model always, and at times grossly, underestimates the actual number of offspring. . . . .	85
Figure 5.3	Here we have the fecundity data for each beaker in Group 2, as well as the fit using our model from Equation (5.1). The fecundity data is depicted by red stars, and gives the actual number of offspring recorded for each beaker. Note that during Phase 2 the density of the beakers in Group 2 increase from 1 daphnid per beaker to 10 daphnids per beaker. The model fit, using the optimal parameter values for that beaker, is depicted by a solid black line. We see that the model always, and at times grossly, underestimates the actual number of offspring. . . . .	86
Figure 5.4	Here we have the fecundity data for each beaker in Group 3, as well as the fit using our model from Equation (5.1). The fecundity data is depicted by red stars, and gives the actual number of offspring recorded for each beaker. The model fit, using the optimal parameter values for that beaker, is depicted by a solid black line. We see that the model always, and at times grossly, underestimates the actual number of offspring. . . . .	87
Figure 5.5	Here we have the fecundity data for each beaker in Group 4, as well as the fit using our model from Equation (5.1). The fecundity data is depicted by red stars, and gives the actual number of offspring recorded for each beaker. Note that during Phase 2 the density of the beakers in Group 4 decrease from 10 daphnids per beaker to 1 daphnid per beaker. The model fit, using the optimal parameter values for that beaker, is depicted by a solid black line. We see that the model always, and at times grossly, underestimates the actual number of offspring. . . . .	88

Figure A.1	This is the data for the number of offspring created by each daphnid. The longitudinal data for each individual daphnid is represented by a line of a single color (for example, the yellow line represents the same daphnid). A clear functional form is not apparent, although the data does appear to be somewhat periodic. . . . .	108
Figure A.2	Here we see a box and whisker plot of the data in Figure A.1. This plot shows the changing and wide variability in the data. Each box and whisker corresponds to the offspring created by each daphnid on a given day. . . . .	109
Figure A.3	This is the data for the number of offspring per brood. The longitudinal data for each individual daphnid is represented by a line of a single color (for example, the yellow line represents the same daphnid). . . . .	110
Figure A.4	The proportion of surviving daphnids from the five groups. . . . .	117
Figure A.5	The number of neonates produced per female daphnid per day for each group. Data was collected daily, and the lines connecting each daily data point are drawn to show general trends. . . . .	118
Figure A.6	Longitudinal population data for Replicates 3 and 4. In each plot the red stars correspond to the juvenile population, and the blue circles correspond to the adult population. Notice that each graph is plot on a different scale. . . . .	120
Figure A.7	Longitudinal population data for Replicates 1 - 4 plotted on separate graphs with the same axes. In each plot the red stars correspond to the juvenile population, and the blue circles correspond to the adult population. Each graph is plot using the same axes for comparison purposes. . . . .	121
Figure A.8	The major axis length for daphnids in Control, Vehicle, and Treatment settings. The longitudinal data for each individual daphnid is represented by dots of a single color (for example, the yellow dots represents the same daphnid). The Control data is identical to the data in Figure 3.2, and is here merely for comparison purposes. . . . .	125
Figure A.9	(left) The number of neonates produced per Vehicle female daphnid per day. Daily data are represented by star symbols and connecting lines are drawn to show general trends. (right) The number of neonates produced per Control female daphnid per day. Daily data are represented by star symbols and connecting lines are drawn to show general trends. This is a copy of Figure 3.3 provided for comparison purposes. Notice that each graph is plot on a different scale. . . . .	126
Figure A.10	The number of neonates produced per Treatment female daphnid per day. Daily data are represented by star symbols and connecting lines are drawn to show general trends. Notice that each graph is plot on a different scale. . . . .	126
Figure A.11	Longitudinal population data for Vehicle females in Replicates 3 and 4. In each plot the red stars correspond to the juvenile population, and the blue circles correspond to the adult population. Notice that each graph is plot on a different scale. . . . .	127

Figure A.12	Longitudinal population data for Treatment females in Replicates 1, 2, 3, and 4. In each plot the red stars correspond to the juvenile population, and the blue circles correspond to the adult population. Notice that each graph is plot on a different scale. . . . .	128
Figure A.13	Longitudinal population data for Treatment males in Replicates 1, 2, 3, and 4. In each plot the red stars correspond to the juvenile population, and the blue circles correspond to the adult population. Notice that each graph is plot on a different scale. . . . .	129
Figure A.14	Longitudinal population data for males in Groups $T_C$ and $T_T$ . In each plot the red stars correspond to the juvenile population, and the blue circles correspond to the adult population. Notice that each graph is plot on a different scale. . . . .	133
Figure A.15	Longitudinal population data for females in Groups $T_C$ and $T_T$ . In each plot the red stars correspond to the juvenile population, and the blue circles correspond to the adult population. Notice that each graph is plot on a different scale. . . . .	134
Figure A.16	Longitudinal population data for Groups $C_C$ and $C_T$ . In each plot the red stars correspond to the juvenile population, and the blue circles correspond to the adult population. Notice that each graph is plot on a different scale. . . . .	135
Figure C.1	Left: Results for naive time points and naive inputs (SE-optimal design criteria). Middle: Results for optimized time points and naive inputs. Right: Results for naive time points and optimized inputs. Protein 1a level = $x(t)$ . RNA3 level = $y(t) + z(t)$ . Observation time points are labeled as 'x'. Experiment times when the input is 'on' are labeled on the x-axis with '*'. . . . .	149
Figure C.2	Results of iterative algorithm for SE (left), D (middle), and E (right) optimal design. Protein 1a level = $x(t)$ . RNA3 level = $y(t) + z(t)$ . Observation time points are labeled as 'x'. Experiment times when the input is 'on' are labeled on the x-axis with '*'. . . . .	150
Figure C.3	Convergence of the iterative algorithm for the sum of normalized standard errors (NSE), the change in time points $\Delta\tau$ (euclidean norm), and the change in inputs $\Delta b$ (euclidean norm). The axis for NSE is on a $\log_{10}(y)$ scale, the $\Delta\tau$ and $\Delta b$ are on a $\log_{10}(y + 1)$ scale. Optimal design criteria: SE = 'x', D = 'circles', E = 'squares'. . . . .	151



# Introduction

Biological investigations have increasingly come to rely on mathematical modeling in order to answer several fundamental questions. These models can be used to predict population and disease levels (e.g., [52, 108]), quantify the degree of an effect seen in a species (such as a mutation or physical growth, e.g., [76, 134]), determine suitable levels of treatment for diseased individuals (e.g., [1, 16]) as well as other applications. The most functional models are based on data, since creating models without data leads to a lack of verification of whether the model actually corresponds to the underlying phenomenon it is trying to explain.

This has led to techniques to try and answer key questions about this modeling process itself. Parameter estimation techniques were developed, and continue to be developed, to find appropriate parameter values for a model using experimental data in order to avoid this lack of verification. Model selection techniques have been created to determine which of a number of suitable models best describes the underlying phenomenon. Sensitivity analysis has been developed to quantify the sensitivity of a model's output to the model's input and parameters, where in biological applications the output typically corresponds to biological outcomes such as fecundity or organismal longevity, and the input and parameters typically correspond to different factors such as environmental predation. Uncertainty quantification has been developed to determine the accuracy of not only our parameter estimates, but of the model itself.

In this dissertation we explore the application of mathematical modeling to different biological problems, and we highlight how modeling and uncertainty quantification can expound upon our knowledge of the underlying biological processes. While the techniques we show in this dissertation are not uniquely applicable to biology (indeed, they can, and have, been used in physics, finance, and other disciplines), we explore their use in multiple biological regimes. We also explore certain

uncertainty quantification techniques themselves, and when they are useful or misleading. We are fortunate enough that the scientific community has found our work relevant and worthy of publication, and we note in this introduction which chapters of this dissertation have been published in slightly altered forms.

Chapter 2, which has been submitted in an alternate form to the International Journal of Pure and Applied Mathematics as [5], looks at different forms of uncertainty quantification. Uncertainty quantification has become an increasingly important field as mathematical modeling has become more ubiquitous in scientific investigations. Some uncertainty quantification techniques give us a way to see the confidence we have not only in our parameter estimates, but also to get a gauge in how our random variable parameter estimators depend on each other. In this project, we considered different ways of visualizing the distribution of these parameter estimators in order to see if there is correlation in our estimators. We do this by taking multiple model parametrizations of three mathematical models (the logistic growth model, the Richards curve, and a damped spring-mass system model) and simulating them with fixed parameters. We then take the model's output at fixed time points and perturb that output by noise to simulate real data. Subsequently, we create random variable parameter estimators, and using that simulated noisy data estimate the original model parameters. Next, we look at the approximate distribution of those estimators using the covariance matrix, correlation coefficients, asymptotic confidence ellipsoids, exact confidence regions [141], and the DRAM algorithm [82, 83], and compare these methods on their efficacy. The concepts elucidated in this chapter, as well as other forms of uncertainty quantification, are used throughout the rest of the dissertation.

The most substantial project throughout this dissertation involves a model organism often used in ecotoxicological studies known as *Daphnia magna*. *Daphnia sp.* is a water flea recommended by the EPA as a model organism in investigations on the effects of different chemicals. As a result, daphnid data makes up 8 percent of all of the experimental data for aquatic animals within toxicological databases [62]. They exhibit several complex behaviors, yet are relatively easy to study (so easy that they have been suggested for use in classrooms to introduce small children to science [69]), and thus are ideal for looking at the effects of toxicants on primary consumers, as well as the transgenerational effects of such toxicants. While *Daphnia sp.* exhibit several complex behaviors, potentially the most interesting is cyclic parthenogenesis.

Cyclic parthenogenesis is the process by which the population begins with asexual females. These females then continue to produce females until they receive certain environmental signaling that informs of environmental change, either from food scarcity [158], overcrowding [86, 127], change in photoperiod [74, 86, 97, 103], temperature changes [90, 102, 150], or a combination thereof [97, 127, 151]. This signaling causes some females to switch to sexual reproduction, while others

produce males. The sexual reproduction of males and females then creates diapause eggs, which can survive in the environment for decades either buried in sediment or carried by birds, storms, and streams. When the environmental signal goes away the diapause eggs hatch into asexual females, and the cycle begins again [48].

Several studies have been conducted on the individual level as to the effects of toxicants on daphnids [79, 105, 106, 125–127, 153, 156, 157], and others have been performed on the effects of toxicants on the population-level dynamics [71, 127, 128, 134]. There has also been work to try and model the growth of daphnids, either unperturbed or when subjected to toxicants, both on the population and individual levels (e.g. [67, 68, 71, 73, 75, 76, 128, 133, 134]). Our work with daphnids is built on the work of the past and is focused on creating a comprehensive multi-scale model for unperturbed daphnid population growth.

There are several important mechanisms that affect populations of daphnids. Not only are there random effects on the individual level (e.g., the number of offspring produced per brood by adult female daphnids is highly variable) but there are also effects that occur at the population level (e.g., daphnids that are in crowded conditions produce less offspring). The modeling efforts of the past have in some cases overlooked important effects, or have not given the same level of experimental, mathematical, and statistical scrutiny that we have. For example, [67, 68, 73] try to model daphnids without the use of data, [75, 76, 133] use a less controlled laboratory setup that cannot be correctly characterized as lab or field data and they do not rigorously check their assumptions in modeling due to the lack of computing power at the time to employ more comprehensive statistics, [134] offers no uncertainty quantification, and [71] doesn't consider crowding, which is known to greatly affect daphnid populations [86, 127, 134].

In order to verify the past results, and to build upon them, we developed a wet lab to run experiments on *Daphnia magna*. We designed experiments, ran those experiments, collected data, and analyzed that data. We developed a discrete time-varying delayed Leslie matrix model for the population growth of daphnids, where the parameters in that model came from extensive modeling on the individual growth of daphnids. For example, the physical size of individual daphnids is a parameter in our population-level model, and so we created a model based on individual-level data from our lab for the size of daphnids, and inserted that individual-based model into the population-level model. This approach allowed us to create a truly multi-scale model which builds upon and extends the models seen in the literature. We quantified the uncertainty that we have in our experimental measurements and parameter estimates to ascertain the accuracy of our model in predicting the size of a population of daphnids. Chapter 3, which appears in an altered form in the August, 2015 edition of Mathematical Biosciences as [3], explores in detail these first round of experiments, the modeling, and initial uncertainty quantification.

Chapter 4, which appears in an altered form in Applied Mathematics Letters in June, 2015 as [4], considers what appears to be our most glaringly incorrect assumption from Chapter 3, and in that chapter we comprehensively explore the validity of the assumption of constant mortality, as well as the use of a discrete-time model. Chapter 5 rounds out our discussion of the *Daphnia magna* modeling by considering a continuous-time model, discovering more important effects in daphnid population growth, and building a case for further work that needs to be completed.

Through our work with *Daphnia magna* we show throughout this dissertation the importance for an iterative approach to modeling that involves initial assumptions based on current and prior knowledge, experiments to test those assumptions and initial models, and then a revisiting of those assumptions. This is a method that is greatly aided by uncertainty quantification, and which is necessary not only for *Daphnia magna*, but also for personalized medicine, as seen in the last project of this dissertation.

This dissertation will thus explore multiple topics in biology, as well as mathematics, and highlights how the marriage of biology, mathematics, and statistics can lead to novel insights about the underlying biological system and lead to tangibly helpful outcomes.

# Methods to Determine Correlation of Parameter Estimates from Inverse Problems Given Different Model Parametrizations <sup>1</sup>

## 2.1 Introduction

In the scientific study of physical and biological systems, mathematical modeling provides a conceptual framework for the quantitative investigation of the processes being considered. The development of this conceptual framework is an iterative process in which an abstracted and mathematized representation of the system is used to make predictions which are then tested experimentally; these tests provide greater insight into the operation of the system and its mathematical representation [31]. The link between a mathematical model and experimental data is described by a statistical model that encodes any uncertainty as a result of model misspecification, measurement error, etc. This leads to the problem of uncertainty quantification [39, 145] to assess the extent to which model

---

<sup>1</sup>Published in altered form as [5]

Contributions:

Literature review and preliminary analysis: Robert Baraldi, John Nardini, and W. Clayton Thompson

Computations, simulations, and writeup: Kaska Adoteye

DRAM algorithm implementation: Kevin Flores

Analysis of results: Kaska Adoteye, H.T. Banks, Robert Baraldi, Kevin Flores, W. Clayton Thompson

Advisor: H.T. Banks

based conclusions are robust to modeling and data errors.

In this chapter, we consider one component of uncertainty quantification: the computation of confidence regions for parameters estimated from noisy data. When multiple model parameters are estimated, it is almost always the case that the estimation of all parameters must be computed simultaneously (e.g., by minimizing the sum of squared errors between the model and the data). As an estimator is formally a random variable [31, 141], uncertainty quantification can be viewed as the study of the properties of the joint distribution of these random variables. Ideally, for any two parameters of the mathematical model, their corresponding estimators will be independent (their joint distribution can be factored) so that uncertainty in the estimation of one parameter will have no effect on the uncertainty in the estimation of the other parameter. In practice, however, this is rarely the case. While various techniques and algorithms exist to identify a subset of parameters that can be estimated with the greatest degree of certainty [54, 55], an alternative problem of interest and utility is how the structure of the model itself has an impact on the joint distribution of the estimators.

In particular, we examine two aspects of this problem. First, we consider how alternative model parameterizations (transformations of the parameter space such that the model solution is unchanged) have an impact on the precision with which the parameters can be estimated. Second, we consider how alternative computational approaches for parameter estimation and/or the construction of confidence regions can improve understanding of the estimator properties. To address these issues, we consider three simple example systems: a logistic growth model, a generalized logistic growth (Richards' curve) model and a damped spring-mass model. In each case, it is shown that the model can be represented by at least two different but ultimately equivalent parameterizations, (e.g., the logistic equation can be equivalently written as  $\dot{P} = rP(1 - P/K)$  or  $\dot{P} = AP - BP^2$  with  $A = r$  and  $B = r/K$ ). For each model, synthetic data is generated by adding pseudo-random measurement error at fixed measurement times. These data are then used to estimate the model parameters, which are compared to the true values used to create the data. For comparison, we consider both frequentist (nonlinear least squares) and Bayesian (delayed rejection adaptive Metropolis - DRAM) methods for parameter estimation. The asymptotic properties of nonlinear least squares estimators are well-characterized [23, 78, 141] and approximate confidence regions are constructed using either an estimate of the covariance matrix or by level sets of the least squares cost function. Confidence regions for the DRAM algorithm are visualized by direct sampling from the estimated posterior distribution.

Even though only scalar examples (with simple forward-solve solutions) are used, these simulation studies provide some interesting insight into the interaction between the parameterization of a mathematical model, the statistical properties of estimators, and the approximation and visualiza-

tion of confidence regions.

We begin in Section 2.2 with a brief outline of the mathematical and statistical framework and associated methodology we employ. This is followed in Section 2.3 by the formulation of the mathematical models we use in our investigations. Finally a summary of our findings is followed by brief concluding remarks.

## 2.2 Methodology

### 2.2.1 Statistical Analysis and Inverse Problem Methods

In order to estimate parameters using asymptotic theory, we will consider a vector mathematical model of the form

$$\frac{dz}{dt} = g(t, z(t), q) \quad (2.1)$$

$$z(t_0) = z_0 \quad (2.2)$$

with observation process

$$f(t, \theta) = \mathcal{C} z(t, \theta)$$

where  $\theta = (q^T, \tilde{z}_0^T)^T$  is our vector of unknown parameters,  $q$  is a vector of our model parameters,  $\tilde{z}_0$  is the portion of our initial condition that is unknown (if any), and  $\mathcal{C}$  maps our model solution  $z(t, \theta)$  in  $\mathbb{R}^m$  to our observed states  $f(t, \theta)$ . In this investigation, our initial condition will always be completely known, and thus  $\theta = q$ . Also, in this investigation our observation operator always produces a scalar, and thus  $\mathcal{C}$  maps  $\mathbb{R}^m$  to  $\mathbb{R}$ .

As experimental data is typically available at discrete times, we will assume that our observations occur at  $n$  discrete times  $t_j$ , and thus our observations will be

$$f(t_j, \theta) = \mathcal{C} z(t_j, \theta), \quad j = 1, \dots, n.$$

It is important to note that very rarely do our experimental observations  $y_j$  match our model observations  $f(t_j, \theta)$ , and thus we need a statistical model to address this discrepancy.

We will thus use the statistical model

$$Y_j = f(t_j, \theta_0) + \mathcal{E}_j, \quad j = 1, \dots, n \quad (2.3)$$

for our observations, where  $\mathcal{E}_j$  is a random variable that represents the random noise that causes our observed data to deviate from our model solution, and  $\theta_0$  is the hypothesized “true” parameter

vector that generates the observations  $\{Y_j\}_{j=1}^n$  (the existence of this parameter vector is a standard assumption in frequentist statistical formulations). We will also assume  $\mathbb{E}(\mathcal{E}_j) = 0$  for each  $j$ , which comes from our implicit assumption that our model in Equations (2.1)-(2.2) correctly describes the underlying phenomenon. In most situations it is possible to assume that  $\mathcal{E}_j, j = 1, \dots, n$  are independent and identically distributed, which is an assumption we will make here as well. In this study, since we are generating the error in a manner described in Section 2.3.4, we will assume  $\mathcal{E}_j, j = 1, \dots, n$  are normally distributed with variance  $\sigma_0^2$ . This tells us that  $Y_j \sim \mathcal{N}(f(t_j, \theta_0), \sigma_0^2)$ .

Since  $\mathcal{E}_j$  is a random variable,  $Y_j$  is a random variable with realizations (i.e., data)  $y_j$ , which for this investigation will be simulated in a manner described in Section 2.3.4. Our goal is to then estimate  $\theta_0$  (which will be known to us throughout this investigation) by creating a random variable estimator  $\Theta$  whose realizations for a given data set  $y_j$  will be estimates  $\hat{\theta}$  of  $\theta_0$ . Our estimates  $\hat{\theta}$  will approximate our “true” parameters  $\theta_0$ , and can be obtained by minimizing the ordinary least squares (OLS) cost functional

$$J(\theta) = \sum_{j=1}^n [y_j - f(t_j, \theta)]^2, \quad (2.4)$$

and thus, with  $\Omega$  being the space of admissible parameters,

$$\theta_0 \approx \hat{\theta} = \arg \min_{\theta \in \Omega} J(\theta).$$

This process of estimating parameters from data is known as an inverse problem, and we will compute all inverse problems in this chapter using *fminsearch* in Matlab.

Once we have our estimate  $\hat{\theta}$ , we wish to ascertain the statistical properties of our estimator  $\Theta$ . Although we do not know the distribution of our estimator  $\Theta$ , we can approximate it under asymptotic theory (as  $n \rightarrow \infty$ ) by the multivariate Gaussian distribution [31, 39, 141]

$$\Theta \sim \mathcal{N}(\theta_0, \Sigma_0^n)$$

where, based on our previous assumptions, our covariance matrix  $\Sigma_0^n$  can be represented as

$$\Sigma_0^n = \sigma_0^2 [\chi^{nT}(\theta_0) \chi^n(\theta_0)]^{-1} \quad (2.5)$$

where

$$\hat{\sigma}^2 = \frac{1}{n-p} \sum_{j=1}^n [y_j - f(t_j, \hat{\theta})]^2 = \frac{J(\hat{\theta})}{n-p}$$

is an unbiased estimate for  $\sigma_0^2$  with  $p$  being the number of parameters being estimated, and  $\chi^n$  is



the sensitivity matrix

$$\chi_{jk}^n(\theta) = \frac{\partial f(t_j, \theta)}{\partial \theta_k}, \quad j = 1, \dots, n, \quad k = 1, \dots, p, \quad (2.6)$$

where  $\theta_k$  is the  $k^{th}$  element of  $\theta$ . The sensitivity matrix can be computed using several different methods including differencing techniques or exact sensitivity equations [31, 39]. Here we use the complex step method which is detailed in Section 2.2.4. For more information on how to treat other cases using asymptotic theory (for example, when there are unknown initial conditions, or there are a vector of observations) consult [31, 39].

In this chapter we will look at ways to visualize and understand the estimated distribution  $\mathcal{N}(\hat{\theta}, \hat{\Sigma}^n)$ . The first such method we will employ is to explore the covariance matrix  $\Sigma_0^n$  of our estimator. Here we will use the estimate

$$\Sigma_0^n \approx \hat{\Sigma}^n = \hat{\sigma}^2 [\chi^{nT}(\hat{\theta}) \chi^n(\hat{\theta})]^{-1}.$$

We will look for correlation in the estimators by inspecting the covariances  $\hat{\Sigma}_{ij}^n, i \neq j$ , since we know that two random variables are independent if their covariance is zero. We will also compute the correlation coefficients

$$\rho_{ij} = \frac{\hat{\Sigma}_{ij}^n}{\sqrt{\hat{\Sigma}_{ii}^n} \sqrt{\hat{\Sigma}_{jj}^n}},$$

where  $\rho_{ij} \in [-1, 1]$  is larger in absolute value the more the estimator components are correlated. In order to determine the confidence we have in our parameter estimates, we also compute the standard error  $SE(\hat{\theta}_k) = \sqrt{\hat{\Sigma}_{kk}^n}$  for the  $k^{th}$  parameter, where we are more confident in our parameter estimate the smaller the standard error is.

## 2.2.2 Confidence “Ellipsoids” or Regions

### 2.2.2.1 Asymptotic Ellipsoids

In order to further understand the distribution of our estimator  $\Theta$ , we will construct ellipsoids based on the covariance matrix. Here we define the quantity

$$Q = (\Theta - \theta_0)^T (\Sigma_0^n)^{-1} (\Theta - \theta_0).$$

and note that, if  $\Sigma_0^n$  is positive definite, then  $Q \sim \chi_p^2$ , a Chi-square distribution with  $p$  degrees of freedom [142, Thm. 2.9]. Recall that, given our statistical assumptions, our covariance matrix  $\Sigma_0^n$  for

our estimator  $\Theta$  can be expressed as in Equation (2.5). Therefore, here we have

$$Q = (\Theta - \theta_0)^T \chi^T \chi (\Theta - \theta_0) / \sigma^2 \sim \chi_p^2.$$

Also, since  $J(\Theta)/(n-p)$  is an unbiased estimator for  $\sigma^2$ , we have  $J(\Theta)/\sigma^2 \sim \chi_{n-p}^2$ , a Chi-square distribution with  $n-p$  degrees of freedom [78].

Letting  $s^2 = J(\Theta)/(n-p)$ , we can define the quantity

$$F(\Theta) = \frac{(\Theta - \theta_0)^T \chi^T \chi (\Theta - \theta_0)}{p s^2}$$

and see that

$$\begin{aligned} F(\Theta) &= \frac{(\Theta - \theta_0)^T \chi^T \chi (\Theta - \theta_0)}{p s^2} \\ &= \frac{(\Theta - \theta_0)^T \chi^T \chi (\Theta - \theta_0) / p}{J(\Theta) / (n-p)} \\ &= \left( \frac{(\Theta - \theta_0)^T \chi^T \chi (\Theta - \theta_0)}{J(\Theta)} \right) \left( \frac{n-p}{p} \right) \\ &= \left( \frac{(\Theta - \theta_0)^T \chi^T \chi (\Theta - \theta_0)}{J(\Theta)} \right) \left( \frac{n-p}{p} \right) \left( \frac{\sigma^2}{\sigma^2} \right) \\ &= \frac{[(\Theta - \theta_0)^T \chi^T \chi (\Theta - \theta_0) / \sigma^2] / p}{[J(\Theta) / \sigma^2] / (n-p)}. \end{aligned}$$

In both the numerator and denominator we have a Chi-squared distribution scaled by its number of degrees of freedom, which is by definition the F-distribution [78]. Thus,

$$F(\Theta) = \frac{(\Theta - \theta_0)^T \chi^T \chi (\Theta - \theta_0)}{p s^2} = \frac{(\Theta - \theta_0)^T (\Sigma_0^n)^{-1} (\Theta - \theta_0)}{p} \sim F_{p, n-p}.$$

It follows that an approximate  $100(1-\alpha)\%$  confidence region is [23, 78]

$$\left\{ \theta : (\theta - \hat{\theta})^T (\hat{\Sigma}^n)^{-1} (\theta - \hat{\theta}) \leq p F_{p, n-p}^\alpha \right\} \quad (2.7)$$

where  $F_{p, n-p}^\alpha$  is the upper- $\alpha$  critical value of the  $F_{p, n-p}$  distribution. This is the asymptotic confidence ellipsoid for the OLS estimate  $\hat{\theta}$ , where we see that this confidence region is completely determined by the covariance matrix  $\hat{\Sigma}^n$  and the confidence level  $\alpha$ , and thus this provides another method of visualizing and understanding the distribution for our estimator  $\Theta$ . In this work we plotted the level curves of the ellipsoid from Equation (2.7) using the command *contour* in Matlab for  $\alpha = 0.01, 0.05$ ,

and 0.1 for the 99,95, and 90% confidence ellipsoids, respectively.

An important note is that we began this section with the assumption that our covariance matrix  $\Sigma_0^n$  is positive definite. It is known that in general a covariance matrix is positive semi-definite, and thus it is positive definite if it is also full rank. Here we are numerically estimating the covariance matrix, and thus we also need the matrix to have a reasonable condition number in order to allow for numerical inversion of the matrix. In this presentation, since we work with basic systems with a low number of parameters, this was not an issue, but in general this matrix may be nearly singular (i.e., ill-conditioned).

### 2.2.2.2 Exact Confidence Regions or “Exact Ellipsoids”

The asymptotic ellipsoids in the previous section are based on the covariance matrix, which by definition considers linear relationships. In order to get a more general representation of the distribution of our estimator  $\Theta$ , we turn to the exact confidence regions or “exact ellipsoids” detailed in [141]. Summarizing [141], we will base these “ellipsoids” on the cost functional in Equation (2.4), and thus it will take the form of the exact confidence region

$$\{\theta : J(\theta) \leq c J(\hat{\theta})\} \quad (2.8)$$

where  $c > 1$ . Now we must find a suitable value for  $c$ . According to [141], we have

$$J(\theta) - J(\hat{\theta}) \approx (\theta - \hat{\theta})^T \chi^T \chi (\theta - \hat{\theta}).$$

Therefore, since

$$(\theta - \hat{\theta})^T \chi^T \chi (\theta - \hat{\theta}) \leq p s^2 F_{p,n-p}^\alpha$$

as shown in the previous section, we can then establish, by substituting  $s^2 = J(\hat{\theta})/(n-p)$ ,

$$J(\theta) - J(\hat{\theta}) \leq J(\hat{\theta}) \frac{p}{n-p} F_{p,n-p}^\alpha.$$

Rearranging this, we get the “exact” confidence region

$$\left\{ \theta : J(\theta) \leq J(\hat{\theta}) \left( 1 + \frac{p}{n-p} F_{p,n-p}^\alpha \right) \right\} \quad (2.9)$$

which is the region described in Equation (2.8) with  $c = 1 + \frac{p}{n-p} F_{p,n-p}^\alpha$ . This will have the required asymptotic confidence level of  $100(1 - \alpha)\%$ , but avoids the linearization seen in the asymptotic ellipsoids.

Since Equation (2.9) requires the computation of the cost functional  $J(\theta)$  at several points, it will be more difficult to compute and display than the asymptotic ellipsoid. With that said, it is likely to provide a more accurate estimation of the real confidence ellipsoid, and thus of the distribution of  $\Theta$  with  $100(1 - \alpha)\%$  confidence. In order to compute the “exact ellipsoids” we created a mesh of values for the parameters. The created mesh was  $100 \times 100$ , which constitutes 10,000 different values for  $\theta$  that were considered. For each value of  $\theta$ , we tested if it satisfied the equality part of the inequality in Equation (2.9) for  $\alpha = 0.01, 0.05$ , and  $0.1$ , and if so, plotted that value. This process is easily parallelizable, but for the purpose of comparing computation time we will run this process in serial.

### 2.2.3 DRAM (Bayesian Analysis)

The above analysis tools assume that there is a true parameter value  $\theta_0$ , while in a Bayesian framework we assume that the parameters are random variables with associated densities. In order to compute these densities, we begin with an initial density  $\pi_0(\theta)$  for the parameters, known as a prior density. We then use data realizations  $y$  in order to create a posterior density  $\pi(\theta|y)$  through the use of a likelihood function  $\pi(y|\theta)$ . In solving the inverse problem under this framework, we use Bayes’ theorem for inverse problems [92] given in Definition 1.

**Definition 1.** (*Bayes’ theorem for inverse problems*) We assume that the parameter vector  $\theta$  is a random variable which has a known prior density  $\pi_0(\theta)$  (possibly non-informative), and corresponding realizations  $y$  of the random variable  $Y$  associated with the measurement process. The posterior density of  $\theta$ , given measurements  $y$ , is then

$$\pi(\theta|y) = \frac{\pi(y|\theta)\pi_0(\theta)}{\pi(y)} = \frac{\pi(y|\theta)\pi_0(\theta)}{\int_{\mathbb{R}^p} \pi(y|\theta)\pi_0(\theta)d\theta} \quad (2.10)$$

where we have assumed that the marginal density  $\pi(y) = \int_{\mathbb{R}^p} \pi(\theta, y)d\theta = \int_{\mathbb{R}^p} \pi(y|\theta)\pi_0(\theta)d\theta \neq 0$  (a normalizing factor) is the integral over all possible joint densities  $\pi(\theta, y)$ . Note here that  $\pi(y|\theta)$  is a likelihood function which describes how likely a data set  $y$  is when given a model solution at the parameter value  $\theta$ .

There have been many techniques developed that can attempt to compute the integral in Definition 1. For a small number of parameters, cubature or Monte Carlo techniques can be used. When the number of parameters increase, a popular method is to construct a Markov chain whose stationary distribution is the posterior density  $\pi(\theta|y)$  of Equation (2.10). With this method we sample the parameter space, accepting the parameters based on closeness of the model solution at the

parameters to the data. It is known that a Markov chain defined by the random walk Metropolis algorithm will converge if the algorithm is allowed to sample the parameter space a large number of times [146]. Here we will use the delayed rejection adaptive Metropolis (DRAM) algorithm, which is described in detail in [7, 82, 83, 146], although there are other algorithms that could have been used. Our implementation of the algorithm is from using the DRAM options of the MCMC toolbox for Matlab, available from Marko Laine at <http://helios.fmi.fi/~lainema/mcmc/>. Our simulations assumed a non-informative prior given by a uniform distribution over a space that served as large bounds on our parameters. We simulated  $M=50,000$  chain iterations to assure mixing. We also assumed the measurement errors are normally distributed, which we can do since we created the error from a normal distribution in a manner described in Section 2.3.4, so that the likelihood function becomes the multivariate normal density.

One benefit to this approach is that the DRAM algorithm samples directly from the posterior distribution, and we can look at these samples graphically through Monte Carlo plots to infer any correlation between parameter distributions. One downside to using DRAM is the long computational times, which have been explored in comparison to the asymptotic approach in [96], and which we will explore in this study as well. It is important to note that while there has been a successful parallel implementation of DRAM [147], here we will use a serial implementation in order to better compare computation times.

#### 2.2.4 Complex-Step Method of Sensitivity Calculations

We briefly describe the complex-step derivative (see [33, 111] for more details) used to calculate an approximation for the sensitivity of a model with respect to model parameters, which is given in Equation (2.6). Essentially, the complex-step derivative is a finite-difference approximation calculated in the complex plane. Recall the forward-difference formula, wherein a common estimate for the first derivative is

$$f'(x) = \frac{f(x+h) - f(x)}{h} + o(h), \quad (2.11)$$

where  $h$  is the finite-difference interval and  $o(h)$  is the truncation error for the first-order approximation. Consider a function  $f = u + iv$  of the complex variable  $z = x + iy$ . Paraphrasing [111], if  $f$  is analytic in the complex plane then the Cauchy-Riemann equations apply and are

$$\frac{\partial u}{\partial x} = \frac{\partial v}{\partial y} \quad (2.12)$$

$$\frac{\partial u}{\partial y} = -\frac{\partial v}{\partial x}. \quad (2.13)$$

Equations (2.12) and (2.13) give the relationship between the real and imaginary parts of the function. We can use the definition of a derivative in the right hand side of the first Cauchy-Riemann Equation (2.12) to write

$$\frac{\partial u}{\partial x} = \lim_{h \rightarrow 0} \frac{v(x + i(y + h)) - v(x + iy)}{h}, \quad (2.14)$$

where  $h$  is a real number. Since the model equations we consider in this manuscript (the models are specified in Section 2.3) are real functions of real variables,  $y = 0$ ,  $u(x) = f(x)$ , and  $v(x) = 0$ . Equation (2.14) can be rewritten as

$$\frac{\partial f}{\partial x} = \lim_{h \rightarrow 0} \frac{\text{Im}[f(x + ih)]}{h} \quad (2.15)$$

and approximated by

$$\frac{\partial f}{\partial x} \approx \frac{\text{Im}[f(x + ih)]}{h}. \quad (2.16)$$

The value of  $h$  is taken to be very small, e.g.,  $h = 10^{-25}$ . This is the *complex-step derivative approximation*, and is not subject to subtractive cancellation errors since there is no difference operation [111]. Of course, in this manuscript we are taking derivatives with respect to the parameters  $\theta_k$ , and thus we have

$$\chi_{j,k}^n(\theta) = \frac{\partial f(t_j, \theta)}{\partial \theta_k} \approx \frac{\text{Im}[f(t_j, \theta_k + ih)]}{h}. \quad (2.17)$$

## 2.3 Mathematical Models

Here we consider three models (the logistic growth model, the Richards curve, and a damped spring-mass system model) and equivalent parametrizations of each model. We wish to explore what effect the different parametrizations have on the distributions for the estimators  $\Theta$ , and how those effects (if any) show up using the methods described above (asymptotic and “exact” ellipsoids, covariance matrices, and DRAM Monte Carlo plots).

### 2.3.1 Logistic

The first model we consider is the widely used logistic model for a bounded, dynamically changing population  $P(t)$ , given by the differential equation

$$\frac{dP}{dt} = rP(t) \left(1 - \frac{P(t)}{K}\right) \quad (2.18)$$

where  $r$  is the intrinsic growth rate, and  $K$  is the carrying capacity for the population under consideration. We call this the  $(r, K)$  parametrization for the logistic curve. Alternatively, we may modify Equation (2.18) to obtain the  $(A, B)$  parametrization for the logistic curve:

$$\frac{dP}{dt} = AP(t) - BP(t)^2. \quad (2.19)$$

Note that if we set  $A = r$  and  $B = \frac{r}{K}$  we see that the models are equivalent. Similarly, we can modify Equation (2.18) to obtain the equivalent  $(C, D)$  parametrization for the logistic curve:

$$\frac{dP}{dt} = CP(t)(D - P(t)), \quad (2.20)$$

which contains the parameters  $C = \frac{r}{K}$  and  $D = K$ . Throughout this presentation we will examine the system using the parameter set  $(r, K) = (50, 10)$  and initial condition  $P(0) = 1$ . Table 2.1 contains plots of the logistic equation with these parameter values.

### 2.3.2 Richards

The second model that we consider is the Richards Curve, which also describes the growth of a bounded, dynamically changing population, here denoted by  $f(t)$ . Letting  $\kappa$  be a birth rate term,  $\alpha$  be the carrying capacity, and  $\delta$  a free parameter, the  $(\kappa, \delta)$  parametrization of the Richards curve is given by

$$\frac{df}{dt} = \frac{\kappa}{1-\delta} f \left[ \left( \frac{f}{\alpha} \right)^{\delta-1} - 1 \right], \quad \delta \neq 1. \quad (2.21)$$

We note that for  $\delta = 2$  this equation is exactly the logistic equation, and that the Richards curve is also a generalization of other population models, such as the Gompertz equation. We also note that  $\kappa = \eta(1-\delta)\alpha^{\delta-1}$  where  $\eta$  is a growth parameter.

Now, if we let  $A = \frac{\kappa}{1-\delta}$  and  $B = \delta$ , then we can rewrite Equation (2.21) as

$$\frac{df}{dt} = Af \left[ \left( \frac{f}{\alpha} \right)^{B-1} - 1 \right], \quad B \neq 1. \quad (2.22)$$

We call this the  $(A, B)$  parametrization for the Richards curve.

Throughout this work, we let  $f(0) = 1$ , fix  $\alpha = 8$ , and only try to estimate  $(\kappa, \delta)$  for Equation (2.21) or  $(A, B)$  for Equation (2.22). We will examine the system using the parameter set  $(\kappa, \delta) = (2, 2)$ , and thus the true dynamics are equivalent to the logistic equation, but now instead of trying to estimate

the carrying capacity we're trying to estimate the inflection of the growth. Table 2.1 contains plots of the Richards curve with these parameter values.

### 2.3.3 Spring Equation

The third model we consider is the spring-mass-dashpot system with mass  $m$ , damping coefficient  $c$ , and spring constant  $k$ . If  $C = c/m$  and  $K = k/m$ , then the oscillating spring (in a standard engineering and mathematical formulation) may be modeled as

$$\begin{aligned}\frac{d^2 x(t)}{dt^2} + C \frac{dx(t)}{dt} + K x(t) &= 0, \\ x(t_0) &= x_0, \quad \dot{x}(t_0) = v_0,\end{aligned}\tag{2.23}$$

which we will call the  $(C, K)$  parametrization for the spring equation. In this project, we take  $x(t_0) = 1$  and  $\dot{x}(t_0) = 0$ , with  $t_0 = 0$ .

Because Equation (2.23) is a homogeneous second order differential equation, we can solve it analytically. This analytic solution will have the form

$$x(t) = e^{-\frac{C}{2}t} (A \cos(\omega t) + B \sin(\omega t)),\tag{2.24}$$

which can be further modified [118] to

$$x(t) = e^{-\frac{C}{2}t} (R \sin(\omega t + \delta)),\tag{2.25}$$

where  $\delta$  (or A and B) can be determined from the initial conditions.

By solving the characteristic polynomial of Equation (2.23), we find that

$$\omega = \frac{\sqrt{4K - C^2}}{2},\tag{2.26}$$

or that, equivalently,

$$K = \omega^2 + \frac{C^2}{4}.\tag{2.27}$$



And thus we can reformulate Equation (2.23) to

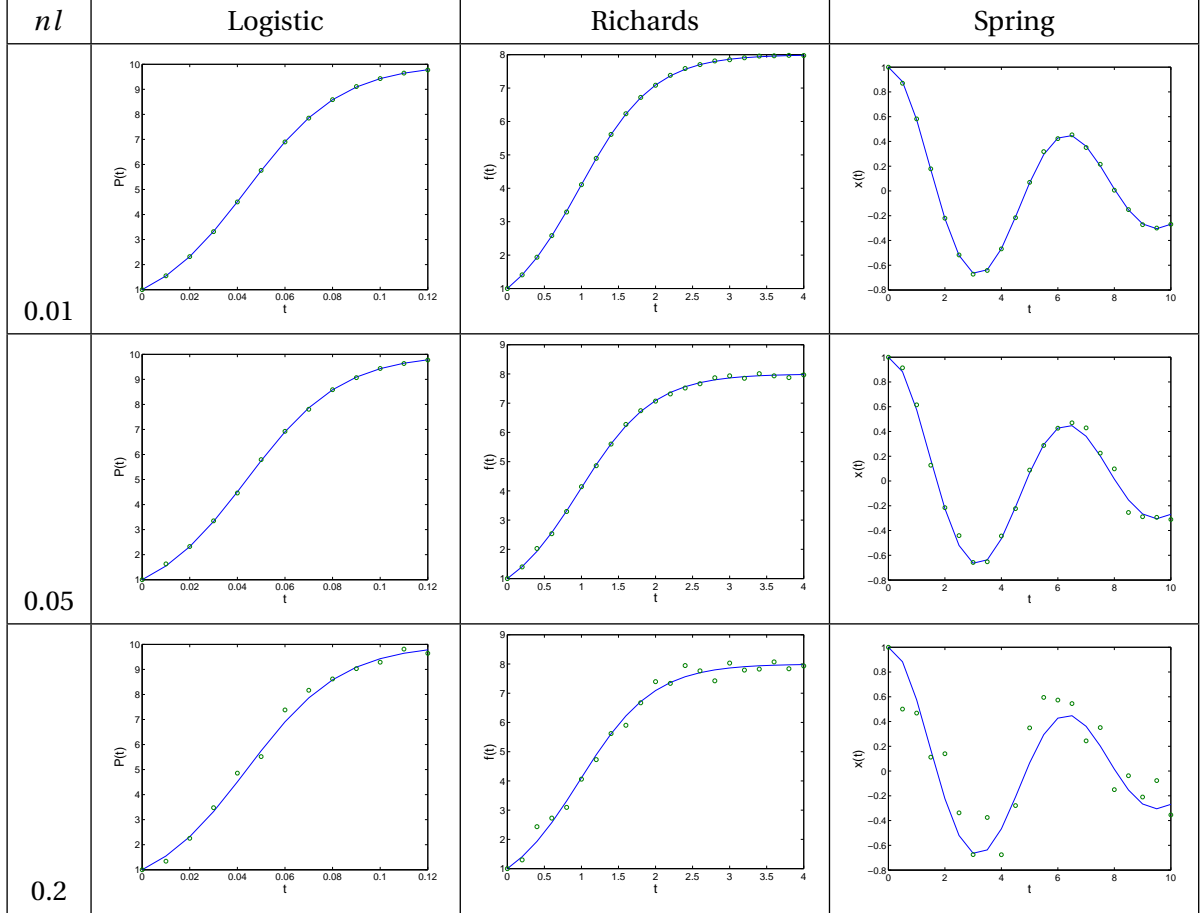
$$\frac{d^2 x(t)}{dt^2} + C \frac{dx(t)}{dt} + \left( \omega^2 + \frac{C^2}{4} \right) x(t) = 0, \quad (2.28)$$

which we will call the  $(C, \omega)$  parametrization for the spring equation. Throughout this presentation, we will examine this system using the parameter set  $(C, K) = (1/4, 1)$ . Table 2.1 contains plots of the spring equation with these parameter values.

### 2.3.4 Adding Noise

For each model above, we simulated the model with the parameter values given and took the model value at evenly spaced times as data points (13 data points for the logistic curve, 21 for the Richards and spring). Looking back at our statistical model in Equation (2.3), these points would translate to  $f(t_j, \theta_0)$ . In order to obtain our “observed” data points  $y_j$ , we then took the points  $f(t_j, \theta_0)$  and perturbed them by realizations of the noise  $\mathcal{E}_j$  from a normal distribution with mean 0 and variance  $\sigma_0^2 = nl^2$  where  $nl = 0.01, 0.05$ , and  $0.2$ . The initial condition was not perturbed by noise, and thus  $y_0 = f(0, \theta_0)$ . Table 2.1 shows the forward solve  $f(t_j, \theta_0)$  for each of the models expressed in Section 2.3, as well as the data points  $y_j$  collected given the various noise levels.

**Table 2.1** These show the forward solves  $f(t_j, \theta_0)$  of the models using the parameters specified in Section 2.3, along with data  $y_j$  collected at evenly spaced time points  $t_j$ , and perturbed by noise  $\mathcal{E}_j$  from a normal distribution with standard deviation  $nl$ . The forward solve is plotted as a solid line, while the data (with noise added) are plotted as open circles. Each column corresponds to a different model, while each row corresponds to a different noise level.



## 2.4 Results

### 2.4.1 Covariance Results

Table 2.2 contains the covariance matrices for each of the models considered for each noise level. In this section we will dissect these matrices to see what information we can glean from them, and what we cannot immediately ascertain. Remembering our parameter values used to generate the data (for the logistic curve  $r = 50, K = 10$ , for the Richards curve  $\kappa = \delta = 2$ , and for the spring

equation  $C = 1/4, K = 1$ ), we see that the variances of the estimators are small relative to the actual parameter values, which suggests that we were able to estimate our parameters in good confidence. To be more precise, Table 2.3 shows the parameter estimates for each model and the corresponding standard errors  $SE(\hat{\theta}_k)$ , which we see are very small compared to our parameter estimates. This tells us that we have high confidence in the estimates of our parameters.

**Table 2.2** These are the covariance matrices for each parametrization for each model, and for each noise level. The first parameter corresponds to the first diagonal, and the second parameter to the second. So, for example, the logistic ( $r, K$ ) covariance matrix has the variance in the  $r$  estimate as the top left entry, and the variance in the  $K$  estimate in the bottom right entry.

	Logistic ( $r, K$ )	Logistic ( $A, B$ )	Logistic ( $C, D$ )
nl = 0.01	$\begin{bmatrix} 0.0023 & -0.0002 \\ -0.0002 & 0.4230 \cdot 10^{-4} \end{bmatrix}$	$\begin{bmatrix} 0.0023 & 0.0003 \\ 0.0003 & 0.0001 \end{bmatrix}$	$\begin{bmatrix} 0.5606 & -0.4351 \\ -0.4351 & 0.4230 \end{bmatrix} \cdot 10^{-4}$
nl = 0.05	$\begin{bmatrix} 0.0362 & -0.0035 \\ -0.0035 & 0.0007 \end{bmatrix}$	$\begin{bmatrix} 0.0362 & 0.0054 \\ 0.0054 & 0.0009 \end{bmatrix}$	$\begin{bmatrix} 0.8769 & -0.6752 \\ -0.6752 & 0.6522 \end{bmatrix} \cdot 10^{-3}$
nl = 0.2	$\begin{bmatrix} 1.1892 & -0.1004 \\ -0.1004 & 0.0176 \end{bmatrix}$	$\begin{bmatrix} 1.1892 & 0.1736 \\ 0.1736 & 0.0279 \end{bmatrix}$	$\begin{bmatrix} 0.0279 & -0.0195 \\ -0.0195 & 0.0176 \end{bmatrix}$
	Richards ( $\kappa, \delta$ )	Richards ( $A, B$ )	
nl = 0.01	$\begin{bmatrix} 0.0859 & 0.0979 \\ 0.0979 & 0.1161 \end{bmatrix} \cdot 10^{-3}$	$\begin{bmatrix} 0.1490 & 0.1301 \\ 0.1301 & 0.1161 \end{bmatrix} \cdot 10^{-3}$	
nl = 0.05	$\begin{bmatrix} 0.0020 & 0.0023 \\ 0.0023 & 0.0027 \end{bmatrix}$	$\begin{bmatrix} 0.0041 & 0.0033 \\ 0.0033 & 0.0027 \end{bmatrix}$	
nl = 0.2	$\begin{bmatrix} 0.0389 & 0.0443 \\ 0.0443 & 0.0525 \end{bmatrix}$	$\begin{bmatrix} 0.0565 & 0.0538 \\ 0.0538 & 0.0525 \end{bmatrix}$	
	Spring ( $C, K$ )	Spring ( $C, \omega$ )	
nl = 0.01	$\begin{bmatrix} 0.4700 & 0.1623 \\ 0.1623 & 0.5401 \end{bmatrix} \cdot 10^{-5}$	$\begin{bmatrix} 0.4700 & 0.0524 \\ 0.0524 & 0.1287 \end{bmatrix} \cdot 10^{-5}$	
nl = 0.05	$\begin{bmatrix} 0.1039 & 0.0358 \\ 0.0358 & 0.1187 \end{bmatrix} \cdot 10^{-3}$	$\begin{bmatrix} 0.1039 & 0.0119 \\ 0.0119 & 0.0287 \end{bmatrix} \cdot 10^{-3}$	
nl = 0.2	$\begin{bmatrix} 0.0027 & 0.0009 \\ 0.0009 & 0.0032 \end{bmatrix}$	$\begin{bmatrix} 0.0027 & 0.0003 \\ 0.0003 & 0.0007 \end{bmatrix}$	

We now consider the off-diagonal elements of the covariance matrices in Table 2.2 for evidence

**Table 2.3** Here we show the parameter estimates  $\hat{\theta}_k$  and standard errors  $SE(\hat{\theta}_k)$  for each parameterization for each model at each noise level considered in this chapter. Each row corresponds to a different parameter. For example, the second to last row corresponds to the parameter  $c$  in the  $(c, \omega)$  parametrization for the spring equation, with the first two columns corresponding to the noise level  $nl = 0.01$ , the next two columns corresponding to the noise level  $nl = 0.05$ , and the last two columns corresponding to the noise level  $nl = 0.2$ .

	nl=0.01		nl=0.05		nl=0.2	
Logistic	Estimate	SE	Estimate	SE	Estimate	SE
$r$	49.9802	0.0481	50.0581	0.1902	51.9379	1.0905
$K$	10.0026	0.0065	9.9830	0.0255	9.8877	0.1327
$A$	49.9802	0.0481	50.0581	0.1902	51.9379	1.0905
$B$	4.9967	0.0075	5.0144	0.0296	5.2528	0.1671
$C$	4.9967	0.0075	5.0144	0.0296	5.2528	0.1671
$D$	10.0026	0.0065	9.9830	0.0255	9.8877	0.1327
Richards	Estimate	SE	Estimate	SE	Estimate	SE
$\kappa$	2.0155	0.0093	1.9828	0.0447	2.0324	0.1972
$\delta$	2.0167	0.0108	1.9798	0.0524	2.0553	0.2291
$A$	-1.9823	0.0122	-2.0238	0.0643	-1.9258	0.2376
$B$	2.0167	0.0108	1.9798	0.0524	2.0553	0.2291
Spring	Estimate	SE	Estimate	SE	Estimate	SE
$c$	0.2482	0.0022	0.2365	0.0102	0.2582	0.0523
$K$	1.0005	0.0023	0.9889	0.0109	1.0162	0.0564
$c$	0.2482	0.0022	0.2365	0.0102	0.2582	0.0523
$\omega$	0.9925	0.0011	0.9874	0.0054	0.9998	0.0273

**Table 2.4** Here we show the correlation coefficients  $\rho_{ij}$  for each parametrization of each model at each noise level considered in this chapter. Each column corresponds to a different noise level, while each row corresponds to a different model parametrization.

	nl=0.01	nl=0.05	nl=0.2
Logistic $(r, K)$	-0.7152	-0.7143	-0.6939
Logistic $(A, B)$	0.9529	0.9529	0.9527
Logistic $(C, D)$	-0.8935	-0.8928	-0.8798
Richards $(\kappa, \delta)$	0.9803	0.9798	0.9808
Richards $(A, B)$	0.9891	0.9899	0.9882
Spring $(c, K)$	0.3222	0.3222	0.3182
Spring $(c, \omega)$	0.2131	0.2181	0.2047

of correlation in our estimators. We cannot immediately say that the estimators are independent, since none of the covariances are zero. We do have that some of the covariances are close to zero, but in no case are they significantly smaller than at least one of the variances, and thus it is difficult to immediately conclude that the covariances are “near” zero. Therefore, it is not immediately apparent from inspecting the covariances that the estimators are independent.

We next turn to the correlation coefficients given in Table 2.4, as these can give us an idea of the degree of correlation in the estimators, if any. For some of the model parametrizations it is clear that there is correlation in the estimators due to the magnitude of the correlation coefficient (close to  $\pm 1$ ). These are the  $(A, B)$  parametrizations for the logistic and Richards curves, as well as the  $(\kappa, \delta)$  parametrization for the Richards curve. There are also some parametrizations where it is clear that there is very little, if any, correlation in the estimators due to the magnitude of the correlation coefficient (close to 0). These are the two parametrizations for the spring equation. At the extremes correlation coefficients are easy to read, but in intermediate values it is more difficult. Therefore, for the  $(r, K)$  and  $(C, D)$  parametrizations for the logistic curve, it is difficult to tell if this is strong correlation in the estimators or not. Typically, accepted values of the correlation coefficient that determine significant correlation differ from discipline to discipline, and we will avoid a discussion on that here. Rather, we will look at our other methods for visualization to see if they can give any further indication of the degree of correlation (or lack thereof) in the estimators, or if they contradict what we’re seeing here.

## 2.4.2 Ellipsoidal and DRAM Results

As a means of comparison we show the results for the asymptotic ellipsoids, “exact ellipsoids”, and DRAM Monte Carlo simulations side by side in Tables 2.5 - 2.11. This is done for each model (each

parametrization of the logistic model, Richards curve, and spring model) and for each noise level ( $nl = 0.01, 0.05$ , and  $0.2$ ). In order to better compare results, the plots for each model have the same axes across noise levels. Thus, for example, the logistic equation using the parameters  $(r, K)$  for noise level  $nl = 0.01$  plots all have the same axes, but those axes will be different than what is seen for the noise level  $nl = 0.05$ , or for the  $(A, B)$  parametrization. The axes used are always  $\hat{\theta} \pm 4 \cdot \max SE(\hat{\theta}_k)$ , where the standard errors  $SE(\hat{\theta}_k)$  can be found in Table 2.3. As expected from the definitions, the sign of the slope of the major axis in the asymptotic ellipsoids is given by the sign of the correlation coefficients in Table 2.4.

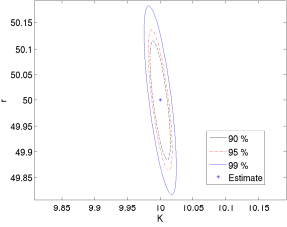
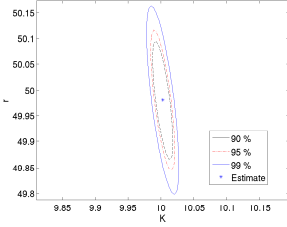
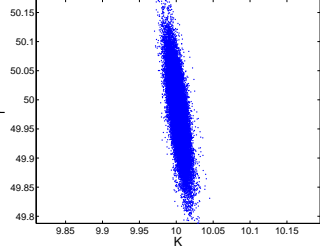
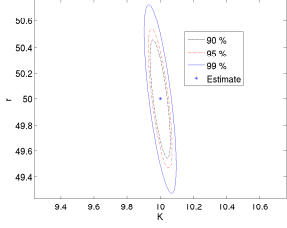
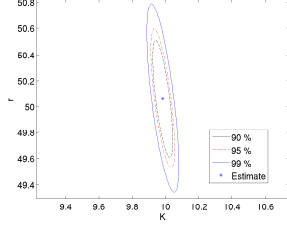
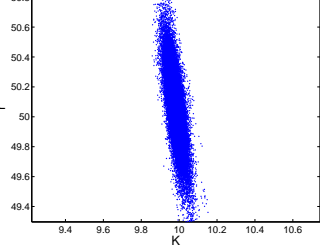
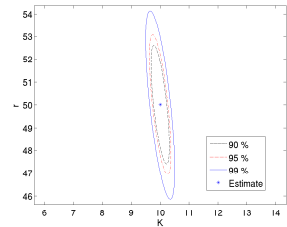
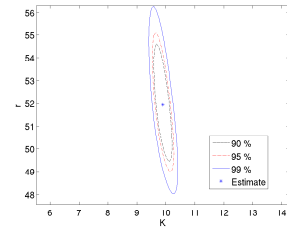
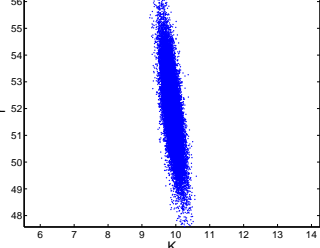
First we will compare what is seen in the asymptotic ellipsoids to what we concluded in the previous section from the covariance matrices, since these two should contain the same information. The asymptotic ellipsoids completely confirm what was seen with the covariance matrices and correlation coefficients for the Richards curve and the spring equation. That is, the asymptotic ellipsoids for the Richards curve are diagonal, which suggests correlation in the estimators, while the asymptotic ellipsoids for the spring curve are not, which suggests no or little correlation in the estimators. For the logistic curve  $(r, K)$  parametrization, we have that the asymptotic ellipsoid is vertical with an incredibly mild tilt, which would suggest little or no correlation in the estimators, while when looking at the correlation coefficients we weren't able to accurately determine whether there was strong correlation or not. For the logistic curve  $(C, D)$  parametrization, we see that the asymptotic ellipsoid is diagonal, which shows clear correlation in the estimators, which we weren't able to accurately ascertain by observing the correlation coefficients. The  $(A, B)$  parametrization of the logistic curve has a slight slope in the asymptotic ellipsoids, which suggests a slight correlation, while the correlation coefficients showed clear correlation. This confirms that the asymptotic ellipsoids provides a quick visualization of the information contained in the covariance matrices, but should be used in conjunction with the covariance matrices to obtain the most information.

While the asymptotic ellipsoids and covariance matrices give information on the linear relationship of the estimators, the "exact ellipsoids" and DRAM Monte Carlo plots visually show the non-linear relationship of the estimators, if any. In the results depicted here, a non-linear relationship only comes up in the  $(A, B)$  parametrization of the Richards curve, and it shows up very clearly in the "exact ellipsoids" and DRAM Monte Carlo plots as a banana shape. It can be very difficult to determine a priori if there will be a non-linear relationship in the estimators, but these methods are able to accurately show when there is.

In addition to the amount of information contained in each plot, it is also important to consider the computational time needed for each method. Therefore, Table 2.12 contains the computation times for each of the plots in Tables 2.5 - 2.11. While the "exact ellipsoids" and DRAM Monte Carlo plots give the most information, that information comes at a cost of a vastly increased computational

time when compared to the asymptotic ellipsoids. It is interesting that the “exact ellipsoids” take significantly less time to compute than the DRAM Monte Carlo plots, which suggests that we can obtain the same information in less time using a frequentist approach. The benefits and drawbacks of each method will be discussed further in the Discussion.

**Table 2.5** These show the results for the logistic curve with the  $(r, K)$  parametrization. The left column of plots are the asymptotic ellipsoids, the middle column of plots are the exact ellipsoids, and the right column of plots are the DRAM Monte Carlo plots. The top row of plots correspond to noise level  $nl = 0.01$ , the middle row to noise level  $nl = 0.05$ , and the bottom row to noise level  $nl = 0.2$ .

nl	Asymptotic	Exact	Dram
0.01			
0.05			
0.2			

**Table 2.6** These show the results for the logistic curve with the  $(A, B)$  parametrization. The left column of plots are the asymptotic ellipsoids, the middle column of plots are the exact ellipsoids, and the right column of plots are the DRAM Monte Carlo plots. The top row of plots correspond to noise level  $nl = 0.01$ , the middle row to noise level  $nl = 0.05$ , and the bottom row to noise level  $nl = 0.2$ .

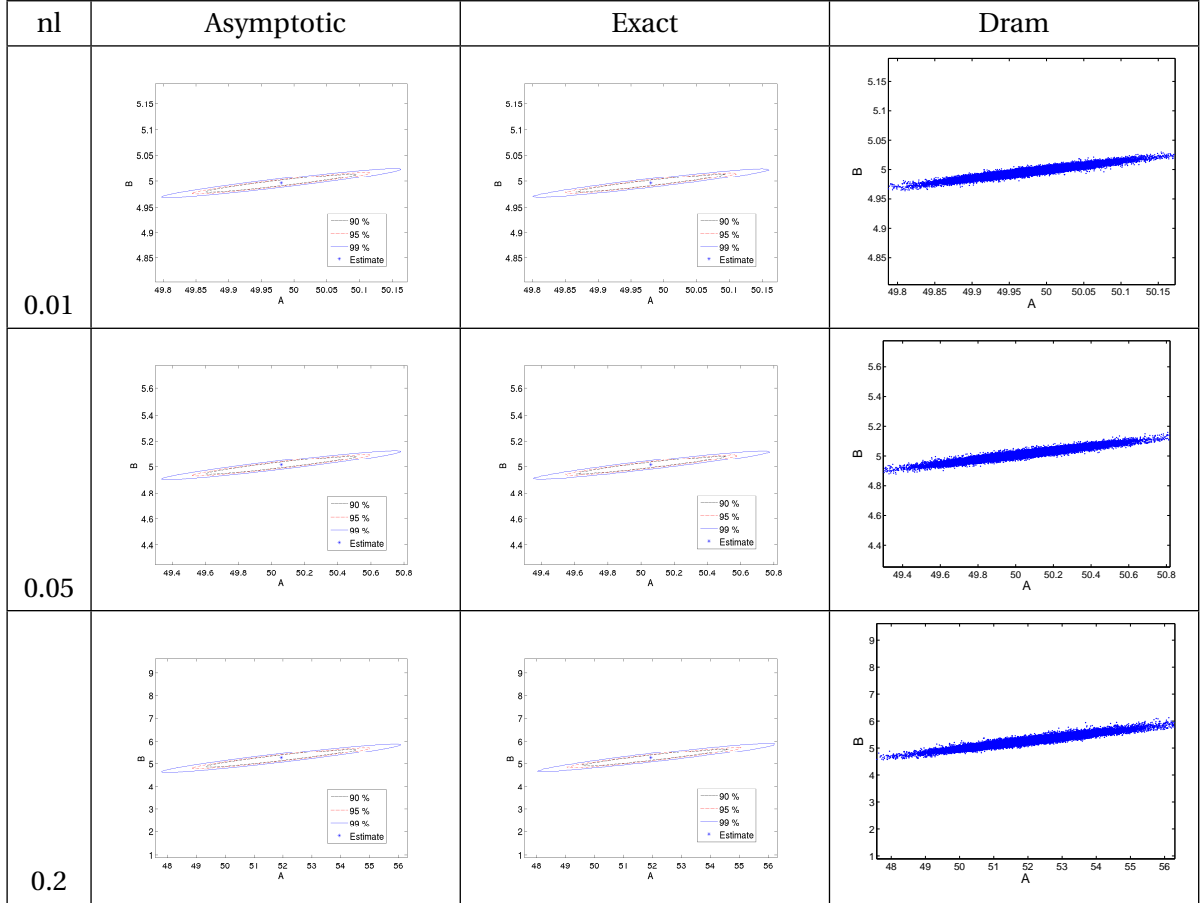




**Table 2.7** These show the results for the logistic curve with the  $(C, D)$  parametrization. The left column of plots are the asymptotic ellipsoids, the middle column of plots are the exact ellipsoids, and the right column of plots are the DRAM Monte Carlo plots. The top row of plots correspond to noise level  $nl = 0.01$ , the middle row to noise level  $nl = 0.05$ , and the bottom row to noise level  $nl = 0.2$ .

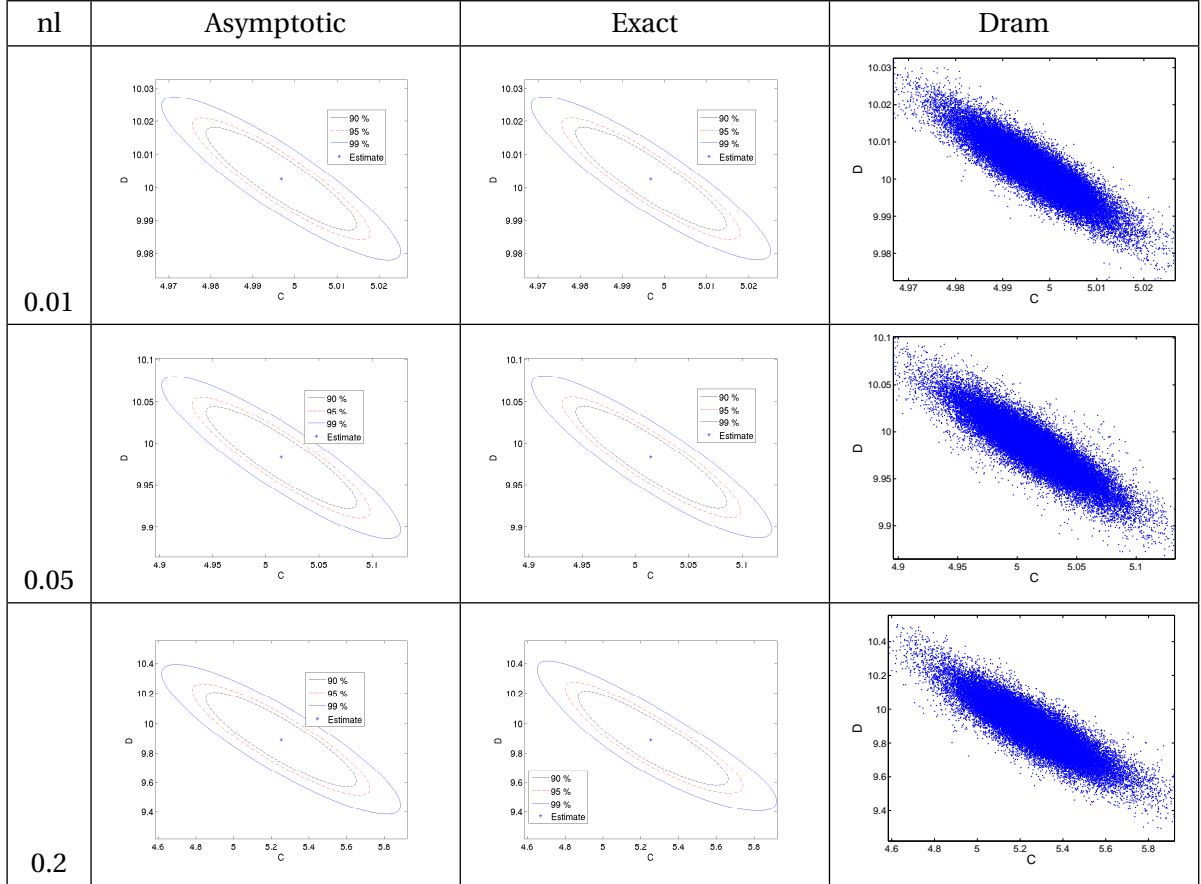


**Table 2.8** These show the results for the Richards curve with the  $(\kappa, \delta)$  parametrization. The left column of plots are the asymptotic ellipsoids, the middle column of plots are the exact ellipsoids, and the right column of plots are the DRAM Monte Carlo plots. The top row of plots correspond to noise level  $nl = 0.01$ , the middle row to noise level  $nl = 0.05$ , and the bottom row to noise level  $nl = 0.2$ .

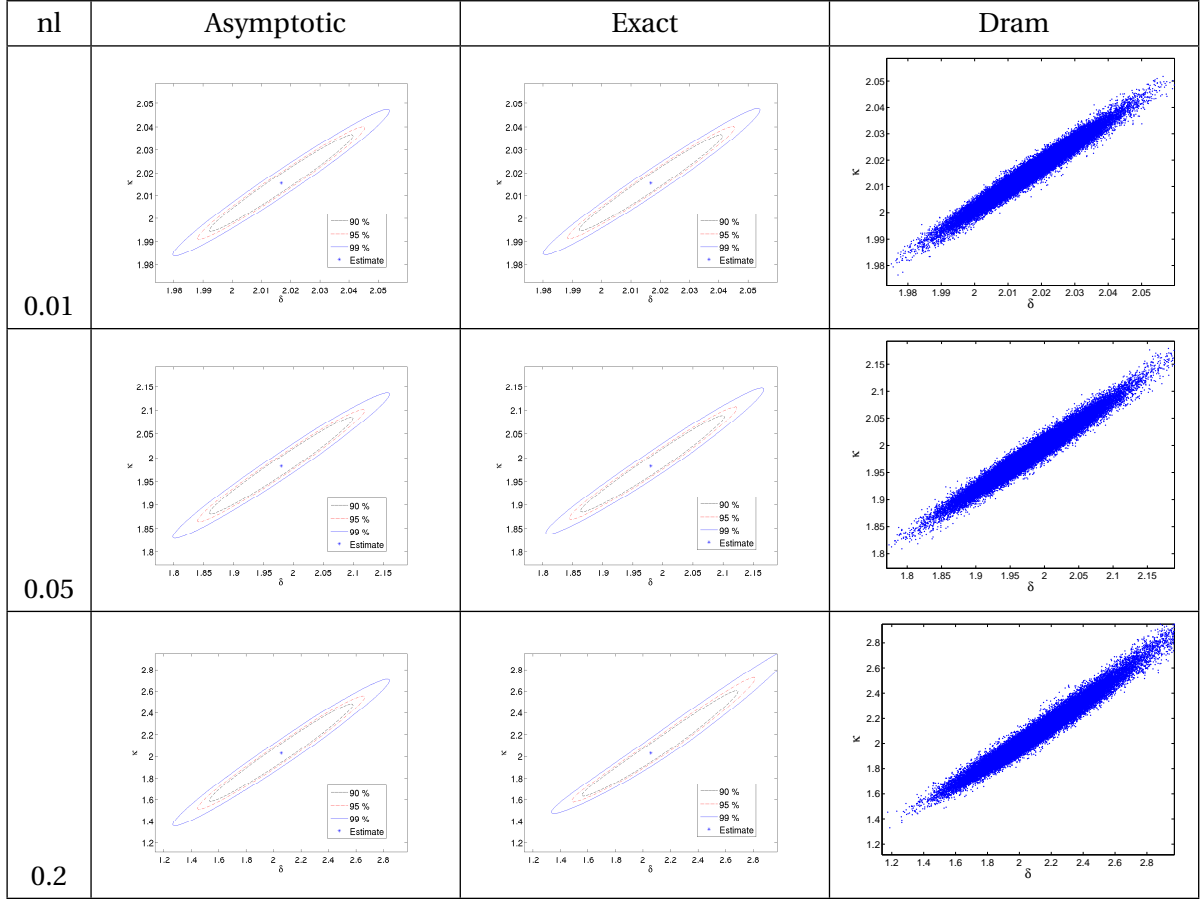


**Table 2.9** These show the results for the Richards curve with the  $(A, B)$  parametrization. The left column of plots are the asymptotic ellipsoids, the middle column of plots are the exact ellipsoids, and the right column of plots are the DRAM Monte Carlo plots. The top row of plots correspond to noise level  $nl = 0.01$ , the middle row to noise level  $nl = 0.05$ , and the bottom row to noise level  $nl = 0.2$ .

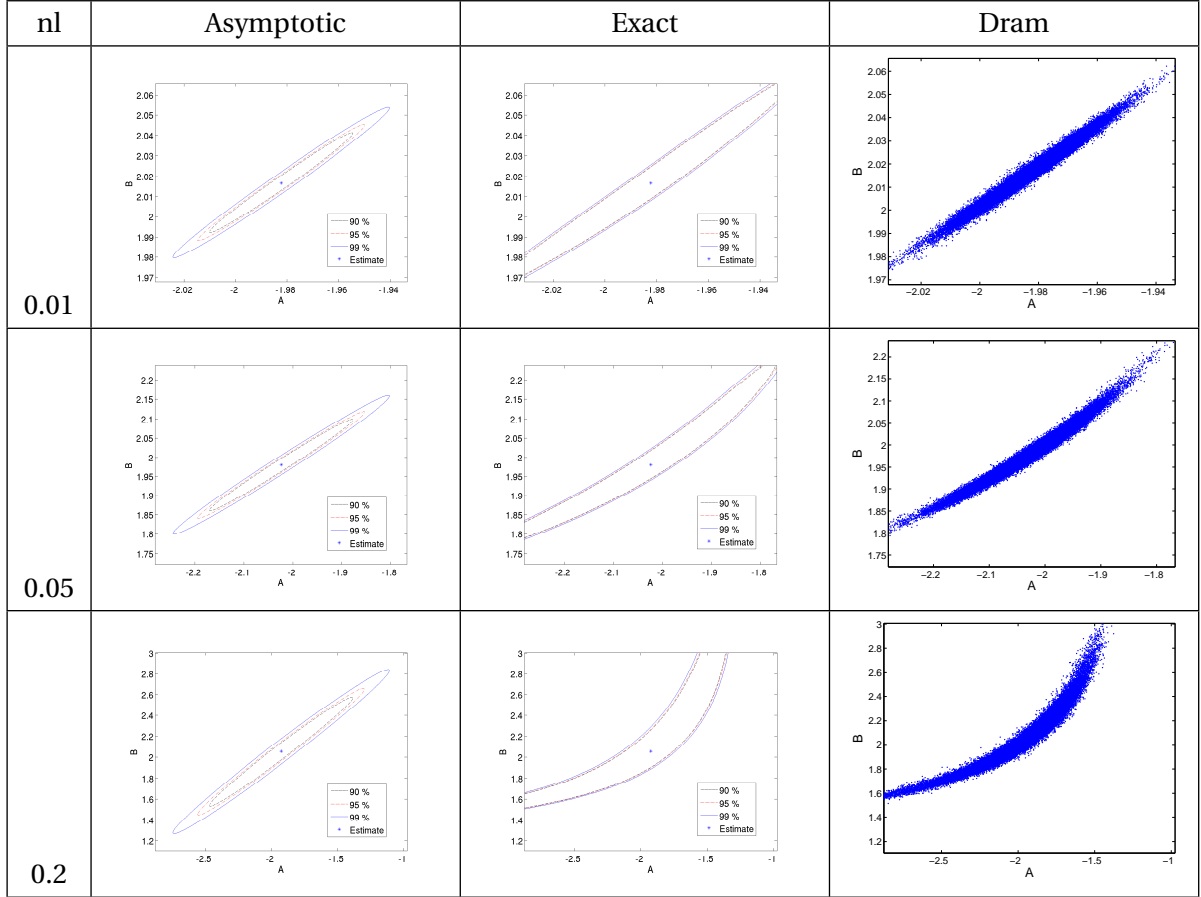


**Table 2.10** These show the results for the spring equation with the  $(C, K)$  parametrization. The left column of plots are the asymptotic ellipsoids, the middle column of plots are the exact ellipsoids, and the right column of plots are the DRAM Monte Carlo plots. The top row of plots correspond to noise level  $nl = 0.01$ , the middle row to noise level  $nl = 0.05$ , and the bottom row to noise level  $nl = 0.2$ .

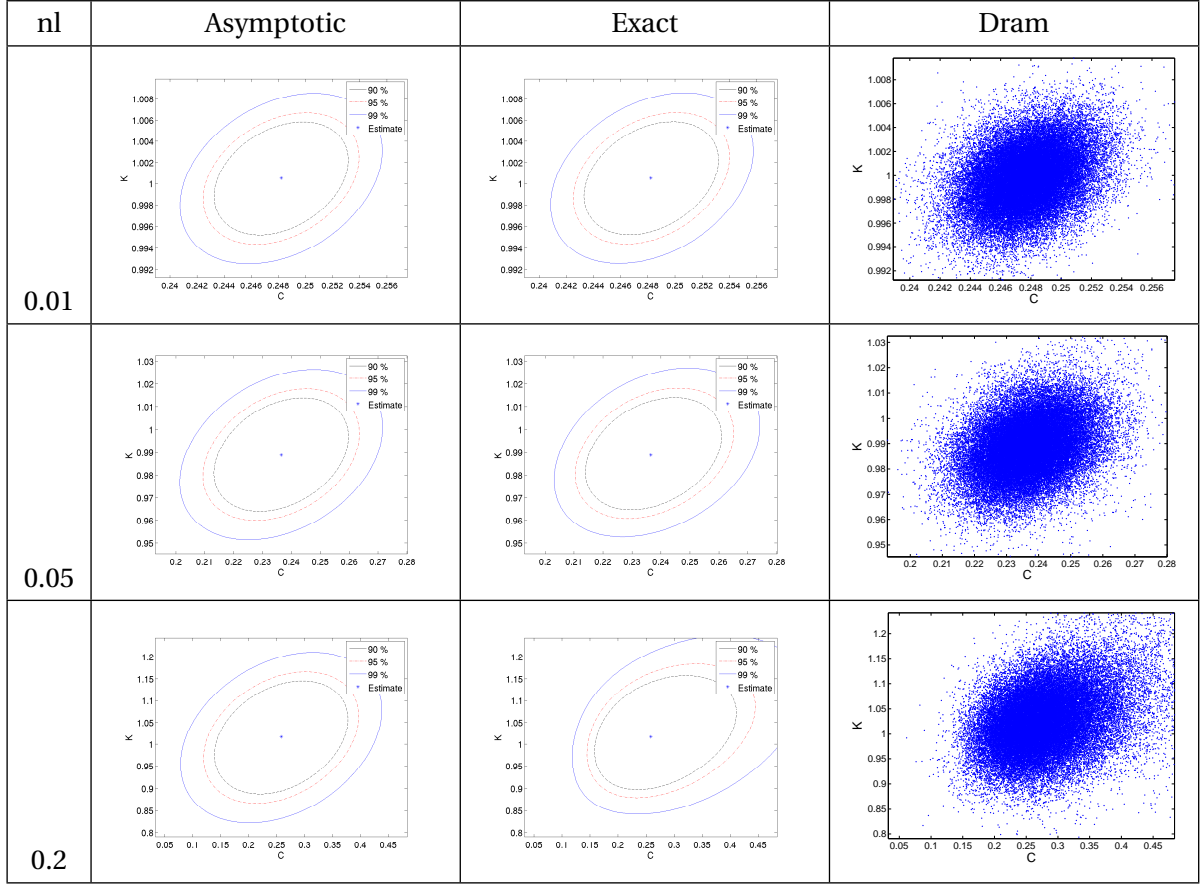


**Table 2.11** These show the results for the spring equation with the  $(C, \omega)$  parametrization. The left column of plots are the asymptotic ellipsoids, the middle column of plots are the exact ellipsoids, and the right column of plots are the DRAM Monte Carlo plots. The top row of plots correspond to noise level  $nl = 0.01$ , the middle row to noise level  $nl = 0.05$ , and the bottom row to noise level  $nl = 0.2$ .

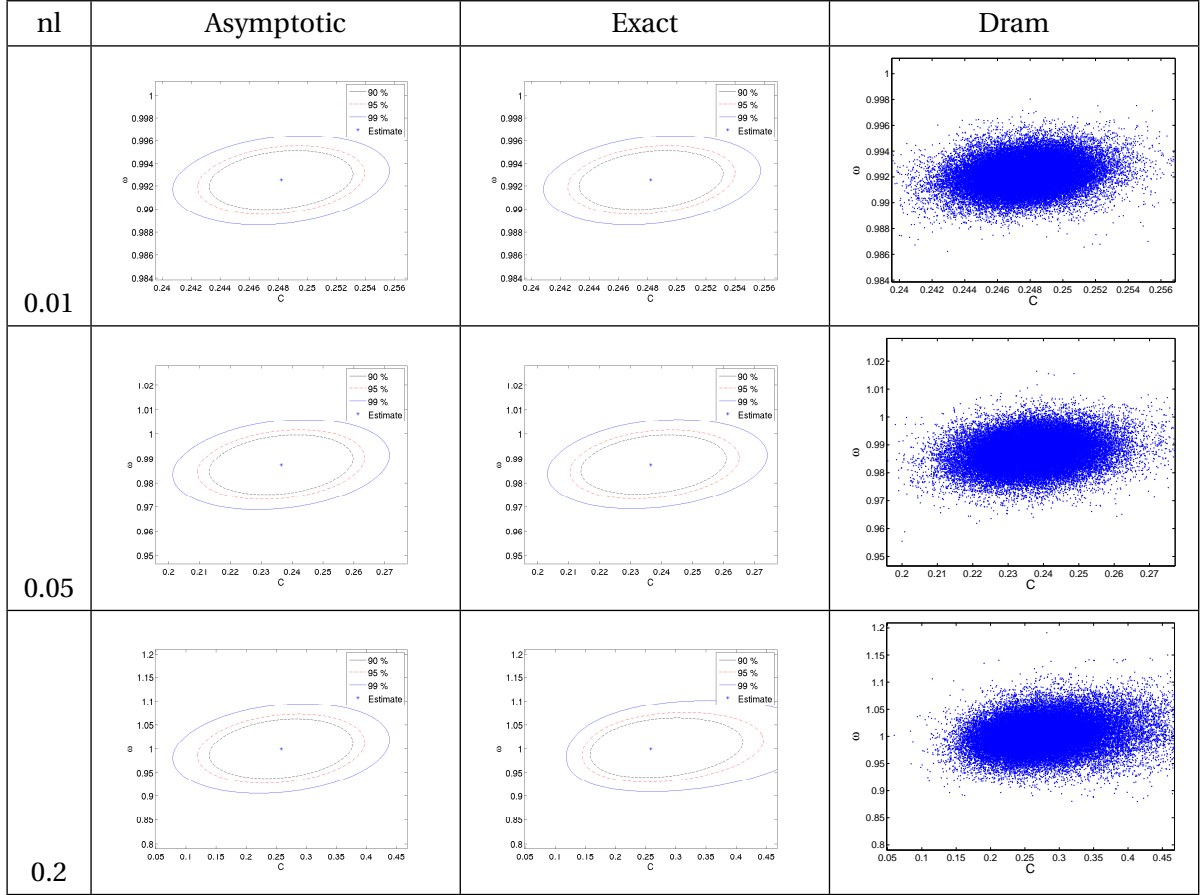


**Table 2.12** This table contains the actual time it took to compute each figure shown in Tables 2.5 - 2.11. Each of these computations were done in serial, and each time is reported in seconds.

	Logistic ( $r, K$ )		
nl	Asymptotic	Exact	DRAM
0.01	3.5629	171.2078	331.3867
0.05	3.5102	159.0493	334.7702
0.2	3.6724	164.0091	334.8415

	Logistic ( $A, B$ )			Logistic ( $C, D$ )		
nl	Asymptotic	Exact	DRAM	Asymptotic	Exact	DRAM
0.01	5.4782	165.1741	327.5574	3.7460	172.8193	333.8275
0.05	3.5826	175.6089	327.8342	3.5053	162.0211	333.5822
0.2	3.6405	170.0562	337.8583	3.6777	170.3691	334.5760
	Richards ( $\kappa, \delta$ )			Richards ( $A, B$ )		
nl	Asymptotic	Exact	DRAM	Asymptotic	Exact	DRAM
0.01	3.7512	163.7019	361.7089	5.7804	244.0324	362.8190
0.05	4.0799	157.7161	360.2998	5.5679	238.2260	370.9050
0.2	3.9228	151.6950	356.3535	6.3256	217.8059	381.949284
	Spring ( $C, K$ )			Spring ( $C, \omega$ )		
nl	Asymptotic	Exact	DRAM	Asymptotic	Exact	DRAM
0.01	7.9877	431.1604	460.5580	8.8229	399.6899	456.4983
0.05	8.3498	399.9744	453.9156	8.6606	430.9618	471.1952
0.2	8.3161	395.9492	466.4205	8.7435	400.0249	505.8148

## 2.5 Discussion and Concluding Remarks

The considerations presented here arose from the simple question of what, if anything, we can say about dependence/independence of parameter estimators arising in inverse problems using simple computational methods related to estimator covariances. Initial findings with several simple one dimensional systems help to clarify the issues involved.

From the asymptotic theory-based covariances alone (see Table 2.2) which employ the linearized sensitivities in their construction, little definitive information can be obtained. If one computes the corresponding correlation coefficients, then in the extreme cases of  $\rho$  near zero (suggesting independence) or near  $\pm 1$  (dependence) some useful information can be obtained about linear

dependence. If one uses this along with the asymptotic based ellipsoids, information content can be enhanced in the non-extreme cases. If one turns to the exact ellipsoids (which are not computed using the linearized sensitivities), one can see not only linear dependence but a nonlinear dependence can be detected if present.

When we compared these methods to the Bayesian DRAM algorithm, we obtain the above mentioned information in addition to other information on the prediction intervals, parameter distributions, etc. [82, 83]. The downside is this takes by far the longest to compute (at least for the examples considered here). Therefore, if all one needs is information about the correlation (or lack thereof) in parameter estimators (with an eye toward reparametrization), then we would not recommend using the DRAM algorithm in a first effort.

One should recognize that effort required in obtaining correlation information can be important factors in larger problems and that run times, and more meaningful measures such as function evaluations, ease in implementation, etc., might be of interest. In that regard, it is important to note that there is a parallel implementation of DRAM [147], and also that the computation of the exact ellipsoids can be easily made parallel (in this note we only used serial implementations). If one considers more elaborate and computationally challenging mathematical models (e.g., such as the nonlinear models for HIV progression [12, 31], models for cell proliferation [39], climate models [145], nonlinear viscoelasticity [96], immune response in transplant patients [38]), then computational costs for the Bayesian approach [96, 145] could be an important consideration.

There are many limitations in our preliminary investigations: while the present study concerns itself exclusively with longitudinal/repeated measurements [60] data, these preliminary insights are not limited to that situation; one only needs a system in which the assumptions of the asymptotic theory and Bayesian based DRAM apply. Moreover, we have not tried to apply optimal design techniques [2, 29, 39, 40] to obtain really efficient computational schemes for the associated inverse problems in our comparisons. Finally we have not addressed at all the motivating issues [141, Chapter 3] of identifiability, ill-conditioning, and reparametrization for systems in which the parametric estimators are found to exhibit dependence.

# A Discrete Multi-Scale Population Model for *Daphnia magna*<sup>1</sup>

## 3.1 Introduction

Structured population models (SPMs) are well characterized for describing aggregate ecological data across a wide variety of species [52, 65]. Numerous studies have exemplified the practical utility of SPMs in conservation biology [59, 70, 152, 154] and hazard assessments [148, 160] by making predictions of population decline or recovery. Importantly, SPMs have been used to analyze factors influencing the imperilment of endangered species populations [64, 77, 87, 95, 162].

The predictive value of a SPM, or of any mathematical model, relies on the degree of fidelity of the model to existing data and in the uncertainty in parameters estimated from that data. Several factors involving data information content can affect the uncertainty in parameters estimated for a structured population model. Beyond the usual issues in optimizing the measurement frequency, variance, and resolution of the structured variable (age/size), a central problem affecting

---

<sup>1</sup>Published in altered form as [3]

### Contributions:

Experimental Design: Kaska Adoteye, Stephanie Eytcheson, and Kevin Flores

Data Collection: Kaska Adoteye, Karissa Cross, Kevin Flores, Timothy Nguyen, Chelsea Ross, Emmaline Smith, Michael Stemkovski, Sarah Stokely

Individual level models conception, design, and implementation: Kaska Adoteye

Population level model conception and design: Kaska Adoteye and Kevin Flores

Population level model implementation: Kaska Adoteye, Kevin Flores, and Michael Stemkovski

Uncertainty quantification and sensitivity analysis: Kaska Adoteye

Writeup: Kaska Adoteye and Kevin Flores

Advisors: H.T. Banks and Gerald A. LeBlanc



SPM parameter uncertainty is that aggregate data may not support the simultaneous estimation of parameters describing multiple biological scales. This “individual dynamics/aggregate data” problem [39] arises due to the interrelation of individual dynamics and aggregate behavior described by SPMs. For example, the mathematical equations describing a fecundity rate in the model might involve a density-independent rate multiplied by a density-dependent rate. Since a lower density-independent rate can be compensated for by a higher density-dependent rate, the multiplication creates a correlation that contributes to a higher level of uncertainty when these rates are concurrently estimated.

An additional confounding factor in estimating parameters for SPMs is encountered when density-independent demographic rates are time- or age-dependent. For example, the rates describing fecundity and survival are known to vary with age in many species. In addition, these age-dependent rates may also be affected by exposure of the organism to exogenous chemicals or other stressful environmental conditions. Although SPMs can be easily modified to describe age-dependent demographic parameters, the accurate estimation of those parameters can be prohibited by practical limitations, e.g., computational tractability [18, 164]. Moreover, the individual dynamics/aggregate data problem is exacerbated because time-dependence is mathematically treated by extending a single parameter to a function described by several parameters.

One approach to redressing the “individual dynamics/aggregate data” problem is to collect, when feasible, demographic data from organisms grown in isolation. This data is then used to estimate density-independent parameters comprised in the demographic rates, which are then fixed in the population model. This enables the estimation of the remaining density-dependent parameters in the population model from longitudinal aggregate data. An added advantage to this approach is that age-dependent rates can also be estimated or directly represented by the collected organismal data, removing the rather complex problem of estimating these rates from aggregate data alone.

Here, we present this approach for estimating density- and age-dependent demographic rates in SPMs for *Daphnia magna*. This species of water flea has been characterized by the National Institutes of Health as a model organism for biomedical research [123]. *D. magna* is also widely used in ecotoxicology to assess the hazard of exogenous chemicals, e.g., pesticides, on ecosystems [105, 106, 156, 157]. These assessments, however, have mainly focused on endpoints below the population level of biological organization, i.e., at the molecular, cellular, or organism levels. SPMs can be used to propagate organismal assessments to the population level, thereby enabling the causal association of organismal responses to ecosystem adversity.

Among the recent literature, several mathematical models were developed to describe the longitudinal dynamics of daphnid populations. Erickson, et al. [71], formulated a SPM to investigate

the impact of stochastic fecundity and survival on the ability of their model to describe data from pesticide treated populations. Importantly, the model from this study was calibrated to data that only captured the early population growth phase of daphnids. Thus, it has not been determined whether a SPM with stochastic demographics can accurately describe the long-term dynamics of daphnid populations, which is qualitatively different from the early growth phase [134]. Preuss, et al. [134], validated an individual-based model in order to predict the effect of variable algae concentration levels on daphnid population dynamics. Other recent efforts [67, 68, 73] to develop daphnid SPMs have focused on qualitative analysis of the general population dynamics rather than model validation.

Here, we collected both individual and population-level data and developed multiple daphnid SPMs in order to test the importance of several biological assumptions. Specifically, we mathematically tested the validity of assuming a time-delay in density-dependent fecundity. We collected daily reproduction data on thirty daphnids to precisely investigate age-dependent fecundity rates for accurate representation in a SPM. We also validated a mathematical description of density-dependent survival and tested whether density-dependent fecundity and survival could be more accurately modeled as a function of total population length (the sum of the lengths of daphnids within the population) rather than total population size (the total number of daphnids within the population). Our investigation of delayed density-dependent fecundity is motivated by previous experimental evidence found in [76, 133]; we note that this assumption has not been tested in the context of SPMs in recent literature and with modern daphnid culture methodology. We also collected precise growth rate data on thirty daphnids (starting at within 2-hours of birth) to calibrate our age-structured observations of juvenile and adult daphnids. We employed quantitative model comparison techniques to assess the validity of our underlying assumptions. Finally, we performed quantitative sensitivity and uncertainty analyses on the SPM with the most accurate biological assumptions among the SPMs we considered.

## **3.2 Methods**

### **3.2.1 Population models**

Each model we describe in the sections below is a specification of the following structured population model:

$$\begin{bmatrix} p(t+1,1) \\ p(t+1,2) \\ p(t+1,3) \\ \vdots \\ p(t+1,i_{max}) \end{bmatrix} = \begin{bmatrix} a(t,1) & a(t,2) & a(t,3) & \dots & a(t,i_{max}) \\ b(t,1) & 0 & 0 & \dots & 0 \\ 0 & b(t,2) & 0 & \dots & 0 \\ \vdots & & \ddots & \dots & \vdots \\ 0 & 0 & 0 & \dots & b(t,i_{max}-1) \end{bmatrix} \begin{bmatrix} p(t,1) \\ p(t,2) \\ p(t,3) \\ \vdots \\ p(t,i_{max}) \end{bmatrix}. \quad (3.1)$$

The population is divided into one-day age classes, ranging from neonates at age  $i = 1$  to a maximum lifespan at age  $i = i_{max}$ , where the number of daphnids of age  $i$  at a time  $t$  is  $p(t, i)$ . Here, we assume  $i_{max} = 74$  based on our individual-level experiments, and based on simulations of our models fit to experimental data, i.e., the maximum life span observed in the simulations was always less than 74 days. The fecundity of each age class  $i$  is given by  $a(t, i)$  and the survival probability is given by  $b(t, i)$ .

We generated several models to investigate the importance of several density-dependent mechanisms in modeling *D. magna* populations. Significance of the different mechanisms was assessed by using statistical comparison tests between different models fit to the same structured population data. We specified the functional forms for  $a(t, i)$  and  $b(t, i)$  in Equation (3.1) to generate four different structured population models for this assessment, which we refer to as models A through D (Table 3.1). The four models we consider are organized by the sequential generalization of the functional forms for fecundity and survival, i.e., models A and D have the least and most number of parameters, respectively.

### 3.2.1.1 Delayed density-dependent fecundity

To evaluate the importance of delayed density-dependent fecundity, we generated models A and B (Table 3.1) with parameters  $\theta = (\mu, q)$  to be estimated. In model A, we assume density-dependent fecundity for all daphnid age classes. We used a functional form for fecundity that decreases with total population size  $N(t)$  [81] (see  $a(t, i)$  in Table 3.1a). The strength of the density-dependent effect on fecundity is represented by the parameter  $q$ ; the fecundity is density-independent when  $q = 0$ . Model A assumes a density- and age-independent survival probability, i.e., the constant  $\mu$ . We did not consider age-dependent survival here, thus the probability  $\mu$  is the same for each age class. We will consider generalizations of  $\mu$  in Chapter 4 and note that constant survival probability has been used previously for structured population modeling of daphnids [76, 133].

Model B generalizes model A by considering a delayed effect of density on fecundity. This generalization is based on previous studies which showed that number of offspring produced by gravid female daphnids in their current cohort was unaffected by increases in population density.

**Table 3.1** Descriptions of models, parameters, and variables with unknown parameters  $\theta = (\mu, q)$  in Models A and B and  $\theta = (\mu, q, c)$  in Models C and D to be estimated.

(a) Age-dependent fecundity,  $a(t, i)$ , and survival probability,  $b(t, i)$  in Equation (3.1).

Model	$a(t, i)$	$b(t, i)$
A	$\alpha(i)(1 - q)^{N(t)}$	$\mu$
B	$\alpha(i)(1 - q)^{N(t-\tau)}$	$\mu$
C	$\alpha(i)(1 - q)^{N(t-\tau)}$	$\mu(1 - c)^{N(t)}$ if $i \leq 4$ , $\mu$ if $i \geq 5$
D	$\alpha(i)(1 - q)^{M(t-\tau)}$	$\mu(1 - c)^{M(t)}$ if $i \leq 4$ , $\mu$ if $i \geq 5$

(b) Parameter/Variable descriptions.

Parameter/ Variable	Description	Units
$p(t, i)$	Number of daphnids of age $i$	# of daphnids
$N(t)$	Total population size at time $t := \sum_{i=1}^{i_{max}} p(t, i)$	# of daphnids
$q$	Density-dependent fecundity constant	dimensionless
$\alpha(i)$	Density-independent fecundity rate	# neonates·daphnid <sup>-1</sup> ·day <sup>-1</sup>
$\mu$	Density-independent survival probability	day <sup>-1</sup>
$\tau$	Delay for density-dependent fecundity	days
$c$	Density-dependent survival constant	dimensionless
$M(t)$	Total population length at time $t := \sum_{i=1}^{i_{max}} p(t, i) \frac{K Z_0 e^{r i}}{K + Z_0(e^{r i} - 1)}$	# · mm
$K$	Average maximum daphnid size (major axis)	mm
$r$	Average daphnid growth rate	mm/hour
$Z_0$	Average neonate size (major axis)	mm

Instead, increased population density had an effect on subsequent cohorts [76, 133]. Since daphnids in their reproductive stage produce neonates approximately every 3 days, we bounded the time-delayed fecundity effect,  $\tau$ , between 0 and 6 days.

### 3.2.1.2 Density- and age-dependent survival

We next evaluated whether density and age were important factors for modeling survival in daphnid populations. To test this, we created model C (with parameters  $\theta = (\mu, q, c)$  to be estimated), which generalizes model B by including a reduced survivorship for daphnids classified as juveniles in our data, i.e., daphnids less than or equal to 4 days old (see Figure 3.1). This generalization is based on the observation that larger daphnids consume more algae than smaller daphnids [139]. The restriction of density-dependent survival to juvenile daphnids is in agreement with previous studies which suggested that the survival of adult daphnids is not affected by competition [119]. This competitive effect is likely an important consideration for the daphnids in our population experiments, since our populations were fed a constant amount of algae each day. Indeed, previous modeling studies have suggested that density-independent daphnid survival rates would best be modeled as a function of age or size rather than as a constant [56, 75, 132, 134].

### 3.2.1.3 A density-dependent model with population length

Lastly, we evaluated whether total population length could more accurately capture the density-dependence of fecundity and survival than the total number of individuals in our daphnid populations. This consideration is in concordance with the generalization in model C, which relies on the observation that larger daphnids contribute more heavily to competition through resource depletion than smaller daphnids [139]. To test our hypothesis about population length dependency, we generated Model D (again with parameters  $\theta = (\mu, q, c)$  to be estimated) by replacing the total population size,  $N(t)$ , in model C by total population length,  $M(t)$  (see Table 3.1). To model total population length, we calculated a weighted population value using a function that relates age to size. Specifically, we found that the logistic function accurately models the average size of daphnids as a function of age based on fits to individual-level experimental data (Figure 3.2). Consequently, we used the logistic function to weight the daphnid size in the model for the total population length  $M(t)$  (see Table 3.1b).

## 3.2.2 Laboratory studies

We conducted two studies in the laboratory to generate data for refining and parameterizing our mathematical model. The first study was performed at the individual daphnid level to track the

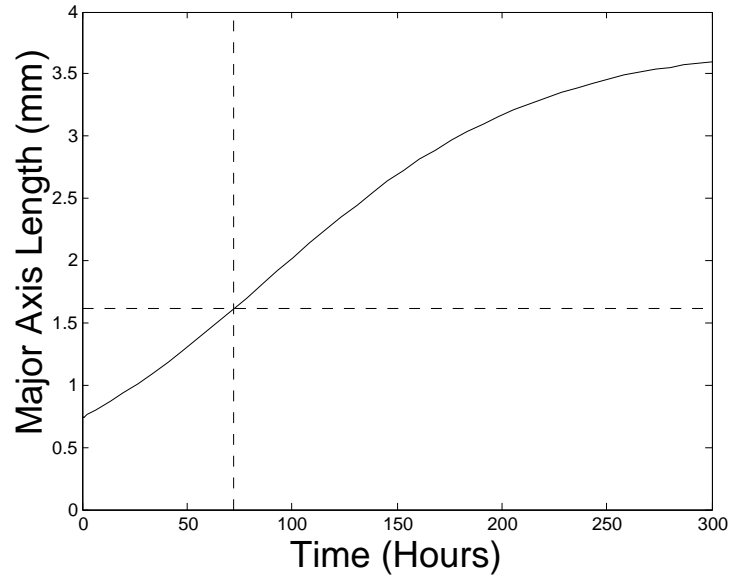


**Figure 3.1** Calibration of the maximum size for classification of juveniles. We determined the maximum juvenile daphnid size by simulating the logistic growth curve with mean parameter values from the non-linear mixed effects model (Figure 3.2, Table 3.2). The pore size of the mesh we used to separate juveniles from adults was 1.62 mm, and this value is plotted as a horizontal line. The vertical line gives the average daphnid age at which their major axis length is equal to the mesh pore size. Based on this calculation, we inferred that the maximum age at which daphnids can fit through the mesh was 4 days old. Thus, we chose to classify juveniles in our models as  $\leq 4$  days old.

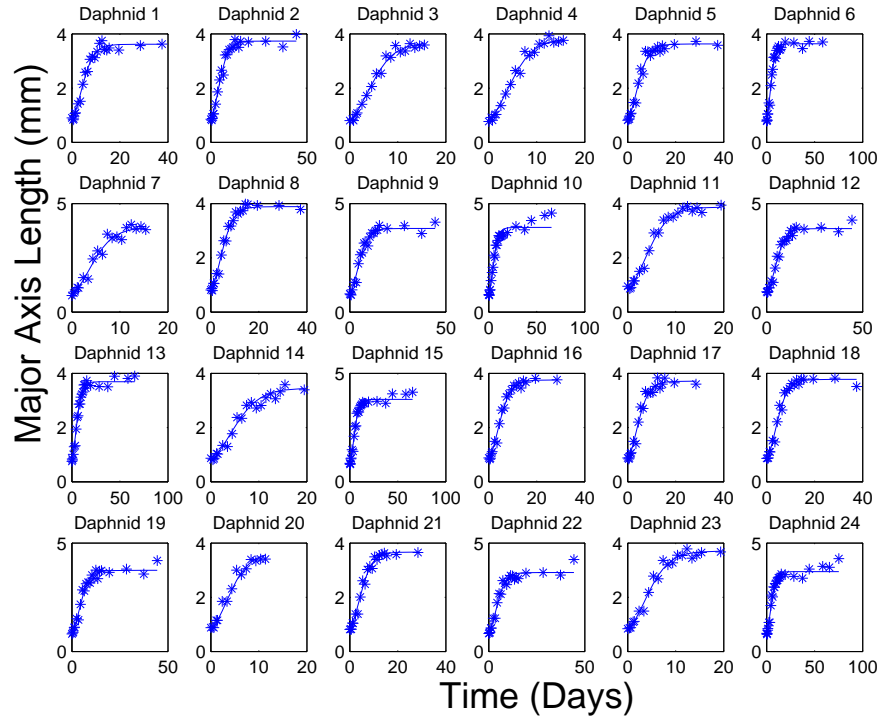


**Figure 3.2** Results for nonlinear regression performed on individual-level growth data using a logistic equation within a nonlinear mixed effects model (NLMEM). Growth data are represented by star symbols (to view growth data on a single graph, see Control Beaker plot in Figure A.8). Best model fits are drawn as lines for each individual. We collected data for thirty daphnids, but these plots show results for twenty four daphnids for which an adequate number of data was collected to fit a NLMEM (the other six daphnids died very early in the experiment). Nonlinear regression was performed using Simbiology in Matlab. We tested several models for growth, including logistic, Gompertz, constant, and linear equations. Based on  $AIC_C$  values, it was determined that the logistic model provided the most accurate fit to the data. See Table 3.2 for estimated parameters and variances, including fixed effects and random effects, and Appendix B.1 for details on how the computation was completed.

baseline fecundity and growth rates in isolation, i.e., density-independent rates. The second study was performed at the population level, in duplicate, for 102 days. The individual-level data was used to estimate the density-independent parameters used in our population model. The population data was then used to estimate the remaining density-dependent parameters. Cultured daphnids were maintained using previously described protocols and conditions [157]. Cultured daphnids were kept in media reconstituted from deionized water [10]. Cultured daphnids for both studies were maintained in an incubator maintained at 20 degrees Celsius with a 16-h light, 8-h dark cycle. The daphnids used in our study came from a colony that was maintained at North Carolina State University for over 20 years (clone NCSU1 [138]).

### 3.2.2.1 Individual study

Thirty daphnids were longitudinally observed to estimate population average rates of fecundity and growth. Less than 2-h old neonates were placed individually into 50mL beakers containing 40mL of media each. Media was changed daily. Daphnids were fed daily with  $7.0 \times 10^6$  cells of algae (*Raphidocelis subcapitata*) and 0.2 mg (dry weight) Tetrafin<sup>TM</sup> fish food suspension prepared as described previously [124]. The number of neonates produced by each individual daphnid was recorded and then removed daily. Fecundity measurements were performed until no daphnids remained (74 days). The size of each individual daphnid was measured with a digital microscope (Celestron, Torrance, CA, USA) at periodic intervals until they died, starting at less than two hours old. The major axis was used to determine size, since the maximum possible length was used to classify daphnids into different size classes, i.e., juveniles and adults (see below).

### 3.2.2.2 Population study

A 102-day population study was conducted, in replicate, using *D. magna*. Two beakers containing 1L of media each were both seeded with five 6-day-old female daphnids. We note that these daphnids did not reproduce prior to the beginning of the population study. Each 1L beaker was fed twice daily (at approximately 10 a.m. and 3 p.m.) with  $1.4 \times 10^8$  cells of algae (*R. subcapitata*) and 4 mg dry weight of fish food suspension. The media was changed and the number of daphnids were counted every Monday, Wednesday, and Friday through the first 40 days of the experiment and once weekly thereafter. During counting, daphnids were separated into two size classes (which we call the juvenile class  $J(t)$  and adult class  $A(t)$  at time  $t$ ) using a fine mesh net with a 1.62-mm pore size. The total number of daphnids  $N(t)$  at time  $t$  was then counted for each size class. Importantly, we note that classification into the juvenile or adult group only defines the size of the daphnid, and does not define whether the daphnid had reached a reproductive stage. We also collected data on



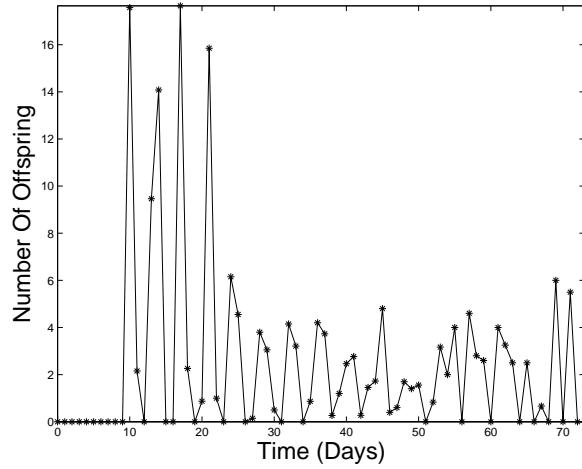


**Figure 3.3** The number of neonates produced per female daphnid per day. Data were collected from thirty female daphnids whose birth was known to within two hours of accuracy. Daily data are represented by star symbols and connecting lines are drawn to show general trends. This data was used as the age-dependent function  $\alpha(i)$  (see Table 3.1).

the number of males produced by examining daphnids microscopically, with males determined by having a longer first antennae [125], but since those numbers were so small (at most 2% of the population was male) and since the males died so quickly (each male died within one week of birth) we do not include that data in our results, or in our modeling.

### 3.2.3 Estimation of density-independent rates

We used data from our individual-level study to estimate the density-independent fecundity rate, which we call  $\alpha(i)$ . We parameterized the function  $\alpha(i)$  defined at age  $i$  by directly using the average number of neonates produced per daphnid per day observed in our individual-level study (Figure 3.3). Using the average number of neonates produced per daphnid per day is an assumption that proved to work best within our population model. Appendix A.1 shows efforts to use the actual number of neonates produced coming from a distribution, which wasn't as effective as the variances in the distributions were so high given the wide variability in daphnid reproduction.

We used the individual-level growth (size) data to estimate the relationship between age and size. We considered several functional forms for  $f(i)$ , the average size of a female daphnid at age  $i$ , within a nonlinear mixed effects model framework and found that the logistic equation  $f(i) = \frac{KZ_0e^{ri}}{K+Z_0(e^{ri}-1)}$  most accurately fit the data for individual daphnid growth (Figure 3.2, Table 3.2)(see Appendix B.1

for computational details). Based on the mean parameter values estimated with the nonlinear mixed effects model, we inferred that the daphnids classified as juveniles in our population experiments were less than or equal to 4 days old, and that adults were greater than 5 days old (Figure 3.1). The function  $f(i)$  was also used to replace total population size with a model for total population length in Model D. We note that we determined that the average size  $f(i)$  was sufficient to replace the total population size, as opposed to using the full distribution of sizes obtained from the nonlinear mixed effects model, since the range of individual parameter values in Table 3.2 was deemed to be too slim to merit more than a delta distribution approximation.

### 3.2.4 Parameter Estimation

Parameters were estimated from the population data using a vector ordinary least squares (OLS) framework [31, 39]. For each model, we consider a vector of parameters  $\theta$  to estimate. Based on our individual-level modeling, the number of juveniles and adults are given by  $f_J(t, \theta) = \sum_{i=1}^4 p(t, i)$  and  $f_A(t, \theta) = \sum_{i=5}^{i_{max}} p(t, i)$ , respectively. The corresponding observation vector is given by  $\mathbf{f}(t, \theta) = [f_J(t, \theta), f_A(t, \theta)]^T$ . We assumed a constant statistical error model of the form

$$\mathbf{Y}_j = \mathbf{f}(t_j, \theta_0) + \mathcal{E}_j, \quad j = 1, 2, \dots, n, \quad (3.2)$$

where  $\mathbf{Y}_j$  is a random variable with realizations  $\mathbf{y}_j = [J(t_j), A(t_j)]^T$  (i.e., the data) and  $\mathbf{f}(t_j, \theta_0)$  is the model observation with the hypothesized “true” parameter vector  $\theta_0$ . The error terms  $\mathcal{E}_j$  are assumed independent and identically distributed (i.i.d) random variables with mean  $E[\mathcal{E}_j] = 0$  and  $V_0 = \text{var}(\mathcal{E}_j) = \text{diag}(\sigma_{J,0}^2, \sigma_{A,0}^2)$ , where  $\sigma_{J,0}^2$  and  $\sigma_{A,0}^2$  are the observation variances for the juvenile and adult observations, respectively. An estimate,  $\hat{\theta}$ , for the true parameter vector  $\theta_0$  is obtained by implementing an iterative algorithm (see [39] for details). We note here that the constant error assumption might be called into question. Below we test that assumption, and verify that it is valid in this case.

The inverse problems here, and when testing the error assumption below, were computed using two routines in Matlab. The first routine is a direct search algorithm implemented by Daniel Finkel as *direct*, and can be found at [http://www4.ncsu.edu/~ctk/Finkel\\_Direct/](http://www4.ncsu.edu/~ctk/Finkel_Direct/). This was used with the following options: options.maxevals = 400; options.maxits = 400; options.maxdeep = 400; and the output was used as the initial condition for the gradient based Matlab search routine *lsqnonlin*. *lsqnonlin* was run with the options ‘TolFun’ and ‘TolX’ set equal to 1e-20, and the option ‘MaxFunEvals’ set equal to 400. The output of *lsqnonlin* was then used as our parameter estimate.

**Table 3.2** Mean parameter estimates and variances along with individual daphnid parameter estimates for the logistic equation using a nonlinear mixed effects model (see Figure 3.2).

(a) Mean values and variances (random effects) estimated for the logistic equation with a nonlinear mixed effects model.

Parameter	$K$	$r$	$Z_0$
Fixed Effect Mean Value	3.7346	0.0157	0.7333
Random Effect Variance	$1.0533 \times 10^{-3}$	$4.8239 \times 10^{-3}$	$6.8978 \times 10^{-7}$

(b) Individual parameter estimates for each daphnid.

Daphnid	$K$	$r$	$Z_0$
1	3.6148	0.0157	0.7333
2	3.7342	0.0160	0.7333
3	3.6834	0.0156	0.7333
4	3.8267	0.0156	0.7333
5	3.6262	0.0162	0.7333
6	3.6340	0.0157	0.7333
7	3.8957	0.0169	0.7334
8	3.8895	0.0154	0.7333
9	3.8556	0.0152	0.7333
10	3.9009	0.0145	0.7333
11	3.8718	0.0170	0.7334
12	3.8482	0.0148	0.7333
13	3.6902	0.0140	0.7333
14	3.4604	0.0138	0.7333
15	3.7969	0.0150	0.7333
16	3.7530	0.0158	0.7333
17	3.7092	0.0162	0.7333
18	3.7758	0.0164	0.7333
19	3.7397	0.0159	0.7333
20	3.6688	0.0178	0.7334
21	3.6662	0.0153	0.7333
22	3.6387	0.0163	0.7334
23	3.7070	0.0166	0.7333
24	3.6806	0.0147	0.7333

### 3.2.5 Testing Constant Error Assumption

We tested the hypothesized error model in Equation (3.2). In order to do this, we will consider the more general error model

$$\mathbf{Y}_j = \mathbf{f}(t_j, \theta_0) + \mathbf{f}^\gamma(t_j, \theta_0) \mathcal{E}_j, \quad j = 1, 2, \dots, n, \quad (3.3)$$

where  $\gamma \in \mathbb{R}$ . This is known as a relative error model, where  $\gamma = 0$  gives us our previously hypothesized constant error model in Equation (3.2).

There is no rigorous test to see which error assumption is correct, but in general in order to test the accuracy of these error models it is common to consider the residuals (using the estimated parameters  $\hat{\theta}$ )

$$r_j^J = \frac{J(t_j) - f_J(t_j, \hat{\theta})}{f_J^\gamma(t_j, \hat{\theta})}, \quad r_j^A = \frac{A(t_j) - f_A(t_j, \hat{\theta})}{f_A^\gamma(t_j, \hat{\theta})},$$

where we notice that the residuals for the juvenile estimation,  $r_j^J$ , and the residuals for the adult estimation,  $r_j^A$ , are obtained by solving for the error in Equation (3.3) with realizations for  $\mathbf{Y}_j$ . Therefore, since the error  $\mathcal{E}_j$  is assumed to be i.i.d. with mean 0 and estimated variance  $\hat{V}_0 = \text{diag}(\hat{\sigma}_{J,0}^2, \hat{\sigma}_{A,0}^2)$ , we would expect the plots of  $r_j^J$  and  $r_j^A$  against time  $t_j$  to be random. Similarly, if our error model is correct and  $\gamma$  is correctly specified, we would expect the plots of  $r_j^J$  and  $r_j^A$  against the model solution,  $f_J(t_j, \hat{\theta})$  and  $f_A(t_j, \hat{\theta})$  respectively, to be random. Consult [31, 39] for more information.

One issue with the above approach of testing the statistical assumption is that it depends heavily on the estimated parameters  $\hat{\theta}$ , which in turn depend on the statistical assumption that was used for the inverse problem. To be more specific, given the statistical model in Equation (3.3), the estimated parameters  $\hat{\theta}$  that are used to compute the residuals  $r_j^J$  and  $r_j^A$  are given by

$$\hat{\theta} = \arg \min_{\theta} \sum_{j=1}^N \frac{(J(t_j) - f_J(t_j, \theta))^2}{\sigma_{J,0}^2 f_J^{2\gamma}(t_j, \theta)} + \frac{(A(t_j) - f_A(t_j, \theta))^2}{\sigma_{A,0}^2 f_A^{2\gamma}(t_j, \theta)},$$

which we can see depend on  $\gamma$ , which is exactly the value we are trying to find by looking at the residual plots. Also, the above approach depends on the assumption that the model perfectly describes the underlying process. The method we describe below avoids these assumptions.

Below we directly test if the error assumption is correct by using nonparametric methods to estimate the error itself for different values of  $\gamma$  (see [36, 114, 155] and the references therein). This approach doesn't use a model, and thus avoids the assumptions of the above approach. Also, using a nonparametric approach, once an optimal value of  $\gamma$  is found we can compare our estimated error

against the residuals  $r_j^J$  and  $r_j^A$  to see if there is any mathematical model error. An investigation of different nonparametric methods was performed in [36], and from that investigation it was seen that a second order differencing of the data was quite accurate for different datasets, and thus we will use that method to estimate the error.

That is, given data  $y_j = [y_{1,j}, y_{2,j}]^T$  at time  $t_j$  in a relative error model as in Equation (3.3), we will estimate a realization  $\varepsilon_{i,j}$  of the error  $f_i^\gamma(t_j, \theta_0)\mathcal{E}_{i,j}$  by

$$\hat{\varepsilon}_{i,j} = \frac{e_{i,j}}{|y_{i,j} - e_{i,j}|^\gamma}, \quad j = 2, 3, \dots, n-1, \quad i = 1, 2, \quad (3.4)$$

where

$$e_{i,j} = \frac{1}{\sqrt{6}}(y_{i,j-1} - 2y_{i,j} + y_{i,j+1}).$$

Here in a switch of notation  $i = 1, 2$  correspond to  $J$  and  $A$  before, so  $y_{1,j} = J(t_j)$ ,  $y_{2,j} = A(t_j)$ ,  $f_1^\gamma(t_j, \theta_0) = f_J^\gamma(t_j, \theta_0)$ , and  $f_2^\gamma(t_j, \theta_0) = f_A^\gamma(t_j, \theta_0)$ . We will plot this estimate  $\hat{\varepsilon}_{i,j}$  against  $t_j$  for values of  $\gamma = 0, 0.05, 0.1, 0.15, \dots, 1.5$ . The plot for the best error estimate should appear random (as in, white noise around the horizontal axis). Once we have the value of  $\gamma$  that provides the best error estimate, we will then use that value of  $\gamma$  to test the error estimate against the model solution.

### 3.2.6 Model Comparisons

#### 3.2.6.1 Model Hypothesis Testing

We used a statistical model comparison test [23, 31] to evaluate the significance in considering various components, e.g., delayed density-dependence, for models A through D. Briefly, this methodology evaluates the significance of a  $\chi^2$  statistic generated by the residual sum of squares to test the null hypothesis,  $H_0$ , that a certain parameter or set of parameters is not needed to describe the system. We note that this method requires nested models. For example, model A is “nested” in model B because model B reduces to model A when  $\tau = 0$ . If we can reject the null hypothesis  $H_0$  then we conclude that the parameters in question cannot be taken equal to zero and infer that they are needed to accurately describe the data. For further details on this hypothesis testing technique and previous applied examples of this methodology see [23, 26, 31].

Model B is “nested” in model C because model C reduces to model B if  $c = 0$ . In order to show that Model C is nested in Model D, we need to show that  $M(t - \tau) = N(t - \tau)$  for appropriate values of  $K, Z_0$ , and  $r \in \mathbb{R}$ . This is equivalent to finding of values of  $K, Z_0$ , and  $r$  such that

$$\frac{K Z_0 e^{ri}}{K + Z_0(e^{ri} - 1)} = 1, \quad \forall i \in \mathbb{N}.$$

If we set  $r = 0$  and  $Z_0 = 1$ , the above equation becomes

$$\frac{K}{K} = 1,$$

which is true for all values of  $K \in \mathbb{R} \setminus \{0\}$ . Therefore, we see that Model C is indeed nested in Model D.

### 3.2.6.2 Akaike Information Criteria

The Akaike Information Criterion ( $AIC$ ) score gives an approximately unbiased form of the Kullback-Leibler Distance, or a measure of the distance between a model and the corresponding data [39]. The  $AIC$  score is used to compare the accuracy of different models to the same data set; a lower  $AIC$  score indicates higher accuracy. We note that the  $AIC$  score is applicable to more model comparisons than the  $\chi^2$  based test described above, since it does not require the compared models to be nested. The  $AIC$  score corrected for small sample size ( $n/p < 40$ ,  $n$  = number of data points,  $p$  = number of parameters) is given by as  $AIC_C = n \ln\left(\frac{RSS}{n}\right) + 2p + \frac{2p(p+1)}{n-p-1}$ , where  $RSS$  is the *residual sum of squares* [39, 49]. We used the  $AIC_C$  score to compare the models tested for the nonlinear mixed effects model for density-independent growth of daphnids (Appendix B.1).

### 3.2.7 Parameter Uncertainty Quantification

We calculated standard errors and 95% confidence intervals for the estimated parameters  $\hat{\theta}$  using asymptotic theory, and used bootstrapping for verification. We provide a brief description of the application of these two methods here, but for more details see [31, 39].

#### 3.2.7.1 Asymptotic Theory

The observation variance  $V_0$  in the vector OLS framework using a constant statistical error model is approximated by

$$V_0 \approx \hat{V} = \text{diag} \left( \frac{1}{n-p} \sum_{j=1}^n [\mathbf{y}_j - \mathbf{f}(t_j, \hat{\theta})][\mathbf{y}_j - \mathbf{f}(t_j, \hat{\theta})]^T \right).$$

The resulting approximation of the covariance matrix is given by

$$\hat{\Sigma}^n = \left( \sum_{j=1}^n D_j^T(\hat{\theta}) \hat{V}^{-1} D_j(\hat{\theta}) \right)^{-1},$$

where the  $2 \times p$  matrix  $D_j(\hat{\theta})$  is given by

$$D_j(\hat{\theta}) = \begin{pmatrix} \frac{\partial f_j(t_j, \hat{\theta})}{\partial \theta_1} & \cdots & \frac{\partial f_j(t_j, \hat{\theta})}{\partial \theta_p} \\ \frac{\partial f_A(t_j, \hat{\theta})}{\partial \theta_1} & \cdots & \frac{\partial f_A(t_j, \hat{\theta})}{\partial \theta_p} \end{pmatrix},$$

where  $p = 2$  in Models A and B and  $p = 3$  in Models C and D. Then asymptotic theory [31, 39] yields that the OLS estimator has a limiting distribution given approximately by a  $\mathcal{N}(\hat{\theta}, \hat{\Sigma}^n)$  distribution.

We calculated standard errors and 95% confidence intervals [31, 39] in order to quantify the uncertainty in estimating each element of the parameter estimate  $\hat{\theta}$  for our best model with vector observation  $\mathbf{f}(t, \theta)$ . The standard error and 95% confidence interval of the  $k^{th}$  parameter  $\hat{\theta}_k$  is given by  $SE(\hat{\theta}_k) = \sqrt{\hat{\Sigma}_{kk}^n}$  and  $[\hat{\theta}_k - 1.96SE(\hat{\theta}_k), \hat{\theta}_k + 1.96SE(\hat{\theta}_k)]$ , respectively [31].

### 3.2.7.2 Bootstrapping

Bootstrapping is implemented for an estimated parameter vector  $\hat{\theta}$  by first calculating standardized residuals

$$\bar{r}_j^i = \sqrt{\frac{n}{n-p}} (y_j^i - f_i(t_j, \hat{\theta})), \quad j = 1, \dots, n,$$

where  $n$  is the number of data points,  $p$  is the number of parameters,  $i = J$  or  $A$  represents either the adult or juvenile observation. Bootstrap sample points are created by sampling the standardized residuals for each observation (J or A) and adding them to the respective model solutions, either  $f_J(t_j, \hat{\theta})$  or  $f_A(t_j, \hat{\theta})$ . We created  $M = 1000$  simulated bootstrap data sets in this fashion and then conducted  $M$  inverse problems to fit the model to each of these simulated data sets. For the  $m^{th}$  simulated bootstrap data set, we then find the corresponding parameter estimate  $\hat{\theta}^m$ . The mean, variance, and standard errors for  $\hat{\theta}$  are approximated by the following formulas [39]:

$$\begin{aligned} \hat{\theta}_{BOOT} &= \frac{1}{M} \sum_{m=1}^M \hat{\theta}^m, \\ Var(\hat{\theta}_{BOOT}) &= \frac{1}{M-1} \sum_{m=1}^M (\hat{\theta}^m - \hat{\theta}_{BOOT})(\hat{\theta}^m - \hat{\theta}_{BOOT})^T, \\ SE_k(\hat{\theta}_{BOOT}) &= \sqrt{Var(\hat{\theta}_{BOOT})_{kk}}. \end{aligned}$$

The 95 % confidence interval for each  $\hat{\theta}_k$  is calculated as the range between the 25-th and 975-th entries in the ordered set of  $M$  parameter estimates from bootstrapping.

## 3.3 Results

### 3.3.1 Model Selection

When comparing models A and B we found that a 6 day time-delay on the effect of density on fecundity provided a significantly improved fit to the daphnid population data versus the non-delayed model for both population data sets ( $P = 5.029\text{e-}4$ , Replicate 1;  $P = 3.219\text{e-}3$ , Replicate 2,  $\chi^2$ -test). We note that we also tested whether larger  $\tau$  values could provide a more accurate fit to population data but found no significant differences in fits to the population data when using  $\tau = 6$  versus  $\tau = 7$  or  $8$  ( $P = .3071$ , Replicate 1;  $P = .1139$ , Replicate 2,  $\chi^2$ -test).

We found that the inclusion of both density and age dependence in the survival probability  $b(t, i)$  provided significantly improved fits to population data for one of the two replicates ( $P = 1.615\text{e-}1$ , Replicate 1;  $P = 3.96\text{e-}2$ , Replicate 2,  $\chi^2$ -test). Overall, these results suggest that model C is more appropriate for modeling our daphnid populations than model B, since it describes a wider range of observed biological dynamics.

We note that we also considered other models that did not significantly increase the accuracy of the model to experimental population data. For example, we considered models in which the density-dependent effects were of different functional forms.

We find that using the total population length in Model D provides a significant improvement to the population fit over using total number of daphnids as in Model C ( $P = 6.8077\text{e-}3$ , Replicate 1;  $4.5812\text{e-}5$ , Replicate 2,  $\chi^2$ -test). These results strongly suggest that model D is better than model C at representing the population data from both replicates. Hence, dependence of birth and death demographics on population density is most likely a function of a total population length rather than the absolute number of daphnids counted regardless of size or age. See Figure 3.10 for fits of model D to the population data. Moreover, the parameter estimates for both replicates were strikingly similar, indicating that our validation of model D is repeatable despite the possibility of biological variability between population experiments.

### 3.3.2 Verification of Constant Error Assumption

We tried several values of  $\gamma$  for a more general error model (Equation (3.3)). As  $\gamma$  increases past 0.5, the plots of  $\hat{\epsilon}_{i,j}$  become progressively less random (see Figures 3.4-3.6). For values of  $\gamma$  between 0.05 and 0.45, the most random observation error plots came from  $\gamma = 0.2$ . Therefore, if we are to use relative error  $\gamma > 0$ , we would need to use  $\gamma = 0.2$ .

Now we must determine if using  $\gamma = 0.2$  is a better assumption than using  $\gamma = 0$ . Figure 3.7 shows the plots of  $\hat{\epsilon}_{i,j}$  for  $\gamma = 0$  and for  $\gamma = 0.2$  side by side. What we want to see is whether the plots for



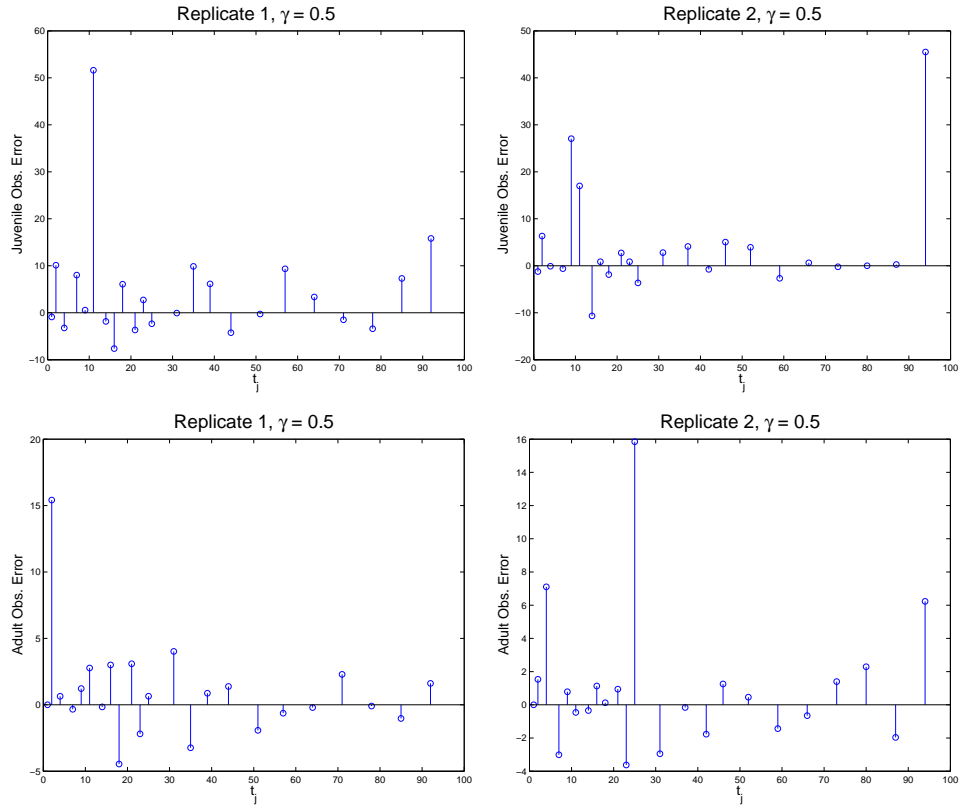


**Figure 3.4** These are the plots of the observation error estimates  $\hat{\epsilon}_{J,j}$  and  $\hat{\epsilon}_{A,j}$  for juveniles and adults, respectively, plotted against time  $t_j$  for  $\gamma = 0.5$ . The plots for Replicate 1 are on the left, and for Replicate 2 are on the right.

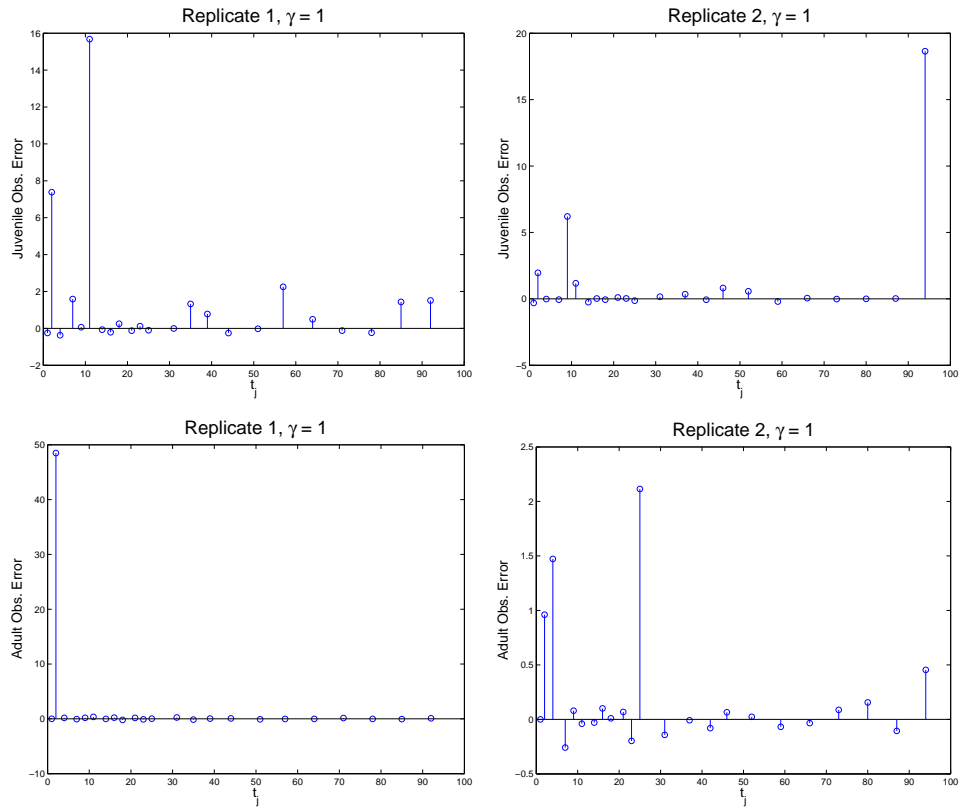


**Figure 3.5** These are the plots of the observation error estimates  $\hat{\epsilon}_{J,j}$  and  $\hat{\epsilon}_{A,j}$  for juveniles and adults, respectively, plotted against time  $t_j$  for  $\gamma = 1.0$ . The plots for Replicate 1 are on the left, and for Replicate 2 are on the right.

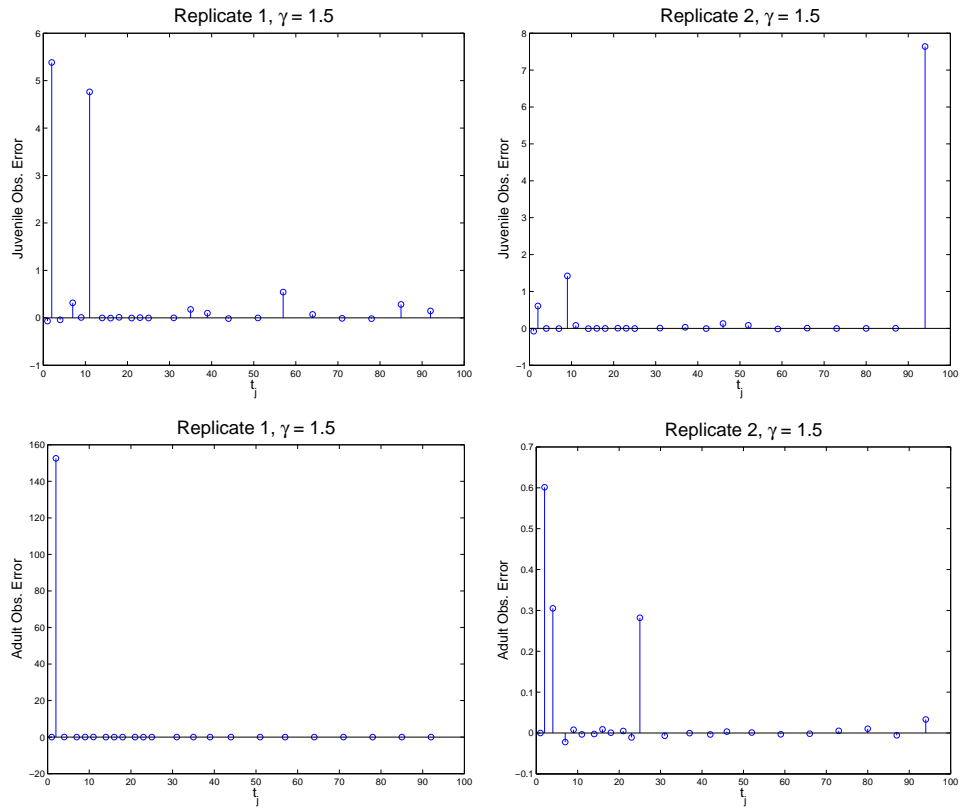


**Figure 3.6** These are the plots of the observation error estimates  $\hat{\epsilon}_{J,j}$  and  $\hat{\epsilon}_{A,j}$  for juveniles and adults, respectively, plotted against time  $t_j$  for  $\gamma = 1.5$ . The plots for Replicate 1 are on the left, and for Replicate 2 are on the right.

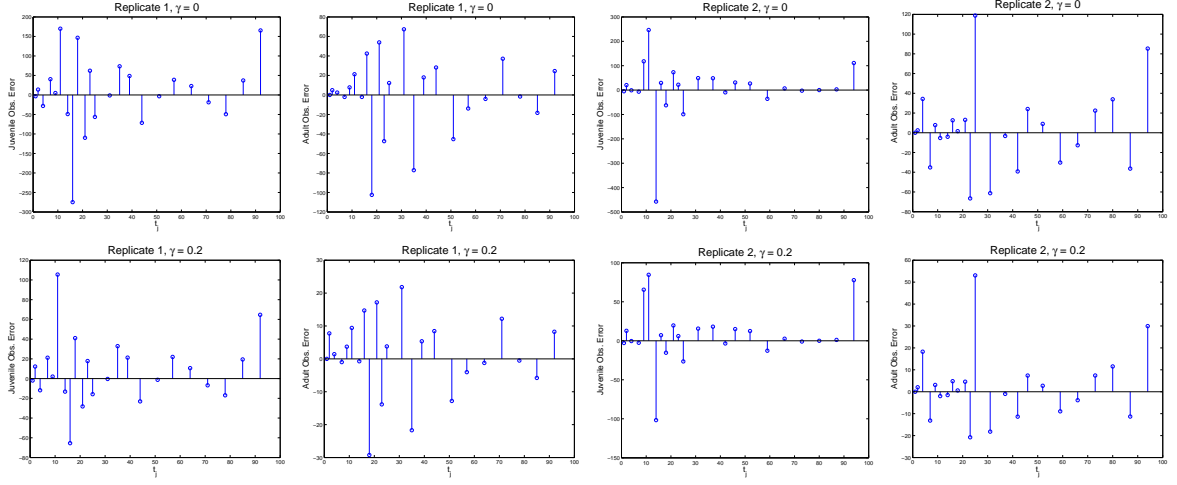


**Figure 3.7** These are the plots of the observation error estimates  $\hat{\epsilon}_{J,j}$  and  $\hat{\epsilon}_{A,j}$  for juveniles and adults, respectively, plotted against time  $t_j$ . The plots for  $\gamma = 0$  are on the top, and the corresponding plots for  $\gamma = 0.2$  are on the bottom.

$\gamma = 0.2$  look more random than the plots for  $\gamma = 0$ . What we do see is that the residual plots look very similar qualitatively, except for the magnitude of the errors. Since there's not enough evidence to say that a relative error model with  $\gamma = 0.2$  is more accurate, we will continue to assume that  $\gamma = 0$ , and thus that we have constant error. Now that we have a reasonable error assumption, we can also inspect the plot of the residual  $r_j^J$  against the model solution  $f_J(t_j, \hat{\theta})$  and  $r_j^A$  against the model solution  $f_A(t_j, \hat{\theta})$  (Figure 3.8), where we see that they appear fairly random.

### 3.3.3 Uncertainty Analysis

We quantified uncertainty in our parameter estimates for model D. Uncertainty quantification provides an estimation of the statistical confidence in each parameter estimate for a given data set, where confidence is determined by estimating a distribution for each parametric estimator. We calculated standard errors and 95% confidence intervals for each parameter using asymptotic theory and bootstrapping (Table 3.3, Figure 3.9). Both the results from asymptotic theory and bootstrapping support that the standard errors were low and the 95% confidence intervals were narrow for the parameter estimates in both replicates. These results indicate a high confidence that our model calibration results are repeatable.

In order to investigate how well our model captures our data, given our observation error (Table 3.4), we plotted our model with one standard deviation of observation error in Figure 3.10, and our model with close to two standard deviations of observation error in Figure 3.11. To be more specific,

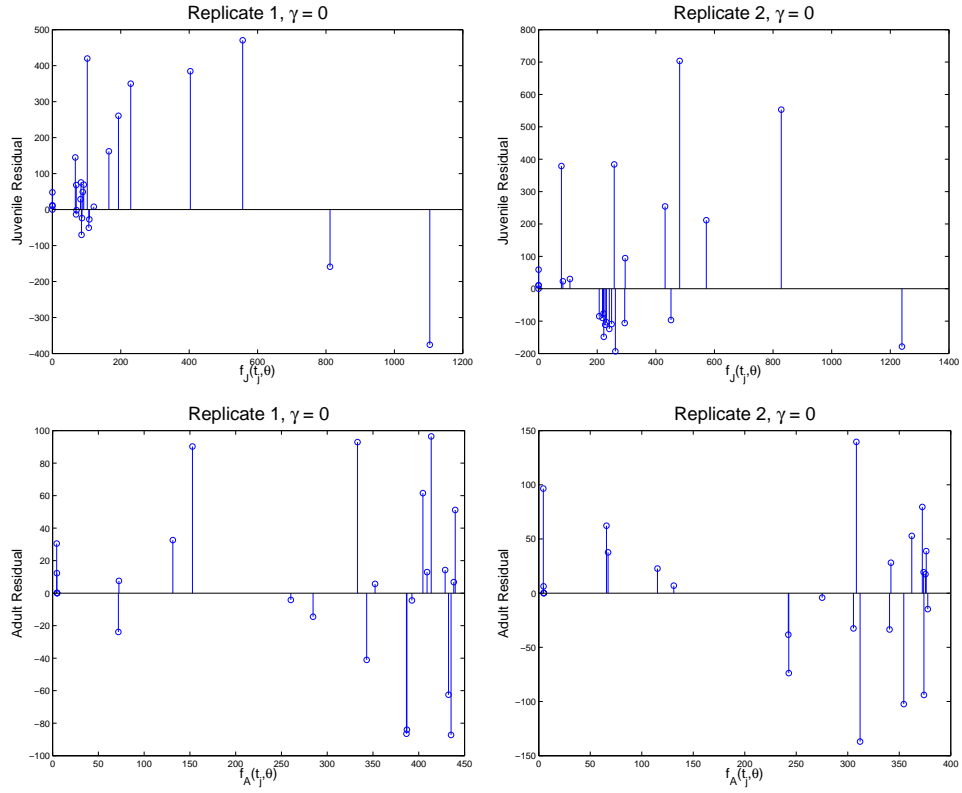


**Figure 3.8** These are the plots of the residual  $r_j^J$  plotted against the model solution for juveniles  $f_j(t_j, \theta)$  on top and  $r_j^A$  plotted against the model solution for adults  $f_A(t_j, \theta)$  on the bottom. The plots for Replicate 1 are on the left, and for Replicate 2 are on the right.

**Table 3.3** Results from uncertainty quantification with asymptotic theory and bootstrapping for model D.

(a) Parameter estimates, asymptotic standard errors, and asymptotic 95% confidence intervals (C.I.) for model D.

Replicate	Parameter	Estimate	Standard Error	95 % C.I.
1	$\mu$	$9.5051 \times 10^{-1}$	$1.0428 \times 10^{-2}$	$(9.2889 \times 10^{-1}, 9.7214 \times 10^{-1})$
1	$q$	$1.7206 \times 10^{-3}$	$1.5426 \times 10^{-4}$	$(1.4007 \times 10^{-3}, 2.0405 \times 10^{-3})$
1	$c$	$1.5153 \times 10^{-4}$	$2.9689 \times 10^{-5}$	$(8.9972 \times 10^{-5}, 2.1310 \times 10^{-4})$
2	$\mu$	$9.8559 \times 10^{-1}$	$8.1785 \times 10^{-3}$	$(9.6863 \times 10^{-1}, 1.0025)$
2	$q$	$1.3542 \times 10^{-3}$	$1.7762 \times 10^{-4}$	$(9.8590 \times 10^{-4}, 1.7225 \times 10^{-3})$
2	$c$	$2.8005 \times 10^{-4}$	$4.1701 \times 10^{-5}$	$(1.9358 \times 10^{-4}, 3.6652 \times 10^{-4})$

(b) Parameter estimates, bootstrap standard errors, and bootstrap 95% confidence intervals (C.I.) for model D.

Replicate	Parameter	Estimate	Standard Error	95 % C.I.
1	$\mu$	$9.5051 \times 10^{-1}$	$8.7505 \times 10^{-3}$	$(8.8922 \times 10^{-1}, 9.2551 \times 10^{-1})$
1	$q$	$1.7206 \times 10^{-3}$	$2.3202 \times 10^{-4}$	$(2.0358 \times 10^{-3}, 2.9980 \times 10^{-3})$
1	$c$	$1.5153 \times 10^{-4}$	$2.3608 \times 10^{-5}$	$(-4.8952 \times 10^{-5}, 4.8953 \times 10^{-5})$
2	$\mu$	$9.8559 \times 10^{-1}$	$2.3660 \times 10^{-2}$	$(9.3715 \times 10^{-1}, 1.0355)$
2	$q$	$1.3542 \times 10^{-3}$	$3.2867 \times 10^{-4}$	$(6.8486 \times 10^{-4}, 2.0517 \times 10^{-3})$
2	$c$	$2.8005 \times 10^{-4}$	$9.7547 \times 10^{-5}$	$(8.3218 \times 10^{-5}, 4.8888 \times 10^{-4})$

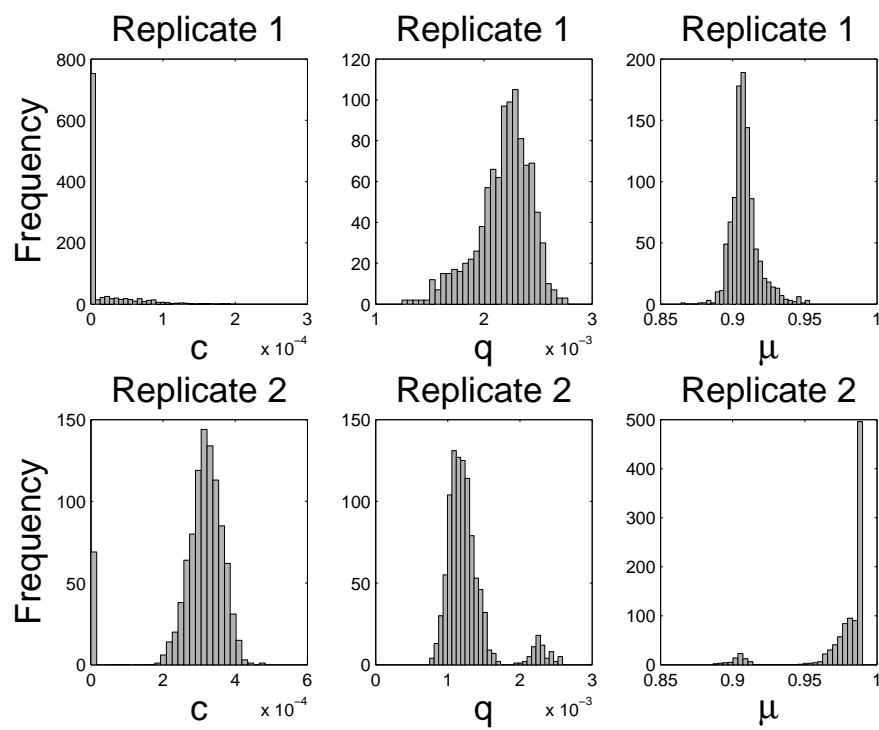


**Figure 3.9** The parameter distributions obtained from bootstrapping for each estimated parameter ( $\mu$ ,  $q$ ,  $c$ ) and each replicate for model D.

**Table 3.4** Our estimates for the observation standard errors are shown here. For example,  $\hat{\sigma}_{A,0}$  is what our uncertainty quantification returned as our best estimate for the standard deviation of the error seen in observing adult daphnids during data collection.

	Replicate 1					
Value	$\hat{\sigma}_{J,0}$	$\hat{\sigma}_{A,0}$	$\hat{\sigma}_{N,0}$	$1.96\hat{\sigma}_{J,0}$	$1.96\hat{\sigma}_{A,0}$	$1.96\hat{\sigma}_{N,0}$
Estimate	171.5502	81.1267	184.6778	336.2385	159.0082	361.9683
	Replicate 2					
Value	$\hat{\sigma}_{J,0}$	$\hat{\sigma}_{A,0}$	$\hat{\sigma}_{N,0}$	$1.96\hat{\sigma}_{J,0}$	$1.96\hat{\sigma}_{A,0}$	$1.96\hat{\sigma}_{N,0}$
Estimate	233.5445	91.6277	253.6872	457.7473	179.5904	497.2268

to make the solid black lines in Figures 3.10 and 3.11, we simulated our model using the parameter estimates  $\hat{\theta}$ . The data itself is shown as black open circles. Therefore, taking only the solid black lines and the open circles, you have a plot of simply our data and our model solutions with the estimated “true” parameter values.

The gray section in the top two plots of Figure 3.10 is the region  $f_J(t_j, \hat{\theta}) \pm \hat{\sigma}_{J,0}$  for each experimental replicate, and the gray section in the middle two plots of Figure 3.10 is the region  $f_A(t_j, \hat{\theta}) \pm \hat{\sigma}_{A,0}$  for each experimental replicate. These gray regions represent the 68 % confidence bands, since they represent one standard deviation away from the model solution. Similarly, the gray section in the top two plots of Figure 3.11 is the region  $f_J(t_j, \hat{\theta}) \pm 1.96\hat{\sigma}_{J,0}$  for each experimental replicate, and the gray section in the middle two plots of Figure 3.11 is the region  $f_A(t_j, \hat{\theta}) \pm 1.96\hat{\sigma}_{A,0}$ . These represent the 95 % confidence bands, as they represent 1.96 standard deviations away from the model solution. Table 3.4 shows the values for  $\hat{\sigma}_{A,0}$  and  $\hat{\sigma}_{J,0}$ , as well as the values  $1.96\hat{\sigma}_{A,0}$  and  $1.96\hat{\sigma}_{J,0}$ , for reference.

In order to make this plot for the total population, we assumed that we used only one observation, the total population  $N(t_j) = A(t_j) + J(t_j)$  at observation times  $t_j$ . Thus, our error model for the total population is now specified as

$$Y_j = f(t_j, \theta_0) + \mathcal{E}_j, \quad j = 1, 2, \dots, n$$

where  $Y_j$  is a random variable with realizations  $y_j = N(t_j)$  (i.e., the data),  $f(t_j, \theta_0) = f_N(t_j, \theta_0) = f_J(t_j, \theta_0) + f_A(t_j, \theta_0)$  is the discrete model solution with the hypothesized “true” parameter vector  $\theta_0$ , where  $f_N(t, \theta_0)$  is the total number of daphnids given by our model at time  $t$ . The error terms  $\mathcal{E}_j$  are assumed to be i.i.d random variables with mean zero and variance  $V_0 = \sigma_{N,0}^2$ . From uncertainty quantification using this new statistical error model we have an estimate for our observation error  $\hat{V}_0 = \hat{\sigma}_{N,0}^2$ .



**Table 3.5** The percentage (% accuracy) and fraction of observed data points that were contained in the 68 % confidence bands of our model solution. Results are shown for the number of juveniles, number of adults, and total population size for each replicate

Daphnid Classification	Replicate	% Accuracy	Fraction
Juvenile	1	80 %	20/25
Adult	1	68 %	17/25
Total	1	84 %	21/25
Juvenile	2	84 %	21/25
Adult	2	84 %	21/25
Total	2	92 %	23/25

Therefore, the gray section in the bottom two plots of Figure 3.10 is the region  $f_N(t_j, \hat{\theta}) \pm \hat{\sigma}_{N,0}$  for each experimental replicate. These gray regions represent the 68 % confidence bands, since they represent one standard deviation away from our model solution. The gray section in the bottom two plots of Figure 3.11 is the region  $f_N(t_j, \hat{\theta}) \pm 1.96\hat{\sigma}_{N,0}$  for each experimental replicate. These gray regions represent the 95 % confidence bands, since they represent 1.96 standard deviations away from the model solution. Table 3.4 shows the values for  $\hat{\sigma}_{N,0}$  and  $1.96\hat{\sigma}_{N,0}$  for reference.

Table 3.5 contains the obtained accuracy of our modeling effort using the 68 % confidence bands. This accuracy could be improved by generally improving our model, but shows that we are already able to generally capture the population dynamics. We see that the estimation of the total population was more accurate than estimating the adult or juvenile population separately. This speaks to our size classifications possibly being incorrect in our data, while our overall modeling is accurate. We know that the maximum size of daphnids decreases as the density of daphnids increases [76, 134, and the references within], an effect which we did not consider in our modeling effort. Incorporating that effect might fix the accuracy of our modeling for the size classes, and is an area for future work.

### 3.3.4 Parameter Sensitivities

We applied a sensitivity analysis to our best validated model (model D) to understand how changes in estimated parameters governing fecundity and survival affect population size and structure. We calculated the relative time-dependent sensitivity functions for juvenile, adult, and total population size (Figure 3.12) (calculations shown in Appendix B.2). Interestingly, we observed that the maximum total population size for our two replicates was achieved on day 19, dividing the population dynamics into two phases, which we call the “early phase” and the “late phase” (Figure 3.13). In the early phase ( $\leq 19$  days) of the population experiments, the population grows rapidly and exceeds its carrying capacity. In the late phase of the population experiments ( $> 19$  days), the total population size

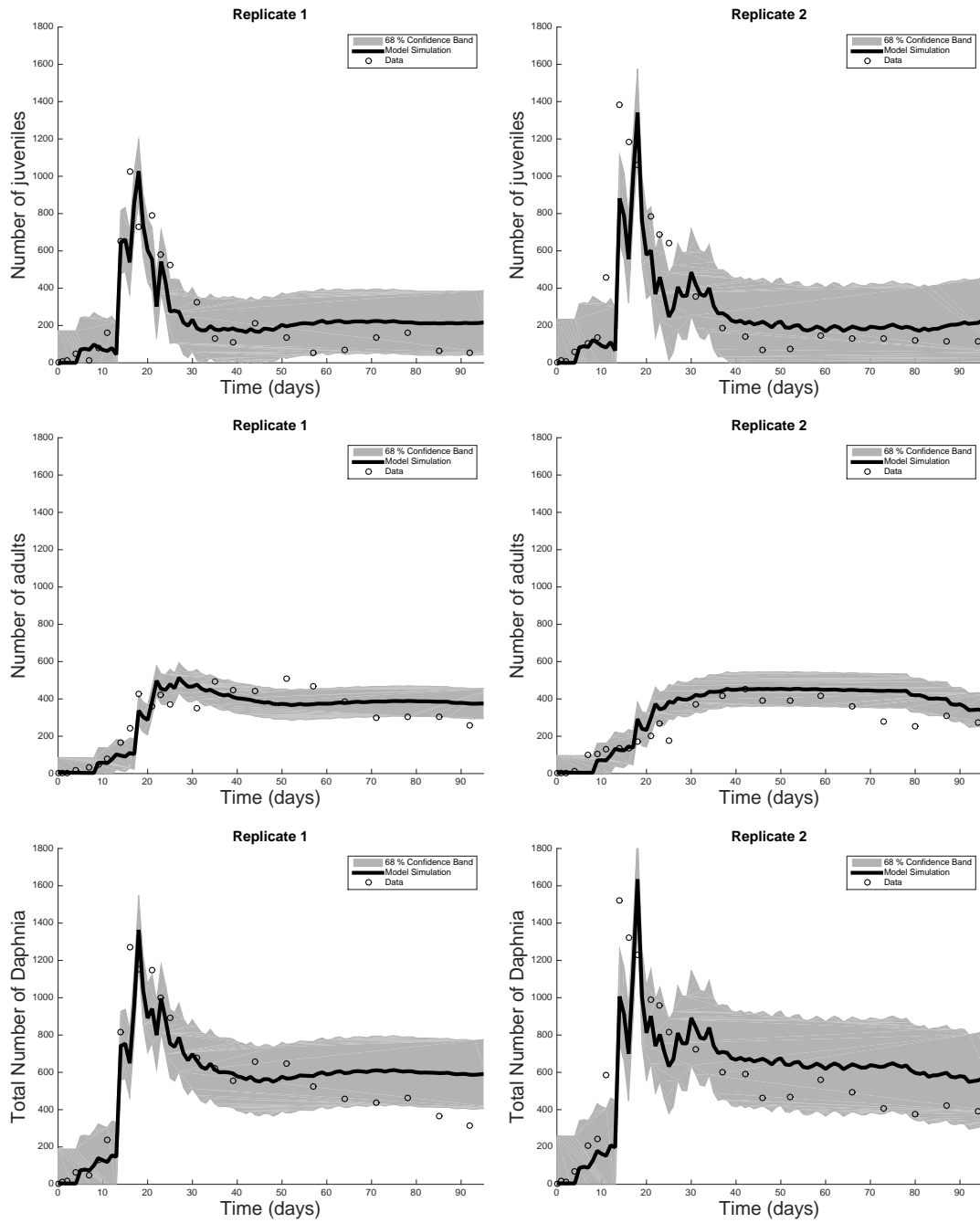


**Figure 3.10** Results from fitting our discrete daphnid population model to adult and juvenile longitudinal data. Black lines: model simulation results using parameter estimates. Black circles: our data. Gray region: 68 % confidence band, with the error coming from our statistical model, which assumes constant error.

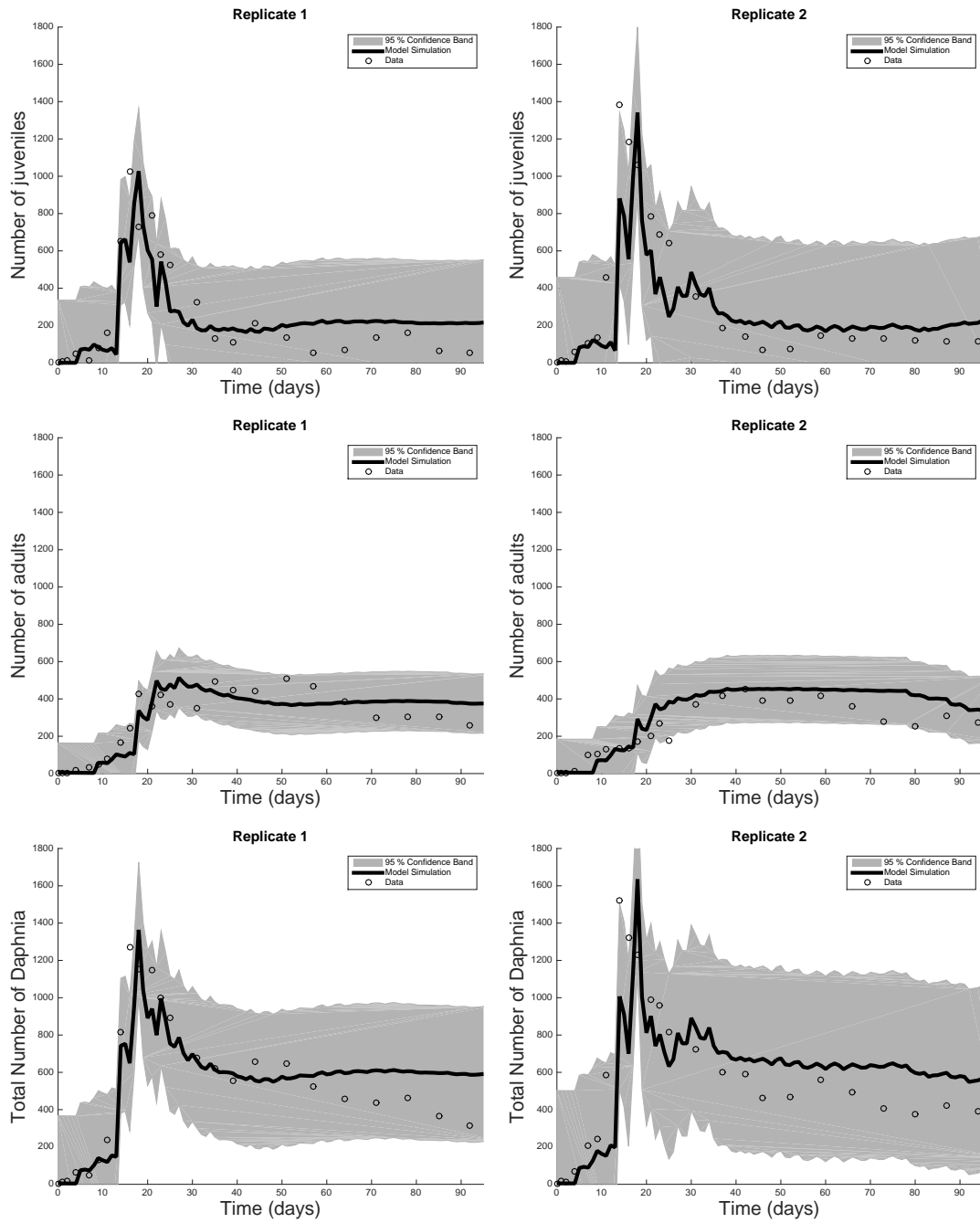


**Figure 3.11** Results from fitting our discrete daphnid population model to adult and juvenile longitudinal data. Black lines: model simulation results using parameter estimates. Black circles: our data. Gray region: 95 % confidence band, with the error coming from our statistical model, which assumes constant error.

converges towards steady state levels as an excess juvenile population rapidly dies off or progresses to the adult stage. Dividing our sensitivity analysis between these two phases revealed that the effect of increasing fecundity or survival is both temporally and life-stage dependent (Figure 3.14).

We found that the juvenile, adult, and total population sizes were most sensitive to changes in  $\mu$  in both the early and late phase as compared to the other estimated parameters  $q$  and  $c$ . The sensitivity analysis indicates that increasing the survival parameter  $\mu$  will increase the juvenile population in the early phase and decrease it in the late phase, whereas an increased  $\mu$  increases the adult population size in both the early and late phase. Although increased survival increases the total population size in the early phase, the late phase is much less sensitive. These findings suggest that increases in the survival parameter  $\mu$  will cause a shift in the population distribution towards the adult stage and that this shift mainly occurs during the early phase of population growth.

Our sensitivity analysis indicates that increasing  $q$ , the effect of density on fecundity, has a greater effect in the late phase of the population experiment than in the early phase for the juvenile, adult, and total population size. This result is expected, since a lower fecundity rate should lead to lower population sizes overall and within specific life stages. We hypothesize that the late phase is more heavily influenced by a decreased density-dependent fecundity rate than the early phase because of the time delayed effect. If so, this would imply that most of the offspring in the early phase are produced by female daphnids whose fecundity has not yet been effected by density.

Lastly, our sensitivity analysis indicates that increasing  $c$ , the effect of density on the survival of juveniles, leads to lower numbers of juveniles and adults, and a lower total population size in the early phase. This relationship is more pronounced in the late phase for both the number of adults and total population size. Unexpectedly, our sensitivity analysis indicates that increasing the parameter  $c$  can cause the number of juveniles to increase during the late phase of the population experiments.

Taken together, these findings suggest that a higher density-dependent juvenile survival probability can cause a shift towards juveniles in the equilibrium age distribution of daphnid populations, even though the total population size decreases overall. Our results highlight the importance of mathematical modeling to understand non-intuitive temporal shifts in the age distribution of daphnid populations that may occur under environmental conditions that increase competition, e.g., if the amount of algae decreases.

### 3.3.5 Parameter Correlation

We considered correlation in our parameter estimators using asymptotic ellipsoids (see Section 2.2.2.1 for details) for the parameters  $\theta = (\mu, q, c)$  for model D. We observed that for both replicates

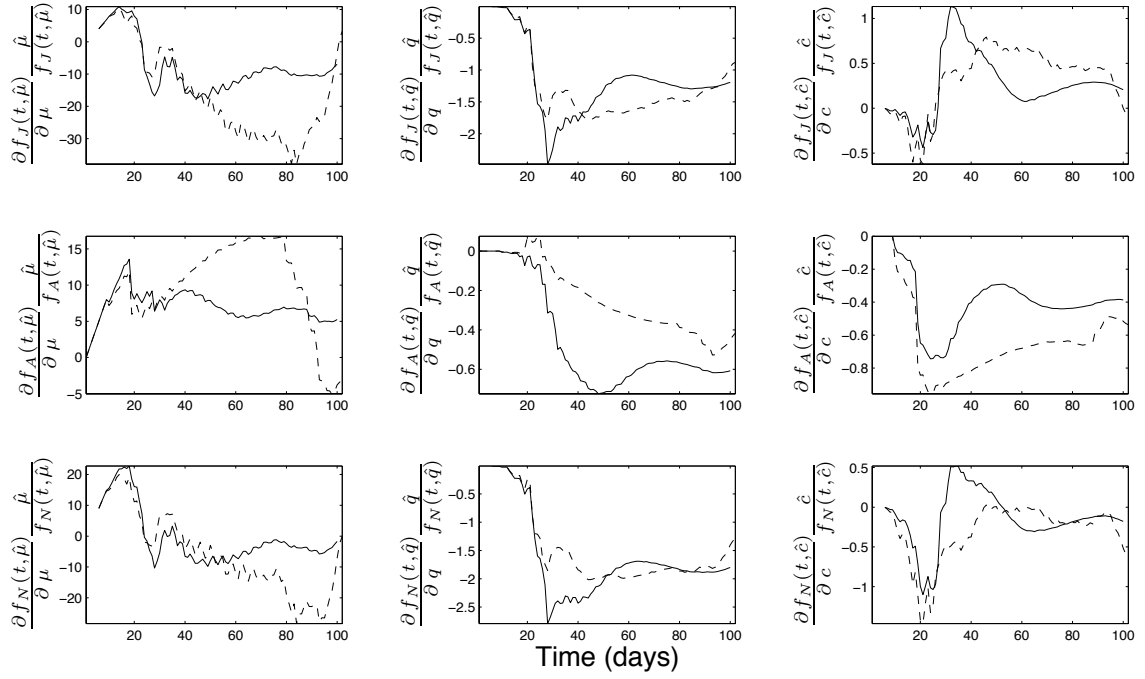


**Figure 3.12** The relative time-dependent sensitivities for juveniles, adults, and the total population with respect to each of the estimated parameters ( $\mu$ ,  $q$ ,  $c$ ) for model D. Sensitivities were calculated for the number of juveniles  $f_J(t, \hat{\theta})$  (top row), the number of adults  $f_A(t, \hat{\theta})$  (middle row), and the total population size  $f_N(t, \hat{\theta})$  (bottom row). The left column corresponds to  $\mu$ , the middle column to  $q$ , and the right column to  $c$ . Solid lines: Replicate 1. Dashed lines: Replicate 2.

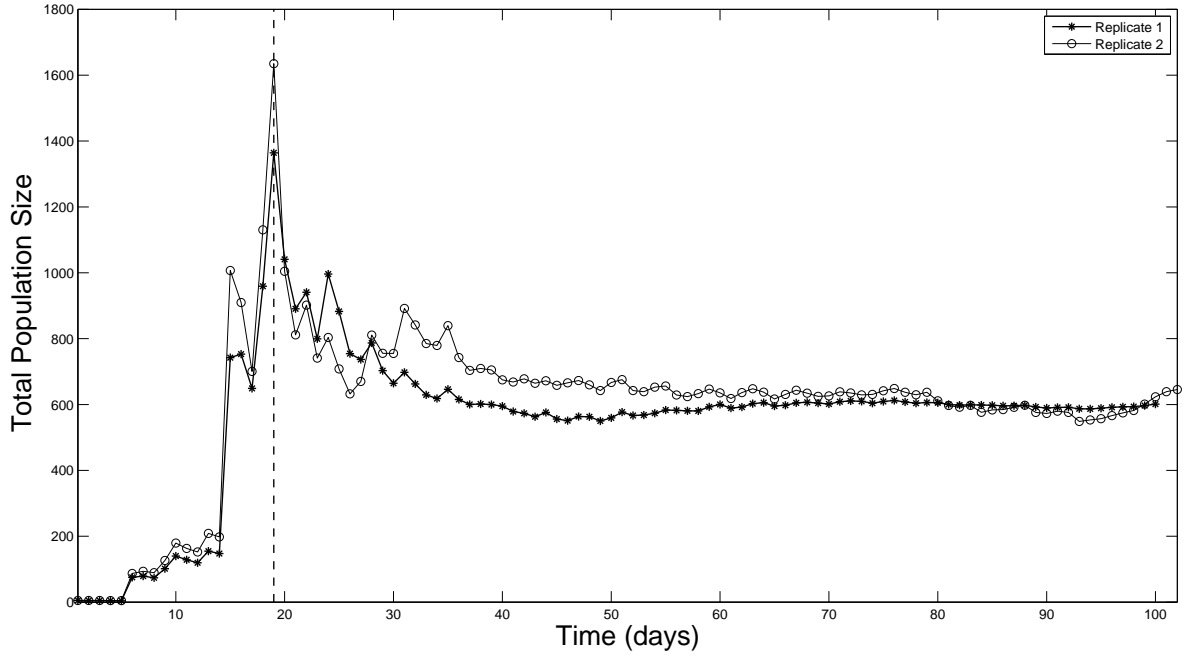


**Figure 3.13** Longitudinal data for the total population size for two population replicates. The vertical dashed line is at 19 days, and shows the division between the early phase and late phase dynamics.

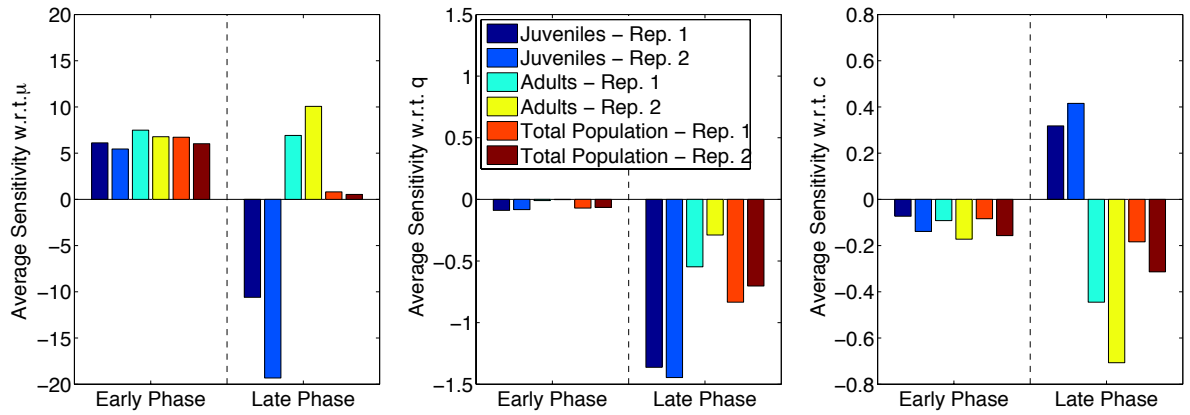


**Figure 3.14** The average of the relative sensitivities during the early and late phases for juvenile,  $J(t)$ , adult,  $A(t)$ , and total population,  $N(t)$ , counts with respect to the survival parameter,  $\mu$ , the effect of density on fecundity,  $q$ , and the effect of density on survival,  $c$ . Sensitivities are divided between the early phase of the population experiments (before the peak size is reached on day 19) and the late phase (after day 19).

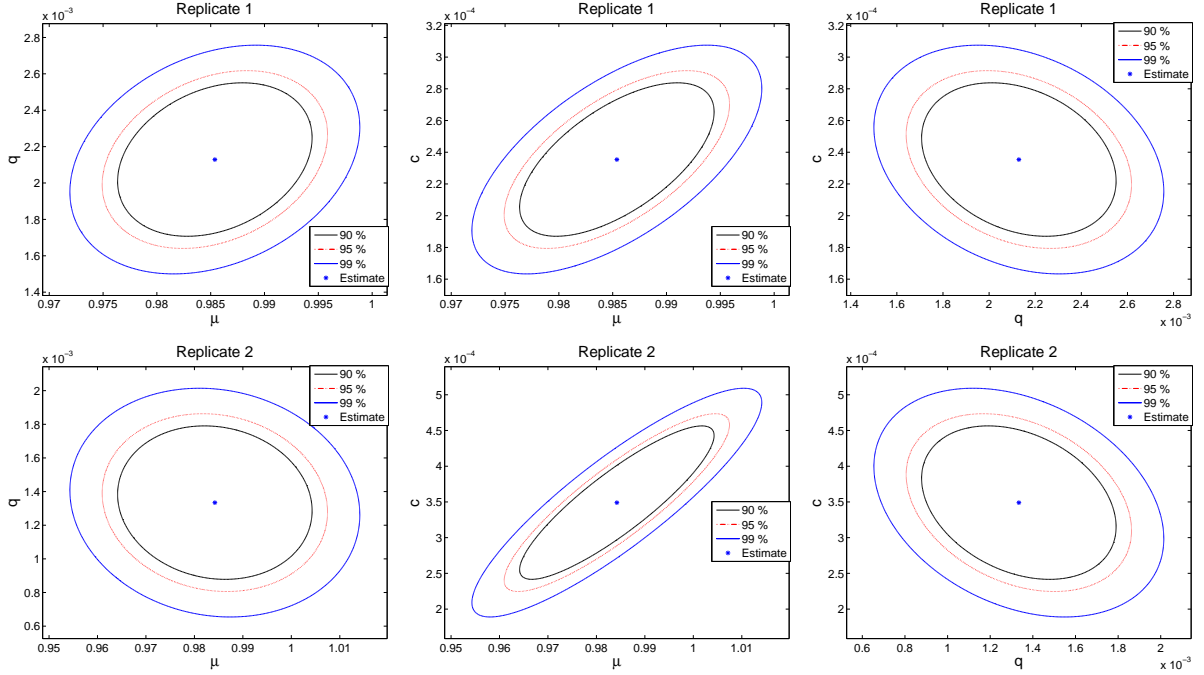


**Figure 3.15** These are the asymptotic confidence ellipsoids for the parameters in model D. In each figure, the solid black line corresponds to the 90% confidence ellipsoid, the dash-dot red line corresponds to the 95% confidence ellipsoid, and the solid blue line corresponds to the 99% confidence ellipsoid. The top row of figures correspond to Replicate 1, while the bottom row correspond to Replicate 2.

the estimators for  $\mu$  and  $c$  are correlated (Figure 3.15). Upon inspection of our model equations for model D (Equation (3.1) with parameters from Table 3.1) we see that  $b(t, i)$  is a function of  $\mu$  and  $c$ , where  $\mu$  is multiplied by a function of  $c$ . What we see in our ellipsoids is that  $\mu$  can compensate for a change in  $c$  in that term. At this point we don't consider a reparametrization of the model, as we believe that other improvements to the model will correct this correlation (see Section 3.4).

### 3.4 Conclusions and Discussion

We tested several hypotheses concerning the significance of several biological assumptions in describing daphnid populations with a structured population model. One assumption we evaluated, delayed density-dependent fecundity, had been suggested previously [76, 133]. Importantly, this hypothesized mechanism was not quantitatively verified due to a lack of statistical comparison tools at the time they were proposed. We applied a  $\chi^2$  based model comparison test and found strong statistical evidence for a time delay in density-dependent fecundity. We also found statistical evidence

for the assumption that intraspecific competition mainly affects juvenile daphnids, previously suggested in [56, 75, 132, 134]. Lastly, we determined that the effect of density on daphnid demographics is more accurately modeled as a function of total population length, rather than total population number [76, 139]. Our findings indicate that the assumptions we investigated can improve the accuracy of future daphnid population modeling efforts and may provide increased accuracy in other daphnid models which may not have considered all of these assumptions [67, 68, 71, 73, 76, 134].

We found that parameterizing the density-independent components of demographic rates with individual-level data enabled the estimation of density-dependent parameters from aggregate structured population data. The most complex density-independent component that we discovered was for daphnid fecundity (Figure 3.3). Our data revealed a clear periodic pattern in the timing of offspring production in which daphnids begin releasing neonates at 9-days-old. Notably, the maximum offspring production rate is significantly higher in the first 4 broods than in subsequent broods ( $P = 0.0011$ , Mann-Whitney U-test). To the best of our knowledge, fecundity oscillations with a consistent frequency and time-dependent amplitude has not previously been observed for daphnids. We note that without employing individual-level time-dependent fecundity data, our attempts to fit daphnid population data gave extremely poor results (data not shown). We suspect that the collection of similarly precise individual-level data will be necessary to parameterize structured models from field data of daphnid populations. For example, daphnids could be sampled in the field and cultured/observed under experimental conditions similar to their natural environment. Alternatively, one may be able to employ computational methods designed to estimate time-dependent rates from aggregate data alone [14, 18–20, 24, 25, 28, 39]. However, these methods have only been previously applied to density-independent structured population models, and thus they remain largely untested and underdeveloped in density-dependent scenarios.

An underlying challenge in performing hazard assessments is to generate a highly repeatable baseline control for comparison. For our best validated model (Model D), the parameter estimates, uncertainty quantification, temporal variations in sensitivity patterns, and overall degree of accuracy to the data were all extremely similar between replicates (Figures 3.13 and 3.14, Tables 3.3 and 3.5). These results highlight the need for comprehensively evaluating biological assumptions about daphnid populations grown under non-stressed environmental conditions, i.e., the control case. Our results also suggest the need for further improvement, which can be seen since Model D underestimated the early phase ( $\leq 19$  days) growth rate and the time at which the peak size was reached for the juvenile population in the second replicate. One possible adjustment that may increase the accuracy of model D is to incorporate an age-dependent daphnid survival probability. From our sensitivity analysis, we infer that increasing the juvenile survival probability will likely remedy the underestimation of the early phase growth rate (Figure 3.14). For simplicity, we assumed



a constant parameter  $\mu$  for the density-independent survival probability in the modeling efforts reported here; however, this assumption is thoroughly investigated in the next chapter where we explore finding an age-varying function for  $\mu$ . Such an age-varying function, if found prior to any parameter estimation on the population level (as  $\alpha(t)$  was in this section), would hopefully also correct issues of correlation in estimators seen between  $\mu$  and  $c$ .

# Estimation of Age-Varying Mortality Rates for *Daphnia magna*<sup>1</sup>

## 4.1 Introduction

The most widely used structured population models in ecology are those in which the structured variable is discrete, i.e., a Leslie matrix model [3, 43, 50, 52, 108, 149]. In such discrete models, one typically assumes (i) constant parameter rates, (ii) that individuals can be lumped into discrete classes, and (iii) that time can be divided into discrete intervals. Although these model attributes enable fast computation and the application of tools for steady state analysis, they can also lead to instabilities in the data fitting process [18, 164]. Moreover, computation with discrete models can become intractable when using more realistic time-dependent parameters rather than constant parameters. As an alternative approach, it has previously been suggested that the Sinko-Streifer population model, which uses partial differential equations (PDEs) with a continuously structured variable, is more amenable to describing age-varying parameters and that its use significantly increases accuracy in fitting population data [11, 42].

In the previous chapter we developed a comprehensive discrete-time structured population model to describe the population growth of *Daphnia magna*, and analyzed ways in which the model could be improved. We determined that our assumptions of constant mortality and a discrete model

---

<sup>1</sup>Published in altered form as [4]

### Contributions:

Literature review and preliminary analysis: Kaska Adoteye and Kevin Flores

Model design, implementation, and analysis: Kaska Adoteye

Writeup: Kaska Adoteye, H.T. Banks, and Kevin Flores

Advisors: H.T. Banks and Gerald A. LeBlanc

could be called into question. In this chapter we compare the accuracy of a discrete matrix model versus a differential equation model in describing density-independent survival data for *Daphnia magna*. With both models we also tested the accuracy of using constant versus age-varying parameters, and we show that a differential equation model with age-varying parameters best describes our daphnid survival data. This work paves the way for the construction of a validated continuously structured population model for daphnids, which we expect will provide an improvement to previously published models [71, 76, 84, 134, 137], as well as the model in Chapter 3.

## 4.2 Data and Methods

### 4.2.1 Density-independent *Daphnia magna* survival data

Ninety daphnids were longitudinally observed and survival was recorded daily. All daphnids were maintained in individual isolation using previously described protocols and conditions [157]. The daphnids were kept in media reconstituted from deionized water [10] and maintained in an incubator at 20 degrees celsius with a 16-h light, 8-h dark cycle. The daphnids used in our study came from a colony that was maintained at North Carolina State University for over 20 years (clone NCSU1 [138]). Less than 2-h old female neonates were placed individually each into 50mL beakers containing 40mL of media which was changed daily. Daphnids were fed daily with  $7.0 \times 10^6$  cells of algae (*Raphidocelis subcapitata*) and 0.2 mg (dry weight) Tetrafin<sup>TM</sup> fish food suspension prepared as described previously [124]. Each beaker was checked daily for the presence of new offspring and these neonates were removed daily. The ninety daphnids came from three equally sized groups: thirty daphnids were constantly exposed to media containing .2  $\mu$ L of a .3nM concentration of pyriproxyfen/40 mL media ("Pyriproxyfen + Carrier" group), thirty daphnids were constantly exposed to media containing .2  $\mu$ L ethanol/40 mL media ("Carrier" group), and thirty daphnids were not treated with any chemicals ("No treatment" group). The amount of ethanol used in the carrier group is the amount that was used to dilute the pyriproxyfen for the "Pyriproxyfen + Carrier" group. Since no statistically significant difference in survival was found between the three daphnid groups (see Section 4.3 below), data from all three groups were combined into a single data set for ninety daphnids ("Combined" group) for all analysis in this chapter.

#### 4.2.2 Mathematical models

To test the accuracy of continuous models for describing daphnid survival data, we used a density-independent form of the Sinko-Striefer PDE model [144]:

$$\begin{aligned} u_t(t, x) + (g(t, x)u(t, x))_x &= -\mu(t, x)u(t, x) \\ g(t, x_0)u(t, x_0) &= \int_{x_0}^{x_1} k(t, \xi)u(t, \xi)d\xi, \end{aligned}$$

where  $x_0$  is the minimum age (0 days) and  $x_1$  is the maximum age (the maximum observed age was 91 days). The state variable  $u(t, x)$  is the population density at age  $x$  and time  $t$ ,  $g(t, x)$  represents the rate at which daphnids age,  $\mu(t, x)$  is the mortality rate, and  $k(t, x)$  is the fecundity rate. The individual-level survival data in the combined data set were time shifted so that the age of all the daphnids was zero at time zero. Hence, age and time progress at the same rate in the survival data and  $g(t, x) \equiv 1$ . We also assume that  $k(t, x) \equiv 0$  since newly born neonates were removed daily. This allows us to simplify our PDE model to

$$\begin{aligned} u_t(t, x) + u_x(t, x) &= -\mu(t, x)u(t, x) \\ u(t, x_0) &= 0. \end{aligned}$$

Using the method of characteristics with  $t(s) = x(s) = s$ ,  $\tilde{u}(s) = u(t(s), x(s))$ , and  $\tilde{\mu}(s) = \mu(s, s)$ , we can show that the PDE can be written

$$\begin{aligned} \frac{d\tilde{u}}{ds} &= -\tilde{\mu}\tilde{u}, \\ \tilde{u}(s_I) &= 90, \end{aligned}$$

where  $s_I = t_I$  is the time at which the initial 90 daphnids (neonates) are introduced. This model was simulated using *ode45* in Matlab with default options. To test the accuracy of discrete models for describing daphnid survival data, we also used the Leslie matrix model in Equation (3.1) with  $a(t, i) \equiv 0$ ,  $b(t, i) \equiv \tilde{\mu}$ , and  $i_{max} = 91$ .

#### 4.2.3 Inverse problem methodology

In order to estimate  $\tilde{\mu}$ , we employed an ordinary least squares framework that is widely used to estimate model parameters from data [31, 39]. This technique, under well known assumptions on the statistical error model of the data observations, is equivalent to maximum likelihood estimation

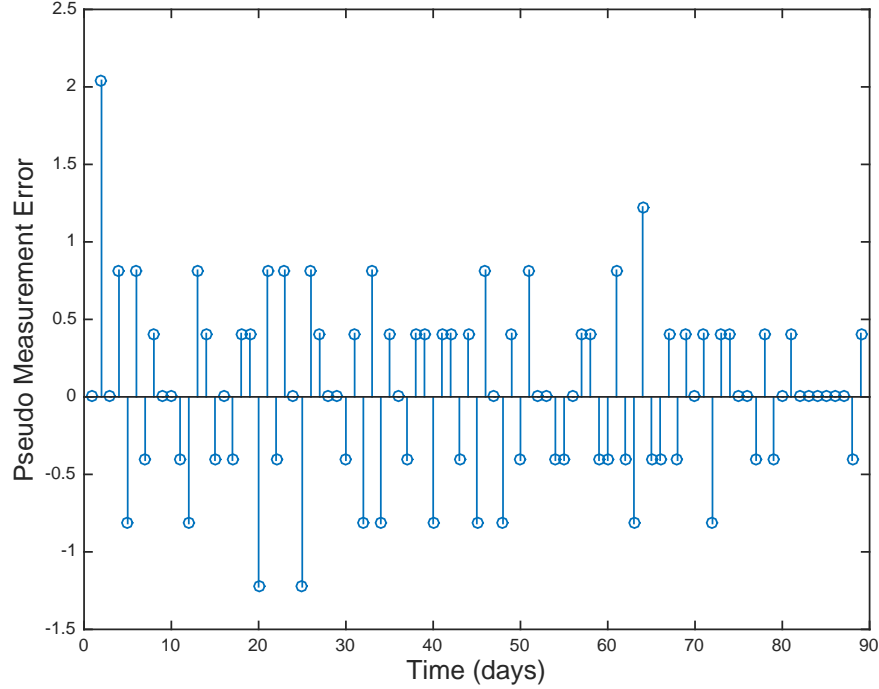


**Figure 4.1** This is the pseudo measurement error based on second-order differencing of the data shown in Figure 4.2 using Equation (3.4).

[31, 39]. Formally, this technique minimizes the residual sum of squares

$$J(\tilde{\mu}) = \sum_{i=1}^n (\tilde{u}(s_i; \tilde{\mu}) - y_i)^2$$

where  $y_i$  is data for the number of living daphnids at time  $s_i$  and  $n$  is the number of data points. For more information on this estimation framework, see [31, 39].

In order to determine the error structure in our statistical model we used a difference-based test. Specifically, we used Equation (3.4) with  $\gamma = 0$  (which gives a second-order differencing of the data) to plot the pseudo measurement error and found that it resembled white noise with mean zero (Figure 4.1). Since the pseudo measurement errors produced white noise, we can assume that the error variance in our statistical model is constant. For more information on this technique, consult Section 3.2.5 as well as [36, 114, 155] and the references therein.

For both the Leslie and PDE models we used multiple forms of  $\tilde{\mu}$ . To model a constant mortality rate, we used  $\tilde{\mu} \equiv \bar{\mu}$  for some constant  $\bar{\mu}$ . To model an age-dependent mortality rate, we described

$\tilde{\mu}$  using a linear spline function for the PDE model and a step function for the Leslie model (a step function was used to provide a discretized version of a linear spline). That is, for the Leslie model we used

$$\tilde{\mu}(t) = \sum_{j=1}^M \hat{\mu}_j \chi_{A_j}(t)$$

and for the PDE model we used

$$\tilde{\mu}(t) = \sum_{j=1}^M \alpha_j \ell_j(t)$$

where  $\hat{\mu}_j$  and  $\alpha_j$  are parameters to be determined,  $\ell_j(t)$  are the standard linear spline functions,  $\chi_A$  is the indicator function,  $A_j$  are evenly spaced intervals over the domain, and the number of nodes  $M$  depends solely on the number of data points and  $m$ , the length of the interval used.

The inverse problems here were computed using two routines in Matlab. The first routine is a direct search algorithm implemented by Daniel Finkel as *direct*, and can be found at [http://www4.ncsu.edu/~ctk/Finkel\\_Direct/](http://www4.ncsu.edu/~ctk/Finkel_Direct/). This was used with the following options: `options.maxevals = 2000`; `options.maxits = 1000`; `options.maxdeep = 400`; and the output was used as the initial condition for the gradient based Matlab search routine *lsqnonlin*. *lsqnonlin* was run with the options ‘TolFun’ and ‘TolX’ set equal to  $1e-20$ , the option ‘MaxFunEvals’ set equal to 4000, and the option ‘MaxIter’ set equal to 2000. The output of *lsqnonlin* was then used as our parameter estimate.

#### 4.2.4 Model comparisons

We used the corrected Akaike Information Criterion ( $AIC_C$ ) score described in Section 3.2.6.2 to compare the accuracy of different models to the combined survival data set for ninety daphnids. We simulated the Leslie model with age-varying mortality with interval lengths  $m \in ([4, 15] \cap \mathbb{N}) \cup \{20, 25, 30, 40\}$  and constant mortality. We also simulated the PDE model with mortality described by a linear spline with interval lengths  $m \in ([4, 15] \cap \mathbb{N}) \cup \{20, 25, 30, 40\}$  and constant mortality. We note that we also determined which interval length (and thus which number of nodes) to use for the linear spline and step functions by seeing which value of  $m$  gave the lowest  $AIC_C$  score.

### 4.3 Results

To test the accuracy of several mathematical models to daphnid survival data, we first generated an experimental data set consisting of survival numbers for ninety daphnids. We used a log-rank test on the Kaplan-Meier survival distributions [93] from the “No treatment”, “Carrier”, and “Pyriproxyfen + Carrier” data sets (Figure 4.2, left) to determine if there was a statistically significant difference

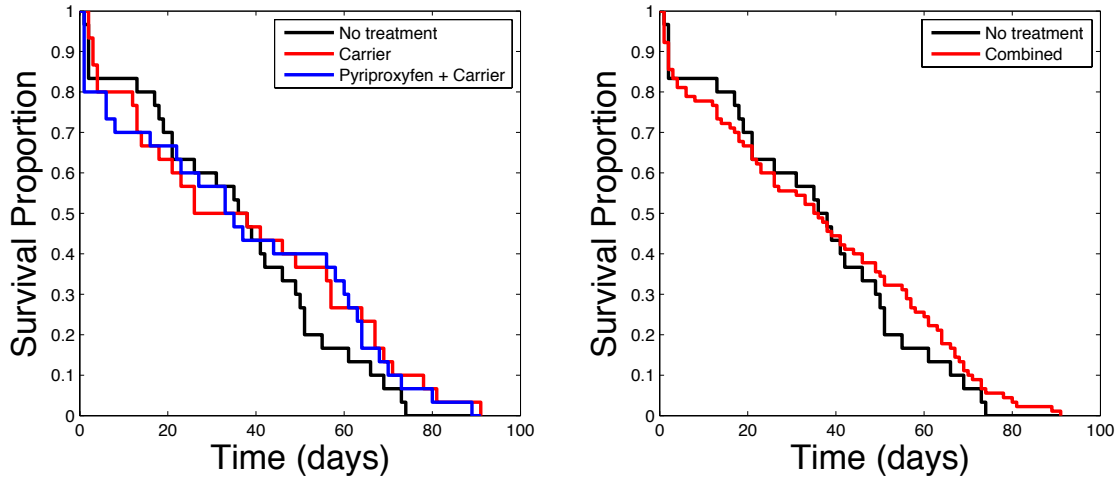


**Figure 4.2** Left: The proportion of surviving daphnids from three groups: no exposure (No treatment), exposure to ethanol (Carrier), or exposure to pyriproxyfen and ethanol (Pyriproxyfen + Carrier). Right: The proportion of surviving daphnids from the no exposure group (No treatment) and the combined set of daphnids from all three groups (Combined).

in mortality between the three corresponding experimental groups. The Kaplan-Meier method provides an estimate of the survival distribution for each experimental group, and the log-rank test is a hypothesis test for the null hypothesis that there is no difference between these distributions [129]. The log rank test shows that the null hypothesis cannot be rejected for the “No treatment” vs “Pyriproxyfen + Carrier” groups ( $P = 0.3783$ ), for the “Pyriproxyfen + Carrier” vs “Carrier” groups ( $P = 0.7335$ ), nor for the “Carrier” vs “No treatment” groups ( $P = 0.7657$ ). This suggests that *there is no statistically significant difference in mortality between any of the three groups*. Similarly, we found no statistical difference between the “No treatment” and “Combined” groups (Figure 4.2, right,  $P = 0.4725$ ). Hence, we used the “Combined” group data set for all subsequent analysis in this chapter.

It was found that the optimal interval length for the age-varying mortality was 4 for the Leslie model and 8 for the PDE model based on  $AIC_C$  scores (Table 4.1). For both the PDE and Leslie models, a constant mortality rate drastically misrepresented the decline in the daphnid population at most ages, while an age-varying mortality rate was better able to capture the survival dynamics at all ages (see Figure 4.3). The  $AIC_C$  values for the Leslie model with constant and age-varying mortality rates (using an interval length of 4) were 327.12 and 30.71, respectively. The  $AIC_C$  values for the PDE model with constant and age-varying mortality rates (using an interval length of 8) were 329.38 and 3.71, respectively. These results confirm that the Sinko-Streifer model with an age-varying mortality rate provides the best fit to the daphnid survival data.

**Table 4.1** The  $AIC_C$  values for the Leslie model and PDE model using age-varying mortality with different interval lengths for the step function (for the Leslie model) and linear splines (for the PDE model)

Interval Length $m$	Leslie	PDE
4	30.7082	125.3541
5	61.6638	284.0119
6	83.9913	365.5346
7	103.6066	75.9273
8	118.0614	3.7118
9	133.3344	11.4706
10	150.0257	31.6695
11	155.8002	67.3963
12	162.8165	88.9536
13	165.7076	101.6404
14	171.7227	108.2198
15	173.7451	117.2300
20	183.9520	140.2571
25	204.6359	152.6786
30	202.9819	157.2818
40	251.9403	176.6617

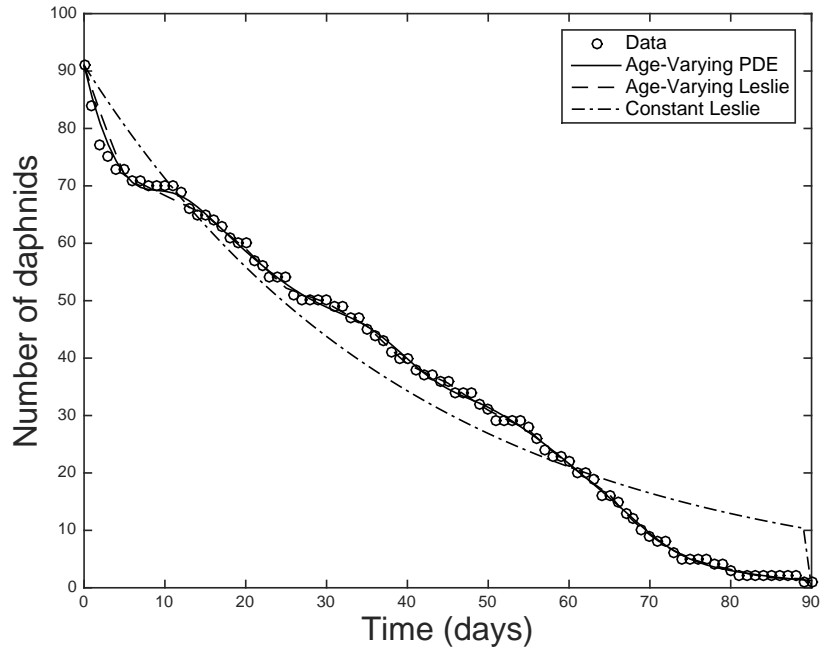


**Figure 4.3** Results from fitting different functional forms for the mortality rate in the PDE and Leslie models.



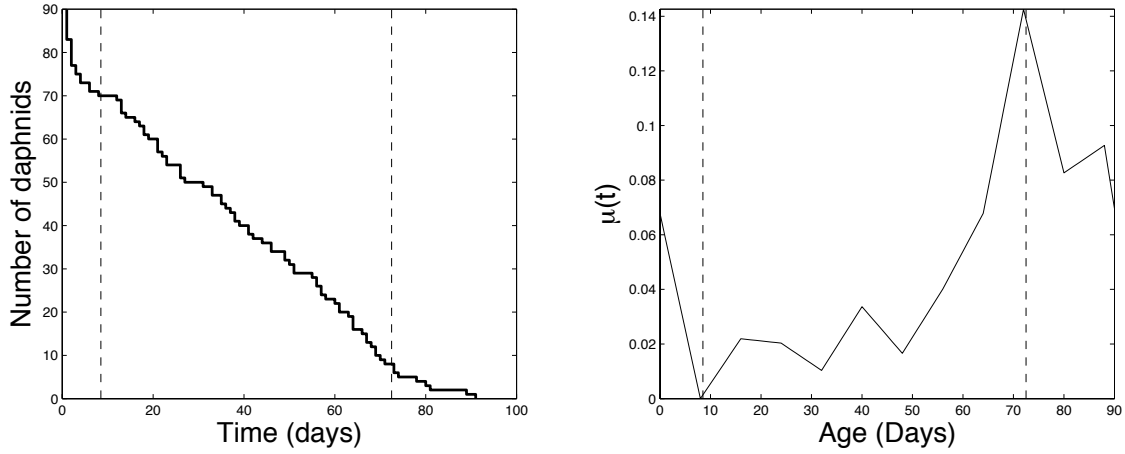


**Figure 4.4** Left: Daphnid survival data. Right: The estimated age-varying mortality function  $\tilde{\mu}(t)$  for the Sinko-Streifer model using linear splines. Both plots are shown with dashed vertical lines representing the division between three possible subpopulations.

## 4.4 Discussion

As seen in this study (Figure 4.3), a constant mortality model will overestimate survival in the first 11 days, underestimate survival between days 11 and 60, and overestimate survival after 60 days, while an age-varying rate can accurately capture the changing survival dynamics. The non-monotone form of the estimated linear spline function for  $\tilde{\mu}(t)$  suggests that the set of daphnids we observed might be composed of at least three subpopulations (Figure 4.4). The first subpopulation experiences rapid mortality, dying within 8 days. The second subpopulation experiences gradual mortality at a logistic rate within 72 days. The third subpopulation lives up to 90 days. The mortality seen in these subpopulations cannot accurately be described by a constant mortality rate, and thus, in addition to providing more accurate fits to the data, we suggest that an age-varying mortality rate might also be used to capture the distribution of mortality rates among a population. In theory, age-varying mortality rate distributions can be estimated from our daphnid survival data using continuous structured population models and a Prohorov metric estimation framework [39]. This framework has previously been used to estimate growth rate distributions from longitudinal size-structured data for shrimp and mosquitofish populations [17–19, 24, 25].

The improved performance of the Sinko-Streifer model over the Leslie model in describing density-independent survival data confirms similar results previously seen for other species [11]. We postulate that incorporating age-varying mortality rates into a density-dependent population model

for *Daphnia magna* might enable more accurate descriptions of density-dependent population data by improving the biological assumptions and allowing for better integration of organismal-level data.

# Determining Delay on Density-Dependent Effect on Fecundity from Experimental Data of *Daphnia magna*, and Ramifications for Future Modeling<sup>1</sup>

## 5.1 Introduction

The dependence of organismal biological outcomes in *Daphnia magna* on the density of other daphnids in proximity is a phenomenon that has been well studied ([3, 56, 81, 134] and the references therein). In Chapter 3 we have shown that not only is the inclusion of density-dependent terms necessary in population-level models for *Daphnia magna*, but also that for fecundity those density-dependent terms need to be delayed. This corroborates what has been previously postulated by other experimenters [76, 133]. Despite this, recent models do not include a delay in the density-dependent effect on fecundity (e.g., [134]), and still others do not include density-dependence at all (e.g., [71]).

While a density-dependent effect on mortality has been discussed [56, 76, 133, 134] to the best of our knowledge there has been no discussion of a delay in such an effect. Through experimentation

---

<sup>1</sup>Contributions:

Continuous model and experimental design: Kaska Adoteye and Kevin Flores

Data collection: Kaska Adoteye, Robert Baraldi, Kevin Flores, Amanda Laubmeier, and Michael Stemkovski

Analysis and writeup: Kaska Adoteye

Advisor: H.T. Banks

we provide evidence for a delayed density-dependent effect on mortality in *Daphnia magna*. This experimentation used daphnids raised in densities no greater than 10 daphnids/beaker, which contrasts the investigation we performed in Chapter 3 which contained uncontrolled daphnid populations. In this experiment we will have four groups of daphnids, with two groups raised in an uncrowded environment and two groups raised in a crowded environment. Partway through the experiment we will switch the density of one crowded group to be uncrowded, and one uncrowded group to be crowded. We will then use the time it takes for those switched daphnids' fecundity and mortality to revert to that of daphnids constantly reared in crowded and uncrowded conditions to determine the delay, if any.

The work of this chapter was motivated by our initial attempt to transform our discrete population model into a continuous model based on evidence from Chapter 4 that such a transformation would improve our results. Section 5.2 provides a thorough treatment of our continuous model and our attempt to recreate our analysis from Chapter 3 that led us to our initial estimates of the delay in the density-dependent effect on fecundity. This leads to inconclusive results, and thus we designed experiments to try and estimate the delay directly from lower density data. Section 5.3 outlines the experiment that we performed, as well as our attempts to model the data from that experiment. The results of this modeling are given in Section 5.4. In Section 5.5 we discuss in detail our findings from this chapter, as well as a suggestion for future daphnid modeling.

## 5.2 Continuous Model

Our continuous model is an extension of the density-dependent form of the Sinko-Streifer PDE model [144] used in Chapter 4:

$$\begin{aligned}\frac{\partial u(t, a)}{\partial t} + \frac{\partial u(t, a)}{\partial a} &= -\mu_{ind}(a)\mu_{dep}(a, M(t))u(t, a) \\ u(t, 0) &= \int_0^{a_{max}} k_{ind}(s)k_{dep}(M(t-\tau))u(t, s)ds\end{aligned}$$

where  $a_0$  is the minimum age of daphnids (0 days) and  $a_{max}$  is the maximum age of daphnids. The state variable  $u(t, a)$  is the population density of daphnids at age  $a$  and time  $t$ ,  $\mu_{ind}(a)$  is the previously determined density-independent mortality rate (Figure 4.4), and  $k_{ind}$  is the previously determined density-independent fecundity rate (Figure 3.3). The density-dependent mortality rate is given by

$$\mu_{dep}(a, M(t)) = 1 + \frac{c_1 M(t)^{h_1}}{c_2^{h_2} + M(t)^{h_1}} \frac{c_3^{h_2}}{c_3^{h_2} + a^{h_2}}$$

and the density-dependent fecundity rate is given by

$$k_{dep} = \frac{q^{h_3}}{q^{h_3} + M(t - \tau)^{h_3}}.$$

Our population length function  $M(t)$  is given by

$$M(t) = \int_0^{a_{max}} u(t, s) \frac{K Z_0 e^{rs}}{K + Z_0 (e^{rs} - 1)} ds,$$

where  $K$ ,  $r$ , and  $Z_0$  have been previously determined (mean values from Table 3.2).

Parameters were estimated from the population data using a vector ordinary least squares (OLS) framework [31, 39]. For each model, we consider a vector of parameters  $\theta$  to estimate. Based on our individual level modeling, the number of juveniles and adults are given by  $f_J(t, \theta) = \int_{a_0}^4 u(t, s) ds$  and  $f_A(t, \theta) = \int_4^{a_{max}} u(t, s) ds$ , respectively. The corresponding observation vector is given by  $\mathbf{f}(t, \theta) = [f_J(t, \theta), f_A(t, \theta)]^T$ . We assumed a constant statistical error model, as verified in Section 3.3.2, of the form

$$\mathbf{Y}_j = \mathbf{f}(t_j, \theta_0) + \mathcal{E}_j, \quad j = 1, 2, \dots, n,$$

where  $\mathbf{Y}_j$  is a random variable with realizations  $\mathbf{y}_j = [J(t_j), A(t_j)]^T$  (i.e., the data, where  $J(t_j)$  and  $A(t_j)$  are the number of juveniles and adults, respectively, at time  $t_j$ ) and  $\mathbf{f}(t_j, \theta_0)$  is the model observation with the hypothesized “true” parameter vector  $\theta_0$ . The error terms  $\mathcal{E}_j$  are assumed independent and identically distributed (i.i.d) random variables with mean  $E[\mathcal{E}_j] = 0$  and  $V_0 = \text{var}(\mathcal{E}_j) = \text{diag}(\sigma_{J,0}^2, \sigma_{A,0}^2)$ , where  $\sigma_{J,0}^2$  and  $\sigma_{A,0}^2$  are the observation variances for the juvenile and adult observations, respectively. An estimate  $\hat{\theta}$  for the true parameter vector  $\theta_0$  is obtained by implementing an iterative algorithm (see [39] for details). The population data used is the same population data from Chapter 3.

The inverse problems were computed using two routines in Matlab. The first routine is a direct search algorithm implemented by Daniel Finkel as *direct*, and can be found at [http://www4.ncsu.edu/~ctk/Finkel\\_Direct/](http://www4.ncsu.edu/~ctk/Finkel_Direct/). This was used with the following options: options.maxevals = 400; options.maxits = 400; options.maxdeep = 400; and the output was used as the initial condition for the gradient based Matlab search routine *lsqnonlin*. *lsqnonlin* was run with the options ‘TolFun’ and ‘TolX’ set equal to 1e-20, and the option ‘MaxFunEvals’ set equal to 400. The output of *lsqnonlin* was then used as our parameter estimate. It should be noted that this method for parameter estimation is exactly the continuous analogue to what was performed in Chapter 3. The model itself was simulated using *hpde* [143] in Matlab (code for *hpde* can be downloaded from <http://faculty.smu.edu/shampine/current.html>).

Similar to Chapter 3, we first estimated the delay  $\tau$  for this model from the population-level data given in Chapter 3. We estimated the model's parameters using values for  $\tau \in \{0, 1, 2, \dots, 13\}$  and investigated the least squares cost from those parameter estimations. The value for  $\tau$  that produces the lowest least squares cost would be considered the delay. Unlike in Chapter 3, there was gross inconsistency between the optimal delays found for each replicate (the optimal delay for one replicate was 2, and for another replicate was 13). Because of this inconsistency, we developed an experiment from which we could determine the delay directly. That experiment, and the proceeding analysis, are detailed below.

## 5.3 Data and Methods

### 5.3.1 Experimental Design and Data

Before the experiment began we raised female daphnids in two densities based on preliminary experiments: 40 daphnids per liter (termed "uncrowded mothers") and 100 daphnids per liter (termed "crowded mothers"). The offspring for these mothers were checked every other day to see if there were enough neonates to begin the experiment; if there were, then the experiment began, and if not then the offspring were discarded.

The experiment consisted of four groups of female daphnids (termed Groups 1 - 4). The daphnids in Groups 2 and 3 were born from the uncrowded mothers and the daphnids in Groups 1 and 4 were born from the crowded mothers. Groups 1 and 4 were started 3 days after Groups 2 and 3, based on when the mothers gave birth to enough offspring. The age of all daphnids is known to within 48 hours, and the daphnids in each beaker are age-matched.

To begin Phase 1 of the experiment, Groups 1 and 4 consisted of 10 beakers with 40 mL of media each, with each beaker containing 10 neonate daphnids. Group 3 consisted of 10 beakers with 40 mL of media each, with each beaker containing 1 neonate daphnid. Group 2 consisted of 100 beakers with 40 mL of media each, with each beaker containing 1 neonate daphnid. For each experimental beaker previously described, there was also a "backup" beaker with the same number of age-matched daphnids as the corresponding experimental beaker. Therefore, if any daphnid in an experimental beaker died, it was replaced with a daphnid from a backup beaker. The backup beakers were consistently kept to around the same density as the experimental beakers. This was done for the entirety of the experiment, to ensure each experimental beaker kept the same density, and that daphnids in the backup beakers experienced the same density as those in experimental beakers.

Table 5.1 contains the mortality data for each beaker. It is important to note that Group 1

experienced high mortality early in the experiment, which we believe is attributable to experimenter error, and thus that mortality (specifically from days 5-8) will not be considered in the analysis provided below. Also, since Group 2 experienced such rapid mortality near the end of the experiment, we needed to reduce the number of experimental breakers for Group 2 as the experiment continued in order to keep each experimental beaker at the required density of daphnids since our backup breakers for Group 2 ran out of daphnids. The experiment ended when there were no longer enough living daphnids for Group 2 to contain at least 6 beakers with 10 daphnids each.

After the second brood (approximately day 17 for Group 2, approximately day 21 for Group 4) the experimental densities in Groups 2 and 4 were switched, while the experimental densities in Groups 1 and 3 remained constant, which begins what we term Phase 2 of the experiment (Table 5.2). That is, at day 18 the 100 experimental breakers for Group 2 were combined to make 10 experimental breakers of 10 daphnids each, and at day 22 the 10 experimental breakers of 10 daphnids each for Group 4 were separated into 10 experimental breakers with 1 daphnid each by taking one daphnid from each of the original 10 experimental breakers.

All daphnids were kept in media reconstituted from deionized water [10] and maintained in an incubator at 20 degrees celsius with a 16-h light, 8-h dark cycle. The daphnids used in our study came from a colony that was maintained at North Carolina State University for over 20 years (clone NCSU1 [138]). Daphnids were fed daily with  $7.0 \times 10^6$  cells of algae (*Raphidocelis subcapitata*) and 0.2 mg (dry weight) Tetrafin™ fish food suspension prepared as described previously [124]. Each beaker was checked daily for the presence of new offspring and those neonates were counted and removed. Figure 5.1 contains the average number of offspring created in each beaker.

### 5.3.2 Statistical Analysis

Upon inspection of Figure 5.1 it appears that the average fecundity in Groups 1 and 3 is not meaningfully impacted during the course of the experiment, and the fecundity seen in Group 3 seems to confirm what was seen in our earlier experiment with solitary daphnid fecundity in Chapter 3 (Figure 3.3). The average fecundity in Groups 2 and 4 seem to meaningfully change 5-7 days into Phase 2. This suggests a delay of 5-7 days for the fecundity density-dependent effect, both for increasing and decreasing densities of daphnids, which would verify what was found through the population data in Chapter 3 (Section 3.3.1). Here we describe a technique that we used to try and confirm this delay past visual inspection. Ideally our analysis in Chapter 3 will match our visual inspection, which will match what we do below.

**Table 5.1** This is the mortality data seen for each Group of the experiment. The data shown here are the total number of deaths seen in that Group (Column 'A'), and the total number of deaths per daphnid each day (Column 'B') in that Group.

	Group 1		Group 2		Group 3		Group 4	
Age	A	B	A	B	A	B	A	B
1	0	0	0	0	0	0	0	0
2	1	0.01	0	0	0	0	0	0
3	1	0.01	1	0.01	0	0	1	0.01
4	1	0.01	2	0.02	0	0	0	0
5	13	0.13	0	0	0	0	0	0
6	13	0.13	0	0	0	0	1	0.01
7	2	0.02	0	0	0	0	0	0
8	2	0.02	0	0	0	0	0	0
9	0	0	0	0	0	0	0	0
10	1	0.01	0	0	0	0	0	0
11	0	0	0	0	0	0	0	0
12	0	0	0	0	0	0	0	0
13	0	0	0	0	0	0	0	0
14	0	0	1	0.01	0	0	0	0
15	0	0	1	0.01	0	0	0	0
16	0	0	1	0.01	0	0	0	0
17	0	0	0	0	0	0	0	0
Phase 2 begins for Groups 2 and 3								
18	0	0	0	0	1	0.1	1	0.01
19	0	0	2	0.02	0	0	1	0.01
20	1	0.01	1	0.01	0	0	2	0.02
21	0	0	1	0.01	0	0	0	0
Phase 2 begins for Groups 1 and 4								
22	0	0	7	0.07	0	0	0	0
23	1	0.01	18	0.18	0	0	0	0
24	1	0.01	15	0.15	0	0	0	0
25	2	0.02	13	0.13	0	0	0	0
26	0	0	8	0.8	0	0	0	0
27	1	0.01	7	0.0778	0	0	0	0
28	0	0	7	0.0875	0	0	0	0
29	0	0	8	0.1143	0	0	0	0
30	0	0	7	0.1	0	0	0	0
Experiment ends for Groups 2 and 3								
31	1	0.01	-	-	-	-	0	0
32	1	0.01	-	-	-	-	0	0
33	2	0.02	-	-	-	-	0	0



**Table 5.2** This table contains the number of daphnids per beaker (labeled density) and the number of beakers for each experimental Group for Phases 1 and 2 of the the experiment.

Group	Phase 1		Phase 2	
	Density	# of Beakers	Density	# of Beakers
1	10 daphnids/40 mL	10 beakers	10 daphnids/40 mL	10 beakers
2	1 daphnid/ 40 mL	100 beakers	10 daphnids/40 mL	10 beakers
3	1 daphnid/40 mL	10 beakers	1 daphnid/40 mL	10 beakers
4	10 daphnids/40 mL	10 beakers	1 daphnid/40 mL	10 beakers

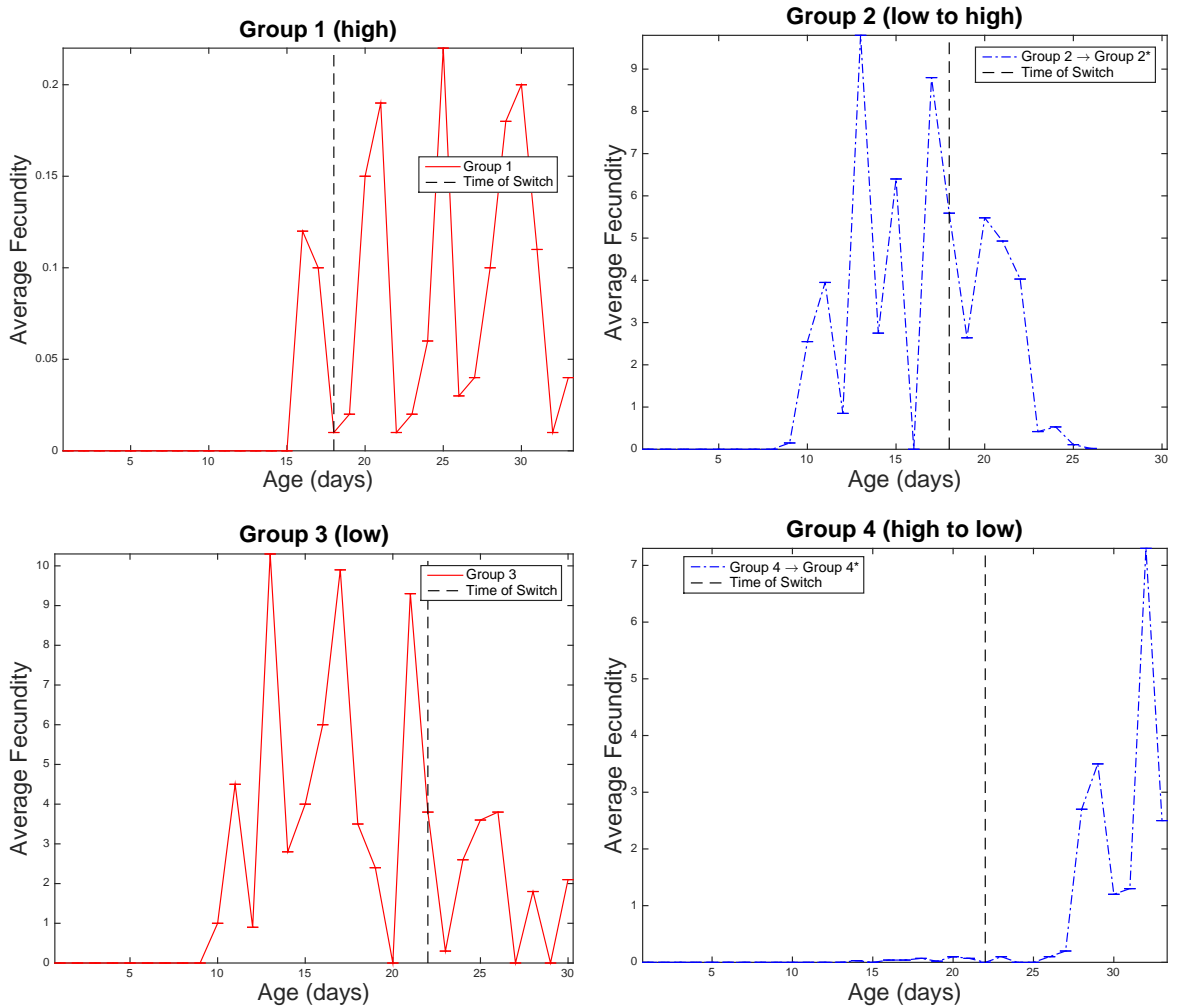


**Figure 5.1** For each experimental group these show the average fecundity per daphnid per day. The vertical dashed line in each graph depicts the time when Phase 2 began for that beaker. So, for example, for Group 2 Phase 2 began on day 18, and so that is the vertical dashed line in that plot, and all data to the left of that vertical dashed line is Phase 1. Notice that each graph is plot on a different scale.

### 5.3.2.1 Mathematical Model and Inverse Problem Methodology

The method we used to determine the delay was a method developed and further expanded upon by Banks et. al. [34, 35]. Their method involves determining the distribution of a delay from data for HIV infections, but is developed in such generality that it can easily be adapted to daphnid modeling. This is the method we will describe and use below.

Using what we know of daphnid growth and reproduction from Chapter 3, we have modeled that, on any given day  $t$ , the number of new daphnid neonates  $f(t, \theta)$  is given by

$$f(t, \theta) = N(t)\alpha(t)(1 - q)^{M(t-\tau)} \quad (5.1)$$

where  $\alpha(t)$ ,  $q$ ,  $N(t)$ , and  $M(t)$  represent the same quantities as in Table 3.1, and  $\theta = (q, \tau)$ . It is important to note that this formulation assumes that the delay  $\tau$  is a point delay as opposed to distributed. Here we take  $\alpha(t)$  to be the same that we used in Chapter 3 (that is, the values for  $\alpha(t)$  are taken directly from Figure 3.3).

In this experiment we have several beakers for each Group, and we will, at least initially, treat each beaker in each Group as separate. We will use 10 beakers from each Group, so for Group 2 in Phase 1 we will pick those 10 beakers randomly from the 100 possible. Our observations are the number of offspring per daphnid at time  $t_j$  for beaker  $i$  and are denoted by  $y_j^i$ , where  $i = 1, \dots, 40$ , so  $i = 1, \dots, 10$  correspond to the 10 beakers in Group 1,  $i = 11, \dots, 20$  correspond to the 10 beakers in Group 2, and so on. For each beaker we had only one observation, and since we are keeping the number of daphnids constant in each beaker we can reasonably assume a constant statistical error model. This leads our statistical model to pertain to a scalar observation with constant error [39], and thus our statistical model is given by

$$Y_j^i = f^i(t_j, \theta_0^i) + \mathcal{E}_j^i, \quad j = 1, 2, \dots, n,$$

where  $Y_j^i$  is a random variable with realizations  $y_j^i$ ,  $\theta_0^i$  is the hypothesized “true” parameter vector for the  $i$ ’th beaker,  $f^i(t_j, \theta_0^i)$  is the model solution for the  $i$ ’th beaker, and the error terms  $\mathcal{E}_j^i$  are assumed independent and identically distributed (i.i.d) random variables with mean  $E[\mathcal{E}_j^i] = 0$  and variance  $V_0 = \sigma_0^2$ . Therefore, in order to find our estimate  $\hat{\theta}^i$  of  $\theta_0^i$  for each beaker we will minimize the cost functional

$$J^i(\theta) = \sum_{j=1}^n [y_j^i - f^i(t_j, \theta)]^2.$$

We thus perform 40 different inverse problems, one for each beaker. The inverse problems were computed using two routines in Matlab. The first routine is a direct search algorithm implemented by

Daniel Finkel as *direct*, and can be found at [http://www4.ncsu.edu/~ctk/Finkel\\_Direct/](http://www4.ncsu.edu/~ctk/Finkel_Direct/). This was used with the following options: `options.maxevals = 2000`; `options.maxits = 1000`; `options.maxdeep = 400`; and the output was used as the initial condition for the gradient based Matlab search routine *lsqnonlin*. *lsqnonlin* was run with the options ‘TolFun’, ‘TolCon’, and ‘TolX’ set equal to 1e-20. The output of *lsqnonlin* was then used as our parameter estimate.

At this point we will have 40 different parameter estimates  $\hat{\theta}^i$ . We will then look at the variability of these parameter estimates to see if it is reasonable to assume that the true delay is a fixed delay or a distributed delay. Our determination of the nature of the delay will lead us down one of two paths:

1. If the delays found are simply small deviations from a single number (for example, if that number is 6 we might have for each  $i$  that  $\hat{\theta}^i \in [5.99, 6.01]$ ), then we can assume that the true delay is fixed and that there is only a single “true” parameter vector  $\theta_0$ . With that assumption we will perform a different inverse problem, where we find a single “true” parameter vector  $\theta_0$  for all beakers. This will be done by having each beaker be an observation as before, but now we put all observations into one vector, and thus perform a single inverse problem with each beaker as a different replicate. Therefore, our statistical model will be

$$\mathbf{Y}_j = \mathbf{f}(t_j, \theta_0) + \mathcal{E}_j, \quad j = 1, 2, \dots, n,$$

where  $\mathbf{f}(t_j, \theta_0) = [f^1(t_j, \theta), f^2(t_j, \theta), \dots, f^{40}(t_j, \theta)]^T$  contains the model solution for each beaker,  $\mathbf{Y}_j = [Y_j^1, Y_j^2, \dots, Y_j^{40}]^T$  is a random variable with realizations  $\mathbf{y}_j = [y_j^1, y_j^2, \dots, y_j^{40}]^T$ , and the error terms  $\mathcal{E}_j$  are assumed independent and identically distributed (i.i.d) random variables with mean  $E[\mathcal{E}_j] = 0$  and variance  $V_0 = \sigma_0^2 I$ . An estimate  $\hat{\theta}$  for the true parameter vector  $\theta_0$  would be obtained by implementing an iterative algorithm (see [39] for details).

2. If we determine that the delays are indeed distributed since they cover a wide range of values (for example, for each  $i$  we have  $\hat{\theta}^i \in [2, 12]$ ), then we will need to use techniques of [34, 35] in order to determine that distribution. That is, we will consider a probability distribution  $P$  which characterizes the distribution of  $\tau$ ’s which are in a set of admissible delays  $T$ . Then, our number of new neonates will be

$$f(t, \theta(P)) = \int_T N(t) \alpha(t) (1 - q)^{M(t-\tau)} dP(\tau). \quad (5.2)$$

In this case we will now no longer consider  $\theta = (q, \tau)$ , but rather  $\theta = (q, p_1, p_2, \dots, p_n)$  where each  $p_i$  is either a parameter that describes the distribution  $P$  (so for example if  $P$  is a Gaussian distribution then  $p_1 = \mu$ , the mean of that distribution, and  $p_2 = \sigma^2$ , the variance of that

distribution) or values from a discretized version of  $P$ . If we are to discretize  $P$ , we will also need to discretize  $T$ , and thus we assume that  $T = \{\tau_1, \tau_2, \dots, \tau_n\}$  and that each  $p_i$  is the probability of the delay being  $\tau_i$ . From there we can transform Equation (5.2) into a sum, with which we can perform a standard inverse problem to determine the  $p_i$ 's.

We discussed here considering whether the delay  $\tau$  is distributed, but the same techniques could be used to determine if the parameter  $q$  is distributed, and to determine the distribution for  $q$ , if one exists.

## 5.4 Statistical Analysis Results

Using the method described in Section 5.3.2.1 we were able to obtain parameter estimates and model fits to the fecundity data using Equation (5.1) (see Figures 5.2-5.5). As we can see, the data is consistently grossly underestimated by our model, and thus our parameter estimates are unreliable. Therefore, we cannot determine the delay using the methods detailed in Section 5.3.2.1. In the Discussion we will explore why this happened, what we have been able to learn from this experiment, and future work.

## 5.5 Discussion and Concluding Remarks

### 5.5.1 Fecundity Delay

Our results from the statistical analysis of our model in Equation (5.1) were inconclusive, pointing to either a flaw in Equation (5.1) or a flaw in our inverse problem methodology in Section 5.3.2.1. Our model in Equation (5.1) was successfully used as part of a much broader population-level model in Chapter 3, and our inverse problem methodology has been successfully used before by Banks et. al. in [34, 35], and thus we are hesitant to disparage either without further considering what might have gone wrong.

A huge crux of our fecundity model is the term  $\alpha(t)$ , which is the density-independent fecundity of daphnids. In Chapter 3 we used the average fecundity per daphnid per day for  $\alpha(t)$ , which worked since even though an individual daphnid's fecundity is random (see Appendix A.1), when there are a lot of daphnids together the law of large numbers takes over and the observed fecundity tends towards the mean. In this case, we have 1 or 10 daphnids per beaker, which is not nearly enough for us to reasonably expect that the law of large numbers can take effect. Since our model here depends so heavily on  $\alpha(t)$ , and we don't have a reliable measure for  $\alpha(t)$  at these densities, we cannot use this model for this investigation (we could use a wide distribution for  $\alpha(t)$  as found in

## Group 1: Individual OLS Fits

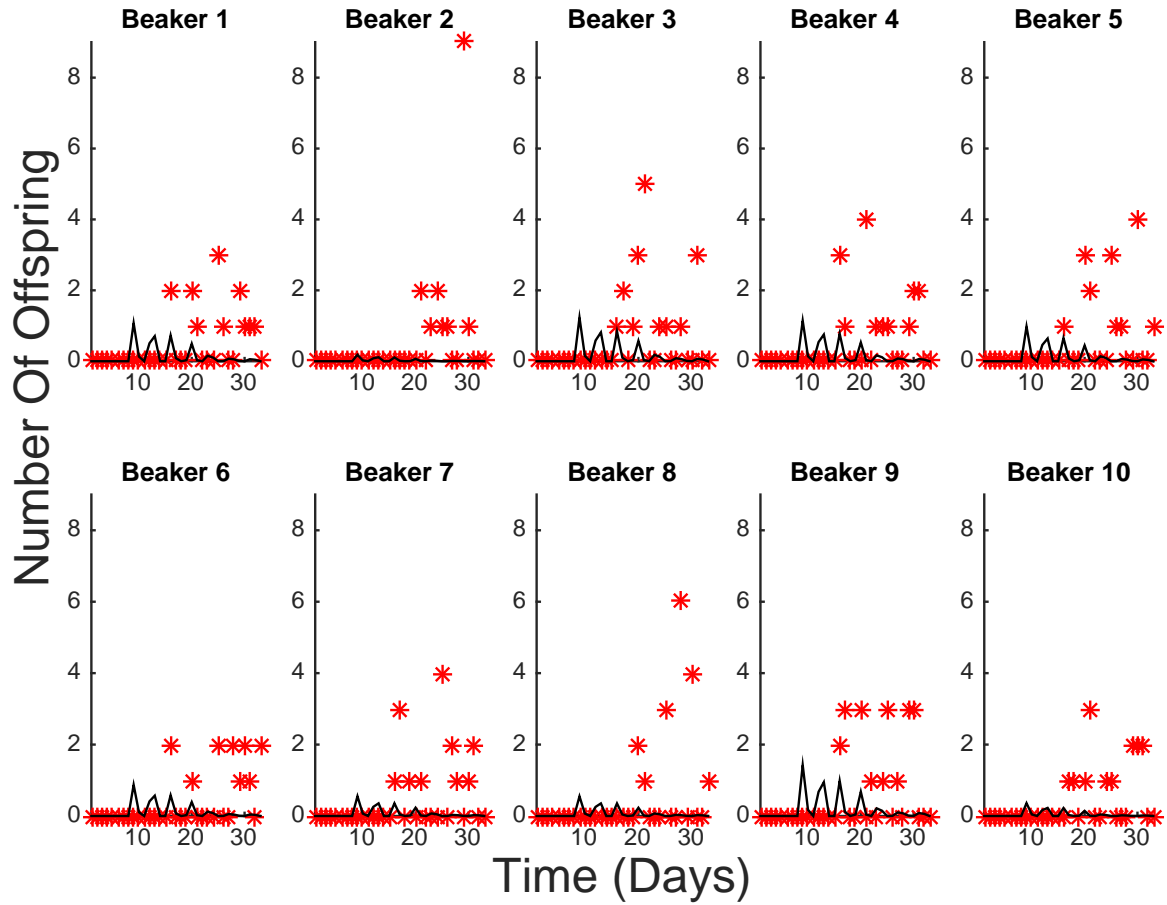


**Figure 5.2** Here we have the fecundity data for each beaker in Group 1, as well as the fit using our model from Equation (5.1). The fecundity data is depicted by red stars, and gives the actual number of offspring recorded for each beaker. The model fit, using the optimal parameter values for that beaker, is depicted by a solid black line. We see that the model always, and at times grossly, underestimates the actual number of offspring.

## Group 2: Individual OLS Fits

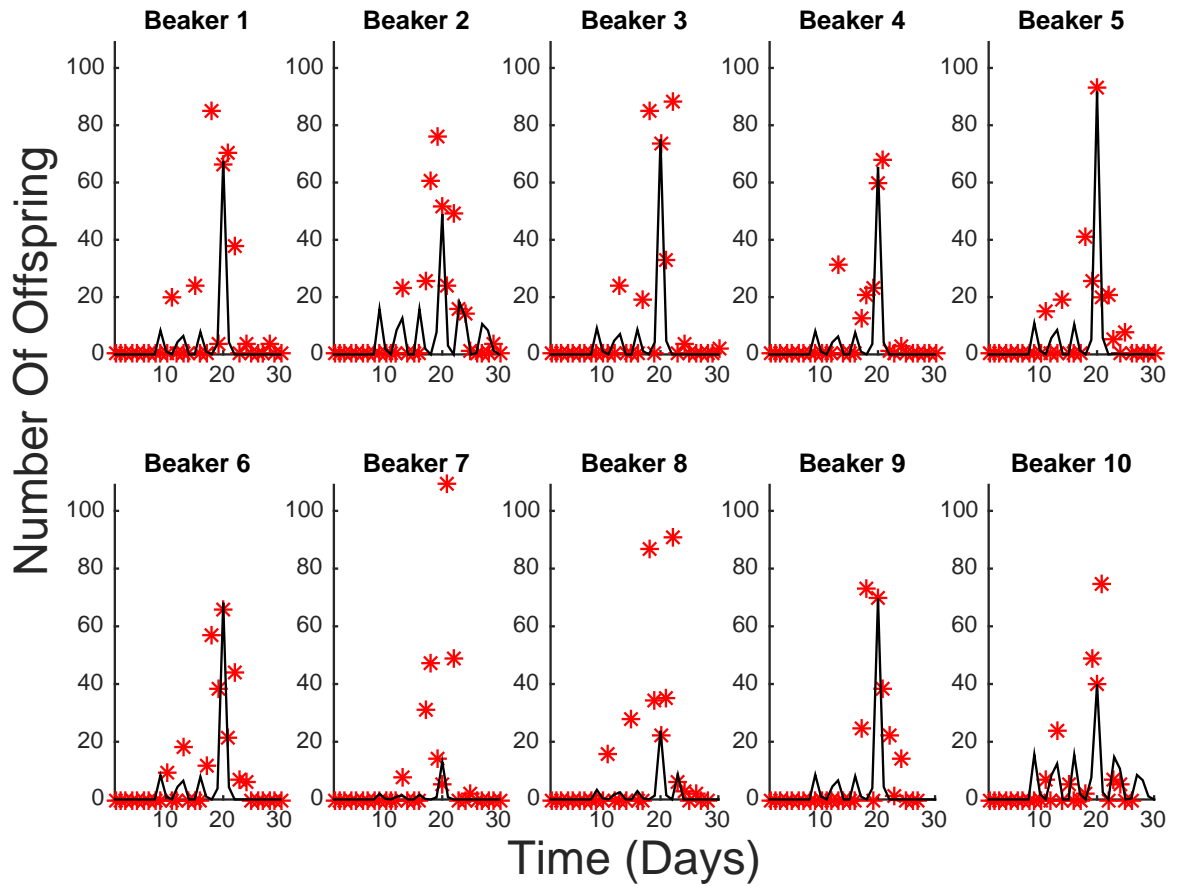


**Figure 5.3** Here we have the fecundity data for each beaker in Group 2, as well as the fit using our model from Equation (5.1). The fecundity data is depicted by red stars, and gives the actual number of offspring recorded for each beaker. Note that during Phase 2 the density of the beakers in Group 2 increase from 1 daphnid per beaker to 10 daphnids per beaker. The model fit, using the optimal parameter values for that beaker, is depicted by a solid black line. We see that the model always, and at times grossly, underestimates the actual number of offspring.

### Group 3: Individual OLS Fits

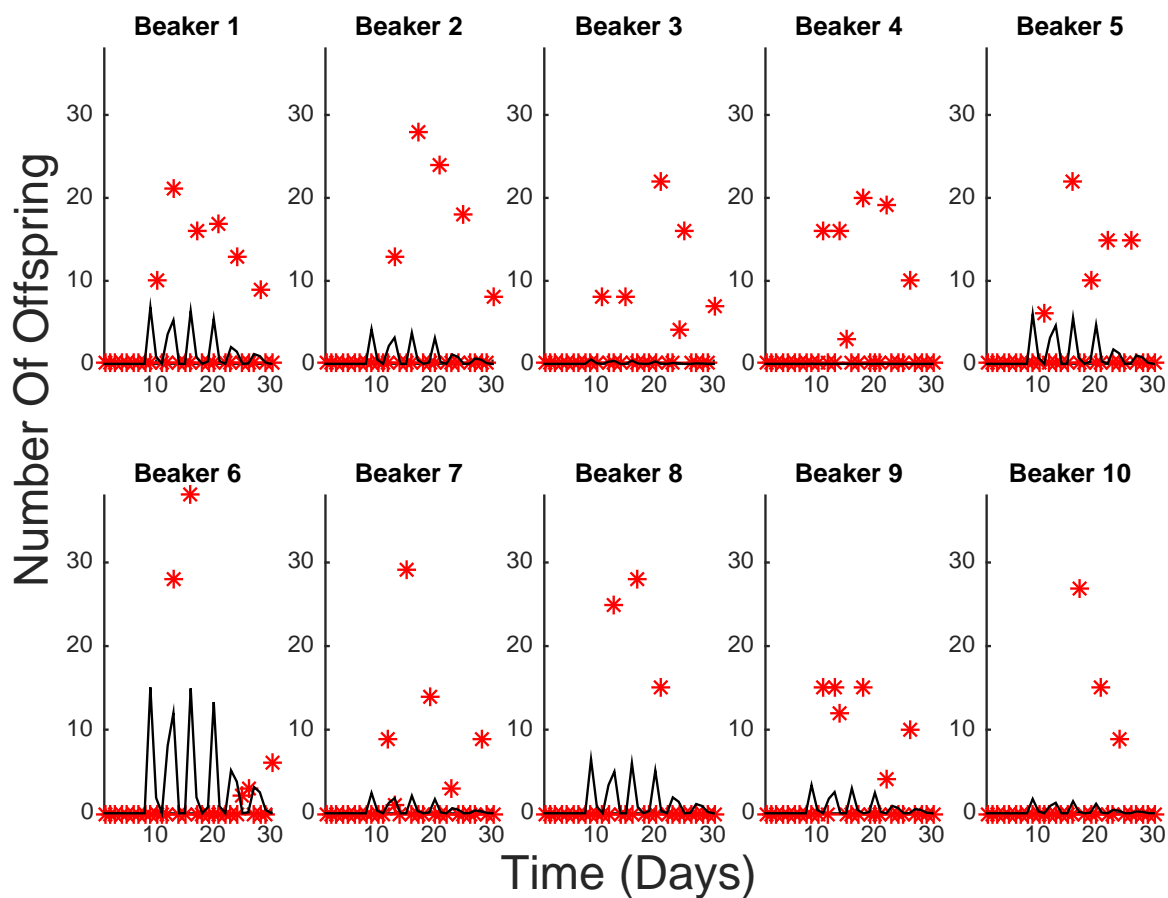


**Figure 5.4** Here we have the fecundity data for each beaker in Group 3, as well as the fit using our model from Equation (5.1). The fecundity data is depicted by red stars, and gives the actual number of offspring recorded for each beaker. The model fit, using the optimal parameter values for that beaker, is depicted by a solid black line. We see that the model always, and at times grossly, underestimates the actual number of offspring.

## Group 4: Individual OLS Fits

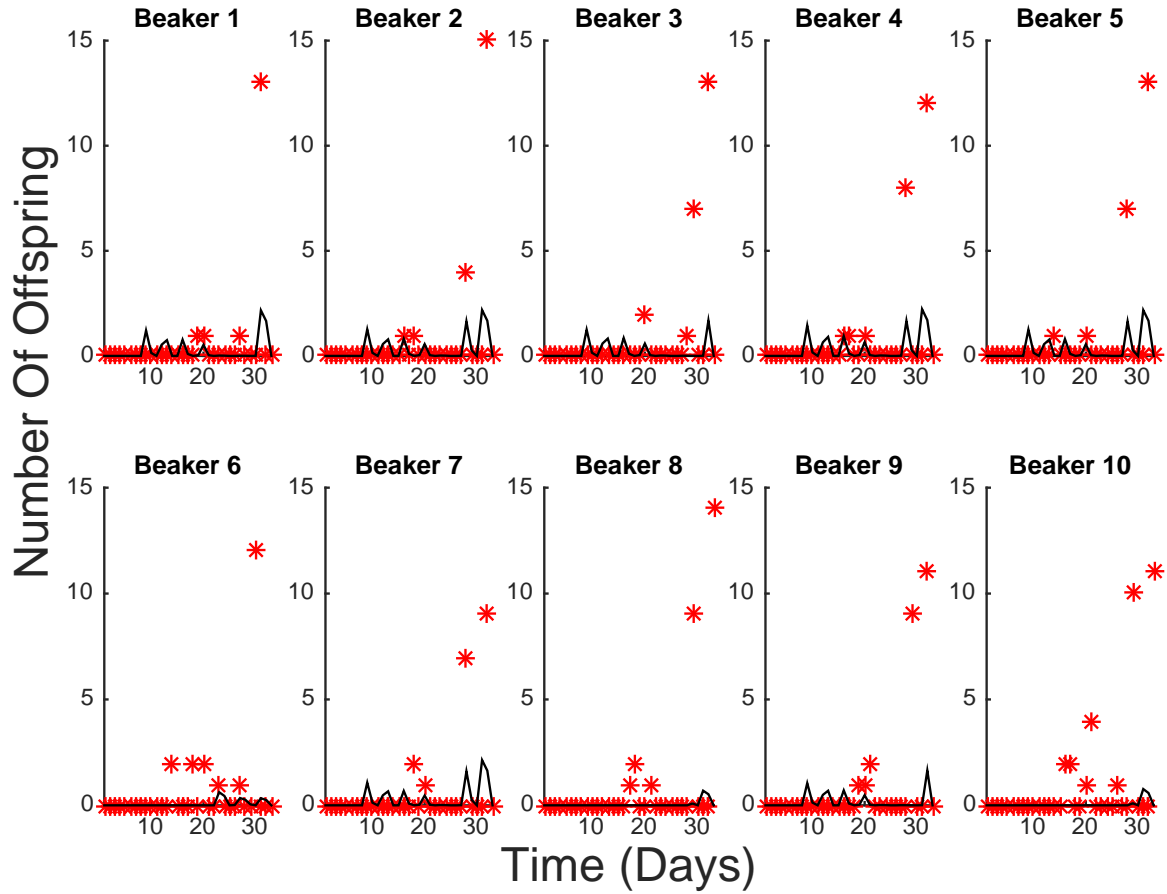


**Figure 5.5** Here we have the fecundity data for each beaker in Group 4, as well as the fit using our model from Equation (5.1). The fecundity data is depicted by red stars, and gives the actual number of offspring recorded for each beaker. Note that during Phase 2 the density of the beakers in Group 4 decrease from 10 daphnids per beaker to 1 daphnid per beaker. The model fit, using the optimal parameter values for that beaker, is depicted by a solid black line. We see that the model always, and at times grossly, underestimates the actual number of offspring.



Appendix A.1, but we don't expect that that would improve upon these results). This means that we cannot now determine the delay mathematically from this new data, and we cannot purport to use the model that we developed in Chapter 3 for small populations of daphnids. Although we cannot determine the delay through this analysis, we still have evidence, simply from the data, that the delay is between 5 and 7 days. This duplicates what was found statistically using the population-level data in Chapter 3, which is hopeful even though we were not able to validate those results using the continuous model in Section 5.2.

Through this experiment we see also that not only is the current density of the daphnids important, but also the density that they grew up in (see Section 5.5.2). This affects size, mortality, and fecundity in a way that to the best of our knowledge no-one has ever considered in daphnid modeling.

### **5.5.2 Mortality Delay and Effect of Developmental Environment**

In Table 5.1 Group 2, which switched from a low density environment (1 daphnid per beaker) to a high density environment (10 daphnids per beaker), began to experience rapid mortality 5-6 days after the switch. Groups 1 and 3, which stayed at high and low densities, respectively, never experience this rapid mortality (again, we are discounting the mortality seen in Group 1 from days 5-8 as experimenter error). Group 4, which switched from a high density to a low density, also never experienced such rapid mortality.

It is important to note that the daphnids that grew up in a low density environment (so Groups 2 and 3) were physically bigger than those that grew up in a high density environment (so Groups 1 and 4), began to reproduce earlier, and that they also had a higher average fecundity as seen in Figure 5.1, which agrees with what has been seen by previous experimenters [56, 81]. This suggests that there is some epigenetic encoding that happens to daphnids that grow in crowded vs uncrowded conditions that affects their size and fecundity. It is also important to note that, while the daphnids that switched density never changed size to reflect the density that they were placed into, their fecundity, after about 6 days, did return back to what would be expected for daphnids originally growing in that density.

The mortality spike seen in Group 2 suggests that daphnids which grew up in uncrowded conditions are not physically able to survive in a crowded condition. This could be since they grew bigger, thus needing more nutrients. The lack of any mortality change in Group 4 suggests that daphnids which grew up in crowded conditions are physically able to survive in uncrowded conditions, possibly since their smaller size requires less nutrients, allowing them to thrive in an uncrowded condition. So we are seeing a daphnid's developmental environment affect their

mortality, fecundity, and size along with their current environment, and now we need to try and formulate a way to describe all of this mathematically.

### 5.5.3 Future Work

What these results suggest is that not only is it important to know the temporal density history of daphnids because of delays in the mortality and fecundity density-dependence of daphnid population dynamics, but that a daphnid's life history is also critical in understanding its biological outputs and outcomes. In addition, the results of Chapter 4 suggest that our model should be continuous with age-varying mortality as opposed to the discrete model with constant mortality used in Chapter 3. The results of Chapter 4 also suggest that daphnids may fall into various subpopulations that could also be modeled, which is similar to what has been found in previous work for other aquatic organisms [13, 25].

All of these point to the need for a much more complex, and more complete, model for daphnid population growth. Here I will outline a theoretical framework for a future model. For this, let us assume that there exists an intrinsic parameter  $\gamma$  that daphnids have, which can represent both their subpopulation as well as the density at which the daphnid was born. Let's assume  $\gamma \in \Gamma$ , where  $\Gamma$  is a range of admissible parameters, and let  $P$  be the distribution of the  $\gamma$ 's in  $\Gamma$ . Let  $a$  be the daphnid's age and  $s$  be the daphnid's size, and thus we have that the density of daphnids at time  $t$ , age  $a$ , size  $s$ , and intrinsic parameter  $\gamma$  is given by

$$u(t, a, s, \gamma).$$

The total population density is then given by

$$v(t, P) = \int_0^{a_{max}} \int_{s_0}^{s_{max}} \int_{\Gamma} u(t, a, s, \gamma) dP(\gamma) ds da,$$

where  $a_{max}$  is the maximum age of daphnids and  $s_0$  and  $s_{max}$  are the minimum and maximum sizes attained, respectively. Using a density-dependent form of the Sinko-Streifer PDE model [144], we then obtain

$$\frac{\partial u}{\partial t} + \frac{\partial u}{\partial a} + \frac{\partial}{\partial s} [g_{ind}(a, s, \gamma) g_{dep}(a, s, \gamma) u(t, a, s, \gamma)] = -\mu_{ind}(a, s, \gamma) \mu_{dep}(a, s, \gamma) u(t, a, s, \gamma)$$

where  $g_{dep}$  and  $\mu_{dep}$  are the density-dependent growth and mortality of daphnids, and  $g_{ind}$  and  $\mu_{ind}$  are the density-independent growth and mortality of daphnids. Here we will have  $\mu_{dep}$  have some delay, potentially distributed, within it, while  $\mu_{ind}$  and  $g_{ind}$  will likely be what was obtained

in Chapters 4 and 3, respectively. Our boundary condition will represent the fecundity, and be given by

$$u(t, 0, s_0, \gamma) = \int_0^{a_{max}} \int_{s_0}^{s_{max}} k_{ind}(a, s, \gamma) k_{dep}(a, s, \gamma) u(t, a, s, \gamma) ds da,$$

where  $k_{dep}$  and  $k_{ind}$  are the density-dependent and density-independent terms for fecundity, where  $k_{dep}$  contains some delay. This model would then need to be modified to permit the use of toxicants, as this is solely creating a comprehensive baseline model.

This dissertation has laid the groundwork from which such a comprehensive model can be built. In exploring these important aspects of daphnid growth, previous models [71, 76, 133, 134] can be revisited with this new knowledge of daphnid dynamics.

## Discussion and Concluding Remarks

What we have seen throughout this dissertation is a confluence of mathematics, statistics, and biology in order to find novel solutions to important problems, as well as to gain biological understanding of organisms. In Chapter 2 we compared the efficacy of analyzing correlation coefficients, covariance matrices, asymptotic and exact confidence regions, as well as the DRAM algorithm in determining correlation in parameter estimators, and found that while it is possible to detect correlation with each method, the DRAM algorithm and exact confidence regions give the most information, albeit for the most computational cost. In Chapter 3 we conducted experiments on *Daphnia magna* on both the individual and population level, and used that experimental data to calibrate a multi-scale daphnid population-level model. In that chapter we used uncertainty quantification and sensitivity analysis to find ways to improve upon that model, and explored those improvements in Chapters 4 and 5. Through these investigations we discovered, and confirmed, several important biological mechanisms that drive daphnid population dynamics as well as individual organismal endpoints.

While the types of models have changed throughout the presentation a common thread permeates all of these discussions: mathematical modeling, married with statistical analysis, can lead to important solutions to biological issues and questions. We have incorporated the use of various mathematical models, but do not disparage the use of other types of models. For example, we have used both a Leslie matrix model [108] and a Sinko-Streifer PDE model [144] for daphnid population dynamics, but recognize that other models (individual-based models, stochastic models, etc.) can also be useful in this context. Some techniques discussed throughout this work we feel should be used more thoroughly in biological investigations, such as testing the error assumption of your model (Section 3.2.5) as well as the uncertainty quantification and sensitivity analysis seen

throughout several chapters of this work.

We have rigorously followed modeling as an iterative approach, much in the fashion suggested by Banks and Tran [31]. For example, we preempted our daphnid modeling by a thorough literature review and experimentation. From those, we were able to determine several important mechanisms for daphnid growth and development, as well as population growth. We transformed those biological concepts into mathematical formulas which we then calibrated using the experimental data, and we then used a statistical model to quantify our uncertainty in that calibration. Interpreting our results at the end of Chapter 3, we found ways in which our original understanding needed to be improved upon, and provided further analysis of our data, and revised our model, in Chapter 4. Our original understanding was tested again in Chapter 5, and there we needed to not only reformulate our model, but to perform further experimentation to provide a deeper understanding of the organism. Each step in this repeated process is important as it has given us further insights as well as aided the robustness of our models, and we urge future modelers to also treat modeling as an iterative process as we have here.

From this dissertation we have explored a wide range of topics, but also left room for further investigations going forward. To build off of our analysis in Chapter 2 we can consider optimal design techniques, parallel computation, as well as questions of identifiability, ill-conditioning, and reparametrization for systems with which there is dependence in parametric estimators. At the end of Chapter 5 we have outlined a comprehensive daphnid population model that incorporates the findings from Chapters 3-5. Also, we motivated our daphnid discussion with the desire to effectively model the effect of toxicants on daphnid populations, as well as the phenomenon of cyclic parthenogenesis, which remains an open problem.

## BIBLIOGRAPHY

- [1] B. M. Adams, H. T. Banks, M. Davidian, and E. S. Rosenberg. Model fitting and prediction with HIV treatment interruption data. *Bulletin of Mathematical Biology*, 69:563–584, 2007.
- [2] K. Adoteye, H. T. Banks, and K. Flores. Optimal design of non-equilibrium experiments for genetic network interrogation. *Applied Mathematics Letters*, 40(84-89):893–9659, 2015.
- [3] K Adoteye, HT Banks, K Cross, S Etchyson, KB Flores, G LeBlanc, T Nguyen, C Ross, E Smith, M Stemkovski, and S Stokley. Statistical validation of structured population models for *Daphnia magna*. *Mathematical Biosciences*, 266:73–84, August 2015.
- [4] Kaska Adoteye, H.T. Banks, Kevin B. Flores, and Gerald A. LeBlanc. Estimation of time-varying mortality rates using continuous models for *Daphnia magna*. *Applied Mathematics Letters*, 44:12–16, June 2015.
- [5] Kaska Adoteye, Robert Baraldi, Kevin Flores, John Nardini, H.T. Banks, and W. Clayton Thompson. Correlation of parameter estimators for models admitting multiple parameterizations. *International Journal of Pure and Applied Mathematics*, 2015. submitted. Preprint: [https://drive.google.com/file/d/0B4Y\\_MUjV9P8idzFXaWYxUFgtYWc/edit](https://drive.google.com/file/d/0B4Y_MUjV9P8idzFXaWYxUFgtYWc/edit).
- [6] I. Alves-Rodrigues, R. P. Galao, A. Meyerhans, and J. Diez. *Saccharomyces cerevisiae*: a useful model host to study fundamental biology of viral replication. *Virus Research*, 120:49–56, 2006.
- [7] C. Andrieu and J. Thomas. A tutorial on adaptive MCMC. *Statistics and Computing*, 18:343–373, 2008.
- [8] Gerald T. Ankley, Richard S. Bennett, Russell J. Erickson, Dale J. Hoff, Michael W. Hornung, Rodney D. Johnson, David R. Mount, John W. Nichols, Christine L. Russom, Patricia K. Schmieder, Jose A. Serrano, Joseph W. Tietge, and Daniel L. Villeneuve. Adverse outcome pathways: a conceptual framework to support ecotoxicology research and risk assessment. *Environmental Toxicology and Chemistry*, 29(3):730–741, 2010.
- [9] Stevan J. Arnold. Morphology, performance and fitness. *American Zoologist*, 23(2):347 – 361, 1983.
- [10] W. S. Baldwin and G. A. LeBlanc. Identification of multiple steroid hydroxylases in *Daphnia magna* and their modulation by xenobiotics. *Environ. Toxicol. Chem.*, 13:1013–1021, 1994.
- [11] H. T. Banks, J. E. Banks, L. K. Dick, and J. D. Stark. Estimation of dynamic rate parameters in insect populations undergoing sublethal exposure to pesticides. *Bull. Math Biol.*, 69(7):2139–2180, 2007.
- [12] H. T. Banks, R. Baraldi, K. Cross, K. B. Flores, C. McChesney, L. Poag, and E. Thorpe. Uncertainty quantification in modeling HIV viral mechanics. *Mathematical Biosciences and Engineering*,

12(5):937–64, 2015. CRSC-TR13-16, Center for Research in Scientific Computation, North Carolina State University.

- [13] H. T. Banks, V. A. Bokil, S. Hu, A. K. Dhar, R. A. Bullis, C. L. Browdy, and F. C. T. Allnutt. Modeling shrimp biomass and viral infection for production of biological countermeasures. *Mathematical Biosciences and Engineering*, 3(4):635–660, 2006.
- [14] H. T. Banks, L. W. Botsford, F. Kappel, and C. Wang. Modeling and estimation in size structured population models, lcms-ccs report 87-13, brown university. *Proc. 2nd Course on Mathematical Ecology*, (1988):521–541, December 1988. (Trieste, December 8-12,1986) Word Press, Singapore.
- [15] H. T. Banks, Amanda Choi, Tori Huffman, John Nardini, Laura Poag, and W. Clayton Thompson. Quantifying CFSE label decay in flow cytometry data. *Applied Math Letters*, 26, 2013.
- [16] H. T. Banks, M. Davidian, S. Hu, G. M. Kepler, and E. S. Rosenberg. Modeling HIV immune response and validation with clinical data. *Journal of Biological Dynamics*, 2:357–385, 2008.
- [17] H. T. Banks and J. L. Davis. A comparison of approximation methods for the estimation of probability distributions on parameters. *Appl. Numer. Math.*, 57:753–777, 2007.
- [18] H. T. Banks, J. L. Davis, S. L. Ernstberger, S. Hu, E. Artimovich, and A. K. Dhar. Experimental design and estimation of growth rate distributions in size-structured shrimp populations. *Inverse Probl.*, 25:095003, 2009.
- [19] H. T. Banks, J. L. Davis, S. L. Ernstberger, S. Hu, E. Artimovich, A. K. Dhar, and C. L. Browdy. A comparison of probabilistic and stochastic formulations in modeling growth uncertainty and variability. *J. Biological Dynamics*, 3:130–148, 2009.
- [20] H. T. Banks, J. L. Davis, and S. Hu. A computational comparison of alternatives to including uncertainty in structured population models. In *Three Decades of Progress in Systems and Control*, pages 19–33. Springer, New York, 2010.
- [21] H. T. Banks and Jimena L. Davis. A comparison of approximation methods for the estimation of probability distributions on parameters. *Applied Numerical Mathematics*, 57:753 – 777, May 2007.
- [22] H. T. Banks, S. Dediu, S. L. Ernstberger, and F. Kappel. Generalized sensitivities and optimal experimental design. *Journal of Inverse and Ill-posed Problems*, 18:25–83, 2010.
- [23] H. T. Banks and B. G. Fitzpatrick. Statistical methods for model comparison in parameter estimation problems for distributed systems. *J. Math. Biol*, 28:501–527, 1990.
- [24] H. T. Banks and B. G. Fitzpatrick. *Estimation of growth rate distributions in size-structured population models*, CAMS Tech. Rep. 90-2, University of Southern California, January, 1990. *Quart. Appl. Math.*, 49:215–235, 1991.

- [25] H. T. Banks, B. G. Fitzpatrick, L. K. Potter, and Y. Zhang. Estimation of probability distributions for individual parameters using aggregate population observations, crsc-tr98-06. In W. McEneaney, G. Yin, and Q. Zhang, editors, *Stochastic Analysis, Control, Optimization, and Applications*. Birkhauser, Boston, 1998.
- [26] H. T. Banks, K. B. Flores, K. Link, L. Poag, T. Huffman, J. Nardini, B. Blasco, J. Jungfleisch, and J. Diez. A mathematical model of RNA3 recruitment in the Brome Mosaic Virus replication cycle. *International Journal of Pure and Applied Mathematics*, 89(2):251–274, 2013.
- [27] H. T. Banks, K. Holm, and F. Kappel. Comparison of optimal design methods in inverse problems. *Inverse Problems*, 27:075002, 2011.
- [28] H. T. Banks and K. Kunisch. *Estimation Techniques for Distributed Parameter Systems*. Birkhausen, Boston, 1989.
- [29] H. T. Banks and K. L. Rehm. Experimental design for distributed parameter vector systems. *Applied Math Letters*, 26(1):10–14, 2013.
- [30] H. T. Banks, D. Robbins, and K. L. Sutton. Theoretical foundations for traditional and generalized sensitivity functions for delay differential equations. *Mathematical Biosciences and Engineering*, 10:1301–1333, 2013.
- [31] H. T. Banks and H. T. Tran. *Mathematical and Experimental Modeling of Physical and Biological Processes*. CRC Press, New York, 2009.
- [32] H.T. Banks, John E. Banks, Sarah Lynn Joyner, and John D. Stark. Dynamic models for insect mortality due to exposure to insecticides. *Mathematical and Computer Modelling*, 48:316–332, 2008.
- [33] H.T. Banks, K. Bekele-Maxwell, L. Bociu, M. Noorman, and K. Tillman. The complex-step method for sensitivity analysis of non-smooth problems arising in biology. Preprint, CRSC-TR15-11, North Carolina State University, 2015. Eurasian Journal of Mathematical and Computer Applications (submitted).
- [34] H.T. Banks and D.M. Bortz. A parameter sensitivity methodology in the context of HIV delay equation models. *J. Math Biol.*, 50(6):607–25, June 2005.
- [35] H.T. Banks, D.M. Bortz, and S.E. Holte. Incorporation of variability into the modeling of viral delays in HIV infection dynamics. *Math Biosci.*, 183(1):63–91, May 2003.
- [36] H.T. Banks, J. Catenacci, and S. Hu. Use of difference-based methods to explore statistical and mathematical model discrepancy in inverse problems. *J. Inverse Ill-Posed Problems*, May 2015. submitted. Preprint: <http://www.ncsu.edu/crsc/reports/ftp/pdf/crsc-tr15-05.pdf>.
- [37] H.T. Banks and Jimena L. Davis. Quantifying uncertainty in the estimation of probability distributions with confidence bands. Technical report, Center for Research in Scientific Computation, North Carolina State University, December 2007.



- [38] H.T. Banks, S. Hu, K. Link, E.S. Rosenberg, S. Mitsuma, and L. Rosario. Modeling immune response to BK virus infection and donor kidney in renal transplant recipients. *J. Inverse Problems in Science and Engineering*, March 2015. CRSC-TR14-09, Center for Research in Scientific Computation, North Carolina State University.
- [39] H.T. Banks, Shuhua Hu, and W. Clayton Thompson. *Modeling and Inverse Problems in the Presence of Uncertainty*. CRC Press, New York, 2014.
- [40] H.T. Banks and K.L. Rehm. Parameter estimation in distributed systems: Optimal design. *Eurasian Journal of Mathematical and Computer Applications*, 2:70–79, 2014.
- [41] H.T. Banks, Danielle Robbins, and Karyn L. Sutton. Generalized sensitivity analysis for delay differential equations. In *Control and Optimization with PDE Constraints*, 2012.
- [42] J. E. Banks, J. K. Dick, H. T. Banks, and J. D. Stark. Time-varying vital rates in ecotoxicology: Selective pesticides and aphnid population dynamics. *Ecological Modeling*, 210:155–160, 2008.
- [43] J. E. Banks and J. D. Stark. What is ecotoxicology? an ad-hoc grab bag or an interdisciplinary science? *Integr. Biol.*, 5:1–9, 1998.
- [44] R. Baraldi, K. Cross, C. McChesney, L. Poag, E. Thorpe, K. B. Flores, and H. T. Banks. Uncertainty quantification for a model of HIV-1 patient response to antiretroviral therapy interruptions. In *Proceedings of the American Control Conference*, pages 2753–2758, 2014.
- [45] Edward J. Bedrick and Chih-Ling Tsai. Model selection for multivariate regression in small samples. *Biometrics*, 50:226–231, 1994.
- [46] C.W.M. Bodar, I. van der Sluis, J.C.P. van Montfort, P.A. Voogt, and D.I. Zandee. Cadmium resistance in *Daphnia magna*. *Aquatic Toxicology*, 16:33–39, 1990.
- [47] Z. I. Botev, J. F. Grotowski, and D. P. Kroese. Kernel density estimation via diffusion. *The Annals of Statistics*, 38(5):2916–2957, 2010.
- [48] L. Brendonick and L De Meester. Egg banks in freshwater zooplankton: evolutionary and ecological archives in the sediment. *Hydrobiologia*, 491:65–84, 2003.
- [49] K. P. Burnham and D. R. Anderson. *Model Selection and Multimodal Inference*. Springer, New York, 2nd edition, 2002.
- [50] P. Calow, R. Sibly, and V. Forbes. Risk assesment on the basis of simplified life history scenarios. *Environ. Toxicol. Chem.*, 16:1983–1989, 2001.
- [51] Gary R. Carvalho and Hans Georg Wolf. Resting eggs of lake-*Daphnia* I. distribution, abundance and hatching of eggs collected from various depths in lake sediments. *Freshwater Biology*, 22:459–470, 1989.

- [52] H. Caswell. *Matrix Population Models: Construction, Analysis, and Interpretation*. Sinauer, Sunderland, MA, 2nd edition, 2001.
- [53] G. Chalancon, C. N. J. Ravarani, S. Balaji, A. Martinez-Arias, L. Aravind, R. Jothi, and M. M. Babu. Interplay between gene expression noise and regulatory network architecture. *Trends in Genetics*, 28(5):221–232, 2012.
- [54] Y. Chu and J. Hahn. Parameter set selection for estimation of nonlinear dynamic systems. *AIChE Journal*, 53:2858–2870, 2007.
- [55] A. Cintron-Arias, H.T. Banks, A. Capaldi, and A. Lloyd. A sensitivity matrix based methodology for inverse problem formulation. *J. Inverse Ill-Posed Problems*, 17:545–564, 2009.
- [56] M. Cleuvers, B. Goser, and H. T. Ratte. Life-strategy shift by intraspecific interaction in *Daphnia magna*: change in reproduction from quantity to quality. *Oecologia*, 110(3):337–345, 1997.
- [57] W. J. Conover and Ronald L. Iman. Rank transformations as a bridge between parametric and nonparametric statistics. *The American Statistician*, 35(3):124–129, August 1981.
- [58] Anja Coors, Joost Vanoverbeke, Tom De Bie, and Luc De Meester. Land use, genetic diversity and toxicant tolerance in natural populations of *Daphnia magna*. *Aquatic Toxicology*, 95:71–79, October 2009.
- [59] D. T. Crouse, L. B. Crowder, and H. Caswell. A stage-based population model for loggerhead sea turtles and implications for conservation. *Ecology*, 68:1412–1423, 1987.
- [60] M. Davidian and D.M. Giltinan. *Nonlinear Models for Repeated Measurement Data*. Chapman Hall/CRC Monographs on Statistics and Applied Probability, 1995.
- [61] André de Roos and Lennart Persson. Competition in size-structured populations: mechanisms inducing cohort formation and population cycles. *Theoretical Population Biology*, 63:1–16, 2003.
- [62] N. Denslow, J. K. Colbourne, D. Dix, J. H. Freedman, C. C. Helbing, S. Kennedy, and P. L. Williams. Selection of surrogate animal species for comparative toxicogenomics. In R. DiGiulio and W. H. Benson, editors, *In Genomic Approaches for Cross-Species Extrapolation in Toxicology*. Taylor and Francis, Washington, DC, 2007.
- [63] Odo Diekmann, Mats Gyllenberg, J. A. J. Metz, Shinji Nakaoka, and Andre M. de Roos. *Daphnia* revisited: local stability and bifurcation theory for physiologically structured population models explained by way of an example. *J. Math Biol.*, 61:277–318, 2010.
- [64] D. Doak, P. Kareiva, and B. Klepetka. Modeling population viability for the desert tortoise in the western mojave desert. *Ecol. Appl.*, 4:446–460, 1994.
- [65] D. F. Doak and W. F. Morris. *Quantitative Conservation Biology: Theory and Practice of Population Viability Analysis*. Sinauer, Sunderland, MA, 2002.

- [66] Marisa C. Eisenberg and Michael A. L. Hayashi. Determining structurally identifiable parameter combinations using subset profiling. 2013. preprint submitted to Mathematical Biosciences.
- [67] M. El-Doma. Stability analysis of a size-structured population dynamic model of *daphnia*. *International Journal of Pure and Applied Mathematics*, 70(2):189–209, 2011.
- [68] M. El-Doma. A size-structured dynamics model of *daphnia*. *Applied Mathematics Letters*, 25:1041–1044, 2012.
- [69] M. El-Doma, editor. *Daphnia Biology and Mathematics Perspectives*. Nova Science Pub Inc, 2014.
- [70] P. Endels, H. Jacquemyn, R. Brys, and M. Hermy. Rapid response to habitat restoration by the perennial *Primula veris* as revealed by demographic monitoring. *Plant Ecol.*, 176:143–156, 2005.
- [71] R. A. Erickson, S. B. Cox, J. L. Oates, T. A. Anderson, C. J. Salice, and K. R. Long. A *Daphnia* population model that considers pesticide exposure and demographic stochasticity. *Ecological Modeling*, 275:37–47, 2014.
- [72] Per J. Færøvig, Tom Andersen, and Dag O. Hessen. Image analysis of *Daphnia* populations: non-destructive determination of demography and biomass in cultures. *Freshwater Biology*, 47:1956–1962, 2002.
- [73] J. Z. Farkas and T. Hagen. Linear stability and positivity results for a generalized size-structured *Daphnia* model with inflow. *Applicable Analysis*, 86:1087–1103, 2007.
- [74] D. Ferrari and P. Herbert. The induction of sexual reproduction in *Daphnia magna*: genetic differences between arctic and temperate populations. *Can. J. Zool.*, 60:2143–2148, 1982.
- [75] P. W. Frank, C. D. Boll, and R. W. Kelly. Vital statistics of laboratory cultures of *daphnia pulex* as related to density. *Physiological Zoology*, 30(4):287–305, 1957.
- [76] Peter W. Frank. Prediction of Population Growth Form in *Daphnia pulex* Cultures. *The American Naturalist*, 94(878):357–372, 1960.
- [77] M. Fujiwara and H. Caswell. Demography of the endangered north atlantic right whale. *Nature*, 414:537–54, 2001.
- [78] A. R. Gallant. *Nonlinear Statistical Models*. Wiley, New York, 1987.
- [79] G. K. Gijupalli and W. S. Baldwin. The time- and age-dependent effects of the juvenile hormone analog pesticide, pyriproxyfen on *Daphnia magna* reproduction. *Chemosphere*, 92:1260–1266, 2013.
- [80] A. E. Girling and B. M. Garforth. Influence of variations in culture medium on the survival and reproduction of *Daphnia magna*. *Bull. Environ. Contam. Toxicol.*, 42:119–125, 1989.

- [81] C. Guisande. Reproductive strategy as population density varies in *daphnia magna* (Cladocera). *Freshwater Biology*, 29(3):463–467, 1993.
- [82] H. Haario, M. Laine, A. Mira, and E. Saksman. Dram: Efficient adaptive MCMC. *Statistics and Computing*, 16(4):339–354, 2006.
- [83] H. Haario, E. Saksman, and J. Tamminen. An adaptive metropolis algorithm. *Bernoulli*, 7(2):223–242, 2001.
- [84] N. Hanson and J. D. Stark. A comparison of simple and complex population models to reduce uncertainty in ecological risk assessments of chemicals: example with three species of *Daphnia*. *Exotoxicology*, 20:1268–1276, 2011.
- [85] Paul D. N. Herbert. The population biology of *Daphnia* (crustacea, daphnidae). *Biol. Rev.*, 53:387–426, 1978.
- [86] A. Hobaek and P. Larsson. Sex determination in *Daphnia magna*. *Ecology*, 71:2255–2268, 1990.
- [87] D. G. Hole, M. J. Whittingham, R. B. Bradbury, G. Q. A. Anderson, P. L. M. Lee, J. D. Wilson, and J. R. Krebs. Widespread local house-sparrow extinctions. *Nature*, 418:931–932, 2002.
- [88] Helen L. Hooper, Richard Connon, Amanda Callaghan, Steve J. Maund, Matthias Liess, Sabine Duquesne, Thomas H. Hutchinson, Jonathan Moggs, and Richard M. Sibly. The use of image analysis to estimate population growth rate in *Daphnia magna*. *Journal of Applied Ecology*, 43:828–834, 2006.
- [89] Mieke Jansen, Anja Coors, Robby Stoks, and Luc De Meester. Evolutionary ecotoxicology of pesticide resistance: a case study in *Daphnia*. *Ecotoxicology*, 20:543–551, May 2011.
- [90] F.J. Janzen and P.C. Phillips. Exploring the evolution of environmental sex determination, especially in reptiles. *J. Evol. Biol.*, 19:1775–1784, 2006.
- [91] Nelson G. Hairston Jr., Winfried Lampert, Carla E. Cáceres, Cami L. Holtmeier, Lawrence J. Weider, Ursula Gaedke, Janet M. Fischer, Jennifer A. Fox, and David M. Post. Rapid evolution revealed by dormant eggs. *Nature*, 401:446, September 1999.
- [92] J. Kaipio and E. Somersalo. *Statistical and Computational Inverse Problems*. Springer, New York, 2005.
- [93] E. L. Kaplan and P. Meier. Nonparametric estimation from incomplete observations. *J. Amer. Statist. Assn.*, 53(282):457–481, 1958.
- [94] Karen Kast-Hutcheson, Cynthia V. Rider, and Gerald A. LeBlanc. The fungicide propiconazole interferes with embryonic development of the crustacean *Daphnia magna*. *Environmental Toxicology and Chemistry*, 20(3):502–509, 2001.
- [95] W. L. Kendall, J. E. Hines, and J. D. Nichols. Adjusting multistate capture-recapture models for misclassification bias: Manatee breeding proportions. *Ecology*, 84:1058–1066, 2003.

- [96] Zackary R. Kenz, H. T. Banks, and Ralph C. Smith. Comparison of frequentist and Bayesian confidence analysis methods on a viscoelastic stenosis model. *SIAM/ASA Journal on Uncertainty Quantification*, 1(1):348–369, 2013.
- [97] O. Klevien, P. Larsson, and A. Hobaek. Sexual reproduction in *Daphnia magna* requires three stimuli. *Oikos*, 65:197–206, 1992.
- [98] Saskia Knillmann, Nathalie C. Stampfli, Yury A. Noskov, Mikhail A. Beketov, and Matthias Liess. Elevated temperature prolongs long-term effects of a pesticide in *Daphnia* spp. due to altered competition in zooplankton communities. *Global Change Biology*, 19:1598–1609, 2013.
- [99] Michiyori Kobayashi and Toru Nezu. Variation of hemoglobin content in *Daphnia magna*. *Physiological Zoology*, 59(1):35 – 42, 1986.
- [100] Sanna Koivisto and Matti Ketola. Effects of copper on life-history traits of *Daphnia pulex* and *Bosmina longirostris*. *Aquatic Toxicology*, 32:255–269, June 1995.
- [101] Michal Komorowski, Maria J. Costa, David A. Rand, and Michael P. H. Stumpf. Sensitivity, robustness, and identifiability in stochastic chemical kinetics models. *PANS*, 108(21):8645–8650, 2011.
- [102] H. Korpelainen. The effects of temperature and photoperiod on life history parameters of *Daphnia magna* (crustacea: Cladocera). *Freshwater Biol.*, 16:615–620, 1986.
- [103] H. Korpelainen. Sex ratios and conditions required for environmental sex determination in animals. *Biol. Rev.*, 65:147 – 184, 1990.
- [104] W. Lampert. Response of the respiratory rate of *Daphnia magna* to changing food conditions. *Oecologia*, 70(4):495–501, 1986.
- [105] G. A. LeBlanc and C. V. Rider. An integrated addition and interaction model for assessing toxicity of chemical mixtures. *Toxicological Sciences*, 87(2):520–528, 2005.
- [106] G. A. LeBlanc, Y. H. Wang, C. N. Holmes, G. Kwon, and E. K. Medlock. A transgenerational endocrine signaling pathway in crustacea. *PLoS One*, 8(4):e61715, 2013.
- [107] Gerald A. LeBlanc. Laboratory investigation into the development of resistance of *Daphnia magna* (strauss) to environmental pollutants. *Environmental Pollution Series A, Ecological and Biological*, 27:309–322, April 1982.
- [108] P. H. Leslie. On the use of matrices in certain population mathematics. *Biometrika*, 33(3):183–212, 1945.
- [109] H. Lilliefors. On the Kolmogorov-Smirnov test for normality with mean and variance unknown. *Journal of the American Statistical Association*, 62:399–402, June 1967.

- [110] Fernando Martínez-Jerónimo, Rafael Villase nor, Guillermo Rios, and Félix Espinosa. Effect of food type and concentration on the survival, longevity, and reproduction of *Daphnia magna*. *Hydrobiologia*, 287:207–214, 1994.
- [111] Joaquim R. R. A. Martins, Ilan M. Kroo, and Juan J. Alonso. An automated method for sensitivity analysis using complex variables. In *Proc. 38th Aerospace Sciences Meeting*, pages 1–12. Amer. Inst. Aeronautics and Astronautics, 2000. paper AIAA-2000-0689.
- [112] MathWorks. Nonlinear mixed-effects modeling: Maximum likelihood estimation. [http://www.mathworks.com/help/simbio/ug/what-is-nonlinear-mixed-effects-modeling.html?searchHighlight=simbiology%20nlme#bui\\_w1q](http://www.mathworks.com/help/simbio/ug/what-is-nonlinear-mixed-effects-modeling.html?searchHighlight=simbiology%20nlme#bui_w1q). Accessed: 2015-09-10.
- [113] Edward McCauley, William A. Nelson, and Roger M. Nisbet. Small-amplitude cycles emerge from stage-structured interactions in *Daphnia*-algal systems. *Nature*, 455, October 2008.
- [114] H.-G. Müller and U. Stadtmüller. Estimation of heteroscedasticity in regression analysis. *Annals of Statistics*, 15:610–625, 1987.
- [115] I. G. Munro and R. W. G. White. Comparison of the influence of temperature on the egg development and growth of *Daphnia longispina* O.F. Müller (Crustacea:Cladocera) from two habitats in southern England. *Oecologia*, 20:157–165, 1975.
- [116] W. W. Murdoch, B. E. Kendall, R. M. Nisbet, C. J. Briggs, W. McCauley, and R. Bolser. Single-species models for many-species food webs. *Nature*, 417:541 – 543, 2002.
- [117] K. F. Murphy, R. M. Adams, X. Wang, G. Balazsi, and J. J. Collins. Tuning and controlling gene expression noise in synthetic gene networks. *Nucleic Acids Research*, 38(8):2712–2726, 2010.
- [118] R. Kent Nagle, Edward Saff, and Arthur Snider. *Fundamentals of Differential Equations and Boundary Value Problems*. Pearson Education, Boston San Francisco New York, fourth edition, 2004.
- [119] W. E. Neill. Experimental studies of microcrustacean competition, community composition and efficiency of resource utilization. *Ecology*, 56:809–826, 1975.
- [120] Gregor Neuert, Brian Munsky, Rui Zhen Tan, Leonid Teytelman, Mustafa Khammash, and Alexander van Oudenaarden. Systemic identification of signal-activated stochastic gene regulation. *Science*, 339, 2013.
- [121] A. Noueiry and P. Ahlquist. Brome mosaic virus RNA replication: revealing the role of the host in RNA virus replication. *Annual Review of Phytopathology*, 41:77–98, 2003.
- [122] E. Oberdörster, D. Rittschof, and G. A. LeBlanc. Alteration of [<sup>14</sup>C]-testosterone metabolism after chronic exposure of *Daphnia magna* to tributyltin. *Arch. Environ. Contam. Toxicol.*, 34:21–25, 1998.

- [123] National Institutes of Health. Daphnia. Model Organisms for Biomedical Research.
- [124] A. W. Olmstead and G. A. LeBlanc. The environmental-endocrine basis of gynandromorphism in a crustacean. *International Journal of Biological Sciences*, 3:77–84, 2007.
- [125] Allen W. Olmstead and Gerald A. LeBlanc. Effects of endocrine-active chemicals on the development of sex characteristics of *Daphnia magna*. *Environmental Toxicology and Chemistry*, 19(8):2107–2113, 2000.
- [126] Allen W. Olmstead and Gerald A. LeBlanc. Insecticidal juvenile hormone analogs stimulate the production of male offspring in the crustacean *Daphnia magna*. *Environmental Health Perspectives*, 111, June 2003.
- [127] A.W. Olmstead and G.A. LeBlanc. Temporal and quantitative changes in sexual reproductive cycling of the cladoceran *Daphnia magna* by a juvenile hormone analog. *J. Exp. Zool.*, 290:148–155, 2001.
- [128] Richard Ottermanns, Kerstin Szonn, Thomas G. Preuß, and Martina Roß-Nickoll. Non-linear analysis indicated chaotic dynamics and reduced resilience in model-based daphnia populations exposed to environmental stress. *PLOS One*, 9(5), May 2014.
- [129] R. Peto and J. Peto. Asymptotically efficient rank invariant test procedures. *J. Royal Statistical Society, Series A (Blackwell Publishing)*, 135(2):185–207, 1972.
- [130] B. Pietrzak, M. Grzesiuk, and A. Bednarska. Food quantity shapes life history and survival strategies in *Daphnia magna* (Cladocera). *Hydrobiologia*, 643:51–54, 2010.
- [131] Barbara Pietrzak, Anna Bednarska, and Malgorzata Grzesiuk. Longevity of *Daphnia magna* males and females. *Hydrobiologia*, 643:71–75, 2010.
- [132] K. G. Porter, D. Orcutt, and J. Gerritsen. Functional response and fitness in a generalist filter feeder, *Daphnia magna* (Cladocera: Crustacea). *Ecology*, 64(4):735–742, 1983.
- [133] D. M. Pratt. Analysis of population development in *daphnia* at different temperatures. *The Biological Bulletin*, 85(2):116–140, 1943.
- [134] T. G. Preuss, M. Hammers-Wirtz, U. Hommen, M. N. Rubach, and H. T. Ratte. Development and validation of an individual based *Daphnia magna* population model: The influence of crowding on population dynamics. *Ecological Modeling*, 220:310–329, 2009.
- [135] Stephanie Prigent, Wafaâ Haffaf, H. T. Banks, M. Hoffmann, Human Rezaei, and Marie Doumic. Size distribution of amyloid fibrils. mathematical models and experimental data. *International Journal of Pure and Applied Mathematics*, 93(6):845–878, 2014.
- [136] Sandy Raimondo and Jr. Charles L. McKenney. Projecting population-level responses of mysids exposed to an endocrine disrupting chemical. *Integr. Comp. Biol.*, 45:151–157, 2005.

- [137] W. E. Ricker. Stock and recruitment. *J. Fish. Res. BD. Canada*, 11(5):559–623, 1954.
- [138] C. V. Rider, T. A. Gorr, A. W. Olmstead, B. A. Wasilak, and G. A. LeBlanc. Stress signaling: coregulation of hemoglobin and male sex determination through a terpenoid signaling pathway in a crustacean. *Journal of Experimental Biology*, 208:15–23, 2005.
- [139] J. H. Ryther. Inhibitory effects of phytoplankton upon the feeding of *daphnia magna* with reference to growth, reproduction, and survival. *Ecology*, 35(4):522–533, 1954.
- [140] M. Schwartz, J. Chen, M. Janda, M. Sullivan, J. A. den Boon, and P. Ahlquist. A positive-strand RNA virus replication complex parallels form and function of retrovirus capsids. *Molecular Cell*, 9:505–514, 2002.
- [141] G. A. Seber and C. J. Wild. *Nonlinear Regression*. Wiley, Hoboken, 2003.
- [142] G. A. F. Seber and A. J. Lee. *Linear Regression Analysis*. Wiley, Hoboken, 2003.
- [143] L. F. Shampine. Solving Hyperbolic PDEs in MATLAB. 2:346 – 358, December 2005.
- [144] J. W. Sinko and W. Streifer. A new model for age-size structure of a population. *Ecology*, 48:910–918, 1967.
- [145] Ralph C. Smith. *Uncertainty Quantification: Theory, Implementation, and Applications*. Computation Science and Engineering. SIAM, 2014.
- [146] A. Solonen. Monte carlo methods in parameter estimation of nonlinear models. Master’s thesis, Lappeenranta University of Technology, Lappeenranta, Finland, 2006.
- [147] A. Solonen, P. Ollinaho, M. Laine, H. Haario, J. Tamminen, and H. Järvinen. Efficient MCMC for climate model parameter estimation: parallel adaptive chains and early rejection. *Bayesian Analysis*, 7(3):715–736, 2012.
- [148] J. D. Stark and J. E. Banks. Selective pesticides: are they less hazardous to the environment? *Bioscience*, 51:980–982, 2001.
- [149] J. D. Stark and J. E. Banks. Population-level effects of pesticides and other toxicants on arthropods. *Annu. Rev. Entomol.*, 48:505–519, 2003.
- [150] R.G. Stross. Photoperiod control of diapause in *Daphnia*. iii. two-stimulus control of long-day, short-day induction. *Biol. Bull.*, 137:359–374, 1969.
- [151] R.G. Stross and J.C. Hill. Diapause induction in *daphnia* requires two stimuli. *Science*, 150:1462–1464, 1965.
- [152] D. M. Thomson. Matrix models as a tool for understanding invasive plant and native plant interactions. *Conserv. Biol.*, 19:917–928, 2005.



- [153] M. B. Vandegehuchte, F. Lemiere, L. Vanhaecke, W. V. Berghe, and C. R. Janssen. Direct and transgenerational impact on *Daphnia magna* of chemicals with a known effect on DNA methylation. *Comparative Biochemistry and Physiology, Part C*, 151:278–285, 2010.
- [154] J. R. Vonesh and O. De la Cruz. Complex life cycles and density dependence: assessing the contribution of egg mortality to amphibian declines. *Oecologia*, 133:325–333, 2002.
- [155] J.A. Vrugt, C.G.H. Diks, H.V. Gupta, W. Bouten, and J.M. Verstraten. Improved treatment of uncertainty in hydrologic modeling: combining the strengths of global optimization and data assimilation. *Water Resources Research*, 41:W01017, 2005.
- [156] H. Y. Wang, A. W. Olmstead, H. Li, and G. A. LeBlanc. The screening of chemicals for juvenoid-related endocrine activity using the water flea *Daphnia magna*. *Aquatic Toxicology*, 74:193–204, 2005.
- [157] Y. H. Wang, G. Kwon, H. Li, and G. A. LeBlanc. Tributyltin synergizes with 20- hydroxyecdysone to produce endocrine toxicity. *Tox. Sci.*, 123:71–79, 2011.
- [158] D.A. Warner, M.B. Lovern, and R. Shine. Maternal nutrition affects reproductive output and sex allocation in a lizard with environmental sex determination. *Proc. Biol. Sci.*, 274:883–890, 2007.
- [159] Denis Weber, Dieter Schaefer, Michael Dorgerloh, Eric Bruns, Gerhard Goerlitz, Klaus Hammel, Thomas G. Preuss, and Hans Toni Ratte. Combination of a higher-tier flow-through system and population modeling to assess the effects of time-variable exposure of isoproturon on the green algae *DESMODESMUS SUBSPICATUS* and *PSEUDOKIRCHNERIELLA SUBCAPITATA*. *Environmental Toxicology and Chemistry*, 31(4):899 – 908, 2012.
- [160] U. Wennergren and J. D. Stark. Modeling long-term effects of pesticides on populations: beyond just counting dead animals. *Ecol. Appl.*, 10:295–302, 2000.
- [161] J. D. Willson, W. A. Hopkins, C. M. Bergeron, and B. D. Todd. Making leaps in amphibian ecotoxicology: translating individual-level effects of contaminants to population viability. *Ecological Applications*, 22(6):1791 – 1802, 2012.
- [162] P. H. Wilson. Using population projection matrices to evaluate recovery strategies for Snake River Spring and Summer Chinook salmon. *Conserv. Biol.*, 17:782–794, 2003.
- [163] Hans Georg Wolf and Gary R. Carvalho. Resting eggs of lake-*Daphnia* II. *In situ* observations on the hatching of eggs and their contribution to population and community structure. *Freshwater Biology*, 22:471–478, 1989.
- [164] S. N. Wood. Obtaining birth and mortality patterns from structured population trajectories. *Ecol. Monogr.*, 64:23–44, 1994.

## **APPENDICES**

## Other Daphnid Work

### A.1 Considering Probabilistic Fecundity <sup>1</sup>

#### A.1.1 Background and Data

Our population model specified in Chapter 3 uses the average fecundity per daphnid per day (Figure 3.3) as a measure of density-independent daphnid fecundity. Here we examine the raw fecundity data from our individual experiment (see Section 3.2.2.1 for experimental details) to determine if using that raw data meaningfully improves upon our population model.

First examination of the raw data suggests that the fecundity follows a periodic pattern with a variance that can be determined (Figure A.1), where the period would be 3-4 days, which is the time between daphnid broods. Upon further investigation, it appears that the variance of the data varies widely from day to day, and contains multiple outliers (Figure A.2). This contrasts with our daphnid growth rate data (Figure A.8), which contained small variances (Table 3.2) and could be estimated using a nonlinear mixed effects model (Figure 3.2). Due to this contrast we require a different approach to model the raw fecundity data.

Considering the daily fecundity appears too difficult for direct modeling, and thus we considered the offspring created per brood (Figure A.3). Here we lose the periodicity seen in the raw data, and are left with still scattered observations that appear to be nondeterministic. These observations of the data caused us to pursue the possibility of probabilistic fecundity. Such a consideration for fecundity has been pursued in previous modeling attempts by other researchers. For example,

---

<sup>1</sup> Contributions:  
 Modeling, analysis, and writeup: Kaska Adoteye  
 Advisor: H.T. Banks

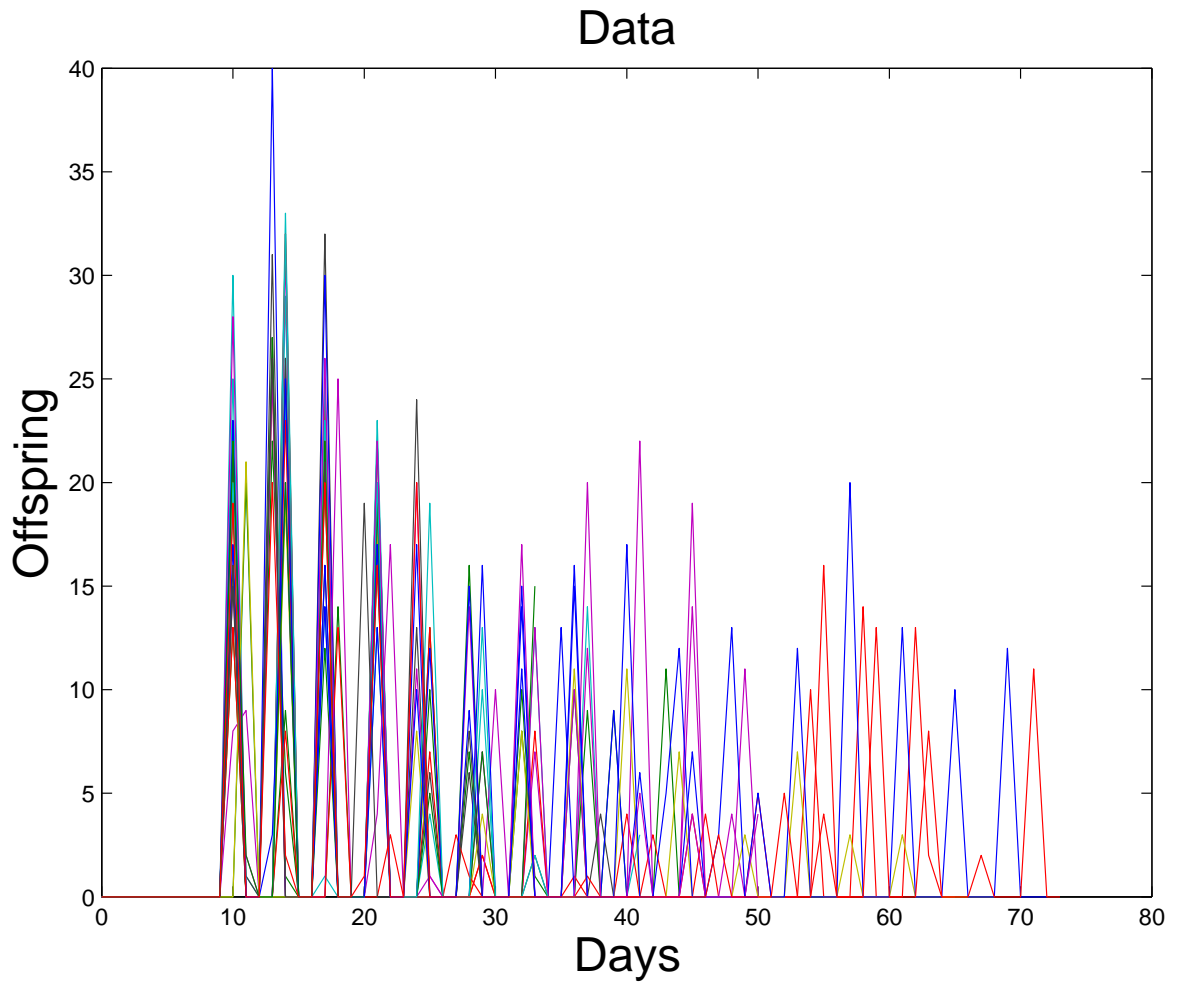


**Figure A.1** This is the data for the number of offspring created by each daphnid. The longitudinal data for each individual daphnid is represented by a line of a single color (for example, the yellow line represents the same daphnid). A clear functional form is not apparent, although the data does appear to be somewhat periodic.

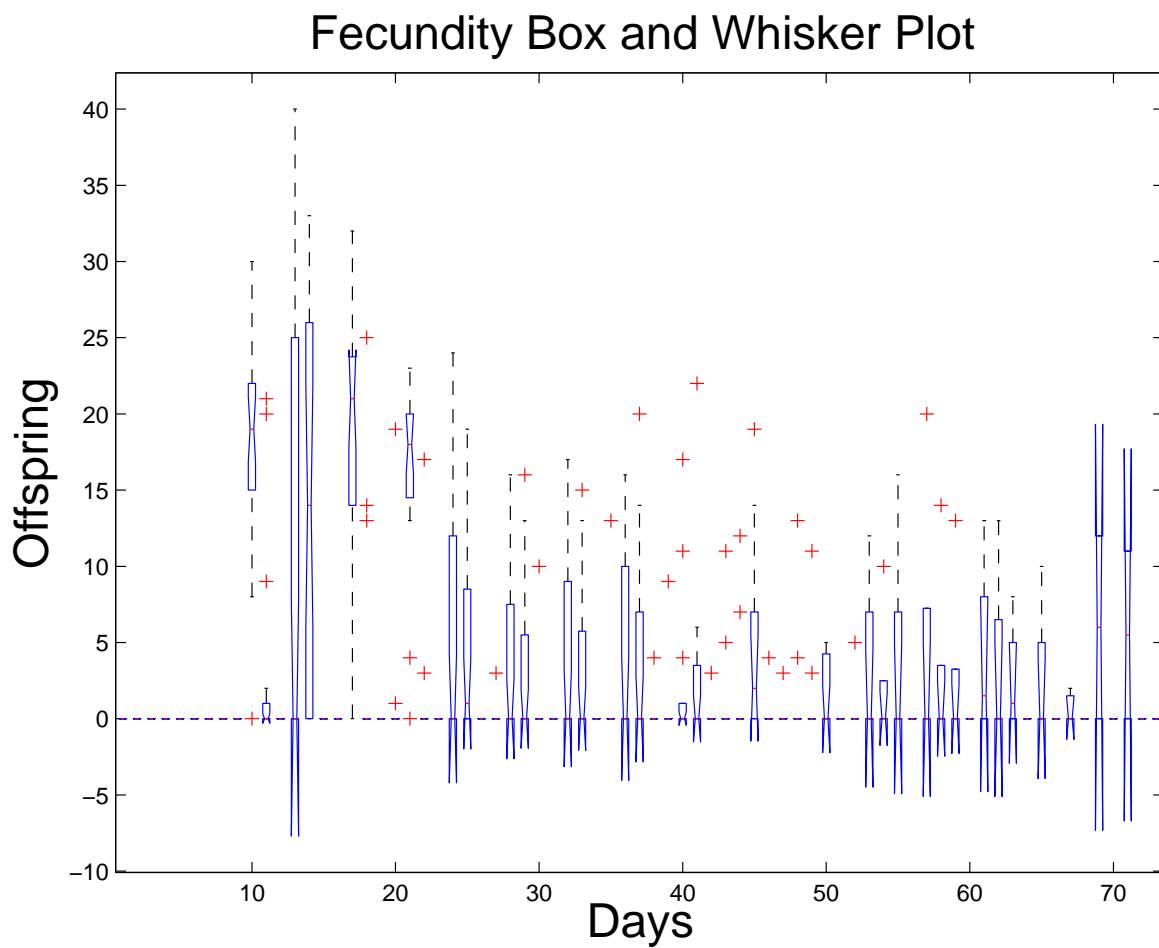


**Figure A.2** Here we see a box and whisker plot of the data in Figure A.1. This plot shows the changing and wide variability in the data. Each box and whisker corresponds to the offspring created by each daphnid on a given day.

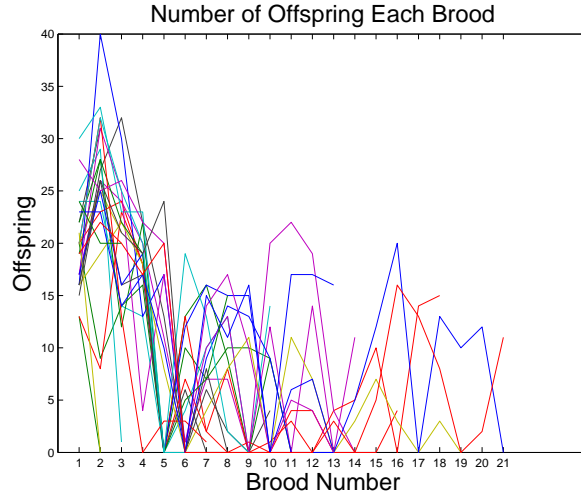


**Figure A.3** This is the data for the number of offspring per brood. The longitudinal data for each individual daphnid is represented by a line of a single color (for example, the yellow line represents the same daphnid).

Preuss et. al. considered fecundity as being normally distributed about a mean [134], and Erickson et. al. considered it to be from a Poisson distribution [71], but here we will consider probabilistic daphnid fecundity in more generality.

### A.1.2 Introducing Probability

When considering probabilistic daphnid fecundity we first attempted to produce a probability density function for the data shown in Figure A.3. This was performed using a kernel density estimator with adaptive bandwidth as outlined by Z.I. Botev et. al. [47] and implemented by Botev in the Matlab function *kde*. A Gaussian kernel density estimator is defined as

$$\hat{f}(x, t) = \frac{1}{N} \sum_{i=1}^N \frac{1}{\sqrt{2\pi t}} e^{-(x-X_i)^2/(2t)} \quad (\text{A.1})$$

where  $x \in \mathbb{R}$ , we are given  $N$  independent realizations  $\chi_N = \{X_1, \dots, X_N\}$  from an unknown continuous probability density function  $f$  on  $\mathcal{X}$ , and  $\sqrt{t}$  is the scale (referred to as bandwidth). This is thus a sum of Gaussian probability density functions around our observations, and is often used to estimate true probability density functions. Botev's approach hinges on the fact that the Gaussian kernel density estimator in Equation (A.1) is the unique solution to the diffusion partial differential

equation

$$\frac{\partial}{\partial t} \hat{f}(x, t) = \frac{1}{2} \frac{\partial^2}{\partial x^2} \hat{f}(x, t), \quad x \in \mathcal{X}, t > 0, \quad (\text{A.2})$$

with  $\mathcal{X} = \mathbb{R}$  and initial condition  $\hat{f}(x, 0) = \frac{1}{N} \sum_{i=1}^N \delta(x - X_i)$ , which is the empirical density of the data  $\chi_N$  where  $\delta(x - X_i)$  is the Dirac measure at  $X_i$ . Therefore, finding the kernel density estimator is simply solving the heat equation, whose solution is well-known. This method avoids some of the pitfalls of other methods to determine Gaussian kernel density estimators, such as boundary bias. For a more comprehensive overview of kernel density estimators, see [47] and the references therein.

We estimated the probability density function for the number of offspring created by all daphnids in a particular brood. The densities appeared normal when the daphnids that produced no offspring in that brood are not considered. At this point we tested if the number of offspring in each brood actually came from a normal distribution. To do this, we performed a Lilliefors test for normality [109] on that data. The Lilliefors test, implemented with the function *lillietest* in Matlab, computes the test statistic

$$\max_x |F(x) - G(x)|$$

where  $F(x)$  is the empirical cumulative distribution function (cdf) computed from the data, and  $G(x)$  is a normal distribution with the same mean and variance of the data. We found that, with 99 % significance the offspring for every brood can be considered normal when not considering daphnids that produced zero offspring.

Thus, in order to quantify the fecundity, there are three parameters for each brood that need to be quantified: the proportion,  $\gamma_i$ , of daphnids that create zero offspring at brood  $i$ , and then for the daphnids that do produce offspring, the mean  $\mu_i$  and variance  $\sigma_i^2$  for the normal distribution that the number of offspring in brood  $i$  is drawn from. Table A.1 contains these parameters for each of the broods. The parameters for the normal distributions were determined using the function *fitdist* in Matlab. It should be noted that if individual longitudinal data is collected, as it was here, then  $\gamma_i$  and  $\mu_i$  can be determined strictly from the data and thus do not need to be estimated. If aggregate data is collected, then all three parameters will need to be estimated for each brood.

### A.1.3 Population Model Incorporating Probabilistic Fecundity/Testing Within a Population Model

This section is a continuation of the population model comparison performed in Chapter 3, where we tested four models (models A-D) and determined that model D provided the best fit to the data. Here we consider model E. This model is a specification of the structured population model in

**Table A.1** Fecundity parameters for our daphnids from our individual experiments.  $\gamma_i$  is the proportion of living daphnids that create zero offspring in brood  $i$ . The other daphnids produce a number of offspring pulled from the distribution  $N(\mu_i, \sigma_i^2)$  for brood  $i$ .

Brood # $i$	Approx. Day $t_i$	$\gamma_i$	$\mu_i$	$\sigma_i$
1	10	0	19.7308	4.2573
2	14	0.0769	25.5	6.97199
3	17	0	19.913	6.75488
4	21	0.0500	17.7368	4.31846
5	23	0.5000	14.3	6.42996
6	25	0.4000	7.83333	5.58949
7	28	0.1500	8.64706	4.89823
8	32	0.2632	10.2857	4.63147
9	36	0.5333	10.8571	4.94734
10	38	0.4667	9.75	5.8493
11	41	0.3636	9.71429	7.29644
12	45	0.3000	10.2857	6.26403
13	48	0.6000	6.75000	6.18466
14	50	0.4286	6.0000	3.4641
15	53	0.2000	8.5	3.10913
16	57	0.2000	10.7500	8.53913
17	59	0.5000	13.5000	0.707107
18	61	0	9.7500	5.37742
19	65	0.66667	10	0
20	69	0	7	7.07107
21	71	0.5000	11	0



Equation (3.1). The terms  $a(t, i)$  and  $b(t, i)$ , which correspond to the fecundity and mortality of daphnids of age  $i$  at time  $t$ , respectively, will be the same as in model D (Table 3.1), except that we will consider a variation on the term  $\alpha(i)$  based on our findings in Appendix A.1.2. Here we will have  $\alpha(t_i) \sim N(\mu_i, \sigma_i^2)$  with probability  $1 - \gamma_i$ ,  $i = 1, 2, \dots, 21$ , and with probability  $\gamma_i$  we have  $\alpha(t_i) = 0$ , where  $t_i, \mu_i, \sigma_i$ , and  $\gamma_i$  are drawn from Table A.1.

We will estimate the parameters  $\theta = (\mu, q, c)$  for model E using the exact same inverse problem methodology outlined in Section 3.2.4, in order for more accurate model comparison. That is, parameters were estimated from the population data using a vector ordinary least squares (OLS) framework [31, 39]. For each model, we consider a vector of parameters  $\theta$  to estimate. Based on our individual-level modeling, the number of juveniles and adults are given by  $f_J(t, \theta) = \sum_{i=1}^4 p(t, i)$  and  $f_A(t, \theta) = \sum_{i=5}^{i_{max}} p(t, i)$ , respectively. The corresponding observation vector is given by  $\mathbf{f}(t, \theta) = [f_J(t, \theta), f_A(t, \theta)]^T$ . We assumed a constant statistical error model, as verified in Section 3.3.2, of the form

$$\mathbf{Y}_j = \mathbf{f}(t_j, \theta_0) + \mathcal{E}_j, \quad j = 1, 2, \dots, n, \quad (\text{A.3})$$

where  $\mathbf{Y}_j$  is a random variable with realizations  $\mathbf{y}_j = [J(t_j), A(t_j)]^T$  (i.e., the data, where  $J(t_j)$  and  $A(t_j)$  are the number of juveniles and adults, respectively, at time  $t_j$ ) and  $\mathbf{f}(t_j, \theta_0)$  is the model observation with the hypothesized “true” parameter vector  $\theta_0$ . The error terms  $\mathcal{E}_j$  are assumed independent and identically distributed (i.i.d) random variables with mean  $E[\mathcal{E}_j] = 0$  and  $V_0 = \text{var}(\mathcal{E}_j) = \text{diag}(\sigma_{J,0}^2, \sigma_{A,0}^2)$ , where  $\sigma_{J,0}^2$  and  $\sigma_{A,0}^2$  are the observation variances for the juvenile and adult observations, respectively. An estimate,  $\hat{\theta}$ , for the true parameter vector  $\theta_0$  is obtained by implementing an iterative algorithm (see [39] for details).

The inverse problems here were computed using two routines in Matlab. The first routine is a direct search algorithm implemented by Daniel Finkel as *direct*, and can be found at [http://www4.ncsu.edu/~ctk/Finkel\\_Direct/](http://www4.ncsu.edu/~ctk/Finkel_Direct/). This was used with the following options: options.maxevals = 400; options.maxits = 400; options.maxdeep = 400; and the output was used as the initial condition for the gradient based Matlab search routine *lsqnonlin*. *lsqnonlin* was run with the options ‘TolFun’ and ‘TolX’ set equal to 1e-20, and the option ‘MaxFunEvals’ set equal to 400. The output of *lsqnonlin* was then used as our parameter estimate. For model E, *randn* in Matlab was used to find normally distributed random numbers, and *rand* was used to find a uniformly distributed random number to account for the  $\gamma_i$ .

We then compared models using Akaike Information Criteria, and more specifically the Akaike weights. The Akaike Information Criterion (AIC) score gives an approximately unbiased form of the Kullback-Leibler Distance, or a measure of the distance between a model and the corresponding data [39]. The AIC score is used to compare the accuracy of different models to the same data set; a lower

$AIC$  score indicates higher accuracy. While we have previously used  $AIC$  to compare models for the growth of daphnids (Section 3.2.6.2), those models used single observations at each time point (the major axis length of the daphnid), while here we use multivariate observations at each time point (the number of juveniles and adults). The  $AIC$  score for independent multivariate normally distributed observations in the case of nonlinear models is given by  $AIC = n \nu \ln\left(\frac{RSS}{n \nu}\right) + n \nu (1 + \ln(2\pi)) + 2(p + 1)$ , where  $RSS$  is the residual sum of squares [39, 49]. The  $AIC$  score corrected for small sample size ( $n/p < 40$ ,  $n$  = number of data points,  $p$  = number of parameters) in the case of multivariate observations ( $\nu$  = number of observables) is given by  $AIC_C = AIC + 2 \frac{\tilde{p}(\nu + p + 1)}{n - (\nu + p + 1)}$ , where  $\tilde{p}$  is the total number of unknown parameters estimated in the mathematical and statistical models. Here, we take  $\tilde{p} = p$ , since we do not estimate directly the variances  $\sigma_{J,0}^2$  and  $\sigma_{A,0}^2$  in addition to the  $p$  parameters for the mathematical model. We note that although this  $AIC_C$  formula was derived for multivariate linear regression models [45], the authors claimed that this formula can be generalized to multivariate nonlinear regression models. We tacitly assume this can be done and hence use the above formulae for our  $AIC_C$  analysis here.

In order to further validate our results, we also computed the Akaike weights  $w_i$ , given by

$$w_i = \frac{\exp\left(\frac{1}{2}(AIC_{C,min} - AIC_{C,i})\right)}{\sum_{r=1}^4 \exp\left(\frac{1}{2}(AIC_{C,min} - AIC_{C,r})\right)}$$

where  $AIC_{C,min}$  is the smallest  $AIC_C$  among the discussed models and  $AIC_{C,i}$  is the  $AIC_C$  value for model  $i$ . The larger the  $w_i$ , the more likely it is that model  $i$  describes the data best [39].

What we find is that, even though model E contains theoretically more detailed information about the fecundity, model D still describes the data best. For Replicate 1, the Akaike weights for models D and E were 0.9025 and 0.0975, respectively. For Replicate 2, the Akaike weights for models D and E were 0.9454 and 0.0546, respectively. It is important to note that since model E used random values, the fits to the data could change wildly depending on simulation. As a result, simulations for model E were run 1000 times and the average of the  $AIC_C$  value found for model E was used when computing weights. Therefore, while we might be able to better describe the random nature of daphnid reproduction using probability densities, those densities do not necessarily aid in population-level modeling as they were implemented. In a sense this is not surprising, as the law of large numbers would suggest that as the number of daphnids increases in a population, the observed number of offspring would tend towards the mean, which is an effect that model D captures. Without improvements to either the probabilistic fecundity modeling or its incorporation into a population-level model, we recommend model D for further analysis and population prediction.

## A.2 Supplemental Experiments<sup>2</sup>

Throughout the dissertation we have outlined multiple experiments that we have then used in our daphnid modeling. Those were but a few of the many experiments that we conducted while expanding our knowledge of the organism. Below we provide a brief description of some of the other experiments we conducted, our reasoning behind conducting the experiment, our results, and any conclusions we could glean. Where appropriate, we will also discuss what these findings could mean for the proposed theoretical model explained in Section 5.5.3, so as to provide a blueprint that future modelers can follow, or at least gain information from.

### A.2.1 Feeding Experiment

#### A.2.1.1 Motivation

There has been extensive work on the response of *Daphnia magna* to changes in food concentration. For example, Lampert considered the response of daphnid respiratory rate to changing food conditions [104]. Martínez-Jerónimo et. al. considered the effects of food type and concentration on the survival, longevity, and reproduction of daphnids [110]. Pietrzak et. al. considered the life history and survival strategies of daphnids to food quantity [130]. In addition, Preuss et. al. considered daphnid populations using both flow-through and semi-batch feeding conditions [134]. Our investigation rested with the question of how our species of daphnid reacts specifically to our species of algae with respect to lifespan and fecundity.

That is, previous work has demonstrated that the quantity and species of algae has dramatic effects on the organismal outcomes of daphnids. We conjectured that the species and clone of daphnid may also play a role. Despite the large body of work on the effect of food on daphnid dynamics, we were unable to find convincing evidence of the effect of varying concentrations of the algae *Raphidocelis subcapitata* on *Daphnia magna*. This question is important, as we calibrated our population model using individual dynamics from daphnids raised in 40mL of media fed 100  $\mu$ L of an algae solution and 50  $\mu$ L of fish food solution daily, which amounts to  $7.0 \times 10^6$  cells of algae (*Raphidocelis subcapitata*) and 0.2 mg (dry weight) Tetrafin<sup>TM</sup> fish food suspension prepared as described previously [124] (Section 3.2.2.1 for more details).

We conjecture that the quantity of food affects daphnid mortality and fecundity, and thus we

---

<sup>2</sup>Contributions:

Experimental design and data collection: Kaska Adotey, Kevin Flores, Timothy Nguyen, Chelsea Ross, Emmaline Smith, Michael Stemkovski, and Sarah Stokely

Writeup and analysis: Kaska Adotey

Advisors: H.T. Banks and Gerald A. LeBlanc

**Table A.2** The food concentrations for each group of the experiment. The algae solution used to feed the beakers contains the number of cells specified, and the fish food solution contains the specified mg of fish food.

Group	$\mu\text{L}$ Algae Solution	Cells of Algae	$\mu\text{L}$ Fish Food Solution	mg Fish Food
1	320	$2.24 \times 10^7$	160	0.64
2	160	$1.12 \times 10^7$	80	0.32
3	100	$7.0 \times 10^6$	50	0.2
4	50	$3.5 \times 10^6$	25	0.1
5	25	$1.75 \times 10^6$	12.5	0.05

will experiment with various amounts of our algae and fish food solutions on individual daphnids. From these experiments we can determine the fecundity and mortality of daphnids under these conditions, which can eventually be incorporated into a daphnid population model which considers changing food concentrations.

#### A.2.1.2 Experimental Design

The experiment consisted of five groups of female daphnids. Daphnids were longitudinally observed to estimate population average rates of fecundity and mortality. Less than 2-h old neonates were placed individually into 50mL beakers containing 40mL of media each. Media was changed daily. The number of neonates produced by each individual daphnid was recorded and then removed daily. Fecundity measurements were performed until no daphnids remained (86 days). Daphnids in each group were fed different concentrations of algae (*Raphidocelis subcapitata*) and Tetrafin<sup>TM</sup> fish food suspension prepared as described previously [124] (Table A.2). Groups 1, 2, 4, and 5 contained 20 daphnids each. Group 3 consists of 30 daphnids, as it is exactly the data obtained from Section 3.2.2.1.

Cultured daphnids were maintained using previously described protocols and conditions [157]. Cultured daphnids were kept in media reconstituted from deionized water [10]. Cultured daphnids for both studies were maintained in an incubator maintained at 20 degrees Celsius with a 16-h light, 8-h dark cycle. The daphnids used in our study came from a colony that was maintained at North Carolina State University for over 20 years (clone NCSU1 [138]).

#### A.2.1.3 Results and Implications for Modeling

The lifespan of daphnids decreased as food concentration increased (Figure A.4). We see that for each food concentration the mortality is not constant, which suggests that a modeling approach

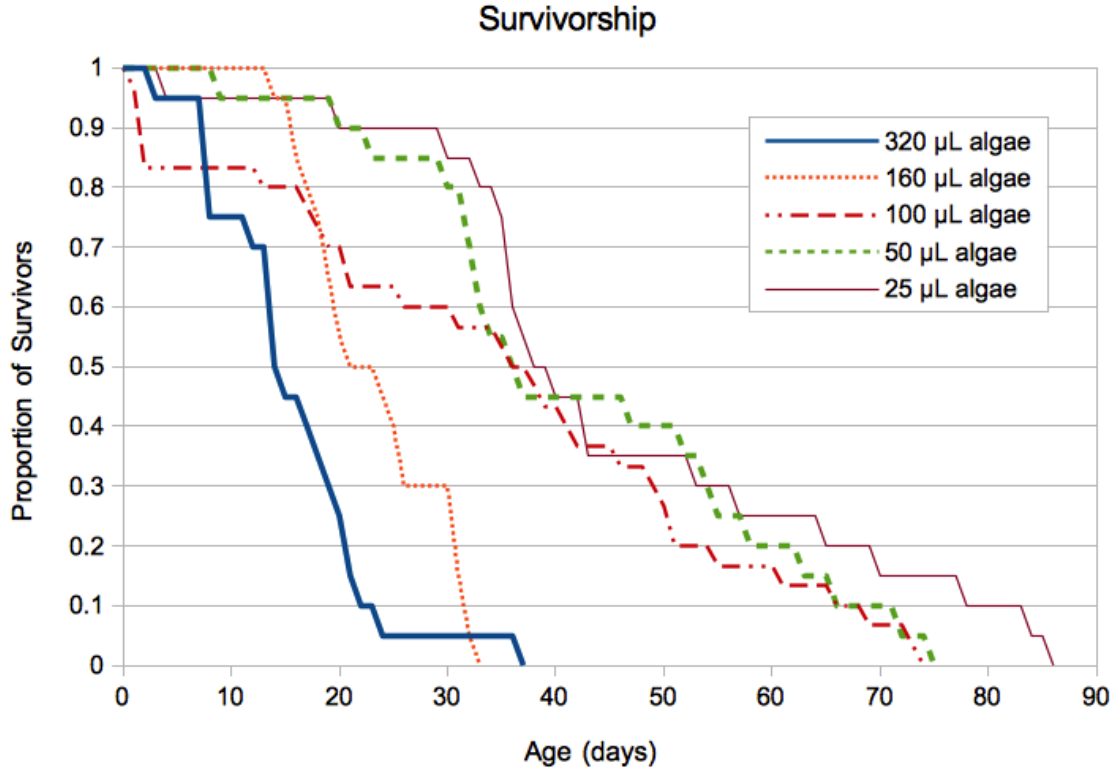


**Figure A.4** The proportion of surviving daphnids from the five groups.

identical to what was performed in Chapter 4 could describe the mortality for each concentration. The fecundity seems to increase as food concentration increases to the 100  $\mu\text{L}$  concentration, and then decreases, showing a nonlinear response of daphnid density-independent fecundity to food concentration (Figure A.5).

These results point to a possible extension to the comprehensive daphnid model hypothesized in Section 5.5.3 which includes food concentration. We will begin with the same theoretical framework, where we assume that there exists an intrinsic parameter  $\gamma$  that daphnids have, which can represent both their subpopulation as well as the density at which the daphnid was born. Let's assume  $\gamma \in \Gamma$ , where  $\Gamma$  is a range of admissible parameters, and let  $P$  be the distribution of the  $\gamma$ 's in  $\Gamma$ . Let  $a$  be the daphnid's age and  $s$  be the daphnid's size, and thus we have that the density of daphnids at time  $t$ , age  $a$ , size  $s$ , and intrinsic parameter  $\gamma$  is given by

$$u(t, a, s, \gamma).$$

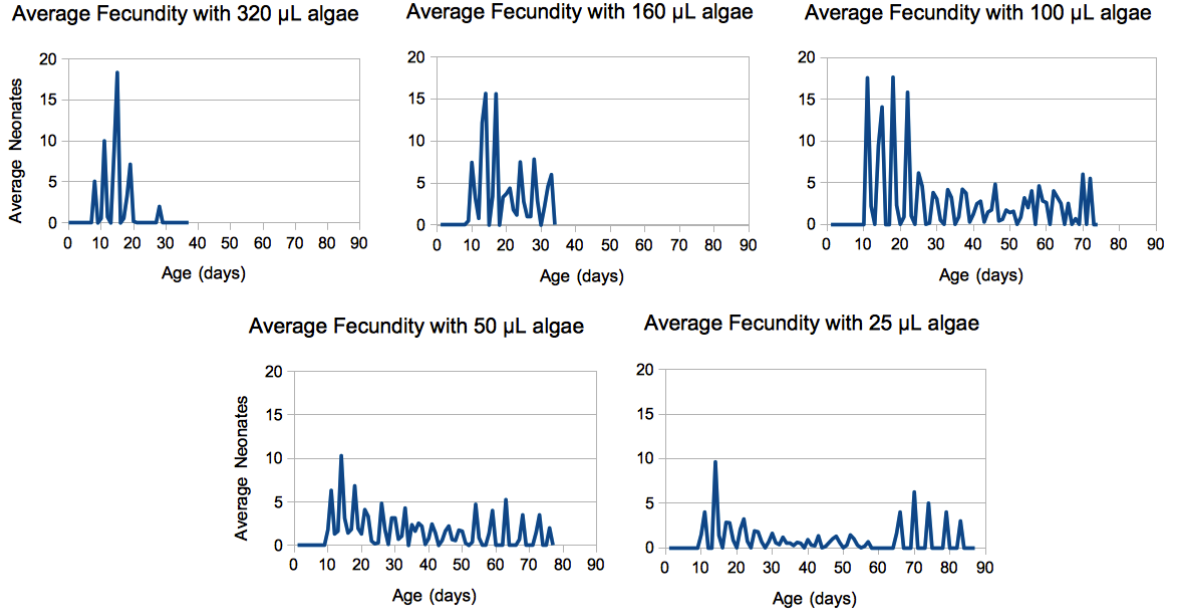


**Figure A.5** The number of neonates produced per female daphnid per day for each group. Data was collected daily, and the lines connecting each daily data point are drawn to show general trends.

The total population density is then given by

$$v(t, P) = \int_0^{a_{max}} \int_{s_0}^{s_{max}} \int_{\Gamma} u(t, a, s, \gamma) dP(\gamma) ds da,$$

where  $a_{max}$  is the maximum age of daphnids and  $s_0$  and  $s_{max}$  are the minimum and maximum sizes attained, respectively. At this point we will include the current food concentration  $\xi$  as a parameter, and using a density-dependent form of the Sinko-Streifer PDE model [144], we then obtain

$$\frac{\partial u}{\partial t} + \frac{\partial u}{\partial a} + \frac{\partial}{\partial s} [g_{ind}(a, s, \gamma) g_{dep}(a, s, \gamma) u(t, a, s, \gamma)] = -\mu_{ind}(a, s, \gamma, \xi) \mu_{dep}(a, s, \gamma) u(t, a, s, \gamma)$$

where  $g_{dep}$  and  $\mu_{dep}$  are the density-dependent growth and mortality of daphnids, and  $g_{ind}$  and  $\mu_{ind}$  are the density-independent growth and mortality of daphnids. Here we will have  $\mu_{dep}$  have some delay, potentially distributed, within it, while  $g_{ind}$  will be what was obtained in Chapter 3,

respectively. Our boundary condition will represent the fecundity, and be given by

$$u(t, 0, s_0, \gamma) = \int_0^{a_{max}} \int_{s_0}^{s_{max}} k_{ind}(a, s, \gamma, \xi) k_{dep}(a, s, \gamma) u(t, a, s, \gamma) ds da,$$

where  $k_{dep}$  and  $k_{ind}$  are the density-dependent and density-independent terms for fecundity, where  $k_{dep}$  contains some delay.

At the food concentrations used in this experiment,  $k_{ind}(a, s, \gamma, \xi)$  would simply be the values in Figure A.5, and  $\mu_{ind}(a, s, \gamma, \xi)$  would be the age-varying mortality functions obtained from performing the same analysis from Chapter 4 on the data in Figure A.4. At other food concentrations, the values for  $k_{ind}(a, s, \gamma, \xi)$  and  $\mu_{ind}(a, s, \gamma, \xi)$  could be a cubic spline interpolation of the functions found for the food concentrations used in this experiment. This is merely a suggestion, and we do not guarantee the accuracy of such a method.

## A.2.2 Replicates 3 and 4 of Population Experiment

### A.2.2.1 Motivation and Experimental Design

In Section 3.2.2.2 we outlined our main population-level study, where we raised two beakers (Replicates 1 and 2) of unmolested daphnid populations for 102 days. A couple months after starting that experiment, we began to raise two additional beakers (Replicates 3 and 4) of unmolested daphnid populations using the same protocol for 85 days. That is, two beakers containing 1L of media each were both seeded with five 6-day-old female daphnids. We note that these daphnids did not reproduce prior to the beginning of the population study. Each 1L beaker was fed twice daily (at approximately 10 a.m. and 3 p.m.) with  $1.4 \times 10^8$  cells of algae (*R. subcapitata*) and 4 mg dry weight of fish food suspension. The media was changed every Monday, Wednesday, and Friday, and the number of daphnids were counted every Monday, Wednesday, and Friday through the first 64 days of the experiment and once weekly thereafter. During counting, daphnids were separated into two size classes (which we call the juvenile class  $J(t)$  and adult class  $A(t)$  at time  $t$ ) using a fine mesh net with a 1.62-mm pore size. The total number of daphnids  $N(t)$  at time  $t$  was then counted for each size class. Importantly, we note that classification into the juvenile or adult group only defines the size of the daphnid, and does not define whether the daphnid had reached a reproductive stage.

Cultured daphnids were maintained using previously described protocols and conditions [157]. Cultured daphnids were kept in media reconstituted from deionized water [10]. Cultured daphnids for both studies were maintained in an incubator maintained at 20 degrees Celsius with a 16-h light, 8-h dark cycle. The daphnids used in our study came from a colony that was maintained at North Carolina State University for over 20 years (clone NCSU1 [138]).

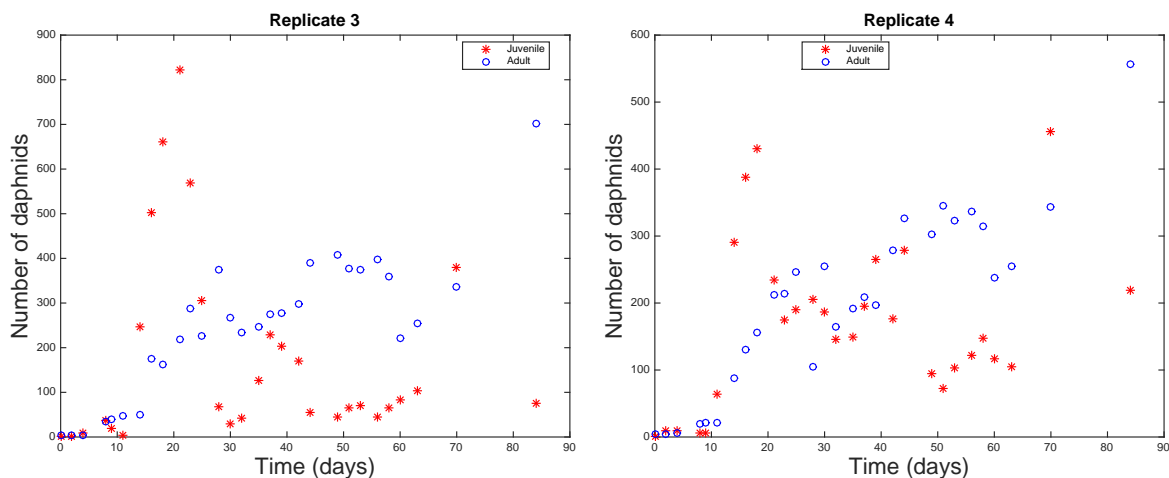


**Figure A.6** Longitudinal population data for Replicates 3 and 4. In each plot the red stars correspond to the juvenile population, and the blue circles correspond to the adult population. Notice that each graph is plot on a different scale.

This experiment was conducted simply to supplement the amount of data we could analyze for Chapter 3, but due to the nature of our results these replicates were not analyzed.

### A.2.2.2 Results

Replicates 3 and 4 both exhibit a similar juvenile spike and decline as was seen in Replicates 1 and 2 (Figure A.6), but the number of juveniles and adults seen in Replicates 3 and 4 is far exceeded by the numbers seen in Replicates 1 and 2 (Figure A.7). The number of daphnids apparent in Replicate 4, and to a smaller extent in Replicate 3, increase near the end of the experiment to levels that meet or exceed the juvenile spike, which is a phenomenon that was not seen in Replicates 1 and 2. This suggests that the population is not reaching steady state, as was seen in Replicates 1 and 2, but rather is experiencing different population shifts.

### A.2.2.3 Analysis

Replicates 1 and 2 were very promising, as there was an extreme similarity in the qualitative population dynamics of those two replicates. Replicates 3 and 4 do not exhibit the same qualitative dynamics. One hypothesis we have for this shift is that the quality of our algae was drastically reduced at the beginning stages of Replicates 3 and 4, while it was pristine at the beginning stages of Replicates 1 and 2. All replicates began with very few daphnids, and the effect of algal quality could



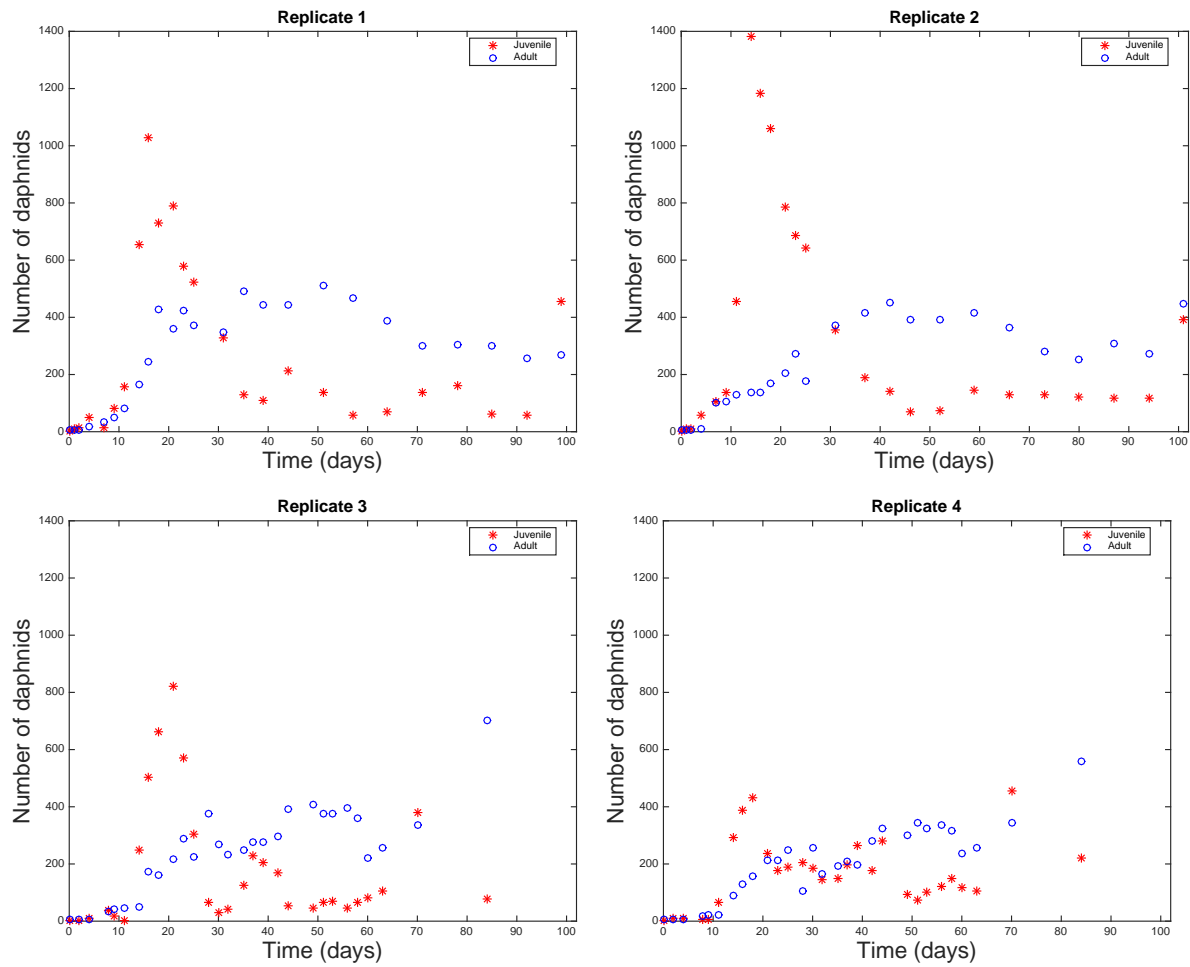


**Figure A.7** Longitudinal population data for Replicates 1 - 4 plotted on separate graphs with the same axes. In each plot the red stars correspond to the juvenile population, and the blue circles correspond to the adult population. Each graph is plot using the same axes for comparison purposes.

have drastically affected early fecundity, which could have affected the rest of the dynamics.

Also, due to the time difference in the start of the experiment, there could have been some epigenetic differences in the original daphnids for each replicate that caused the different dynamics to occur. We do not know exactly what difference the few months could have had on the daphnids, but since that represents multiple generations, this possibility cannot be ruled out.

Another possibility for the different results between Replicates 3 and 4 and Replicates 1 and 2 is simply the random nature of daphnid fecundity (Appendix A.1). While the random nature doesn't affect daphnid populations in aggregate, the effect would be pronounced at the beginning of our experiments when there are only 5 daphnid mothers.

It is interesting to note that while Replicates 3 and 4 do not agree with Replicates 1 and 2, they do agree slightly with each other, which suggests that there is some quality in the originating daphnids themselves or the algae that caused the disparity. We have given a few suggestions as to the root of the disparity, but since it exists, and since we are not assured of our algal quality throughout the experiment, we did not use these replicates in our modeling, and we cut our consideration of Replicates 1 and 2 to 102 days, which represents the time until we found our algal quality had decreased substantially.

### **A.2.3 Pyriproxyfen and Ethanol Population and Individual Experiments**

#### **A.2.3.1 Motivation**

Several studies have been conducted on the individual level as to the effects of toxicants on daphnids [79, 105, 106, 125–127, 153, 156, 157], and others have been performed on the effects of toxicants on the population-level dynamics [71, 127, 128, 134]. There has also been work to try and model the growth of daphnids, either unperturbed or when subjected to toxicants, both on the population and individual levels (e.g. [67, 68, 71, 73, 75, 76, 128, 133, 134]). Our work throughout this dissertation with daphnids built on the work of the past and focused on creating a comprehensive multi-scale model for unperturbed daphnid population growth. In this section we outline experiments we performed, on both the population and individual level, for the effect of pyriproxyfen, a juvenile hormone analog, on daphnids, and ethanol, the substance used to transport pyriproxyfen into daphnid media. While our work did not focus on modeling this data, future work can and should be used to modify our model to allow for work with this data.

Other experimenters have observed pyriproxyfen increasing male offspring and decreasing overall fecundity [79, 126, 156]. In this section we explore those effects of pyriproxyfen, consider how pyriproxyfen exposure affects the physical size of daphnids, and also look at how these effects come into play in population dynamics. It is important to note that while other studies have used varying

concentrations of pyriproxyfen, or exposed daphnids for only short amounts, here we constantly expose daphnids to a single concentration of pyriproxyfen. The results of this section, as well as the past literature, show how sensitive daphnids are to this pesticide, and demonstrate the need for care when using this pesticide, and possibly others, in areas that can run off to bodies of water containing daphnids.

#### **A.2.3.2 Experimental Design/Methods**

We conducted two studies in the laboratory using pyriproxyfen and ethanol, the substance used to dilute the pyriproxyfen. The first study was performed at the individual daphnid level to track the baseline fecundity and growth rates in isolation (mortality was also tracked, and that data, along with analysis of it, can be found in Chapter 4). The second study was performed at the population level in four Replicates. Experiments on Replicates 1 and 2 consisted of a 102 day study began concurrently with the daphnids described in Section 3.2.2.2, while Replicated 3 and 4 consisted of a 85 day study run concurrently with the daphnids in Appendix A.2.2.1. Cultured daphnids were maintained using previously described protocols and conditions [157]. Cultured daphnids were kept in media reconstituted from deionized water [10]. Cultured daphnids for both studies were maintained in an incubator maintained at 20 degrees Celsius with a 16-h light, 8-h dark cycle. The daphnids used in our study came from a colony that was maintained at North Carolina State University for over 20 years (clone NCSU1 [138]).

##### **A.2.3.2.1 Individual study**

Sixty daphnids were longitudinally observed to estimate population average rates of fecundity and growth. Less than 2-h old neonates were placed individually into 50mL beakers containing 40mL of media each. Media was changed daily. Daphnids were fed daily with  $7.0 \times 10^6$  cells of algae (*Raphidocelis subcapitata*) and 0.2 mg (dry weight) Tetrafin™ fish food suspension prepared as described previously [124]. The number of neonates produced by each individual daphnid was recorded and then removed daily. Fecundity measurements were performed until no daphnids remained. We also collected data on the number of males produced by examining daphnids microscopically, with males determined by having a longer first antennae [125]. The size of each individual daphnid was measured with a digital microscope (Celestron, Torrance, CA, USA) at periodic intervals until they died, starting at less than two hours old. The major axis was used to determine size. The sixty daphnids came from two equally sized groups: thirty daphnids were constantly exposed to media containing .2  $\mu$ L of a .3nM concentration of pyriproxyfen/40 mL media ("Treatment" group) and thirty daphnids were constantly exposed to media containing .2  $\mu$ L ethanol/40 mL media

("Vehicle" group). An unexposed, "Control" group, was also considered, and data from that group can be found in Chapter 3, although some is recreated below for comparison purposes.

#### A.2.3.2.2 Population study

Each replicate consisted of a "Treatment" beaker which was exposed constantly to media containing 5  $\mu\text{L}$  of a 60  $\mu\text{M}$  concentration of pyriproxyfen/L media, and Replicates 3 and 4 also consisted of an additional "Vehicle" beaker which was exposed constantly to media containing 5  $\mu\text{L}$  of ethanol/L media. Each beaker contained 1L of media and were seeded with five 6-day-old female daphnids. We note that these daphnids did not reproduce prior to the beginning of the population study. Each 1L beaker was fed twice daily (at approximately 10 a.m. and 3 p.m.) with  $1.4 \times 10^8$  cells of algae (*R. subcapitata*) and 4 mg dry weight of fish food suspension. For all replicates the media was changed every Monday, Wednesday, and Friday. The number of daphnids were counted every Monday, Wednesday, and Friday through the first 40 days of the experiment for Replicates 1 and 2, the first 64 days of the experiment for Replicates 3 and 4, and once weekly thereafter. During counting, daphnids were separated into two size classes (which we call the juvenile class  $J(t)$  and adult class  $A(t)$  at time  $t$ ) using a fine mesh net with a 1.62-mm pore size. Importantly, we note that classification into the juvenile or adult group only defines the size of the daphnid, and does not define whether the daphnid had reached a reproductive stage. We also collected data on the number of males produced by examining daphnids microscopically, with males determined by having a longer first antennae [125].

#### A.2.3.3 Results and Data Analysis

The major axis length of daphnids is meaningfully impacted by the application of pyriproxyfen (Figure A.8). The effect becomes more apparent when trying to model this growth (see Appendix B.1, Table B.1). While the application of ethanol doesn't appear to meaningfully impact daphnid reproduction other than a spike in reproduction for the few remaining daphnids late in the experiment (Figure A.9), the application of pyriproxyfen has a major effect. Not only is there an introduction of males from female daphnid mothers exposed to pyriproxyfen, but also those mothers produce drastically less female daphnids (Figure A.10).

We see that these individual dynamics play themselves out on the population level in a large way. As the application of ethanol didn't meaningfully impact the daphnid individual dynamics, the daphnid population dynamics remain seemingly unchanged from what was seen from unexposed daphnids (Figure A.11). This contrasts greatly what occurs for daphnids exposed to pyriproxyfen. There are significantly less females present than in the unexposed beakers, and the growth of the

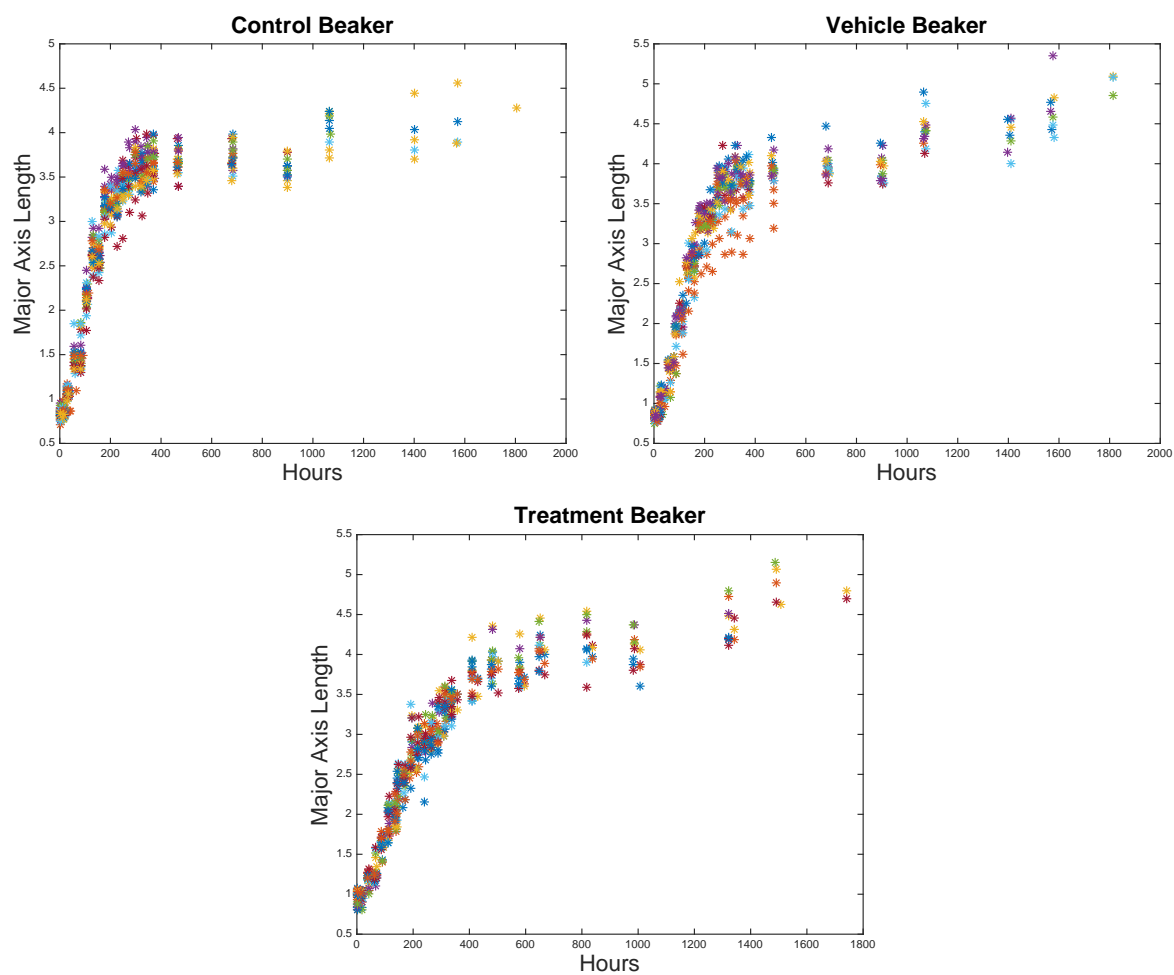


**Figure A.8** The major axis length for daphnids in Control, Vehicle, and Treatment settings. The longitudinal data for each individual daphnid is represented by dots of a single color (for example, the yellow dots represents the same daphnid). The Control data is identical to the data in Figure 3.2, and is here merely for comparison purposes.

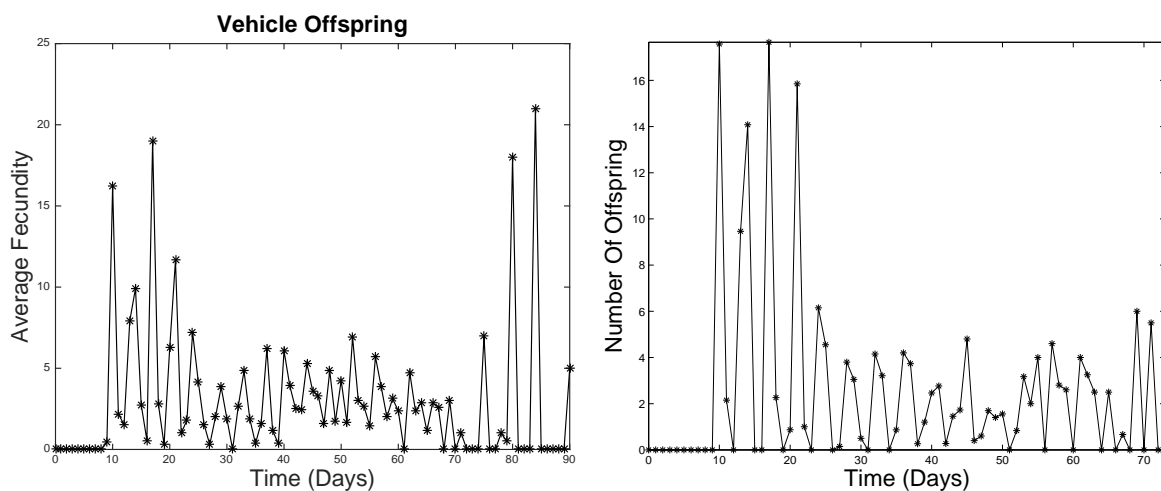


**Figure A.9** (left) The number of neonates produced per Vehicle female daphnid per day. Daily data are represented by star symbols and connecting lines are drawn to show general trends. (right) The number of neonates produced per Control female daphnid per day. Daily data are represented by star symbols and connecting lines are drawn to show general trends. This is a copy of Figure 3.3 provided for comparison purposes. Notice that each graph is plot on a different scale.

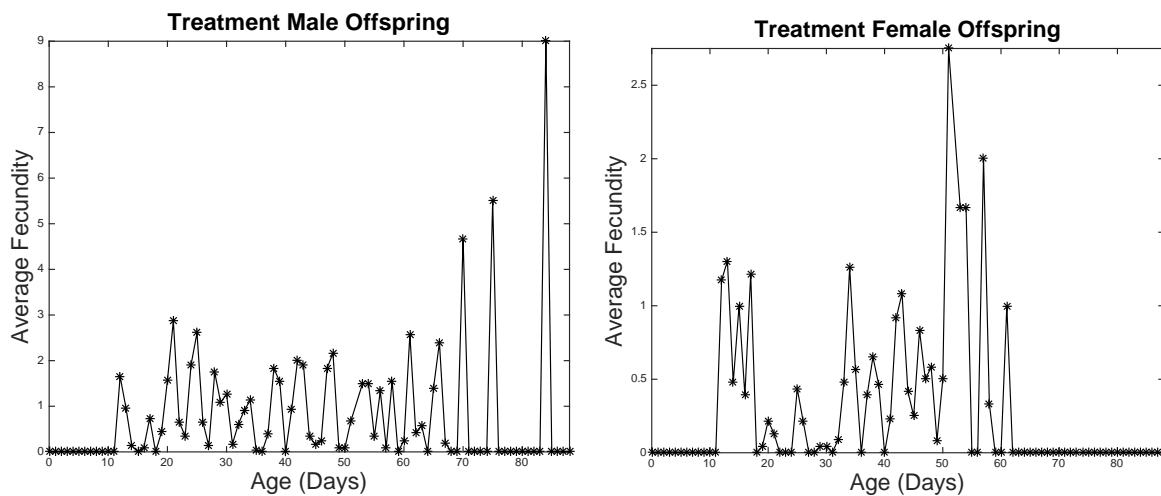


**Figure A.10** The number of neonates produced per Treatment female daphnid per day. Daily data are represented by star symbols and connecting lines are drawn to show general trends. Notice that each graph is plot on a different scale.

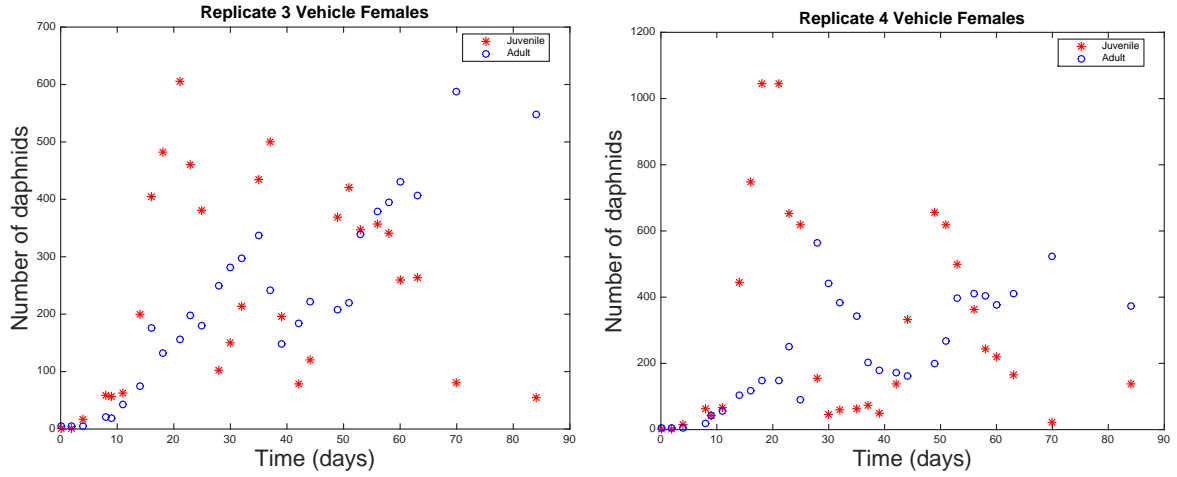


**Figure A.11** Longitudinal population data for Vehicle females in Replicates 3 and 4. In each plot the red stars correspond to the juvenile population, and the blue circles correspond to the adult population. Notice that each graph is plot on a different scale.

female population is slow to begin with, and then spikes around day 50 (Figure A.12). We also see that the introduction of males on the individual level creates nontrivial male population-level dynamics (Figure A.13). This is quite interesting, as in our unexposed populations we saw that cyclic parthenogenesis was barely a factor, but here the introduction of pyriproxyfen makes it a driving force.

In this study we introduced an incredibly small amount of pyriproxyfen into the daphnid media, yet it had dramatic repercussions on the population. This highlights the sensitivity of daphnids to this pesticide, and points to the possible effect other exogenous substances can have on daphnid population dynamics. In the next section we discuss briefly how these effects can be included into a daphnid population model, and note that this analysis can also be performed for other chemicals.

#### A.2.3.4 Future Modeling

These results point to a possible extension of the comprehensive daphnid model hypothesized in Section 5.5.3. We will begin with the same theoretical framework, where we assume that there exists an intrinsic parameter  $\gamma$  that daphnids have, which can represent their subpopulation, the density at which that daphnid was born, the pyriproxyfen concentrations they have been exposed to, as well as their gender. Let's assume  $\gamma \in \Gamma$ , where  $\Gamma$  is a range of admissible parameters, and let  $P$  be the distribution of the  $\gamma$ 's in  $\Gamma$ . Let  $a$  be the daphnid's age and  $s$  be the daphnid's size, and thus we

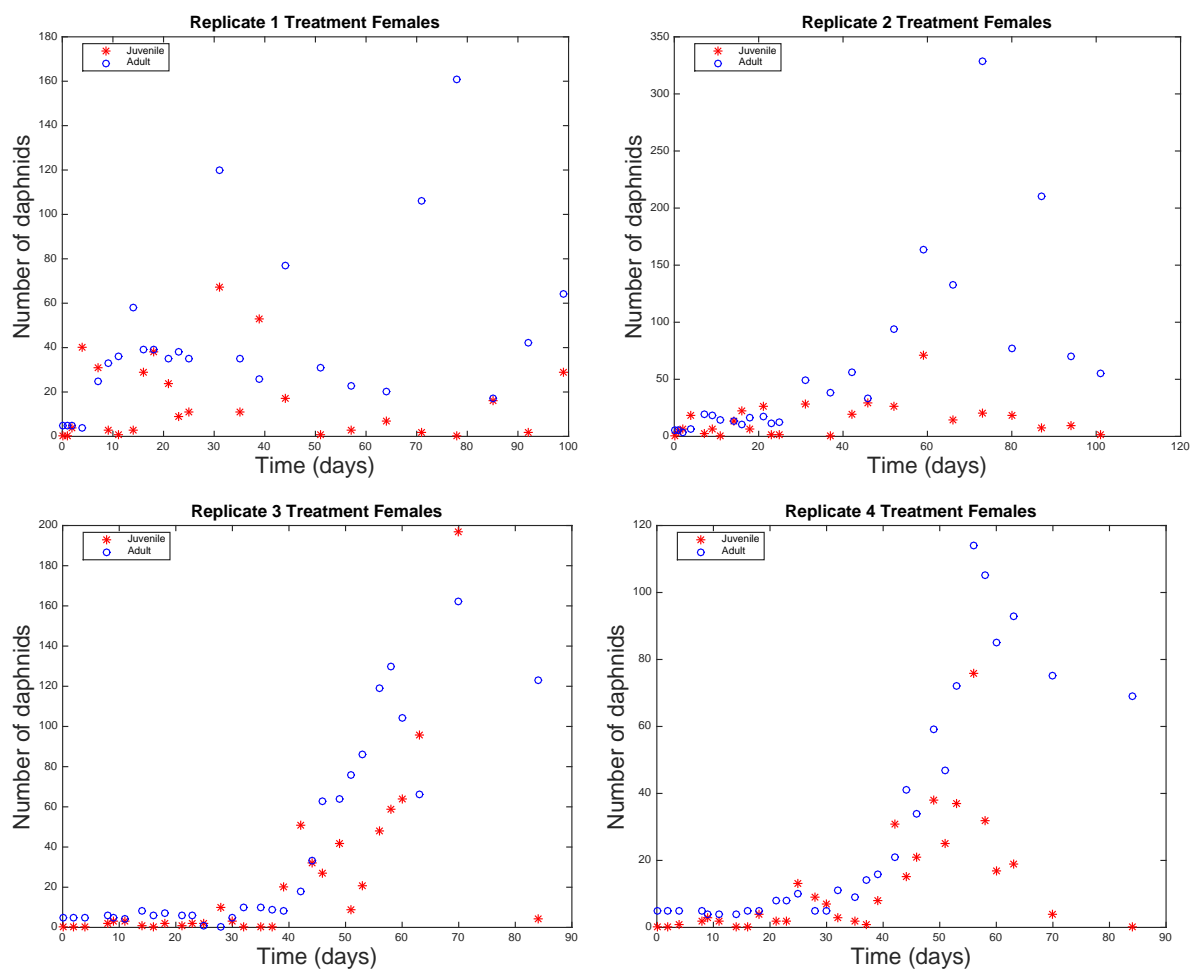


**Figure A.12** Longitudinal population data for Treatment females in Replicates 1, 2, 3, and 4. In each plot the red stars correspond to the juvenile population, and the blue circles correspond to the adult population. Notice that each graph is plot on a different scale.



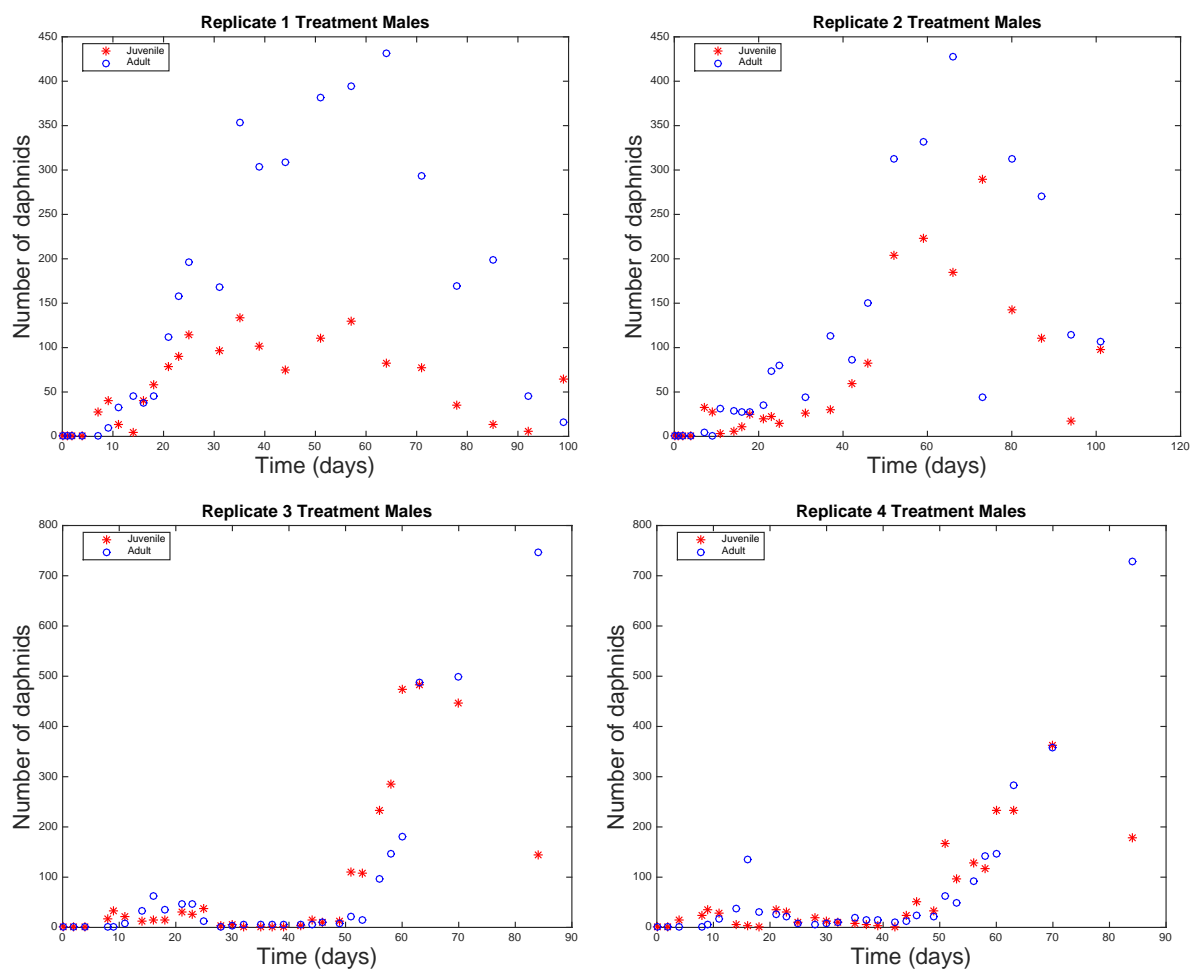


**Figure A.13** Longitudinal population data for Treatment males in Replicates 1, 2, 3, and 4. In each plot the red stars correspond to the juvenile population, and the blue circles correspond to the adult population. Notice that each graph is plot on a different scale.

have that the density of daphnids at time  $t$ , age  $a$ , size  $s$ , and intrinsic parameter  $\gamma$  is given by

$$u(t, a, s, \gamma).$$

The total population density is then given by

$$v(t, P) = \int_0^{a_{max}} \int_{s_0}^{s_{max}} \int_{\Gamma} u(t, a, s, \gamma) dP(\gamma) ds da,$$

where  $a_{max}$  is the maximum age of daphnids and  $s_0$  and  $s_{max}$  are the minimum and maximum sizes attained, respectively. Using a density-dependent form of the Sinko-Streifer PDE model [144], we then obtain

$$\frac{\partial u}{\partial t} + \frac{\partial u}{\partial a} + \frac{\partial}{\partial s} [g_{ind}(a, s, \gamma) g_{dep}(a, s, \gamma) u(t, a, s, \gamma)] = -\mu_{ind}(a, s, \gamma) \mu_{dep}(a, s, \gamma) u(t, a, s, \gamma)$$

where  $g_{dep}$  and  $\mu_{dep}$  are the density-dependent growth and mortality of daphnids, and  $g_{ind}$  and  $\mu_{ind}$  are the density-independent growth and mortality of daphnids. Here we will have  $\mu_{dep}$  have some delay, potentially distributed, within it, while  $\mu_{ind}$  will be what was obtained in Chapter 4.  $g_{ind}$  will be what was obtained in Chapter 3 for unexposed daphnids, or a model based on the Treatment data in Figure A.8 for daphnids exposed to pyriproxyfen. Our boundary condition will represent the fecundity, and be given by

$$u(t, 0, s_0, \gamma) = \int_0^{a_{max}} \int_{s_0}^{s_{max}} k_{ind}(a, s, \gamma) k_{dep}(a, s, \gamma) u(t, a, s, \gamma) ds da,$$

where  $k_{dep}$  and  $k_{ind}$  are the density-dependent and density-independent terms for fecundity, where  $k_{dep}$  contains some delay.  $k_{ind}$  would come directly from Figure 3.3 for unexposed daphnids or Figure A.10 for daphnids exposed to pyriproxyfen.

It should be noted that the data from this section comes from daphnids constantly exposed to a set concentration of pyriproxyfen. For other toxicants, other exposure levels, and other exposure durations, it can be expected that the growth, fecundity, and possibly mortality in the case of lethal concentrations of toxicants, will be different from what has been observed here. Therefore, the density-independent terms would need to be altered to adjust for those differences.

## A.2.4 Pesticide Resistance

### A.2.4.1 Motivation

Pesticide resistance has been widely studied in environmental toxicology and evolutionary ecology for several organisms, and has specifically been considered for *Daphnia magna*. Resistance is the increase of relative fitness over time of an individual or population in the presence of a harmful substance, in our case pyriproxyfen. Fitness has several components, including fecundity, survivorship, growth rate, and ability to compete. To fully measure relative fitness, lifetime studies which take into account all of these components need to be done [9]. This is unrealistic in most cases, and thus most studies, including ours, only consider some of these components.

Resistance in a population can arise from phenotypic plasticity (acclimatization) or response to selection (genetic or epigenetic). To decouple these effects and detect genetic resistance, populations should be studied in parallel. In daphnids, resistance to toxicants has been attributed to phenotypic plasticity [46, 100, 107] as well as genetic resistance [58, 89]. All of these studies have made these assessments using individually kept animals, and to the best of our knowledge a study has not been completed to measure population-level impacts. Our contribution to this body of work is the consideration of these population-level dynamics.

This experiment is further motivated by surprising population dynamics seen in our pyriproxyfen population dynamics (Figures A.12 and A.13). In those experiments we witnessed a major spike in reproduction of our populations around day 50 following slow population growth at the onset of the experiment. This suggests that there was some resistance to pyriproxyfen that later generations developed relating specifically to reproductive fitness cost (as the minimum reproductive time of *Daphnia magna* is 9 days, 50 days is enough for 5 generations of daphnids). To exaggerate this effect, daphnids in this experiment came from beakers treated with a constant amount of pyriproxyfen for 213 days, which corresponds to 23 generations.

### A.2.4.2 Experimental Design/Methods

Before the experiment began we raised female daphnid mothers in unmolested populations in two different conditions. The "Treatment" 1L beaker had been exposed daily to 5  $\mu$ L of 60  $\mu$ M of pyriproxyfen for 213 days, while the "Control" 1L beaker was not exposed.

The experiment consisted of four different groups of female daphnids (termed Groups  $C_C$ ,  $C_T$ ,  $T_C$ , and  $T_T$ ), with each group consisting of two beakers containing 200mL of media. The daphnids in Groups  $C_C$  and  $T_C$  were born from mothers in the Control beaker and daphnids in Groups  $C_T$  and  $T_T$  were born from mothers in the Treatment beaker. Daphnids in Groups  $C_C$  and  $C_T$  were kept as

Control beakers (that is, unexposed) and daphnids from Groups  $T_C$  and  $T_T$  were kept as Treatment beakers (that is, exposed daily to  $5\ \mu\text{L}$  of  $60\ \mu\text{M}$  of pyriproxyfen per 1L of media).

Each experimental beaker was initially seeded with four 6-day-old daphnids. We note that these daphnids did not reproduce prior to the beginning of the population study. Each 200mL beaker was fed twice daily (at approximately 10 a.m. and 3 p.m.) with  $2.8 \times 10^7$  cells of algae (*R. subcapitata*) and 0.8 mg dry weight of fish food suspension. The experiment lasted 27 days, which slightly exceeds the time for the "early phase" of our initial population study (Figure 3.13). The media was changed and the number of daphnids were counted every Monday, Wednesday, and Friday through the full 27 day experiment. During counting, daphnids were separated into two size classes (which we call the juvenile class  $J(t)$  and adult class  $A(t)$  at time  $t$ ) using a fine mesh net with a 1.62-mm pore size. Importantly, we note that classification into the juvenile or adult group only defines the size of the daphnid, and does not define whether the daphnid had reached a reproductive stage. We also collected data on the number of males produced by examining daphnids microscopically, with males determined by having a longer first antennae [125].

Cultured daphnids were maintained using previously described protocols and conditions [157]. Cultured daphnids were kept in media reconstituted from deionized water [10]. Cultured daphnids for both studies were maintained in an incubator maintained at 20 degrees Celsius with a 16-h light, 8-h dark cycle. The daphnids used in our study came from a colony that was maintained at North Carolina State University for over 20 years (clone NCSU1 [138]).

#### A.2.4.3 Results

Daphnids in Groups  $T_C$  and  $T_T$  produced a significant number of males (Figure A.14), and the number of females produced are quite less than those produced for Groups  $C_C$  and  $C_T$  (comparing Figure A.15 to Figure A.16). This is consistent with what we would predict for daphnids that had never previously been exposed to pyriproxyfen. We hypothesized that pesticide resistance would be apparent if Groups  $T_T$  and  $C_C$  produced similar amounts of daphnids, which was not experienced here. For this reason, we do not believe that the daphnids developed a resistance to pyriproxyfen.

As our results do not show evidence of resistance to pyriproxyfen, there is no need to attempt to incorporate such an effect in a population-level model for daphnids. We suggest that similar experiments be conducted with other pesticides to verify that resistance isn't seen in those regimes as well. We also note that here we did not consider a partial resistance to pyriproxyfen, which might be present and should be tested for. In addition, since our experimental daphnids came from unmolested beakers, these daphnids could be experiencing delayed density-dependent effects on mortality and fecundity throughout this experiment, which could have affected our results.

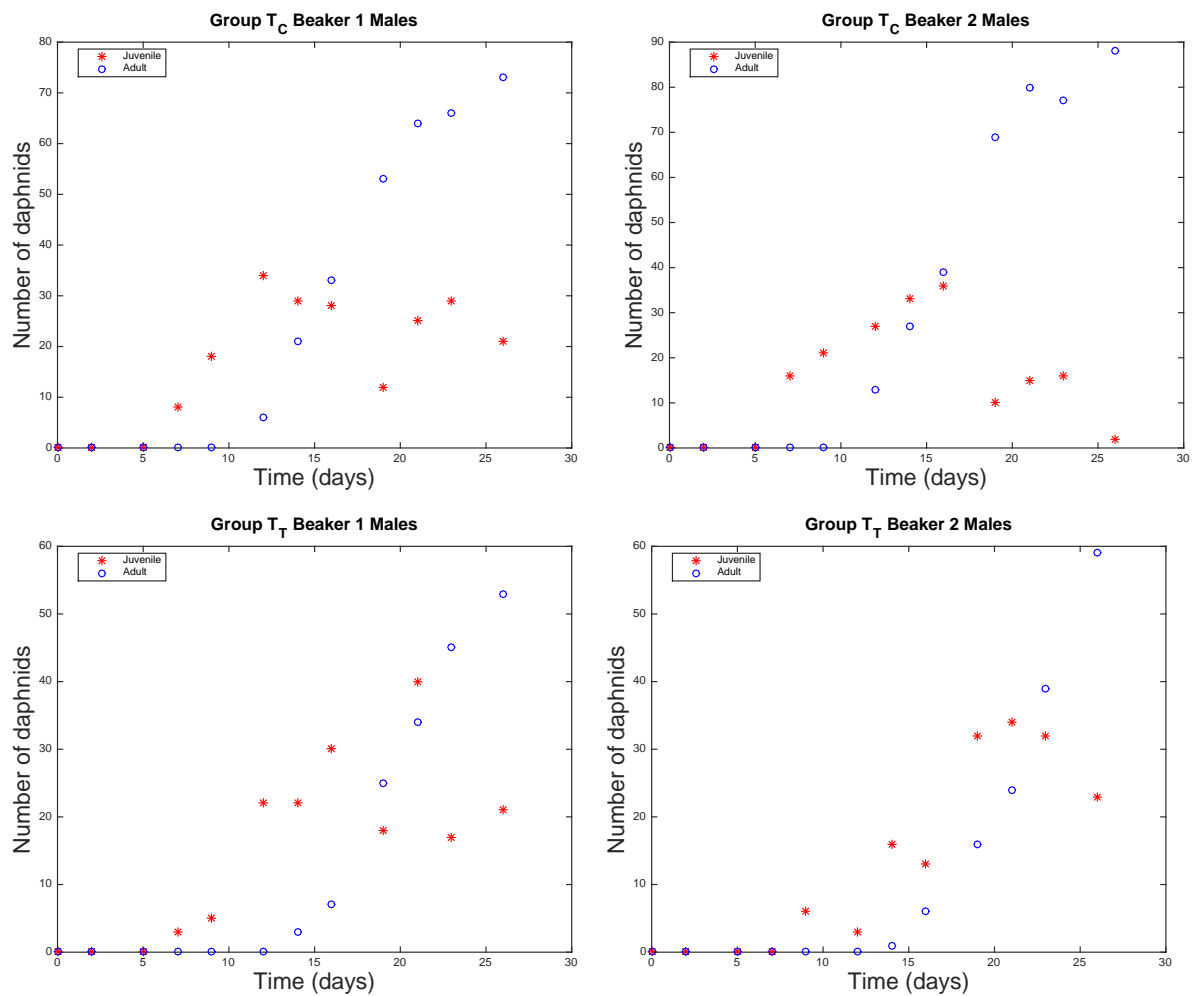


**Figure A.14** Longitudinal population data for males in Groups  $T_C$  and  $T_T$ . In each plot the red stars correspond to the juvenile population, and the blue circles correspond to the adult population. Notice that each graph is plot on a different scale.

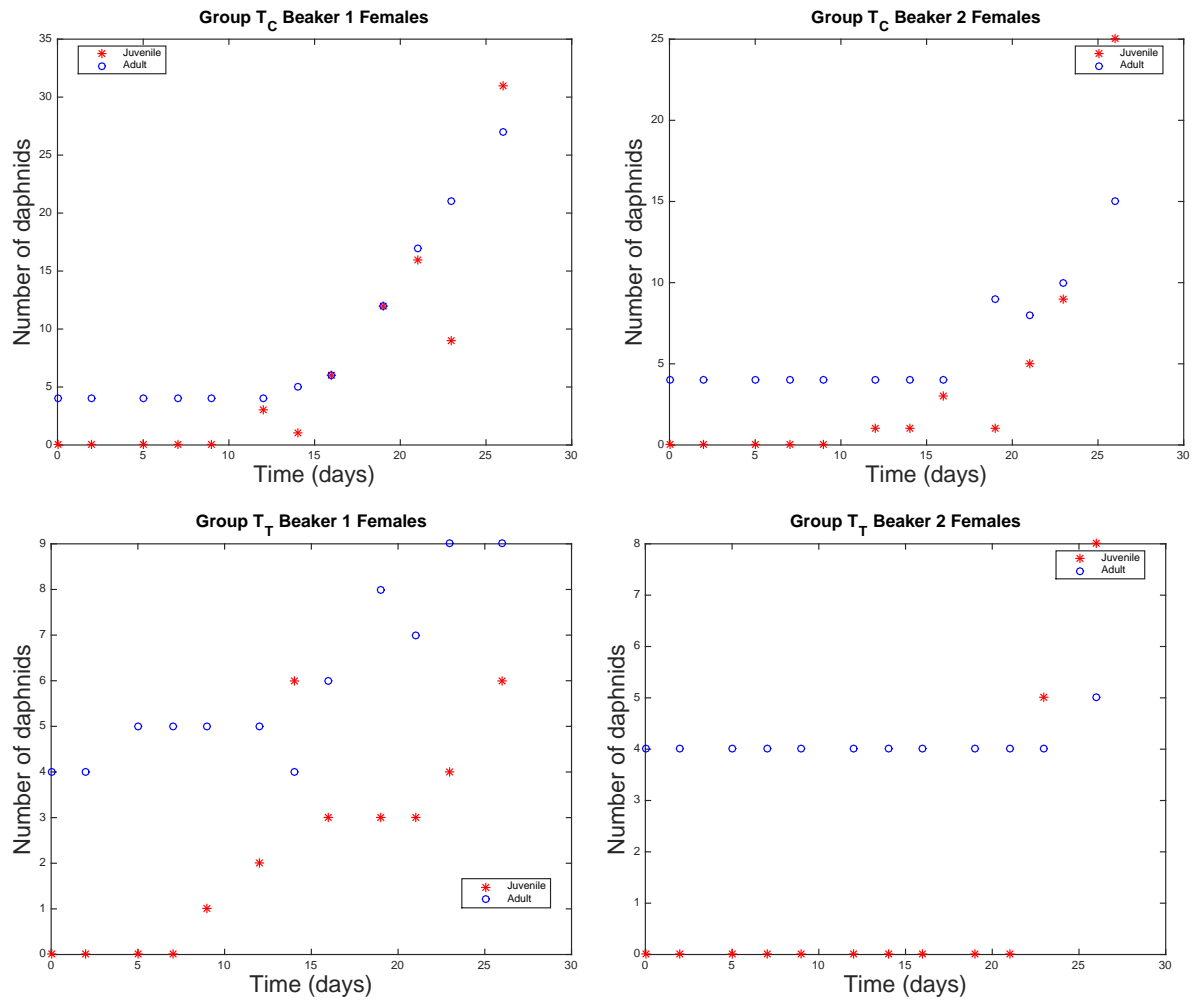


**Figure A.15** Longitudinal population data for females in Groups  $T_C$  and  $T_T$ . In each plot the red stars correspond to the juvenile population, and the blue circles correspond to the adult population. Notice that each graph is plot on a different scale.

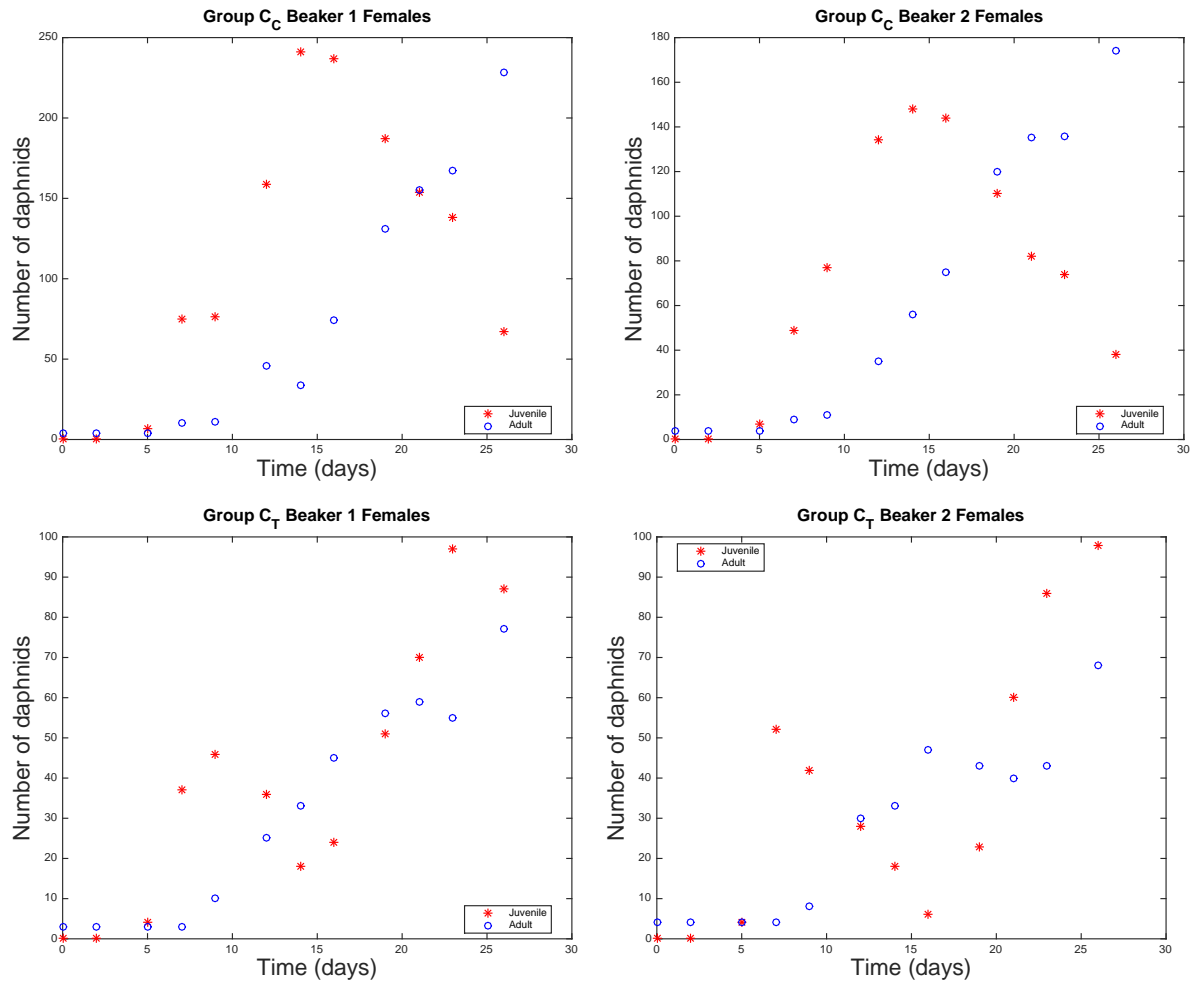


**Figure A.16** Longitudinal population data for Groups  $C_C$  and  $C_T$ . In each plot the red stars correspond to the juvenile population, and the blue circles correspond to the adult population. Notice that each graph is plot on a different scale.

# Implementation Details for Chapter 3<sup>1</sup>

## B.1 Computing Non-linear Mixed Effects Model

We computed a nonlinear mixed effects (NLME) model for the major axis length of *Daphnia magna* (Figure 3.2), and in this section we detail how we determined which specific NLME model to use, and how we estimated the parameters for that model. Appendix B.1.1 details our initial attempt which involved several inverse problems, model selection using Akaike weights, and normality tests for the random effects' variances. This initial attempt led to our second method detailed in Appendix B.1.2: using built-in functionality within a Matlab package called Simbiology. Simbiology's method requires certain assumptions to be filled, which we tested in Appendix B.1.1. The results of Simbiology were what was used in Chapter 3, and coincided with what was found in Appendix B.1.1.

In this investigation four different models were considered: a logistic model  $f_1(t) = \frac{K_1 Z_0 e^{r_1 t}}{K_1 + Z_0 (e^{r_1 t} - 1)}$ , a linear model  $f_2(t) = r_2 t + b$ , a Gompertz growth model  $f_3(t) = K_3 e^{\ln(\frac{Z_0}{K_3}) e^{-r_3 t}}$ , and an exponential model  $f_4(t) = K_4 + (Z_0 - K_4) e^{-r_4 t}$ , where  $K_i$  are maximum size parameters,  $Z_0$  is the initial size of the daphnid, and  $r_i$  are growth rates. Appendix B.1.1 only considers models  $f_1$ ,  $f_2$ , and  $f_3$ , while Appendix B.1.2 also considers model  $f_4$ . Both methods will consider each parameter  $\theta$  as a combination of a fixed effect  $\bar{\theta} \in \mathbb{R}$  and a random effect  $\tilde{\theta} \sim N(0, \sigma^2)$ , where the normality assumption for the random effects will be tested and verified in Appendix B.1.1. Both methods will then, for each parameter, determine  $\bar{\theta}$  and  $\sigma$ .

---

<sup>1</sup> Contributions:

Calculations and writeup: Kaska Adoteye  
Advisor: H.T. Banks



### B.1.1 Initial NLME Growth Model Computation

Our data came from an experiment consisting of 30 daphnids placed in different beakers (see Section 3.2.2.1 for experimental details), but for growth modeling we only used daphnids with 10 or more data points, which amounted to 24 daphnids. Our observations are the major axis length for daphnid  $k$  at time  $t_j$  and are denoted by  $y_j^k$ , where  $k = 1, 2, \dots, 24$ . We had one daphnid per beaker and performed observations under a digital microscope (Celestron, Torrance, CA, USA), and thus we can reasonably assume a constant statistical error model. This leads our statistical model to pertain to a scalar observation with constant error [39], and thus our statistical model for model  $i$  is given by

$$Y_j^k = f_i^k(t_j, \theta_0^k) + \mathcal{E}_j^k, \quad j = 1, 2, \dots, n,$$

where  $Y_j^k$  is a random variable with realizations  $y_j^k$ ,  $\theta_0^k$  is the hypothesized “true” parameter vector for the  $k$ ’th daphnid,  $f_i^k(t_j, \theta_0^k)$  is the model solution for the  $k$ ’th daphnid using the model  $f_i$ , and the error terms  $\mathcal{E}_j^k$  are assumed independent and identically distributed (i.i.d) random variables with mean  $E[\mathcal{E}_j^k] = 0$  and variance  $V_0 = \sigma_0^2$ . Therefore, in order to find our estimate  $\hat{\theta}^k$  of  $\theta_0^k$  for each beaker we will minimize the cost functional

$$J_i^k(\theta) = \sum_{j=1}^n [y_j^k - f_i^k(t_j, \theta)]^2.$$

We thus perform 24 different inverse problems for each model. The inverse problems were computed using the gradient based Matlab search routine *lsqnonlin* run with the options ‘TolX’ and ‘TolFun’ set equal to 1e-9 and ‘MaxFunEvals’ set equal to 400.

For each daphnid we computed the  $AIC_C$  for each model  $f_i$  (see Section 3.2.6.2 for details on  $AIC_C$ ) in order to determine which of the models  $f_i$  provided the best fit to the data for daphnid  $k$ . In order to further validate our results, we also computed the Akaike weights  $w_i$ , given by

$$w_i = \frac{\exp(\frac{1}{2}(AIC_{C,min} - AIC_{C,i}))}{\sum_{r=1}^3 \exp(\frac{1}{2}(AIC_{C,min} - AIC_{C,r}))}$$

where  $AIC_{C,min}$  is the smallest  $AIC_C$  among the discussed models and  $AIC_{C,i}$  is the  $AIC_C$  value for model  $f_i$ . The larger the  $w_i$ , the more likely it is that model  $f_i$  describes the data best [39]. In this study we also considered the minor axis length, as well as daphnids exposed to ethanol (termed the “Carrier” group) and pyriproxyfen (termed the “Pyriproxyfen + Carrier” group) in a manner as specified in Section 4.2.1, although we did not consider those in any of our analysis besides computing Akaike weights. Table B.1 shows, for each group, which model had the highest Akaike

**Table B.1** This table shows which model had the largest Akaike weight for each daphnid given each type of measurement. So, for example, when trying to model the major axis length for the Control daphnids, the Gompertz curve had the largest Akaike weight for one of the 24 daphnids used, the logistic curve had the largest weight for 23 daphnids, and the linear model had the largest weight for none of the 24 daphnids, and all of this is expressed in the first row of this table.

	Gompertz	Logistic	Linear	Total
Control Major Axis	1	23	0	24
Control Minor Axis	1	23	0	24
Carrier Major Axis	3	20	1	24
Carrier Minor Axis	2	22	0	24
Pyriproxyfen + Carrier Major Axis	11	10	0	21
Pyriproxyfen + Carrier Minor Axis	9	12	0	21

weight for each daphnid, where the "Control" group denotes daphnids not exposed to pyriproxyfen or ethanol, and thus central to our study. We see that the logistic model provides the best fit for almost all Control daphnids. We then determined our fixed effects  $\bar{\theta}$  by taking an average of our parameter estimates  $\hat{\theta}^k$  for the logistic model.

At this point we tested if the obtained parameters came from a normal distribution. To do this, we performed a Lilliefors test for normality [109] on the parameter estimates  $\hat{\theta}^k$  for each model  $f_i$ . The Lilliefors test, implemented with the function *lillietest* in Matlab, computes the test statistic

$$\max_x |F(x) - G(x)|$$

where  $F(x)$  is the empirical cumulative distribution function (cdf) computed from the data, and  $G(x)$  is a normal distribution with the same mean and variance of the data. We found that for each parameter we could not reject the null hypothesis that the parameter values are normally distributed across the population ( $p \geq 0.4665$  for each parameter in models  $f_i$ ,  $i = 1, 2, 3$ , except  $K_3$  which had  $p = 0.2069$ ). Given that the parameters come from a normal distribution, we can simply find the standard deviation of the parameter values by finding the standard deviation of the 24 parameter estimates that we have, which gives us the standard deviation  $\sigma$  for each parameter.

### B.1.2 Simbiology NLME Growth Model Computation

Above we first estimated the fixed effects, did a model comparison, and then estimated the random effects. Simbiology simultaneously estimates the fixed effects  $\bar{\theta}$ , the standard deviation  $\sigma$  for the random effect, and performs model comparison. Simbiology assumes that the random effects come from a normal distribution, and therefore even though the method Simbiology uses as described

**Table B.2** These are the  $AIC_C$  values computed by Simbiology for the logistic model  $f_1$ , the linear model  $f_2$ , the Gompertz growth model  $f_3$ , and the exponential model  $f_4$  using the major axis length data for each daphnid. Here we see that the logistic model provides the best fit to the data since it has the lowest  $AIC_C$  score.

Model	$AIC_C$ Value
Logistic	-357.482849072019
Linear	1211.34095476
Gompertz	-302.22996426
Exponential	-91.5244004750864

below is more compact, the analysis performed in Appendix B.1.1 was necessary to test the normality.

Simbiology simultaneously estimates the fixed and random effects by maximizing the likelihood function

$$p(y|\theta, \sigma^2, \Psi) = \int p(y|\theta, \eta, \sigma^2) p(\eta|\Psi) d\eta$$

where  $y$  is the response data (so here the major axis length),  $\theta$  is the vector of fixed effects,  $\sigma^2$  is the observation error variance,  $\Psi$  is the covariance matrix for random effects,  $\eta$  is the vector of random effects,  $p(y|\theta, \sigma^2, \Psi)$  is the marginal density of  $y$ ,  $p(y|\theta, \eta, \sigma^2)$  is the conditional density of  $y$  given the random effects  $\eta$ , and  $p(\eta|\Psi)$  is the prior distribution of  $\eta$ . Simbiology has multiple methods based on the Statistics and Machine Learning Toolbox to solve the above integral, but the method we used involves using the likelihood for the linear mixed-effects model at the current estimates of  $\theta$  and  $\eta$ . For more information, consult [112]

In doing this Simbiology is able to compute an  $AIC_C$  value for the likelihood function directly, which allows for model comparison that incorporates both the fixed and random effects. Table 3.2 contains the estimated parameters for the logistic model for the major axis length, and Table B.2 contains the  $AIC_C$  values for the models, which we see confirms that the logistic model provides the best fit.

## B.2 Sensitivity Equations for Discrete Model D

Here we derive the relative sensitivities shown in Figure 3.12 for Model D given by Equation (3.1) with variables and parameters given in Table 3.1. That is, with  $\theta = (\mu, q, c)$ , we wish to find  $\frac{\partial f_J(t, \hat{\theta})}{\partial \theta_k} \frac{\hat{\theta}_k}{f_J(t, \hat{\theta})}$  where  $f_J(t, \theta) = \sum_{i=1}^4 p(t, i)$  are the number of juveniles predicted by our model, and  $\frac{\partial f_A(t, \hat{\theta})}{\partial \theta_k} \frac{\hat{\theta}_k}{f_A(t, \hat{\theta})}$

where  $f_A(t, \theta) = \sum_{i=5}^{74} p(t, i)$  are the number of adults predicted by our model. Note that since

$$\frac{\partial f_J(t, \theta)}{\partial \theta_k} = \sum_{i=1}^4 \frac{\partial p(t, i)}{\partial \theta_k} \quad \text{and} \quad \frac{\partial f_A(t, \theta)}{\partial \theta_k} = \sum_{i=5}^{74} \frac{\partial p(t, i)}{\partial \theta_k},$$

we can derive the required sensitivities by finding  $\frac{\partial p(t, i)}{\partial \theta_k}$  for each  $i \in [1, 74] \cap \mathbb{N}$ . To do this we'll first compute for  $i = 1$ , and then  $i = 2, 3, 4$ , and then  $i \geq 5$ , due to the similarity in the equations for  $p(t, i)$  for those values of  $i$ , which we will explore below.

For this exploration we will heavily use the Chain Rule from calculus. Recall that if  $u = f(x(s, t), y(s, t), s)$  where  $x$  and  $y$  are functions of variables  $s$  and  $t$ , then

$$\frac{\partial u}{\partial s} = \frac{\partial f}{\partial x} \frac{\partial x}{\partial s} + \frac{\partial f}{\partial y} \frac{\partial y}{\partial s} + \frac{\partial f}{\partial s}.$$

- **$i = 1$ :** From Equation (3.1) with variables and parameters given in Table 3.1 we see that

$$p(t+1, 1) = \sum_{i=1}^{74} p(t, i) \alpha(i) (1-q)^{M(t-\tau)}, \quad (\text{B.1})$$

where  $\alpha(i)$  is the known age-dependent function depicted in Figure 3.3 and

$M(t) = \sum_{j=1}^{74} p(t, j) \frac{K Z_0 e^{rj}}{K + Z_0 (e^{rj} - 1)}$  is the total population length with  $K, Z_0$ , and  $r$  given by the fixed effect means in Table 3.2. Differentiating both sides of Equation (B.1) with respect to  $\mu$  using the Product Rule from calculus, and recalling that both  $p(t, i)$  and  $M(t)$  are functions of

$\mu$ , and that  $\frac{da^x}{dx} = a^x \ln(a)$  for  $a \in \mathbb{R}^+$ , we see

$$\begin{aligned}
& \frac{\partial p(t+1, i)}{\partial \mu} \\
&= \sum_{i=1}^{74} \frac{\partial}{\partial \mu} [p(t, i) \alpha(i) (1-q)^{M(t-\tau)}] \\
&= \sum_{i=1}^{74} \frac{\partial [p(t, i) \alpha(i) (1-q)^{M(t-\tau)}]}{\partial p(t, i)} \frac{\partial p(t, i)}{\partial \mu} + \frac{\partial [p(t, i) \alpha(i) (1-q)^{M(t-\tau)}]}{\partial M(t-\tau)} \frac{\partial M(t-\tau)}{\partial \mu} \\
&= \sum_{i=1}^{74} \frac{\partial p(t, i)}{\partial \mu} \alpha(i) (1-q)^{M(t-\tau)} + [p(t, i) \alpha(i) (1-q)^{M(t-\tau)}] \ln(1-q) \frac{\partial M(t-\tau)}{\partial \mu} \\
&= \sum_{i=1}^{74} \frac{\partial p(t, i)}{\partial \mu} \alpha(i) (1-q)^{M(t-\tau)} \\
&\quad + [p(t, i) \alpha(i) (1-q)^{M(t-\tau)}] \ln(1-q) \left( \sum_{j=1}^{74} \frac{\partial p(t-\tau, j)}{\partial \mu} \frac{K Z_0 e^{rj}}{K + Z_0 (e^{rj} - 1)} \right),
\end{aligned}$$

where we assume  $p(s, i) = p(0, i)$  for  $s < 0$ . Similarly, we have

$$\begin{aligned}
& \frac{\partial p(t+1, i)}{\partial c} \\
&= \sum_{i=1}^{74} \frac{\partial p(t, i)}{\partial c} \alpha(i) (1-q)^{M(t-\tau)} \\
&\quad + [p(t, i) \alpha(i) (1-q)^{M(t-\tau)}] \ln(1-q) \left( \sum_{j=1}^{74} \frac{\partial p(t-\tau, j)}{\partial c} \frac{K Z_0 e^{rj}}{K + Z_0 (e^{rj} - 1)} \right).
\end{aligned}$$

Now, differentiating both sides of Equation (B.1) with respect to  $q$ , and recalling the Power Rule  $\frac{dx^n}{dx} = n x^{n-1}$  for  $n \in \mathbb{R} \setminus \{0\}$ , we obtain

$$\begin{aligned}
& \frac{\partial p(t+1, i)}{\partial q} \\
&= \sum_{i=1}^{74} \frac{\partial}{\partial q} [p(t, i) \alpha(i) (1-q)^{M(t-\tau)}] \\
&= \sum_{i=1}^{74} \frac{\partial [p(t, i) \alpha(i) (1-q)^{M(t-\tau)}]}{\partial p(t, i)} \frac{\partial p(t, i)}{\partial q} + \frac{\partial [p(t, i) \alpha(i) (1-q)^{M(t-\tau)}]}{\partial q} \\
&\quad + \frac{\partial [p(t, i) \alpha(i) (1-q)^{M(t-\tau)}]}{\partial M(t-\tau)} \frac{\partial M(t-\tau)}{\partial q} \\
&= \sum_{i=1}^{74} \frac{\partial p(t, i)}{\partial q} \alpha(i) (1-q)^{M(t-\tau)} + M(t-\tau) p(t, i) \alpha(i) (1-q)^{M(t-\tau)-1} (-1) \\
&\quad + [p(t, i) \alpha(i) (1-q)^{M(t-\tau)}] \ln(1-q) \left( \sum_{j=1}^{74} \frac{\partial p(t-\tau, j)}{\partial q} \frac{K Z_0 e^{rj}}{K + Z_0 (e^{rj} - 1)} \right).
\end{aligned}$$

- $i = 2, 3, 4$ : From Equation (3.1) with variables and parameters given in Table 3.1 we see that, for  $i = 2, 3, 4$ ,

$$p(t+1, i) = p(t, i-1) \mu (1-c)^{M(t)}. \quad (\text{B.2})$$

Differentiating both sides of Equation (B.2) with respect to  $\mu$  gives

$$\begin{aligned}
& \frac{\partial p(t+1, i)}{\partial \mu} \\
&= \frac{\partial [p(t, i-1) \mu (1-c)^{M(t)}]}{\partial p(t, i-1)} \frac{\partial p(t, i-1)}{\partial \mu} + \frac{\partial [p(t, i-1) \mu (1-c)^{M(t)}]}{\partial \mu} \\
&\quad + \frac{\partial [p(t, i-1) \mu (1-c)^{M(t)}]}{\partial M(t)} \frac{\partial M(t)}{\partial \mu} \\
&= \frac{\partial p(t, i-1)}{\partial \mu} \mu (1-c)^{M(t)} + p(t, i-1) (1-c)^{M(t)} \\
&\quad + [p(t, i-1) \mu (1-c)^{M(t)}] \ln(1-c) \left( \sum_{j=1}^{74} \frac{\partial p(t, j)}{\partial \mu} \frac{K Z_0 e^{rj}}{K + Z_0 (e^{rj} - 1)} \right).
\end{aligned}$$

Differentiating both sides of Equation (B.2) with respect to  $c$  gives

$$\begin{aligned}
& \frac{\partial p(t+1, i)}{\partial c} \\
&= \frac{\partial [p(t, i-1)\mu(1-c)^{M(t)}]}{\partial p(t, i-1)} \frac{\partial p(t, i-1)}{\partial c} + \frac{\partial [p(t, i-1)\mu(1-c)^{M(t)}]}{\partial c} \\
& \quad + \frac{\partial [p(t, i-1)\mu(1-c)^{M(t)}]}{\partial M(t)} \frac{\partial M(t)}{\partial c} \\
&= \frac{\partial p(t, i-1)}{\partial c} \mu(1-c)^{M(t)} + M(t)p(t, i-1)\mu(1-c)^{M(t)-1}(-1) \\
& \quad [p(t, i-1)\mu(1-c)^{M(t)}] \ln(1-c) \left( \sum_{j=1}^{74} \frac{\partial p(t, j)}{\partial c} \frac{K Z_0 e^{rj}}{K + Z_0 (e^{rj} - 1)} \right).
\end{aligned}$$

Now, differentiating both sides of Equation (B.2) with respect to  $q$  gives

$$\begin{aligned}
& \frac{\partial p(t+1, i)}{\partial q} \\
&= \frac{\partial [p(t, i-1)\mu(1-c)^{M(t)}]}{\partial p(t, i-1)} \frac{\partial p(t, i-1)}{\partial q} + \frac{\partial [p(t, i-1)\mu(1-c)^{M(t)}]}{\partial M(t)} \frac{\partial M(t)}{\partial q} \\
&= \frac{\partial p(t, i-1)}{\partial q} \mu(1-c)^{M(t)} \\
& \quad + [p(t, i-1)\mu(1-c)^{M(t)}] \ln(1-c) \left( \sum_{j=1}^{74} \frac{\partial p(t, j)}{\partial q} \frac{K Z_0 e^{rj}}{K + Z_0 (e^{rj} - 1)} \right).
\end{aligned}$$

- $i \geq 5$  From Equation (3.1) with variables and parameters given in Table 3.1 we see that,

$$p(t+1, i) = \mu p(t, i-1) \quad (\text{B.3})$$

Differentiating this is straightforward, and so we quickly see (using the product rule)

$$\begin{aligned}
\frac{\partial p(t+1, i)}{\partial \mu} &= p(t, i-1) + \mu \frac{\partial p(t, i-1)}{\partial \mu} \\
\frac{\partial p(t+1, i)}{\partial c} &= \mu \frac{\partial p(t, i-1)}{\partial c} \\
\frac{\partial p(t+1, i)}{\partial q} &= \mu \frac{\partial p(t, i-1)}{\partial q}.
\end{aligned}$$

# Optimal Design of Non-Equilibrium Experiments for Genetic Network Interrogation<sup>1</sup>

## C.1 Introduction

Recent efforts in modeling the host immune response to HIV infection have illuminated the relationship between perturbations that drive biological systems away from equilibrium and information content in data measured from such systems [12, 44]. For example, the HIV model developed by Banks, et al. [1, 16] describes how anti-retroviral therapy (ART) drives viral load in patients toward an equilibrium level that is undetectable, even by ultra-sensitive assays. When ART is interrupted, e.g., due to patient non-adherence, the HIV model converges toward an equilibrium with high viral load. Indeed, these are the dynamics observed in clinical patient data [16]. Banks, et al. fit their HIV model to clinical patient data and exhibited that the number of HIV model parameters that could be estimated with high statistical confidence increased with the number of treatment interruptions [12]. Thus, non-equilibrium dynamics, induced by ART perturbations, increased the data information content as calculated through asymptotic standard errors for estimated model parameters.

We hypothesized that this positive relationship between information content and system pertur-

---

<sup>1</sup>Contributions:

Algorithm development: H.T. Banks and Kevin Flores

Algorithm implementation: Kaska Adotey

Writeup: Kaska Adotey, Kevin Flores, and H.T. Banks

Advisor: H.T. Banks



bations may exist for more general mathematical models, and in particular for models describing biological networks. To investigate this relationship, we employed an optimal experimental design theory framework [22, 27, 29] to develop an algorithm that minimizes parameter standard errors by choosing optimal perturbations to experimental inputs. Specifically, we describe how the algorithm for optimizing selection of observation times can be extended to include optimization of experimentally controlled perturbations in order to produce data sets with maximal information content. Although we do not propose intentional perturbations in a clinical setting with patients, such a framework could be useful for gaining information from in vitro experiments where there may exist limitations on the number of observable states and observation times.

A particularly useful application of our algorithm involves interrogation of genetic networks. Data from genetic networks can be collected by measuring longitudinal gene expression, either pre- or post-translational, from in vitro cell lines. Importantly, there are also several methods for experimentally perturbing in vitro gene expression at the pre- and post-transcriptional levels [53, 117]. Banks et. al. recently estimated kinetic parameters for a model of a synthetically constructed gene network for the recruitment module of the Brome Mosaic Virus replication cycle [6, 26]. In the BMV synthetic system, gene expression is tuned by the concentration of experimentally controlled chemicals. Here, we report how optimization of the experimentally controlled inputs (chemicals) for the BMV system can lead to more informative experiments, and thereby dramatically decrease standard errors for estimated model parameters, i.e., reduce dramatically the uncertainty in estimating model parameters.

## C.2 Data and Methods

### C.2.1 Mathematical models, statistical models, and parameter uncertainty quantification

In this chapter, we formulate an optimal design framework for experimental systems with a scalar time-dependent input  $b(t)$ . In practice,  $b(t)$  is assumed to be known since it is controlled by the experimenter.

The mathematical model we consider is

$$\begin{aligned} \frac{d\vec{x}}{dt} &= \vec{g}(t, \vec{x}(t; \vec{\theta}, b(t)), \vec{q}, b(t)), \quad t \in [t_0, t_f], \\ \vec{x}(t_0, \vec{\theta}) &= \vec{x}_0, \quad \vec{f}(t, \vec{\theta}, b(t)) = C \vec{x}(t, \vec{\theta}, b(t)) \end{aligned} \tag{C.1}$$

where  $\vec{x}(t, \vec{\theta})$  is the vector of state variables of the system generated using a parameter vector

$\vec{\theta} = (\vec{x}_0, \vec{q}) \in \mathbb{R}^p$ ,  $p = N + r$ , that contains  $N$  initial values and  $r$  system parameters listed in  $\vec{q}$ . The map  $\vec{g} : \mathbb{R}^{1+N+r} \rightarrow \mathbb{R}^N$  has the corresponding observation process  $\vec{f}(t, \vec{\theta}, b(t)) = C \vec{x}(t, \vec{\theta}, b(t))$  with observation operator  $C$  that connects the model solution to observed data. Here,  $C$  is a  $K \times N$  matrix, where  $K \leq N$  is allowed. The times  $t_0$  and  $t_f$  are initial and final experiment times, respectively. To illustrate the inverse problem methodology, we use a constant i.i.d statistical error model, although more general error formulations can be readily derived and treated. Further statistical details, including a description of the associated  $K \times K$  covariance matrix  $V_0$ , can be found in [39]. In this work we consider the simple case where  $b(t)$  can be described as a binary vector  $\vec{b}$  of length  $H$ , with values in  $\{0, 1\}$  that represent whether the experimental input is on or off in the time intervals  $[t_{i-1}^b, t_i^b]$ ,  $i = 1, \dots, H$ .

For a given member  $\theta_k$  of the estimated parameter vector  $\vec{\theta}$  the standard error ( $SE_k$ ) is computed by standard methods from asymptotic theory. For Tables C.1 and C.2, the normalized standard error (NSE) is defined as  $\frac{\theta_k}{SE_k}$ ; the 95% confidence interval (CI) is given by  $[\theta_k - 1.96SE_k, \theta_k + 1.96SE_k]$  (see [39] for details).

### C.2.2 Optimal design measures

We follow the optimal design formulation using the Generalized Fisher Information Matrix [22, 27, 29]. Let  $\mathcal{P}_1([t_0, t_f])$  denote the set of all bounded distributions on the interval  $[t_0, t_f]$ . Let  $B = \mathbb{Z}_2^H$ , the set of binary vectors  $\vec{b}$  of length  $H$  that represent the input perturbation  $b(t)$ . Let  $\mathcal{P}_2(B)$  represent the set of all bounded distributions  $\mathcal{P}_2(b)$  on  $B$ . Then the GFIM may be written

$$\mathcal{F}(\mathcal{P}_1, \mathcal{P}_2, \vec{\theta}_0) = \int_{t_0}^{t_f} \int_{\mathbb{Z}_2^H} \nabla_{\vec{\theta}_0}^T \vec{f}(t, \vec{\theta}_0, b(t)) (V_0^{-1}(t)) \nabla_{\vec{\theta}_0} \vec{f}(t, \vec{\theta}_0, b(t)) d\mathcal{P}_2(b) d\mathcal{P}_1(t) \quad (\text{C.2})$$

We consider the case of observations collected at discrete times where we choose a set of  $n$  time points  $\tau = \{t_j\}$ ,  $j = 1, 2, \dots, n$ , and  $t_0 = t_1 < t_2 < \dots < t_n = t_f$ . The corresponding discrete  $p \times p$  Fisher information matrix (FIM) for a discrete input  $b$  measured at discrete times  $\tau$  is

$$F(\tau, b, \vec{\theta}_0) = \sum_{j=1}^n \nabla_{\vec{\theta}_0}^T \vec{f}(t_j, \vec{\theta}_0, b(t_j)) (V_0^{-1}(t_j)) \nabla_{\vec{\theta}_0} \vec{f}(t_j, \vec{\theta}_0, b(t_j)). \quad (\text{C.3})$$

Methods for calculating the sensitivities  $\nabla_{\vec{\theta}} \vec{f}(t, \vec{\theta}, b(t))$  for delay differential equations, such as the model we consider below, are described in [30]. The choice of optimal design criteria is given by the minimization of a functional  $\mathcal{J}(\mathcal{F}) : \mathbb{R}^{p \times p} \rightarrow \mathbb{R}^+$ ; a description of SE-, D-, and E-optimal design criteria can be found in [27].

### C.2.3 Non-equilibrium experimental design algorithm

The algorithm is initialized with an an initial experimental design consisting of an ordered set of  $n$  sampling times,  $\tau$ , and a vector  $\vec{b}$  of  $H$  ones for the experimental input  $b(t)$ . This initial design represents the unoptimized, or naive, experimental design in which the input is always on. Calculating the optimal  $(\tau, \vec{b})$ -pair requires a computationally demanding nonlinear optimization of  $n$  time points and  $2^H$  possible input vectors (a total of  $n + 2^H$  dimensions). We instead iteratively solve the set of coupled equations

$$\vec{b}^* = \underset{\{\vec{b} | \mathcal{P}_{\vec{b}} \in \mathcal{P}_2(B)\}}{\operatorname{argmin}} \mathcal{J}(F(\tau^*, \vec{b}, \vec{\theta}_0)) \quad (\text{C.4})$$

$$\tau^* = \underset{\{\tau | \mathcal{P}_{\tau} \in \mathcal{P}_1([t_0, t_f])\}}{\operatorname{argmin}} \mathcal{J}(F(\tau, \vec{b}^*, \vec{\theta}_0)) \quad (\text{C.5})$$

where  $\mathcal{J}$  represents the SE-, D-, or E-optimal design criterion.

## C.3 Results

### C.3.1 A gene network model for RNA3 recruitment in Brome Mosaic Virus

We applied our optimal design framework to the following previously validated model [26] of RNA3 recruitment in the Brome Mosaic Virus (BMV) replication cycle.

$$\begin{aligned} \frac{dx}{dt} &= b(t) \frac{r_x}{1 + A e^{-x(t)}} - d_x x(t) \\ \frac{dy}{dt} &= r_y - d_y y(t) - m x(t-s) y(t) \\ \frac{dz}{dt} &= m x(t-s) y(t) - d_z z(t) \end{aligned} \quad (\text{C.6})$$

This model was developed to investigate the recruitment process in the replication cycle of BMV, a positive strand RNA virus. This replication cycle is highly conserved across positive strand RNA viruses, such as Severe Acute Respiratory Syndrome (SARS) and Hepatitis C, and the BMV system has been used to gain insights into interactions of the virus with host factors [6, 121, 140]. Briefly, the mathematical model describes the interaction between Protein 1a ( $x(t)$ ) and RNA3 in the unstabilized ( $y(t)$ ) and stabilized ( $z(t)$ ) forms; for an in-depth description see [26]. The levels of Protein 1a ( $x(t)$ ) and total RNA3 ( $y(t) + z(t)$ ) are measured at time points designed by

the experimenter. Parameters describing Protein 1a ( $r_x, d_x, A$ ) were estimated prior to estimating parameters for RNA3. Thus, below we treat Protein 1a parameters as known and only estimate the RNA3 parameters:  $r_y, d_y, m, d_z$ , and the time delay  $s$ . The values we used for estimated model parameters and the variance of the statistical error model can be found in [26].

The model was developed to describe an experiment performed in synthetic yeast that contained plasmids for RNA3 and protein 1a whose expression is controlled by the concentration of copper and galactose, respectively. Data were collected under equilibrium experimental conditions, i.e., both copper and galactose were given at constant concentrations and the biological system described by Eq. (C.6) converged toward a constant equilibrium. Importantly, previous data did not support a high confidence in the estimation of several RNA3 parameters [26]. We subsequently hypothesized that creating a non-equilibrium experiment in which the galactose input is allowed to vary on or off, and copper is held constant, would lead to increased statistical confidence in RNA3 parameter estimates. The function  $b(t)$  represents the input and, below, we discretize  $b(t)$  into an  $H = 10$  dimensional binary vector,  $\vec{b}$ .

#### C.3.1.1 Naive experimental design and non-iterative algorithm results

We first compared results from the unchanged naive experimental design (such as used in [26]) to a non-iterative version of the optimal design algorithm described above, i.e., optimizing only the observation times ( $\tau$ ) or the input  $\vec{b}$ . For each case, we considered a scenario with 27 experimental observation times of total RNA3 over 26 hours, where the initial and final times were fixed at  $t = 0$  hours to  $t = 26$  hours, respectively (Figure C.1). Only results from SE-optimal design criteria were plotted in Figure C.1, since this criteria, unsurprisingly, results in the lowest standard errors for each parameter. We also consider the simple case in which the time intervals over which  $\vec{b}$  is discretized,  $[t_{i-1}^b, t_i^b]$ ,  $i = 1, \dots, H$ , are of equal length.

We found that optimizing the input  $\vec{b}$  with the SE- optimal design criteria resulted in lower normalized standard errors (NSE) for each parameter as compared to optimizing the time points  $\tau$  or the naive experimental design (Table C.1). Among optimizations of  $\vec{b}$ , SE- optimal design criteria outperformed the D- and E- criteria when considering the overall sum of the NSEs.

#### C.3.1.2 Iterative algorithm results

We next compared results from SE-, D-, and E- optimal design criteria when iterating between Eqs. (C.4) and (C.5). We found that the effectiveness in using the algorithm allowed the use of less observation time points, hence in the results below we used 14 observation time points instead of 27. Overall, the iterative algorithm outputs an experimental design which may result in significantly

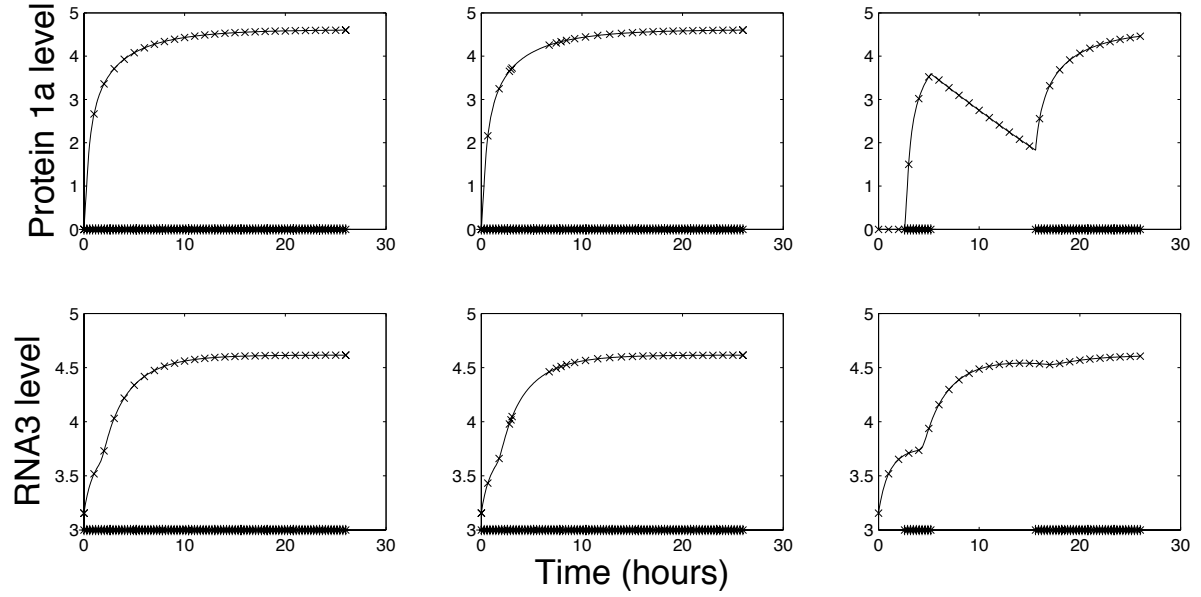


**Figure C.1** Left: Results for naive time points and naive inputs (SE-optimal design criteria). Middle: Results for optimized time points and naive inputs. Right: Results for naive time points and optimized inputs. Protein 1a level =  $x(t)$ . RNA3 level =  $y(t) + z(t)$ . Observation time points are labeled as 'x'. Experiment times when the input is 'on' are labeled on the x-axis with '\*'.

**Table C.1** BMV model results for naive time points and naive inputs (A), optimized time points and naive inputs for D-, E-, and SE-optimal design (B-D through B-SE), or naive time points and optimized inputs for D-, E-, and SE- optimal design (C-D through C-SE). NSE = normalized standard error.

Parameter	$r_y$	$d_y$	$d_z$	$m$	$s$
Estimate	31.641	0.7562	0.3139	0.5557	1.2374
NSE (A)	0.2223	0.6651	0.1947	2.9583	0.4318
95% CI (A)	(17.8575,45.4245)	(-0.22964,1.742)	(0.19414,0.43366)	(-2.6663,3.7777)	(0.19025,2.2846)
NSE (B-D)	0.1632	0.5402	0.1444	2.0333	0.3385
95% CI (B-D)	(21.52,41.762)	(-0.0445,1.5569)	(0.22508,0.40272)	(-1.6589,2.7703)	(0.41635,2.0584)
NSE (B-E)	0.1526	0.5152	0.1356	1.9022	0.3218
95% CI (B-E)	(22.1797,41.1023)	(-0.0074757,1.5199)	(0.2305,0.3973)	(-1.5161,2.6275)	(0.45694,2.0179)
NSE (B-SE)	0.1482	0.5032	0.1329	1.8226	0.3256
95% CI (B-SE)	(22.4505,40.8315)	(0.010449,1.502)	(0.23214,0.39566)	(-1.4294,2.5408)	(0.44772,2.0271)
NSE (C-D)	0.0744	0.0820	0.0940	0.3082	0.0454
95% CI (C-D)	(27.0296,36.2524)	(0.63472,0.87768)	(0.25607,0.37173)	(0.22,0.8914)	(1.1273,1.3475)
NSE (C-E)	0.0519	0.1669	0.0587	0.3471	0.0770
95% CI (C-E)	(28.4206,34.8614)	(0.50884,1.0036)	(0.2778,0.35)	(0.17765,0.93375)	(1.0507,1.4241)
NSE (C-SE)	0.0607	0.0813	0.0643	0.2981	0.0530
95% CI (C-SE)	(27.8745,35.4075)	(0.63564,0.87676)	(0.27431,0.35349)	(0.23107,0.88033)	(1.1089,1.3659)

lower standard errors for all parameter estimates as compared to the naive experimental design regardless of the optimal design criteria choice (Figure 3 (left), zero iterations = naive experimental design). Between optimal design criterion, the SE-optimal design resulted in the lowest sum of NSE's, followed by D-optimal and E-optimal designs, although we note that there was variability in this comparison for each individual parameter (Table C.2).

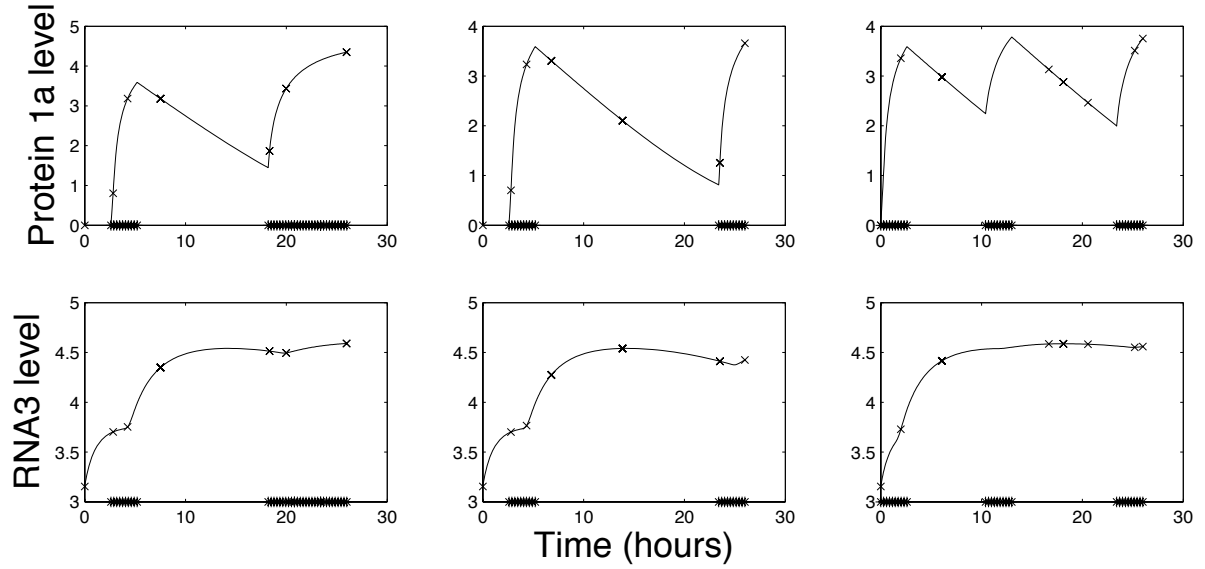


**Figure C.2** Results of iterative algorithm for SE (left), D (middle), and E (right) optimal design. Protein 1a level =  $x(t)$ . RNA3 level =  $y(t) + z(t)$ . Observation time points are labeled as 'x'. Experiment times when the input is 'on' are labeled on the x-axis with '\*'.

**Table C.2** BMV model results for optimized time points and inputs using D-optimal design criteria (D), E-optimal design criteria (E), or SE-optimal design criteria (SE).

Parameter	$r_y$	$d_y$	$d_z$	$m$	$s$
Estimate	31.641	0.7562	0.3139	0.5557	1.2374
NSE (D)	0.0852	0.1052	0.1049	0.3210	0.0583
95% CI (D)	(26.3558,36.9262)	(0.60023,0.91217)	(0.24935,0.37845)	(0.20603,0.90537)	(1.0958,1.379)
NSE (E)	0.0541	1.5602	0.0901	1.0197	0.9503
95% CI (E)	(28.2845,34.9975)	(-1.5563,3.0687)	(0.25845,0.36935)	(-0.55494,1.6663)	(-1.0676,3.5424)
NSE (SE)	0.0599	0.0840	0.0701	0.3173	0.0665
95% CI (SE)	(27.9255,35.3565)	(0.63163,0.88077)	(0.27075,0.35705)	(0.21005,0.90135)	(1.0761,1.3987)

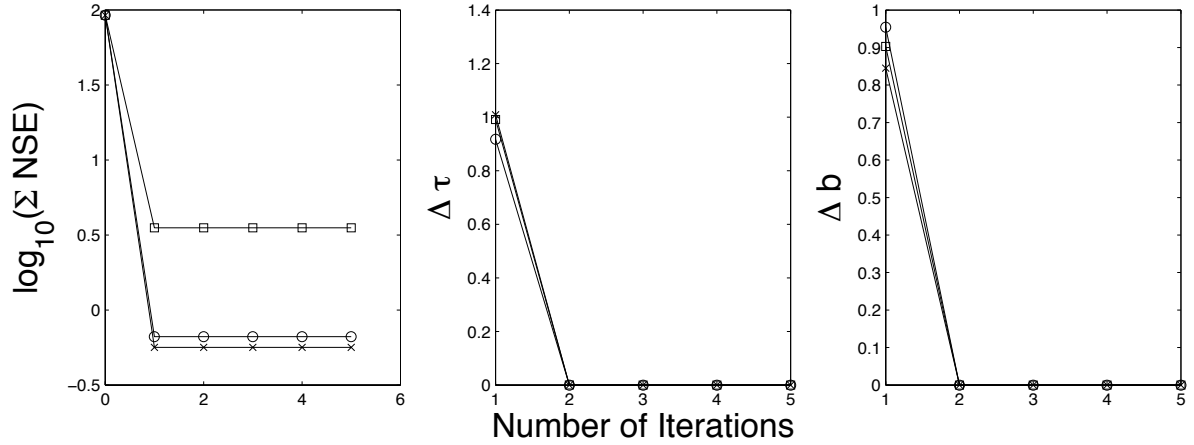


**Figure C.3** Convergence of the iterative algorithm for the sum of normalized standard errors (NSE), the change in time points  $\Delta \tau$  (euclidean norm), and the change in inputs  $\Delta b$  (euclidean norm). The axis for NSE is on a  $\log_{10}(y)$  scale, the  $\Delta \tau$  and  $\Delta b$  are on a  $\log_{10}(y+1)$  scale. Optimal design criteria: SE = 'x', D = 'circles', E = 'squares'.

## C.4 Discussion

Overall, our results suggest that experimental input manipulation can produce non-equilibrium system dynamics, leading to a greater information content in collected data. *Taking the non-iterative algorithm results together with the iterative algorithm results, our findings suggest that input manipulation is a more powerful tool for reducing standard errors in parameter estimates than optimizing*

*observation times for the BMV system.* For example, optimizing only the observation times still resulted in unreasonably large confidence intervals for the parameter  $m$ , whereas optimizing only the experimental input resulted in acceptably narrow confidence intervals for  $m$ , as well as extremely narrow confidence intervals for all other parameters regardless of the choice of optimal design criteria (Table C.1).

In future investigations, we will extend the BMV model to consider multiple time-dependent inputs for both Protein 1a and RNA3, since they are controlled separately by the concentration of galactose and copper, respectively. We postulate that, in general, lower standard errors can be achieved when a greater number of system variables are manipulated with experimentally controlled inputs. In addition, we are currently exploring the use of the iterative algorithm (Eqs. (C.4), (C.5)) in other genetic network systems that approach a periodic equilibrium to test whether the structure of the  $\omega$ -limit set affects algorithm convergence.